Advanced Techniques for Achieving Near Maximum-Likelihood Soft Detection in MIMO-OFDM Systems and Implementation Aspects for LTE/LTE-A

Sébastien Aubert

Thèse

THESE INSA Rennes
sous le sceau de l'Université européenne de Bretagne
pour obtenir le titre de
DOCTEUR DE L'INSA DE RENNES
Spécialité : Traitement du signal et télécommunications

présentée par
Sébastien Aubert
ECOLE DOCTORALE : *MATISSE*
LABORATOIRE : *IETR*

Advanced Techniques for Achieving Near Maximum-Likelihood Soft Detection in MIMO-OFDM Systems and Implementation Aspects for LTE/LTE-A

Thèse soutenue le 23.09.2011
devant le jury composé de :

Christophe Jégo
Professeur, Polytech' Bordeaux / *rapporteur*
Raymond Knopp
Professeur, Institut Eurecom / *rapporteur*
Maryline Hélard
Professeur, INSA IETR / *examinatrice*
Mohamed-Slim Alouini
Professeur, KAUST / *examinateur*
Marc Soler
Algorithm Senior Principal, ST-Ericsson / *examinateur*
Fabrizio Tomatis
Algorithm Development Manager, ST-Ericsson / *examinateur*
Andrea Ancora
Senior Algorithm Development, ST-Ericsson / Co-directeur de thèse
Fabienne Nouvel
Maître de conférence, INSA IETR / Directrice de thèse

Techniques Avancées ayant pour but de s'Approcher des Performances du Maximum de Vraisemblance à Décision Souple pour les Systèmes *MIMO-OFDM* et Étude des Aspects d'Implantation pour les Normes *LTE/LTE-A*

Sébastien Aubert

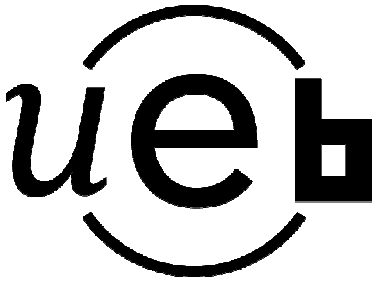

En partenariat avec

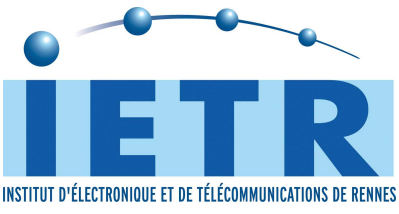

Acknowledgements

First of all, I am indebted to both my company - ST-Ericsson (previously ST-NXP Wireless, previously NXP Semiconductors) - and my laboratory - *Institut National des Sciences appliquées Institut d'Électronique et des Télécommunications de Rennes* -, without whom this thesis would not exist.

I would like to express my greatest gratitude towards my supervisor Fabienne Nouvel. I really appreciated the complete freedom in the thesis subject - making it useful for industry - and her encouragement.

I would like to express my sincerest thanks to Fabrizio Tomatis - my competent and appreciated team Manager - and to Andrea Ancora - my technical leader - who was my strongest guide.

I am also very grateful towards Manar Mohaisen - assistant professor, met at VTC and with whom I worked on a Spawc conference and on a book chapter -, Youssef Nasser - PhD, with whom I worked on a Spawc conference -, Amor Nafkha - assistant professor, who I collaborated with on a VTC conference -, Matthieu Crussière - assistant professor, for his helpful advices and support - and Philippe Mary - assistant professor - met at a Spawc conference and for all the good times.

I would like to express my gratitude to Marc Soler with whom I collaborated and who was full of pertinent and comforting advices.

I would like to mention some of the PhD candidates I was fortunate to met: Pierre Oudomsack Paquero, Loïc Marnat, Ayman Khalil, Lahatra Rakotondrainibe, Philippe Tanguy, Clément Yann, Emmanuel Amador, Pierre Viland, Christophe Le Guellaut and R&D engineer Yvan Kokar. Hopping not to forget anyone, I thank the whole INSA IETR team for its warm welcoming.

I would like to acknowledge all the PhD candidates within the ST-E algorithm team: Sebastian Wagner - reliable un-anonymous reviewer -, Romain Couillet and R&D engineers Éric Alliot, Pierre Demaj, Martial Gander, Stefania Sesia, Dominique Brunel, Christophe Danchesi, Jean-Marc Aznar.

I would like to acknowledge my dearest ST-E colleagues Lionel Sinègre, Catherine Renaud, Éric Queille, Olivier Rouah, Patrice Declémenti, Bruno Casals, Jérôme Velardi, Xavier Lowagie, Patrick Da Silva, Hatem Ayari, Brice Dufour, Julien Aguilar, Gregory Prieur, Michel Zamaron, Nicolas Roirand, Éric Verriest, Laurent Segard, Patrick Valdenaire, Rose-Marie Garino, Laurence Trouchaud, Nicolas Bacquet, Laurent Pilot, Frédéric Maccotta, Xavier Bonafos, Xavier Duperthuy, Issam Toufik, Pascal Bernard, Emmanuel Alie, Laurent Noel and the dearly departed Joël Cornau who make each (working-)day a bit better.

This work is dedicated to my family, my parents, Jane my wife (who makes every (working- and non-working-)day a bit better and who is the most loyal un-anonymous reviewer) and Martin my son.

Contents

List of Abbreviations

3GPP	3^{rd} Generation Partnership Project
ACK	ACKnowledgement
ADC	Analog-to-Digital Converter
AMC	Adaptive Modulation and Coding
APP	A Posteriori Probability
AWGN	Additive White Gaussian Noise
BCJR	Bahl-Cocke-Jelinek-Raviv
BER	Bit Error Rate
BICM	Bit-Interleaved Coded Modulation
BLAST	Bell Labs Layered Space-Time Transmission
BP	Babai Point
BPSK	Binary Phase-Shift Keying
BS	Base Station
C-SC	Capacity-Selection Criterion
CDF	Cumulative Density Function
CED	Cumulated Euclidean Distance
CF	Cholesky Factorization
CL	Closed-Loop
CLA	Complex LLL Algorithm
COST	Committee On Science and Technology
CP	Cyclic Prefix
CQI	Channel Quality Indicator
CRC	Cyclic Redundancy Check
CSI	Channel State Information
D-BLAST	Diagonal-Bell Labs Layered Space-Time Transmission
DAC	Digital-to-Analog Converter
DFD	Decision-Feedback Detection
DFT	Discrete Fourier Transform
DL	DownLink
DSP	Digital Signal Processing
DSS	De-normalized, Shifted then Scaled
ELC	Empirical Log-Likelihood Ratio Clipping
eNB	eNodeB
EPA	Extended Pedestrian A
ETU	Extended Typical Urban
EVA	Extended Vehicular A
EVP	Embedded Vector Processor
FFT	Fast Fourier Transform
FLC	Fixed Log-Likelihood Ratio Clipping
FLOP	FLoating-point OPeration
FP	Fincke-Pohst
FRC	Fixed Reference Channel
FSD	Fixed-complexity Sphere Decoder
GR	Givens Rotations
GS	Gram-Schmidt
HARQ	Hybrid-Automatic Repeat reQuest

HH	HouseHolder
i.i.d.	independent and identically distributed
iff	if and only if
IFFT	Inverse Fast Fourier Transform
ILI	Inter-Layer Interference
IPS	Instruction Per Second
ISI	Inter-Symbol Interference
ITU	International Telecommunication Union
LA	LLL Algorithm
LC	Log-Likelihood Ratio Clipping
LD	Linear Detection
LDPC	Low-Density Parity-Check
LFG	Likelihood Function Generation
LLE	Last list Entry
LLR	Log-Likelihood Ratio
LMMSE	Linear Minimum-Mean Square Error
LR	Lattice-Reduction
LRA	Lattice-Reduction-Aided
LRA-LD	Lattice-Reduction-Aided Linear Detection
LRA-MMSE	Lattice-Reduction-Aided Minimum-Mean Square Error
LRA-MMSEE	Lattice-Reduction-Aided Minimum-Mean Square Error Extended
LRA-ZF	Lattice-Reduction-Aided Zero-Forcing
LSB	Least Significant Bit
LSD	List Sphere-Decoder
LTE	Long-Term Evolution
LTE-A	Long-Term Evolution-Advanced
LU	Lower-Upper
LUT	Look-Up Table
LZF	Linear Zero-Forcing
MAC	Multiply ACcumulate
MAP	Maximum A Posteriori
MCS	Modulation and Coding Scheme
ML	Maximum-Likelihood
ML-SC	Maximum Likelihood-Selection Criterion
MLC	Multi-level Log-Likelihood Ratio Clipping
MLD	Maximum-Likelihood Detector
MMSE	Minimum-Mean Square Error
MMSE-VB	Minimum-Mean Square Error-based Vertical-Bell Labs Layered Space-Time Transmission
MSB	Most Significant Bit
MU-MIMO	Multiple-User-Multiple-Input Multiple-Output
NACK	Negative ACKnowledgement
NP-hard	Non-deterministic Polynomial time
OD	Orthogonal Deficiency
ODFD	Ordered Decision-Feedback Detection
ODN	Original-Domain Neighbourhood
OFDM	Orthogonal Frequency-Division Multiplexing
OFDMA	Orthogonal Frequency-Division Multiple-Access
OL	Open-Loop
OPS	Operation Per Second

P/S	Parallel-to-Serial
PAM	Pulse-Amplitude Modulation
PAPR	Peak-to-Average-Power Ratio
PDCCH	Physical Downlink Control Channel
PDF	Probability Density Function
PED	Partial Euclidean Distance
PGR	Parallel Givens Rotations
PLL	Phase-Locked Loop
PSA	Post-Sorting-Algorithm
QAM	Quadrature Amplitude Modulation
QRD	QR Decomposition
RB	Resource-Block
RDN	Reduced-Domain Neighbourhood
RE	Resource-Element
RF	Radio Frequency
RF	Radio Frequency
RM	Rate-Matching
RMS	Root Mean Square
RS	Reference Signal
S/P	Serial to Parallel
SA	Seysen's Algorithm
SC	Single Carrier
SD	Sphere Decoder
SDMA	Space-Division Multiple Access
SE	Schnorr-Euchner
SER	Symbol Error Rate
SISO	Single-Input Single-Output
SLA	Sorted QR Decomposition-based LLL Algorithm
SLC	Signal-to-Noise Ratio Aware Log-Likelihood Ratio Clipping
SM-MIMO	Spatial Multiplexing-Multiple-Input Multiple-Output
SNR	Signal-to-Noise Ratio
SSN	re-Scaled, re-Shifted then Normalized
ST-E	ST-Ericsson
STBC	Space-Time Block Codes
STTC	Space-Time Treillis Codes
SU-MIMO	Single-User Multiple-Input Multiple-Output
SVD	Singular Value Decomposition
UE	User Equipment
UMTS	Universal Mobile Telephone System
V-BLAST	Vertical-Bell Labs Layered Space-Time Transmission
VIQRD	Variable Incremental QR Decomposition
w.r.t.	with respect to
WSSUS	Wide-Sense Stationary Uncorrelated Scattering
ZF	Zero-Forcing
ZF-VB	Zero-Forcing-based Vertical-Bell Labs Layered Space-Time Transmission

Chapter 1

Introduction

Contents

1.1 Motivation and Problem Statement

Immutably, digital communication aims at providing increasingly higher data rates to users. In the particular case of wireless environments and mobile receivers, challenges are numerous. Given a transmit power, the transmission is subject to a physical bandwidth limit and propagation issues such as both time and frequency fading. Sophisticated signal processing techniques have been developed for decades and allow reaching these limits while ensuring reliable communications. Hence, further improvements become insignificant and costly.

For over ten years, using multiple antennas at both the transmitter and the receiver has been shown to linearly boost the channel capacity by the number of independent sub-channels possibly established, without requiring additional spectral resources.

In order to achieve the 3GPP LTE and 3GPP LTE-A requirements, spatial multiplexing-MIMO communication schemes have been implemented. In such a configuration, a linear superposition of separately transmitted information symbols is observed by the receiver, due to multiple transmit antennas that simultaneously send independent data streams. The detector seeks to recover the transmitted symbols while approaching the channel capacity, which corresponds to an inverse problem with a finite-alphabet constraint. The design of detection schemes with high performance, low latency and applicable computational complexity is a challenging research topic due to the power and latency limitations of mobile communication systems.

The challenge of demultiplexing the transmitted symbols via spatial multiplexing techniques, *i.e.*, detection techniques, stands as one of the main limiting factors of these systems. It makes the detector step in wireless communication systems a key point. In particular, despite its large computational complexity and latency, incorrect choices would lead to a dramatic performance loss.

Ideally, such a research subject aims to achieve near-optimum performance at the detection step, while offering polynomial computational complexity. The primary goal of this work is to provide a solution to this problem, while carefully considering implementation issues. Parallel and non NP-hard algorithms selection are strongly favoured. Also, an efficient performance/complexity trade-off in the LTE(-A) background is achieved.

1.2 Outline and Contributions

The present work has been split into four distinct chapters.

Chapter 2 presents the background and briefly introduces useful preliminaries, notations and considerations with an increasing level of details. The LTE(-A) norm is considered and leads to remarks, assumptions of limitations that go with the flow. Starting from a simple SISO system, general tools are introduced provided they are useful to the rest of the presented work. Thus, some points that might be considered as fundamentals in a different background are made smaller or even overlooked. In particular, time, frequency and space dimensions are addressed through channel coding, OFDM and MIMO schemes, respectively. The classical system model introduction follows the general detection problematic.

The heart of the subject is addressed in Chapter 3. It consists in making an inventory of the main existing solutions, which offers an academical interest. The most promising trends are explored in depth and their behaviour in our background is further discussed, by restricting the discussion to general remarks. Thus, some techniques are clearly overlooked. The classical QR decomposition-based decision-feedback detectors and sphere decoding techniques are introduced. Also, both layer and symbol re-ordering are presented. Implementation issues are considered which logically brings about the introduction of particular sphere decoding like techniques. Further issues explain the interest in lattice-reduction-aided techniques, particularly promising when associated with a neighbourhood study. By aiming at shifting a large part of the detector's computational complexity to the preprocessing step, the combination of the lattice-reduction and an efficiently centred sphere decoding is explored. Finally, an original detector is proposed and its advantage over existing solutions is exposed.

Chapter 4 might have been addressed in Chapter 5 since it constitutes a practical requirement. However, the soft-decision extension of any detector presented in the previous chapter is not necessarily straightforward and induces a significant impact on the detector computational complexity, on system performance or both of them. Consequently, it is the object of a whole chapter where the main trends are described and discussed. With this slant, the log-likelihood ratios calculation is detailed first and the standard approximations are stated. Subsequently, the classical detection algorithms updates are introduced, namely the maximum-likelihood, linear and decision-feedback detectors. The soft-decision extension is also presented in the case of the lattice-reduction-aided linear detectors and of the sphere decoder. In the case of the association of both lattice-reduction and sphere decoder, new issues arise, which induces particular considerations.

Chapter 5 is closely related to our background and in particular to the 3GPP LTE(-A) norm requirements. First, the particular aspects that have been considered in the present work are presented. In particular, LTE(-A) norm parameters are introduced, which induces some convenient assumptions and limitations. Their exploration offers an advantage over a general study, namely a computational complexity and latency reduction. For example, the provided precoding for spatial multiplexing-MIMO systems with OFDM modulation are considered and induce computational complexity reduction at the preprocessing step.

1.3 Following Publications

The present work has led to the publication of several national and international articles. A list of selected communications is given below.

The hard-decision near-maximum-likelihood detector is the key part of the present work. Since it constitutes an active research field, it requires a complete state-of-the-art review of the existing solutions and promising ideas. The preprocessing step of QR decomposition-based algorithms has been generally neglected in the literature, such as one contribution has been presented in the following international publication:

[**Aub09a**] **Aubert S., Nouvel F., and Nafkha A. Complexity gain of QR Decomposition based Sphere Decoder in LTE receivers,** ***Vehicular Technology Conference, IEEE*****, 2009.**

[**Aub09b**] **Aubert S., Nouvel F., and Nafkha A. Décodeur Sphérique associé à une Décomposition QR à Complexité Réduite dans les Systèmes MIMO OFDM,** ***Groupe d'Études du Traitement du Signal et des Images*****, 2009.**

Through the novel and promising association of both the lattice-reduction and a sphere decoding techniques, original techniques were described and led to the filing of two European patents owned by ST-Ericsson:

[**Aub11a**] **Aubert S. Detection process for a receiver of a wireless MIMO communication system,** ***European Patent*****, 2011.**

[**Aub11b**] **Aubert S. Detection process for a receiver of a wireless MIMO communication system, and receiver for the same,** ***European Patent*****, 2011.**

A state-of-the art overview of the main existing trends is proposed, by means of a pedagogical point of view, in:

[**Aub11c**] **Aubert S., and Mohaisen M.** ***From Linear Equalization to Lattice-Reduction-Aided Sphere-Detector as an answer to the MIMO Detection problematic in Spatial Multiplexing Systems*****, Vehicular Technologies, 978-953-307-976-9, INTECH, Feb. 2011.**

The soft-decision near-maximum-likelihood detector is an essential step due to practical requirements. In numerous famous publications, this point is not addressed since it is not necessary from an academic point of view. One contribution was presented in the following international publication:

[**Aub11d**] **Aubert S., Ancora A., and Nouvel F. Multi-Level Log-Likelihood Ratio Clipping in a Soft-Decision Near-Maximum Likelihood Detector,** ***International Conference on Digital Telecommunications*****, April 2011.**

Its commercial application was previously protected through the filing of one European patent owned by ST-Ericsson:

[**Aub10a**] **Aubert S., Ancora A. Process for performing log-Likelihood-ratio clipping in a soft-decision near-ML detector, and detector for doing the same,** ***European Patent*****, Feb. 2010.**

The present work relies on a specific background, namely the LTE(-A) norm. In particular,

the OFDM requirement induces computational complexity reduction in the preprocessing step, thus leading to the following international publications:

[**Aub11e**] **Aubert S., Tournois J., and Nouvel F. On the Implementation of MIMO-OFDM Schemes Using Perturbation of the QR Decomposition: Application to 3GPP LTE-A Systems, *Acoustics, Speech, and Signal Processing, International Conference on*, May 2011.**

Implementation issues have also been considered. In particular, the potential parallelism of the preprocessing step has been addressed in the following international publications:

[**Aub10b**] **Aubert S., Mohaisen M., Nouvel F., and Chang K. Parallel QR Decomposition in LTE-A Systems, *Signal Processing Advances in Wireless Communication, IEEE Workshop on*, May 2010.**

Finally, the OFDM particular case and the MIMO precoding scheme, respectively, have led to the filing of two European patents owned by ST-Ericsson:

[**Aub11f**] **Aubert S. Process for performing QR decomposition of a channel matrix in a MIMO wireless communication system, and receiver for the same, *European Patent*, 2011.**

[**Aub11g**] **Aubert S., and Ancora A. Precoding Matrix Index selection process for a MIMO receiver based on a near-ML detection, and apparatus for doing the same, *European Patent*, 2011.**

Chapter 2

Preliminaries

Contents

2.1 Wireless Communication Systems

To introduce basic principles used in this manuscript, a complex baseband Single-Input Single-Output (SISO) system is first considered. By introducing the convolution operation $*$, the continuous-time system is described through the relation:

$$y(t) = x(t) * h(t) + n(t) = \int_{-\infty}^{\infty} x(\tau)\, h(t-\tau)\, d\tau + n(t), \tag{2.1}$$

where $y(t)$ is the received signal at time t, $x(t)$ is the transmitted signal, $h(t)$ is the channel impulse response and $n(t)$ is a corrupting noise - that characterises imperfect electronic components or some interfering signals.
A discrete-time system results in a sampled version of the aforementioned continuous-time signals:

$$y_k = x_k * h_k + n_k = \sum_{l \in \mathbb{Z}} x_l h_{k-l} + n_k, \tag{2.2}$$

where - among others - $y_k = y(kT)$, where k is an integer and T is the sampling period.

For the sake of simplicity and without loss of generality since Orthogonal Frequency-Division Multiplexing (OFDM) techniques are considered in the present manuscript, the narrow-band flat-fading assumption is admitted. The filter convolution operation thus becomes a trivial multiplication [Pro95] operation and - for each sampling period - the equivalent SISO system simply reads:

$$y = hx + n, \tag{2.3}$$

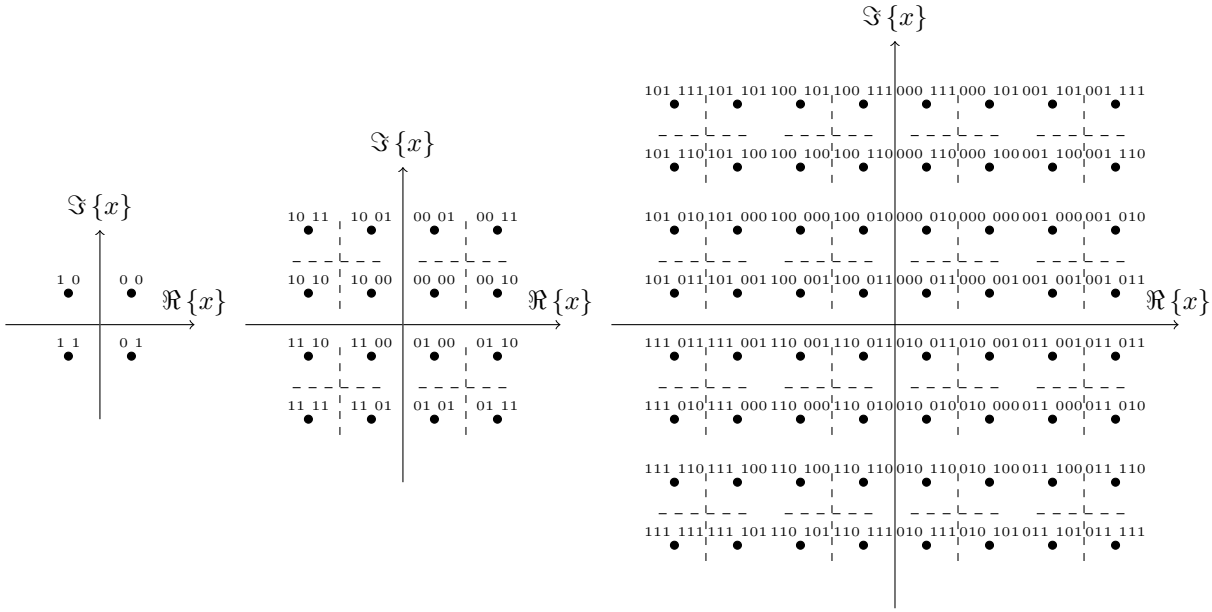

Figure 2.1: 4-QAM, 16-QAM and 64-QAM modulation constellations for LTE(-A) downlink [3GP09c].

where y is the received symbol, h is the channel coefficient, the transmitted symbol x is drawn from a finite constellation set ξ and n is an Additive White Gaussian Noise (AWGN).
In the present work and due to LTE(-A) requirements, only square $|\xi|$-ary QAM constellations are considered, with $|\xi| = 2, 4, 16, 64$. Each symbol is mapped from a bit pattern of length $\log_2\{|\xi|\} = 1, 2, 4, 6$, as depicted in Figure 2.1. The average power of the presented constellation is ensured to be normalized to one, thus the available transmit power is not exceeded. The symbols are mapped using Gray labelling. Subsequently two nearest neighbours only differ in a single bit while they can easily be mistaken thus leading to a smaller BER P_B, given a SER P_S.

In wireless communications, the transmission is subject to fading. It results in an important variation of the attenuation experienced by a signal, over a certain propagation link. In particular, a fading in time, frequency or both arise. A differentiation must be made between slow fading - that may be resolved by the system - and fast-fading - that may lead to irreparable data loss. The coefficient h denotes the complex attenuation factor of the transmission link. At first, h is modelled as a random process, according to a Rayleigh distribution. This way, the channel coefficient is randomly generated by a zero mean and unit variance complex Gaussian distribution:

$$h \backsim \mathcal{CN}(0, 1). \tag{2.4}$$

The signal hx is considered to be randomly corrupted by the noise term n. In the present work, it is randomly generated by a zero mean and σ_n^2 variance complex Gaussian distribution:

$$n \backsim \mathcal{CN}\left(0, \sigma_n^2\right), \tag{2.5}$$

where σ_n^2 is the power spectral density, also commonly denoted as N_0 [Pro95]. We refer to the average SNR at the receiver:

$$\frac{E\{(hx)^*(hx)\}}{E\{n^*n\}} = \frac{E\{x^*x\}\,E\{h^*h\}}{E\{n^*n\}} = \frac{E_S}{N_0}, \tag{2.6}$$

where $E\{\cdot\}$ denotes the expectation and E_S is the average symbol energy, due to independence between x and h and to the unit variance of the channel. The SNR is an essential quantity for performance estimation, under the AWGN assumption [Bar03c].

In the sequel, classical results are introduced. Also, coherent detection is assumed, namely the carrier phase is considered to be perfectly recovered. In practical applications, the carrier phase is estimated with a Phase-Locked Loop (PLL) circuit [Ses09].
In the SISO AWGN (no presence of channel) case, the exact SER expression for $|\xi|$-QAM modulations - and for an even number of bits per symbol since square constellations are considered in the LTE(-A) standard - is determined from the SER expression for a $\sqrt{|\xi|}$-PAM [Pro95]:

$$P_S^{\sqrt{|\xi|}\text{-PAM}} = 2\left(1-\frac{1}{\sqrt{|\xi|}}\right)Q\left(\sqrt{\frac{3}{|\xi|-1}\frac{E_S}{N_0}}\right), \tag{2.7}$$

where the Q-function [Pro95] reads:

$$Q(z) = \frac{1}{\sqrt{2\pi}}\int_z^\infty e^{\frac{-t^2}{2}}dt,\ z \geq 0, \tag{2.8}$$

and with

$$P_S^{|\xi|\text{-QAM}} = 1-\left(1-P_S^{\sqrt{|\xi|}\text{-PAM}}\right)^2. \tag{2.9}$$

Since it is clear - with independent errors on bits - that $P_S = 1-(1-P_B)^{\log_2\{|\xi|\}}$ in the $|\xi|$-QAM case, the BER is well-approximated for small P_B [Pro95] as:

$$P_B \approx \frac{P_S}{\log_2\{|\xi|\}}. \tag{2.10}$$

By assuming the knowledge of the instantaneous channel realization h, the corresponding instantaneous SNR reads $\gamma = |h|^2 E_S/N_0$. Thus, the mean error probability is calculated by averaging over all channel realizations:

$$P_S^{|\xi|\text{-QAM},Rayleigh} = \int_0^\infty P_S^{|\xi|\text{-QAM},AWGN}\,p(\gamma)\,d\gamma, \tag{2.11}$$

where

$$p(\gamma) = \frac{1}{E_S/N_0}e^{\frac{-\gamma}{E_S/N_0}}. \tag{2.12}$$

Subsequently, in the SISO case and in presence of a Rayleigh slow fading channel, the exact SER expression for a $|\xi|$-QAM modulation is obtained through an integration by parts and a change of variables [Pro95]:

$$P_S^{|\xi|\text{-QAM},Rayleigh} = 2\frac{\sqrt{|\xi|}-1}{\sqrt{|\xi|}}\left(1-\frac{1}{s}\right)-\left(\frac{\sqrt{|\xi|}-1}{\sqrt{|\xi|}}\right)^2\left(\frac{2}{\pi s}\tan^{-1}\left\{\frac{1}{s}\right\}-\frac{1}{s}+\frac{1}{2}\right), \tag{2.13}$$

where

$$s = \sqrt{1+\frac{2(|\xi|-1)}{3\log_2\{|\xi|\}}}. \tag{2.14}$$

As introduced in [Pro95, Shi06] and when adapted to the SISO case, the theoretical SER is strongly related to the minimal distance - between two symbols within the constellation - and the number of nearest neighbours - the definition is given below -, denoted as d_{min} and N_e, respectively. In particular, it reads:

$$d_{min}^2 = \min_{x_1,x_2\in\xi,\ x_1\neq x_2}|h(x_1-x_2)|^2, \tag{2.15}$$

and

$$N_e = \sum_{i=1}^{|\xi|} N_{e_i}, \tag{2.16}$$

where N_{e_i} is the number of nearest neighbours of x_i, namely the symbols that are set at a distance $d_{\min}$ from x_i. Assuming Maximum-Likelihood (ML) detection at the receiver, the corresponding SER reads [Pro95]:

$$P_S \approx \frac{1}{|\xi|}\left(\sum_{i=1}^{|\xi|} N_{e_i}\right) Q\left(d_{min}\sqrt{\frac{E_S}{2N_0}}\right), \tag{2.17}$$

thus clearly exhibiting the point that the introduced error probability is the mean error probability. For example in the 16-QAM case, a difference must be made between a symbol inside, on the border or on the corner of the constellation since the number of the nearest neighbours is different for each case. Consequently, their particular SER read:

$$P_S^{|\xi|\text{-QAM,corner}} \approx 2Q\left\{\sqrt{\frac{E_S}{5N_0}}\right\}, \tag{2.18}$$

$$P_S^{|\xi|\text{-QAM,border}} \approx 3Q\left\{\sqrt{\frac{E_S}{5N_0}}\right\}, \tag{2.19}$$

$$P_S^{|\xi|\text{-QAM,inside}} \approx 4Q\left\{\sqrt{\frac{E_S}{5N_0}}\right\}. \tag{2.20}$$

In conclusion, while high order modulations offer large spectral efficiencies, a significant vulnerability to interference is induced, leading to a decreased capacity. According to this consideration, there exists an efficient modulation/data rate - addressed in Section 2.2 - that reaches (in theory) the system capacity. The modulation choice is made depending on any selected Modulation and Coding Scheme (MCS) given channel conditions and required data rate.

In the LTE(-A) downlink case [3GP09c], $|\xi|$-QAM modulations with Gray mapping can be partitioned into square subsets with a minimum mean intra-subset Euclidean distance. It is clearly depicted in Figure 2.1. In particular, any $|\xi|$-QAM constellation may be represented as a weighted sum of 4-QAM constellations [Tar03], leading to the expression below:

$$x^{|\xi|-QAM} = \sum_{i=0}^{\log_2\{|\xi|\}-1} 2^i \left(\frac{\sqrt{2}}{2}\right) x_i^{4-QAM} \tag{2.21}$$

where $x^{|\xi|-QAM}$ belong to a $|\xi|$-QAM constellation. The multi-level bit mapping nature of a QAM constellation induces different symbol characterization by different mean Euclidean distances. Hence, bits are subject to different levels of protection against noise and amplitude impairments, depending on their position within the bit sequence.

2.2 Theoretical Aspects of Channel Coding

The objective of digital communication systems is to transmit a source information to a sink over a channel with the highest reliability, namely with the lowest probability of error. This simple and general idea has rallied researchers for decades, from the founding theoretical formulation established by Shannon [Sha48] to the "astonishingly" efficient iterative turbo codes [Ber93].

At the beginning, Shannon introduced the concept of coding. Directly from the fundamental noisy-channel coding theorem [Sha48], the definition of the channel capacity is offered:

$$C = \log_2 \left\{ 1 + |h|^2 \frac{E_S}{N_0} \right\}. \tag{2.22}$$

This is the capacity for an AWGN memoryless channel, according to the notations in Equation (2.3) and with complex-valued variables.

Subsequently, the Shannon theorem states that given a noisy channel with channel capacity C and information transmitted at a rate of R, then if $R < C$ there exist codes that allow the probability of error at the receiver to be made arbitrarily small. Thus, the concept of channel coding had been introduced. In particular and in order to achieve channel capacity, the practical way of processing lies in providing redundancy - the basic idea - and interleaving - for practical reasons only -, denoted as channel coding.

Although Shannon works were the first to provide an upper bound on the reliable transmissions rate, it did not bring convenient code design. It led to an active research field, initiated by Hamming [Ham50] in 1950. By focusing on the performance-complexity optimization, modern capacity-approaching codes lie in probabilistic coding schemes [Cos07] and a sequence of significant advances in this field is provided.
A first acceptable solution was offered by convolutional codes [Eli55] at the expense of an exponential complexity (see Section 2.7.3) - in the code lengths - with the use of a Viterbi decoder [Vit67]. While it is a first practically feasible solution - for relatively small length of codes -, it offers performance that remains far away - of about 3 dB - from the Shannon limit.
Later, Low-Density Parity-Check (LDPC) codes have been introduced in [Gal62]. The advantageous iterative nature of the associated - bipartite graph-based - decoders makes them rediscovered nowadays [Ric01] due to their low complexity.
More recently, Berrou *et al.* introduced turbo codes in [Ber93]. This approach offers near-Shannon limit performance [Ber96]. However, its leads to a high-complexity - even if iterative thus adjustable - implementation. The BCJR decoder that is proposed in [Bah74] can be used. The first iteration is similar to the Viterbi decoder, thus its computational complexity as well. While their advantage over LDPC codes is not clearly stated, turbo codes are nowadays included in the LTE(-A) standard [3GP10]. Consequently, they are considered in the present work and clearly introduced in the sequel.

As depicted in Figure 2.2, turbo encoders consist of a - parallel in the present case - concatenation of two identical rate-$\frac{1}{2}$ convolutional encoders - denoted as E_1 and E_2 -, by introducing the convenient D-transform, where D is a delay. It returns to the - well-known in the digital filtering field - Z-transform in the modulo-two domain, with each D being replaced by z^{-1}. In particular, E_1 processes the input data while E_2 processes a pseudo-randomly interleaved [3GP10] version of the same data. The codeword produced at the output of the turbo encoder is a concatenation of its unmodified input $\mathbf{u}^l$ - commonly denoted as systematic bits - and of the two convoluted signals $\mathbf{u}^{l,(1)}$ and $\mathbf{u}^{l,(2)}$ - commonly denoted as parity bits -, thus resulting in a coded sequence of bits $\mathbf{b}_k^l$. Each constituent encoder is required to be terminated by tail bits [3GP10] that do not contain information, thus reducing their efficiency for small blocks. In particular in Figure 2.2, the nominal code rate of the turbo code is $\frac{1}{3}$.

In such schemes, soft-decisions of coded symbols are typically produced from the detector output, plus any available side information, and passed on to the decoder in the form of bit-wise Log-Likelihood Ratios (LLR). In the latter, the sign and the magnitude represent the decision and the reliability, respectively. This aspect will be further introduced in Section 4.1.1. From the

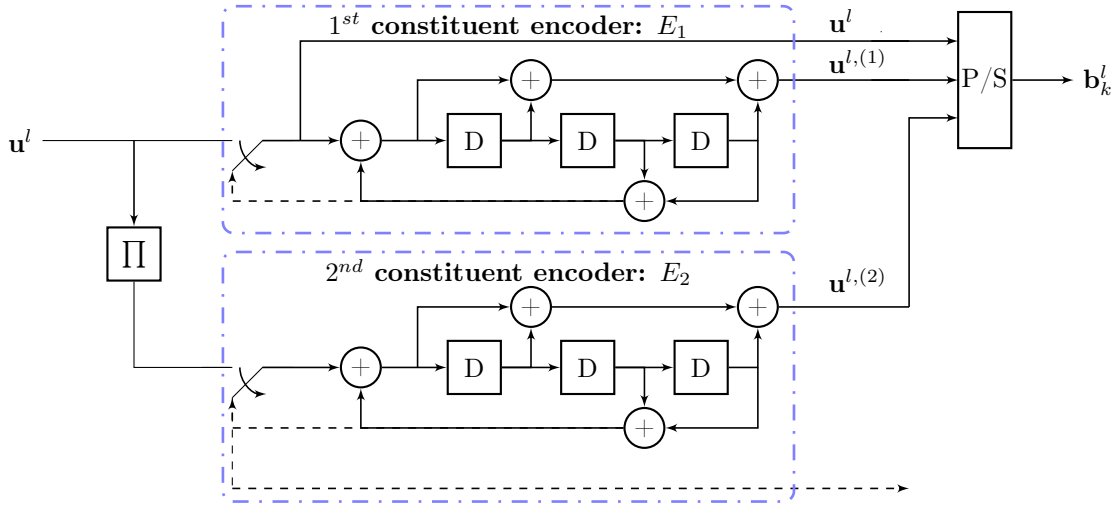

Figure 2.2: Structure of rate $\frac{1}{3}$ turbo encoder (dotted lines apply for treillis termination only).

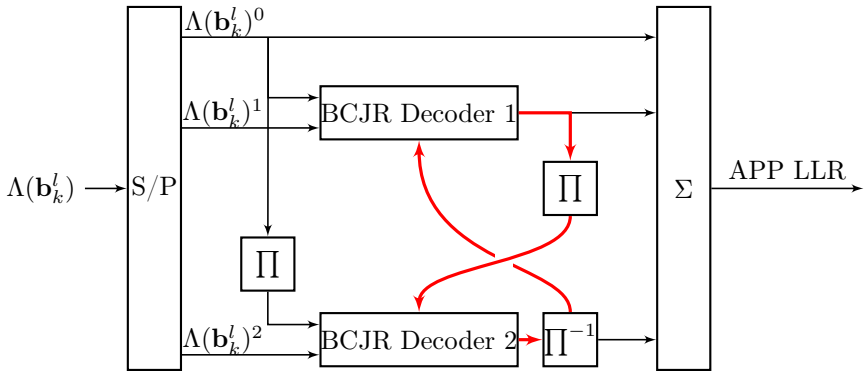

Figure 2.3: Structure of iterative turbo decoder (thick lines describe the iterative procedure).

decoder point of view, a close-to-zero reliability corresponds to an unreliable bit.
While a hard-decoder provides an estimation of the transmitted symbol by making decision with a memoryless slicer, a soft-decoder proceeds differently. In particular, it makes decisions over a range of intermediate values, thus considering the reliability of each input that the slicer would waste in the uncoded case. Consequently, a soft-decision decoder performs better in the presence of corrupted data than its hard-decision counterpart. The difference from a performance point of view is denoted as coding gain.
The optimal decoder for turbo codes would ideally be the Maximum A Posteriori (MAP) decoder. However the number of states in the trellis of a turbo code is large due to the length of the interleaver, thus making an optimal decoding infeasible for significant block sizes. Consequently, the interest of iterative decoding arises [Ber93] and relies on a - suboptimal - separate while cooperative decoding. This key point is depicted in Figure 2.3.

In Figure 2.3, the vector observation at the channel's output $\Lambda(\mathbf{b}_k^l) = [\Lambda(\mathbf{b}_k^l)^0, \Lambda(\mathbf{b}_k^l)^1, \Lambda(\mathbf{b}_k^l)^2]$ [Bar03c] is turbo decoded. In particular, the receiver iterates between two low-complexity *A Posteriori Probability* (APP) convolutional decoders - BCJR Decoders 1 and 2 in the present work -, by first ignoring $\Lambda(\mathbf{b}_k^l)^2$. The APP decoder simultaneously generates an APP LLR value for each

information bit and extrinsic LLRs for each information (see Section 4.1.1), which subsequently feed the other decoder as a priori information after suitable (de)interleaving [Ses09]. Thus, the two decoders cooperate by iteratively exchanging the extrinsic information via the (de)interleaver. Finally, the APP LLR estimates are obtained by adding both the systematic and extrinsic LLRs.

At each iteration within the decoder, the detection belief of the decoded bit increases. After an efficient number of iterations - typically 10-20 [Cos98, Bar03c] and 10 in the present work -, the APP LLR output can be used to obtain final hard decision estimates of the information bits.

2.3 Orthogonal Frequency-Division Multiplexing

The main interest in the use of multi-carrier techniques lies in the aforementioned multipath propagation nature of wireless transmissions, and in particular the channel impulse response length L. We consider a trivial communication system. It is defined by the sequences $\mathbf{x}[k]$, $\mathbf{h}[k]$ and $\mathbf{n}[k]$ of the sampled transmitted signal, the channel impulse response and the AWGN, respectively. We denote T_U as the symbol duration. At the rate of $1/T_U$, the received signal reads:

$$y[k] = \sum_{\tau=0}^{L-1} h[\tau]x[k-\tau] + n[k] = h[0]x[k] + \underbrace{\sum_{\tau=1}^{L-1} h[\tau]x[k-\tau]}_{\text{ISI}} + n[k]. \tag{2.23}$$

Equation (2.23) exhibits the point that the generated Inter-Symbol Interference (ISI) grows up with L, given a sampling rate of $1/T_U$. This aspect would require a complex equalization procedure, namely a computational complexity of $\mathcal{O}\left(L^2\right)$.

As presented in [Ses09, Wan00], multi-carrier communication systems were first introduced in the 1960s [Cha66, Sal67], with the first OFDM - that is a special case of multi-carrier transmission - patent being filed at Bell Labs in 1966. Initially, only analogue design was proposed [Wan00], using banks of sinusoidal signal generators and demodulators to process the signal for the multiple sub-channels. In 1971, the Discrete Fourier Transform (DFT) was proposed in [Wei71], which made OFDM implementation cost-effective.

The typical block diagrams of an OFDM system are depicted in Figures 2.4 and 2.5.

At the OFDM transmitter pictured in Figure 2.4, a serial stream of binary signals is first demultiplexed - through a Serial to Parallel (S/P) converter - into parallel streams $\mathbf{b}_k$. Subsequently, each parallel data stream is independently - by assuming that feedback informations are available - QAM-modulated, as stated by ξ_0, ξ_1, ξ_{N-2} and ξ_{N-1} blocks in Figure 2.4. The sub-channel gain may differ between sub-carriers, which induces different carried data-rates. As a result, the frequency-domain complex symbols vector $\mathbf{X}_k$ is produced, where the subscript k is the index of an OFDM symbol. An Inverse Fast Fourier Transform (IFFT)-based schemes is computed on each set of symbols, which results in a set of N time-domain complex samples $\mathbf{x}_k$.
In practical systems, the number of processed sub-carriers N - namely the FFT/IFFT sizes - is greater than the number of modulated sub-carriers N_U - namely the number of useful sub-carriers -, *i.e.*:

$$N \geq N_U, \tag{2.24}$$

with the unmodulated sub-carriers being padded with zeros [Ses09].
The Cyclic Prefix (CP) - of size G - adding is also depicted. The output of the IFFT is then

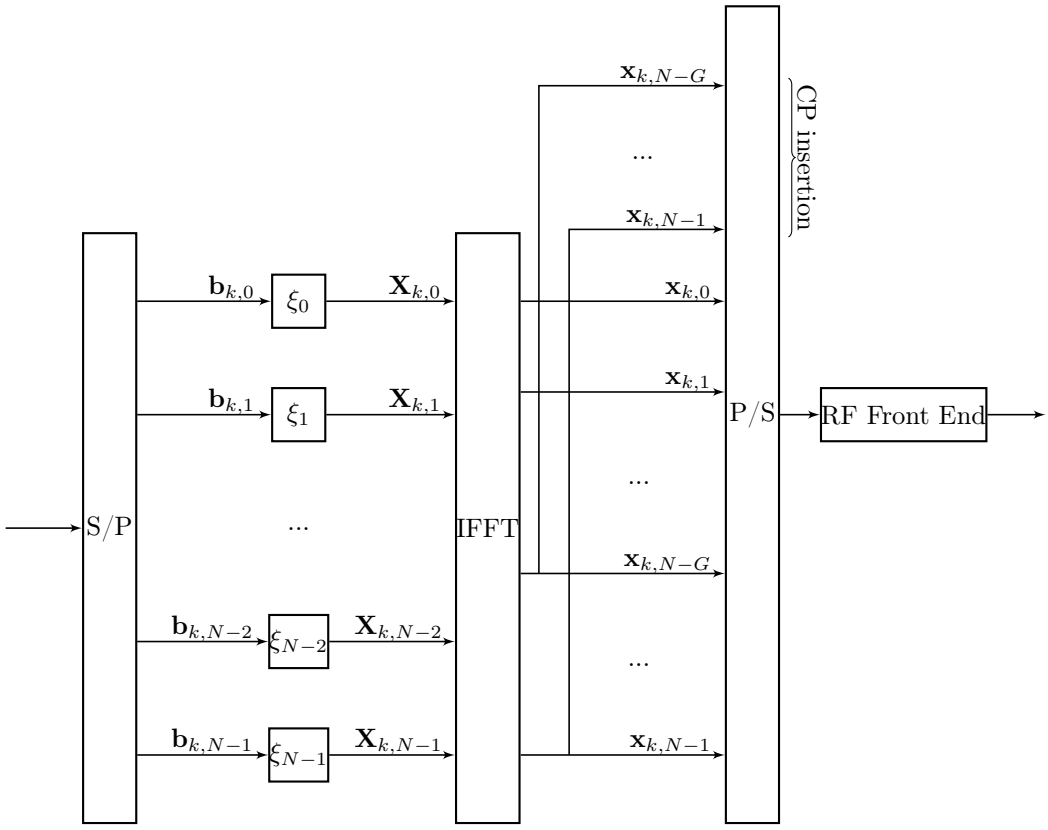

Figure 2.4: OFDM transmitter.

Parallel-to-Serial (P/S) converted for transmission through the frequency-selective channel. Finally, the signal is converted to a baseband signal through a Digital-to-Analog Converter (DAC). This step is came down to a Radio Frequency (RF) front end block in the figure.

At the OFDM receiver pictured in Figure 2.5, the reverse operations are performed to demodulate the OFDM signal. Assuming that time and frequency synchronization are achieved, the baseband signals are then sampled and digitised using an Analog-to-Digital Converter (ADC) that performs the reverse operation of a DAC. This step is came down to a RF front end block in the figure. A number of samples G corresponding to the length of the CP are removed, such that only an ISI-free block of samples is passed to the DFT. Among the N parallel streams output from the Fast Fourier Transform (FFT), the modulated subset of N sub-carriers is selected and further processed by the receiver. This returns N parallel streams. Each of them is converted to a binary stream using an appropriate symbol detector, symbolized by ξ_0^{-1}, ξ_1^{-1}, ξ_{N-2}^{-1} and ξ_{N-1}^{-1} blocks in Figure 2.5.

In order to achieve a full ISI removal, G must be at least equal to L. The drawback of this solution lies in the induced loss of spectral efficiency.
It could be demonstrated, through the introduction of the unitary DFT matrix:

$$\mathbf{F} = \frac{1}{\sqrt{N}} e^{-\frac{j2\pi}{N}(km)},\ 0 \leq k, m \leq N-1, \tag{2.25}$$

that the circular convolution is transformed by means of an FFT into a multiplicative operation in the frequency domain [Ses09, Ben02]. Hence, the transmitted signal over a frequency selective channel is converted into a transmission over N parallel flat-fading channels in the frequency

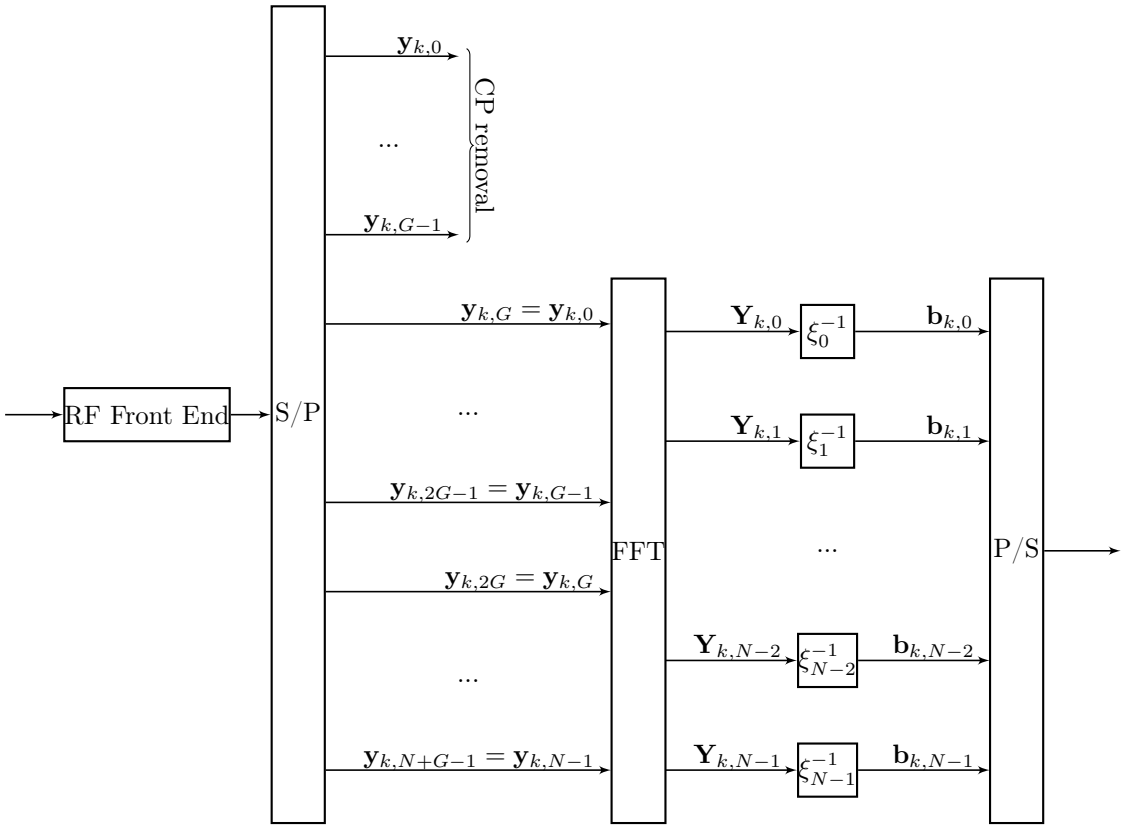

Figure 2.5: OFDM receiver.

domain:

$$\begin{bmatrix} \mathbf{y}_{k,0} \\ \mathbf{y}_{k,1} \\ \vdots \\ \mathbf{y}_{k,N-1} \end{bmatrix} = \begin{bmatrix} \mathbf{x}_{k,0} & 0 & \cdots & 0 \\ 0 & \mathbf{x}_{k,1} & & \\ & & \ddots & 0 \\ 0 & \cdots & 0 & \mathbf{x}_{k,N-1} \end{bmatrix} \begin{bmatrix} \mathbf{H}_{k,0} \\ \mathbf{H}_{k,1} \\ \vdots \\ \mathbf{H}_{k,N-1} \end{bmatrix} + \begin{bmatrix} \mathbf{n}_{k,0} \\ \mathbf{n}_{k,1} \\ \vdots \\ \mathbf{n}_{k,N-1} \end{bmatrix}. \tag{2.26}$$

Consequently, the channel filter convolution becomes one complex multiplication per sub-carrier, thus leading to a simplified (sub-carrier by sub-carrier) equalization scheme. This consideration is made under the assumption that the time-varying channel impulse response remains roughly constant during the transmission of each modulated OFDM symbol, which induces system impairments in the case of extreme fading conditions.

The OFDM scheme is sensitive to Doppler shifting, which leads time synchronisation errors and subsequently a loss of orthogonality of its sub-carriers. Also, high Peak-to-Average-Power Ratio (PAPR) [Han04, Ses09] arises. It is due to constructive and destructive combinations of independent sub-carriers and leads to increased non-linear distortions. Nevertheless, induced advantages are numerous.
One of the major advantages in the OFDM implementation lies in the introduction of the DFT [Wei71] that induces the use of the low-complexity FFT/IFFT [Bur91]. We recall that the FFT/IFFT order is N. In particular, it is required to be a power of two and again $N \geq N_U$.
While it induces high sensitivity to time synchronization errors, the orthogonality of sub-carriers - despite their overlapping spectra through cardinal sinus properties (0 values at each $1/T_U$) - avoids the need to separate the carriers by means of guard-bands. Therefore, OFDM is spectrally

highly efficient.
In OFDM, the high-rate stream of data symbols is actually converted into a low-rate stream of data symbols. The resulting increased QAM symbol duration - by a factor of approximately N - is such that it becomes significantly longer than the channel impulse response length. Thus, ISI are drastically reduced. Consequently, the OFDM modulation scheme has been shown to be particularly convenient in the multi-path environment where ISI are induced by the channel time characteristics (see Section 2.6). In addition and for complete ISI elimination, a guard period is introduced. It consists in adding a CP by duplicating the last G samples of the IFFT output and appending them at the beginning of $\mathbf{x}$, which has been shown to change the linear convolution into a circular one [Wan00].
An additional advantage makes the OFDM suitable for LTE(-A) requirements. The parametrization allows the system designer to balance tolerance of Doppler and delay spread depending on the deployment scenario [Ses09]. In particular, the sub-channel gain may differ between sub-carriers, thus inducing different carried data-rates. Therefore and based on feedback informations: modulation, channel coding and power allocation are advantageously applied independently to each sub-carrier.
Finally and while MU is not considered in the present work, it should be noted that a multiple-access scheme is achieved in a straightforward manner by assigning different OFDM sub-channels to different users. It is denoted as Orthogonal Frequency-Division Multiple-Access (OFDMA), the latter being used - among others - in the LTE(-A).
These factors together have made OFDM a choice technology for the LTE(-A) (among others) downlink.

2.4 MIMO Schemes

2.4.1 Array Gain

By assuming the Channel State Information (CSI) availability at the transmitter with sufficient quality - namely in low mobility scenarii -, a convenient eigen-mode of the channel can be addressed, thus resulting in the concentration of energy in one or more directions [God97]. Consequently, the general idea of beamforming lies in leading to a well defined directional pattern. Its approach is similar in multiple antennas receivers except that the transmit beamforming cannot simultaneously maximize the signal level at all of the received antennas [Fos98].
That is why in the MIMO case, the precoding aims at minimizing the transmit power necessary for achieving the transmission at a given data rate. It can be considered as a multi-stream beamforming, which is made possible through constructive addition of the transmitted signals at different antennas. Again, the CSI must be known at the transmitter, with all well-known associated issues. Such a scheme advantageously catches a large part of the detector's computational complexity since it makes the receiver perceive almost independent parallel streams. Since the Inter-Layer Interferences (ILI) are mainly reduced, low-complexity classical detection schemes are efficient.
When taken to extremes, a Singular Value Decomposition (SVD) of the channel matrix can be processed in order to transmit data into the eigen-modes of the channel [Ral98]. Such a scheme is denoted SVD-MIMO and allows - in an ideal manner - the transmit signal separation into parallel streams.
Also and although it is out of our scope, array gain allows multiple User Equipments (UE) - located in different directions - to be served simultaneously [Ses09] (so-called Multiple-User-MIMO (MU-MIMO)), which is denoted as Space-Division Multiple Access (SDMA).

2.4.2 Diversity Gain

As a complementary point of view to both the time and frequency diversities, the spatial diversity can be offered by multi-antenna techniques thus improving the transmission robustness against fading. In such a scheme, there is no increase of the spectral efficiency compared to the SISO case. With no CSI knowledge at the transmitter, the channel is made to be fully orthogonal - or near orthogonal, according to the number of antennas - through the use of Space-Time Block Codes (STBC) [Ala98], thus making low-complexity classical detection schemes efficient. In each STBC block, some data is transmitted over a certain time interval, which corresponds to a certain code rate. During this time interval, the channel is considered to be constant, which is a strong constraint in extreme scenarii. Otherwise, the orthogonality of the code is not guaranteed.
In order to provide additional coding gain, Space-Time Treillis Codes (STTC) relies on Treillis coding at the transmitter [Tar98] which induces a large computational complexity.

2.4.3 Spatial Multiplexing Gain

When both time and frequency diversities are sufficient, the SM scheme increases the system's spectral efficiency by splitting a high rate signal into multiple low rate streams that are transmitted in parallel, through parallel sub-channels. These multiple streams can be transmitted to a single user on multiple spatial layers created by combinations of the available antennas. A layer ν being defined as a spatial stream, the number of SM data streams is:

$$\nu = \min\{n_R, n_T\}. \tag{2.27}$$

Spatial multiplexing can also be used for simultaneous transmission to multiple receivers, known as space-division multiple access. By scheduling receivers with different spatial signatures, good separability can be assured.
Due to the impact of symbol ordering - within the transmitted signal - on the set of sub-channel gains, a first practical Spatial Multiplexing-MIMO (SM-MIMO) scheme has been proposed and is denoted as BLAST [Fos96]. The interesting aspect is that it achieves acceptable performance while employing a sub-optimal detector. Two different scheme may be used: Diagonal-BLAST (D-BLAST) and Vertical-BLAST (V-BLAST) that will be further introduced in 2.7. None of these rely on CSI knowledge at the transmitter.
In the present work, the low complexity Bit-Interleaved Coded Modulation (BICM) [Cai98] strategy is considered. It consists in encoding, interleaving and modulating any transmitted block that is subsequently mapped onto the transmit antenna. The main object of the detector step is approaching the channel capacity with a polynomial computational complexity (see Section 2.7.3) at the receiver.

2.5 System Model Introduction and Notations

In the present work, the Single-User MIMO (SU-MIMO) assumption is considered. The presented results can be straight-forwardly extended to MU-MIMO systems with detectors that do not rely on a finite-alphabet constraint assumption (see Section 2.7.2). Otherwise, additional knowledge - such as user received energies and transmission delays - is necessary [Pro95] and properties - namely system dimensions and channel correlation [Ses09] - of encountered systems differ, thus inducing different calibrations.
Consider a n_T-transmit and n_R-receive $n_T \times n_R$ MIMO system model associated to the (k,l)-th Resource-Element (RE) in the grid-represented Resource-Block (RB) - the RB allocation will

be detailed in Section 5.1.2. By considering that the channel is flat-fading within each RE, the corresponding n_R-dimensional complex received vector $\mathbf{y}_{k,l}$ reads:

$$\mathbf{y}_{k,l} = \mathbf{H}_{k,l}\mathbf{x}_{k,l} + \mathbf{n}_{k,l}, \tag{2.28}$$

where $0 \leq k \leq 6, \quad 0 \leq l < N_U$ (see Section 2.3), and $N_U \in \{72,\ 180,\ 300,\ 600,\ 1200\}$ [3GP07]. The channel $\mathbf{H}_{k,l}$ is a $n_R \times n_T$ complex valued matrix and is assumed to be perfectly known at the receiver, unless otherwise specified. The n_R-dimensional complex vector $\mathbf{n}_{k,l}$ is an AWGN of variance $\sigma_n^2/2$ for each dimension. The entries of the transmitted symbol vector $\mathbf{x}_{k,l}$ are independently drawn from a complex constellation set ξ and such that $\mathbf{x}_{k,l}$ belongs to the set ξ^{n_T}.

Each channel input $\mathbf{b}_k^l \in \{\pm 1\}^{\log_2\{|\xi|\}}$ is assigned to a symbol according to any encoding scheme, where n is any given layer (see Section 2.4.3) and k is any bit position within the corresponding symbol. The whole symbols vector is mapped from a block of bit stream $\mathbf{c}_m$, by denoting m as the number of bits of the codeword with $1 \leq m \leq \nu \log_2\{|\xi|\}$. At this step, the uncoded or coded case is not distinguished. The block code may consider channel coding through the addition of redundancy and correlation, by introducing the code rate $R \leq 1$ - where $R = 1$ makes $\mathbf{c}$ correspond to uncoded bits -, and interleaving [Ben98]. By applying an efficient modulation and code rate scheme, the channel capacity is almost achieved at any SNR point [Ber93].

At this point, the vital aspects have been introduced and are now put together. In particular in Figure 2.6, the general structure of the considered SM-MIMO-OFDM system is depicted in a block-diagram manner. We shed light on the DownLink (DL) transmission introduced in the LTE(-A) standard [3GP07].

From a global point of view, a digital source is communicating over a MIMO channel $\mathbf{H}_{k,l}$ to a digital sink. At the transmitter, also denoted as DL encoding, parallel independent raw bit streams $\mathbf{u}^l$ are independently turbo encoded - according to what was previously defined in Section 2.2 - at a desired rate through puncturing. The resulting codewords $\mathbf{b}_k^l$ are then pseudo-interleaved, scrambled and QAM modulated, such as complex-valued constellation symbols are fed to the layer mapper block. Inside this block, the latter symbols are mapped onto one or several transmission layers. The corresponding output is then eventually precoded (see Section 5.1.3) on each layer for transmission on the antenna ports. Finally and for each antenna port, a time-domain OFDM signal is generated for each antenna port, as defined beforehand in Section 2.3. The MIMO channel is modelled in accordance with the notations of Equation (2.28). At the receiver, that is also denoted as DL decoding, the inverse operations are processed. Particular attention will be paid to the Detection/Antenna mapping block since it is the object of the present work.

In a MIMO system and by assuming the aforementioned distribution of the complex channel matrix [Tel99], the ergodic channel capacity of the equivalent transmission model Equation (2.28) reads:

$$C = E\left\{\log_2 \det\left(\mathbf{I}_{n_R} + \frac{E_S}{N_0}\mathbf{H}_{k,l}\mathbf{H}_{k,l}^H\right)\right\}, \tag{2.29}$$

where the expectation is processed over the entries of $\mathbf{H}_{k,l}$ and N_0 is the noise spectral density.

For the case of i.i.d. noise at the receiver and with perfect CSI at both the transmitter and the receiver - which allow for an SVD -, the expression above rewrites [Tel99]:

$$C = \sum_{i=1}^{\nu} \log_2\left(1 + \lambda_i \frac{E_S}{N_0}\right), \tag{2.30}$$

by assuming water filling power allocation [Tse05] where λ_i are the singular values of the channel matrix. This equation clearly shows that the capacity grows linearly with the number of layers,

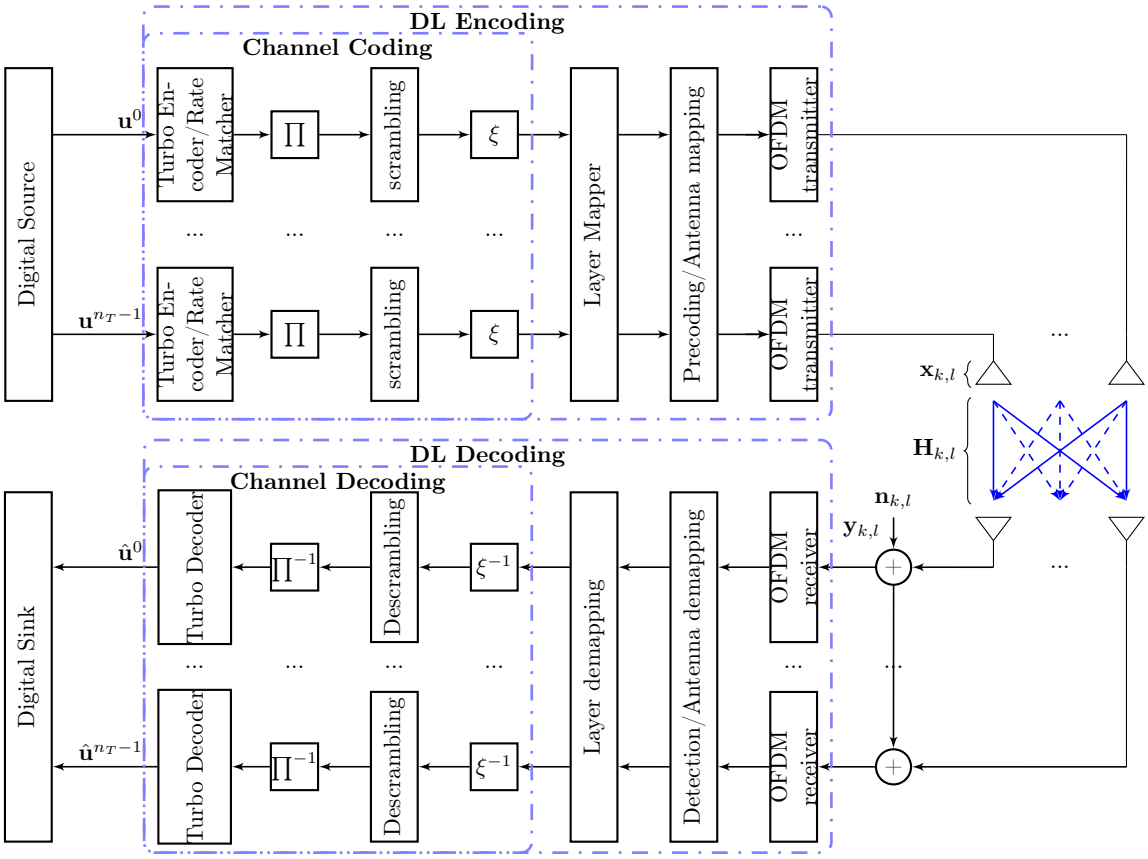

Figure 2.6: Overview of DL baseband signal, SM-MIMO-OFDM scheme.

which was claimed in Section 2.4.3.

In the MIMO case, the global SNR at the receiver is written as:

$$\text{SNR} = \frac{E_S}{N_0} = \frac{E\left\{\mathbf{x}_{k,l}^H \mathbf{H}_{k,l}^H \mathbf{H}_{k,l} \mathbf{x}_{k,l}\right\}}{E\left\{\mathbf{n}_{k,l}^H \mathbf{n}_{k,l}\right\}}. \tag{2.31}$$

In the present work, simulation results are provided in the form of BER curves as a function of the average energy per bit - denoted as E_b - to the power spectral density ratio. The ratio E_b/N_0 is useful in the comparison of the BER performance of different digital modulation schemes without taking bandwidth into account. As introduced in [Hoc03], it can be advantageously seen as a normalized measure of the SNR, thus leading - without considering the spectral efficiency loss due to channel coding - to the relation:

$$\left.\frac{E_b}{N_0}\right|_{dB} = \left.\frac{E_S}{N_0}\right|_{dB} + 10\log_{10}\frac{n_R}{n_T \log_2\{|\xi|\}}. \tag{2.32}$$

Consequently, by considering an equal number of transmit and receive antennas and since the capacity grows linearly with the number of layers, capacity for a given constellation is attained at approximatively [Hoc03] the same E_b/N_0 whatever the number of antennas.

In some scenarii, it may be advantageous to catch the benefits of the spatial diversity and of

the spatial multiplexing gain. In the rest of the manuscript and unless otherwise specified, the SM-MIMO design will be considered.

2.6 General MIMO Channel Model

Due to reflection and scattering in the environment, radio wave propagation is commonly described by a finite number of L distinct paths - that denote the arriving signal at the receiver -, in the continuation of ITU channel models [M.197]. In particular, each path approximates a cluster of paths with similar delays. Thus, $h(t,\tau)$ denotes time-varying complex baseband impulse response - at time instant t and delay τ - for the radio channel and may be written as the well-known tapped-delay line model [3GP09a]:

$$h(t,\tau) = \sum_{i=0}^{L-1} a_i(t)\,\delta(t,\tau_i), \tag{2.33}$$

where a_i and $\delta(\cdot)$ denote any path amplitude and the delta function, respectively. Due to scattering of each wave in the vicinity of a moving mobile, each path approximates the superposition of a large number of scattered waves with approximately the same delay. Paths of similar amplitudes interfere constructively and destructively, thus inducing frequency fading.
The channel coherence bandwidth B_C denotes the minimum frequency separation required for a sufficient change in the channel magnitude so that it becomes uncorrelated from its previous value. It induces a distinction between a flat-fading - the channel coherence bandwidth of the channel is larger than the signal bandwidth - and a frequency-selective fading - the coherence bandwidth of the channel is smaller. Subsequently, the level of frequency diversity depends on the ratio of the system bandwidth to the channel coherence bandwidth [Ray97]. As a rule of thumb, the 50% coherence bandwidth can be estimated from the maximum excess delay of the latest significant multi-path tap [Pro95, Yee93]:

$$B_C \propto \frac{1}{\tau_{\mathrm{RMS}}}. \tag{2.34}$$

The Wide-Sense Stationary Uncorrelated Scattering (WSSUS) channel model, introduced by Bello [Bel63] is a classical assumption for the computation of tap gains of the discrete-time representation of a slowly time-varying multipath channel experienced in mobile communications [Hoe92]. According to this, each path module $|a_i|$ is subject to time-varying fading, which is modelled by varying Rayleigh distributed amplitudes. A mobile receiver induces a Doppler spread, *i.e.* temporal correlation of the process $h(t,\tau)$. It is commonly modelled according to Jakes model-based Doppler power spectrum $S_{a_i}(f)$ [Jak74]. By introducing the maximum occurring Doppler frequency:

$$f_{d,\max} = v\frac{f_c}{c}, \tag{2.35}$$

where v, f_c and c denote the mobile speed, the carrier frequency and the propagation speed, respectively. The Doppler power spectrum reads:

$$S_{a_i}(f) = \begin{cases} \frac{1}{\pi f_{d,\max}\sqrt{1-\left(\frac{f}{f_{d,\max}}\right)^2}} & \text{for } |f| \le f_{d,\max}, \\ 0 & \text{otherwise.} \end{cases} \tag{2.36}$$

A motion at the receiver causes a Doppler shift, itself inducing time fading.
The channel coherence time T_C denotes the minimum time required for a sufficient channel magnitude change such as it becomes uncorrelated from its previous value. It induces a distinction

between slow and fast fading. Slow fading - the coherence time of the channel is large compared to the delay constraint of the channel - is when the amplitude and phase change - imposed by the channel - can be considered as roughly constant over the period of use. Fast fading - the coherence time of the channel is small relative to the delay constraint of the channel - is when the amplitude and phase vary considerably over the period of use. As a rule of thumb, the level of time diversity can be estimated by relating the OFDM symbol duration with the channel coherence time. The latter depends on the maximum occurring Doppler frequency [Ray97]:

$$T_C \propto \frac{1}{f_{d,\max}} \tag{2.37}$$

Spatial correlation arises due to spatial scattering conditions. Despite its simplicity, the correlation-based analytical Kronecker model is used in the 3GPP standard [3GP09d]. By considering the correlation between transmit antennas and between receive antennas as independent, the transmit and receive correlation matrices can be denoted $\mathbf{T}$ and $\mathbf{R}$, respectively. With this assumption, the spatially correlated channel rewrites $\mathbf{H}_{\text{corr}} = \mathbf{R}^{1/2}\mathbf{H}\mathbf{T}^{1/2}$, where $\mathbf{T}$ and $\mathbf{R}$ result in Toeplitz structure matrices and read:

$$\mathbf{T} = \begin{bmatrix} 1 & \cdots & \alpha^{l_T^2/(n_T-1)^2} \\ \vdots & \ddots & \vdots \\ (\alpha^{l_T^2/(n_T-1)^2})^* & \cdots & 1 \end{bmatrix}, \mathbf{R} = \begin{bmatrix} 1 & \cdots & \beta^{l_R^2/(n_R-1)^2} \\ \vdots & \ddots & \vdots \\ (\beta^{l_R^2/(n_R-1)^2})^* & \cdots & 1 \end{bmatrix}, \tag{2.38}$$

where $l_T = \{0, \cdots, n_T - 1\}$, $l_R = \{0, \cdots, n_R - 1\}$ and α and β represent the fading correlation between two adjacent transmit and receive antenna elements, respectively, averaged over all possible orientations of the two antennas in a given wave-field [Dur99]. This simplistic model (only a single coefficient per transmit or receive antenna) will be further discussed in Section 5.1.1.
A strong spatial correlation will increase correlation between column-vectors in the MIMO channel matrix. Consequently, it induces ill-conditioned channel matrices. Numerous tools may be used to measure a matrix orthogonality or conditioning. In the present work, the level of space diversity depends on the *Orthogonal Deficiency* (OD) measurement [Zha07b] that reads:

$$OD\left(\mathbf{H}_{k,l}\right) = 1 - \frac{\det\left(\left(\mathbf{H}_{k,l}\right)^H \mathbf{H}_{k,l}\right)}{\prod_{j=1}^{n_T} \left\|\left(\mathbf{H}_{k,l}\right)_{:,j}\right\|^2}, \tag{2.39}$$

where $0 \leq OD\left(\mathbf{H}_{k,l}\right) \leq 1$ and $OD\left(\mathbf{H}_{k,l}\right) = 0$ iff $\mathbf{H}_{k,l}$ is a unitary matrix. Also, by defining $\sigma_{\max}\left(\mathbf{H}_{k,l}\right)$ and $\sigma_{min}\left(\mathbf{H}_{k,l}\right)$ as the maximal and minimal singular values of $\mathbf{H}_{k,l}$, the conditioning number reads:

$$\kappa\left(\mathbf{H}_{k,l}\right) = \frac{\sigma_{\max}\left(\mathbf{H}_{k,l}\right)}{\sigma_{min}\left(\mathbf{H}_{k,l}\right)}, . \tag{2.40}$$

where $\kappa\left(\mathbf{H}_{k,l}\right) \geq 1$ and $\kappa\left(\mathbf{H}_{k,l}\right) = 1$ if $\mathbf{H}_{k,l}$ is a unitary matrix. According to the MIMO system capacity definition introduced in Section 2.5, it is obvious that it is solely the spatial correlation characteristics of the MIMO channel $\mathbf{H}_{k,l}$ that determine the theoretical capacity as a function of the SNR.

2.7 Detection Problematic and Background

From the receiver point of view, the general detection problematic can be summarized as how to separate the transmitted symbols, while taking into consideration that they appear as a linear superposition of separately transmitted streams.

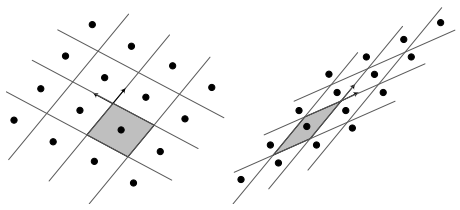

(a) (b)

Figure 2.7: Example of 2-dimensional real lattices with orthogonal bases (a) and correlated bases (b).

The quality of any detector is determined by its ability in recovering the transmitted symbols while approaching the channel capacity [Ber93], which corresponds to an inverse problem with a finite-alphabet constraint [Lar09]. This the case for the Maximum-Likelihood Detector (MLD).

2.7.1 Maximum Likelihood

For the sake of readability, the system model introduced in Equation (2.28) is re-defined as following:

$$\mathbf{y} = \mathbf{H}\mathbf{x} + \mathbf{n}, \tag{2.41}$$

from this chapter to Chapter 4 and otherwise specified.
Working on the transmitted vector $\mathbf{x}$, $\mathbf{H}$ generates the complex lattice:

$$\mathcal{L}(\mathbf{H}) = \{\mathbf{z} = \mathbf{H}\mathbf{x} | \mathbf{x} \in \xi^{n_T}\} = \{\mathbf{x}_1\mathbf{H}_{1,:} + \mathbf{x}_2\mathbf{H}_{2,:} + \cdots + \mathbf{x}_{n_T}\mathbf{H}_{n_T,:} | \mathbf{x}_k \in \xi\}, \tag{2.42}$$

where the columns of $\mathbf{H}$, $\{\mathbf{H}_{:,1}, \mathbf{H}_{:,2}, \cdots, \mathbf{H}_{:,n_T}\}$, are known as the basis vectors of the lattice $\mathcal{L} \in \mathbb{C}^{n_R}$ [Lov86]. Also, n_T and n_R refer to the *rank* and *dimension* of the lattice $\mathcal{L}$, respectively, and the lattice is said to be *full-rank* if $n_T = n_R$.

Figure 2.7(a) shows an example of a 2-dimensional real lattice whose basis vectors are $\mathbf{H}_{:,1} = [0.39 \;\; 0.59]^T$ and $\mathbf{H}_{:,2} = [-0.59 \;\; 0.39]^T$, and Figure 2.7(b) shows another example of a lattice with basis vectors $\mathbf{H}_{:,1} = [0.39 \;\; 0.60]^T$ and $\mathbf{H}_{:,2} = [0.50 \;\; 0.30]^T$. The elements of the transmitted vector $\mathbf{x}$ are drawn independently from the real constellation set $\{-3, -1, 1, 3\}$. The OD of the lattices depicted in Figure 2.7(a) and Figure 2.7(b) are 1 and 2.28, respectively. This indicates that the first set of basis vectors is perfectly orthogonal while the second set is correlated, which implies ILIs and induces among others the advantage of joint detectors. The form of the resulting Voronoi regions of the different lattice points - an example is indicated in gray in Figure 2.7 - also indicates the orthogonality of the basis; when the basis vectors are orthogonal with equal norms, the resulting Voronoi regions are squares, otherwise different shapes are obtained.
In light of the above and from a geometrical point of view, the signal detection problem is defined as finding the lattice point $\hat{\mathbf{z}} = \mathbf{H}\hat{\mathbf{x}}$, such that $\|\mathbf{y} - \hat{\mathbf{z}}\|^2$ is minimized, where $\|\cdot\|$ is the Euclidean norm and $\hat{\mathbf{x}}$ is the estimate of the transmitted vector $\mathbf{x}$.

The optimum detector for the transmit vector estimation is the well-known MLD [Van76]. MLD employs a brute-force search to find the vector $\mathbf{x}_k$ such that the a-posteriori probability $P\{\mathbf{x}_k \,|\, \mathbf{y}\}$, $k \in [\![1; |\xi|^{n_T}]\!]$, is maximized; that is:

$$\hat{\mathbf{x}}_{\text{ML}} = \underset{\mathbf{x} \in \xi^{n_T}}{\arg\max} \{P\{\mathbf{x}_k | \mathbf{y}\}\}. \tag{2.43}$$

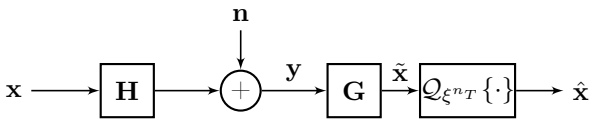

Figure 2.8: Block diagram of the linear detection algorithms.

After some basic probability manipulations and by assuming equally likely symbols, the optimization problem in Equation (2.43) is reduced to:

$$\hat{\mathbf{x}}_{\mathrm{ML}} = \underset{\mathbf{x}\in\xi^{n_T}}{\arg\max} \left\{ p\left(\mathbf{y}|\mathbf{x}_k\right) \right\}, \tag{2.44}$$

where $p\left(\mathbf{y}|\mathbf{x}_k\right)$ is the probability density function of $\mathbf{y}$ given $\mathbf{x}_k$. By assuming that the elements of the noise vector $\mathbf{n}$ are i.i.d. and follow Gaussian distribution, the noise covariance matrix becomes $\Sigma_n = \sigma_n^2 \mathbf{I}_{n_R}$. As a consequence, the received vector is modelled as a multivariate Gaussian random variable whose mean is $\mathbf{H}\mathbf{x}_k$ and covariance matrix is Σ_n. The optimization problem in Equation (2.44) thus rewrites as follows:

$$\hat{\mathbf{x}}_{\mathrm{ML}} = \underset{\mathbf{x}\in\xi^{n_T}}{\arg\max} \left\{ \frac{1}{\pi^{n_R} \det\left(\Sigma_n\right)} \exp^{-(\mathbf{y}-\mathbf{H}\mathbf{x}_k)^H \Sigma_n^{-1} (\mathbf{y}-\mathbf{H}\mathbf{x}_k)} \right\} = \underset{\mathbf{x}\in\xi^{n_T}}{\arg\min} \left\{ \left\|\mathbf{y}-\mathbf{H}\mathbf{x}_k\right\|^2 \right\}. \tag{2.45}$$

This result coincides with the conjuncture based on the lattice theory given above in this section.

By focusing on hard-decision detection, the MLD offers optimal performance.
However and for mobile communications systems that are computationally and latency limited, MLD is infeasible. More details are provided in Section 2.7.3.

Differently to MLD, Linear Detectors (LD) do not consider the finite-alphabet constraint [Lar09].

2.7.2 Linear Detection

The idea behind LD schemes is to treat the received vector by a filtering matrix $\mathbf{G}$, constructed using a performance-based criterion, as depicted in Figure 2.8 [Pau03, Win04, Sch06]. The well-known Zero-Forcing (ZF) and Minimum-Mean Square Error (MMSE) performance criteria are considered in the Linear ZF (LZF) and Linear MMSE (LMMSE) detectors.

LZF detector treats the received vector by the pseudo-inverse of the channel matrix, resulting in the full cancellation of interference with coloured noise. The detector in matrix form is given by:

$$\mathbf{G}_{\mathrm{ZF}} = \left(\mathbf{H}^H\mathbf{H}\right)^{-1}\mathbf{H}^H = \mathbf{H}^{\dagger}, \tag{2.46}$$

where $(\cdot)^H$ is the Hermitian transpose and $(\cdot)^{\dagger}$ the pseudo-inverse.
Figure 2.9 depicts a geometrical representation of the LZF detector. Geometrically, to obtain the k-th detector's output, the received vector is processed as follows:

$$\tilde{\mathbf{x}}_k = \mathbf{G}_{k,:}\mathbf{y} = \frac{\left((\mathbf{H}_{:,k})^{\perp}\right)^H}{\left\|(\mathbf{H}_{:,k})^{\perp}\right\|^2}\mathbf{y} = \mathbf{x}_k + \mu_k, \tag{2.47}$$

where $\mathbf{G}_{k,:}$ is the k-th row of $\mathbf{G}$, $(\mathbf{H}_{:,k})^{\perp}$ is the perpendicular component of $\mathbf{H}_{:,k}$ on the interference space, and μ_k equals $\mathbf{G}_{k,:}\mathbf{n}$. Note that $(\mathbf{H}_{:,k})^{\perp}$ equals $\left(\mathbf{H}_{:,k} - (\mathbf{H}_{k,:})^{||}\right)$, where $(\mathbf{H}_{:,k})^{||}$ is the parallel component of $\mathbf{H}_{:,k}$ to the interference subspace. Then, the mean and variance of the

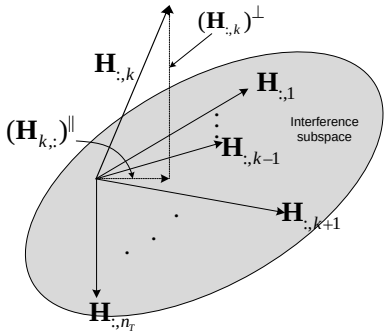

Figure 2.9: Geometrical representation of the linear ZF detection algorithm.

noise μ_k at the output of the LZF detector are 0 and $\|\mathbf{G}_{k,:}\|^2 \sigma_n^2$, respectively. When the channel matrix is ill-conditioned, *e.g.* if a couple of more of columns of the channel matrix are correlated, $(\mathbf{H}_{:,k})^{||}$ becomes large, and the noise is consequently amplified. To alleviate the noise enhancement problem induced by the ZF equalization, LMMSE can be used. The MMSE algorithm optimally balances the residual interference and noise enhancement at the output of the detector. This is accomplished by the filtering matrix $\mathbf{G}_{\text{MMSE}}$ given by:

$$\mathbf{G}_{\text{MMSE}} = \arg\min_{\mathbf{G}} \left\{ \text{E}\left\{ \|\mathbf{G}\mathbf{y} - \mathbf{x}\|^2 \right\} \right\}. \tag{2.48}$$

Due to the orthogonality between the received vector and the error vector given in Equation (2.48), we have:

$$\text{E}\left\{ (\mathbf{G}_{\text{MMSE}}\mathbf{y} - \mathbf{x})\, \mathbf{y}^H \right\} = \mathbf{0}, \tag{2.49}$$

and by extending the left side of Equation (2.49), it directly follows that:

$$\mathbf{G}_{\text{MMSE}} = \left(\Phi_{\mathbf{xx}}^{-1} + \mathbf{H}^H \Phi_{\mathbf{nn}}^{-1} \mathbf{H}\right)^{-1} \mathbf{H}^H \Phi_{\mathbf{nn}}^{-1} = \left(\mathbf{H}^H\mathbf{H} + \frac{\sigma_n^2}{\sigma_x^2}\mathbf{I}_{n_T}\right)^{-1} \mathbf{H}^H, \tag{2.50}$$

where $\Phi_{\mathbf{nn}} = \sigma_n^2 \mathbf{I}_{n_R}$ and $\Phi_{\mathbf{xx}} = \sigma_x^2 \mathbf{I}_{n_T}$ and denote the covariance matrices of the noise and the transmitted vectors, respectively. Theoretically and at high SNR, the LMMSE optimum filtering converges to the LZF solution. However, Mohaisen *et al.* show in [Moh09b] that the improvement by the LMMSE detector over the LZF detector is not only dependent on the plain value of the noise variance, but also on how close σ_n^2 is to the singular values of the channel matrix. They proved that the ratio between the condition number of the filtering matrices of the linear MMSE and ZF detectors is approximated as follows:

$$\frac{\kappa(\mathbf{G}_{\text{MMSE}})}{\kappa(\mathbf{G}_{\text{ZF}})} \approx \frac{1 + \frac{\sigma_n^2}{\sigma_{\max}^2(\mathbf{H})}}{1 + \frac{\sigma_n^2}{\sigma_{\min}^2(\mathbf{H})}}, \tag{2.51}$$

where $\sigma_{\min}(\mathbf{H})$ and $\sigma_{\max}(\mathbf{H})$ are the minimal and maximal singular values of the channel matrix $\mathbf{H}$, which is different from the noise variance σ_n^2.

Figure 2.10 shows the uncoded BER of the LDs in a 4×4 SM-MIMO-Single Carrier (SC) system, using 4-QAM signalling. Although the BER performance of LMMSE is close to that of MLD for

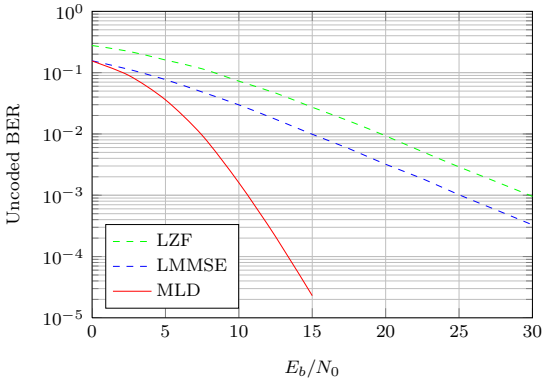

Figure 2.10: Uncoded BER as a function of E_b/N_0, Complex Rayleigh 4×4 SM-MIMO-SC system, LZF, LMMSE and ML detectors, 4-QAM modulations at each layer.

low E_b/N_0 values, the error rate curves of the two linear detection algorithms have a slope of -1, *viz.* diversity order equals one, whereas the diversity order of the MLD equals $n_R = 4$. Thus LDs lead to poor performance.

The advantage of one receiver compared to others comes from the - meticulous - study of its cost while meeting specific requirements, *e.g.* the achievable throughput. Since the concept of algorithm complexity plays a leading role in the present work, a clear introduction of the used definitions and notations is necessary.

2.7.3 Computational Complexity Assumptions

The $\mathcal{O}\{\cdot\}$ notation is widely used in the analysis of algorithms to describe an algorithm's usage of computational resources as a function of the length of its input. By designated $f(n)$ and $g(n)$ as two functions defined on some subset of the real numbers, its formal definition reads:

$$f(n) \underset{n\to a}{=} \mathcal{O}\{g(n)\} \Leftrightarrow \frac{f(n)}{g(n)} \underset{n\to a}{\to} c \in \mathbb{R}, \tag{2.52}$$

where a is any real number.
The *polynomial complexity* class is denoted as the set of algorithms such that their complexity is $\mathcal{O}\left(n^k\right)$ and varies with n, with k being real constant.
The *exponential complexity* class is denoted as the set of algorithms such that their complexity is $\mathcal{O}\left(k^n\right)$ and varies with n.
The *NP-hard* class is denoted as the set of algorithms such that their complexities are not deterministic and lead to an exponential complexity in the worst-case, while a given solution can be checked for correctness in a polynomial time.

The *Computational Complexity* is denoted as the cost of an algorithm which is widely used to measure the efficiency of the algorithm.
The cost of an algorithm is the product of the execution time - *i.e. time complexity* - and the number of processors employed. In [Li 99], the problem of time/processor complexity is summarized and its issues highlighted. We consider the useful example of matrix multiplication of size n. The corresponding total computational complexity can be summarized as follow:
– in $\mathcal{O}(n^3)$ time complexity by using 1 processor;

– in $\mathcal{O}(n^2)$ time complexity by using n processors;
– in $\mathcal{O}(n)$ time complexity by using n^2 processors;
– in $\mathcal{O}(\log n)$ time complexity by using $\mathcal{O}(n^{2.8074})$ processors [Li 98];
– in $\mathcal{O}(1)$ time complexity by using n^3 processors.

The number of parallel processors is a key factor in LTE(-A) inner receivers. To simplify the architecture and reach high computational applications, ST-Ericsson (ST-E) strategy relies on highly parallel DSP architectures allowing to operate on 16 16-bit words vectors, namely the Embedded Vector Processor (EVP) processor [van05]. Since the LTE(-A) SM-MIMO-OFDM background makes a rule to provide up to 8×8 antennas in the downlink, we consider in the present work a feasible trade-off consisting in n^2 available processors. A matrix multiplication time complexity thus becomes $\mathcal{O}(n)$.

While a number of FLoating-point OPerations (FLOP) is a common measure of the cost of computing - and in particular in the estimation of various algorithms' computational complexities -, it induces the same weight for both a real addition and square root. Thus, it sheds light on the necessity to introduce relevant computational complexity assumptions. In particular, the time complexity generally depends on a specific hardware target. The results of the present work rely on Digital Signal Processing (DSP)-oriented assumptions that are introduced below.
First and foremost, real additions ADD_{RR} are neglected since they are seen as being processed in parallel with real multiplications MUL_{RR} - this is assumed in the present work. Such a consideration is possible due to the assumption of using parallel processors. In particular, a Multiply ACcumulate (MAC) operation simultaneously performs a real addition and a real multiplication. Also and from a DSP implementation point of view, a real division DIV_{RR} is considered to be equivalent to 16 real multiplications since its trivial implementation is realized with a conditional add/subtract non-restoring division algorithm. As its name implies, the algorithm functions by adding (subtracting) the divisor to (from) the dividend. In particular, it depends on the previously generated quotient bit. Each add/subtract operation produces a new partial remainder - which will be used in the next step - over the assumed format of the 16-bit words.
Concerning the real square root $SQRT_{RR}$ weight approximation, it relies on the general principle of the normalization of the dynamic between $\frac{1}{4}$ and 1, which makes Taylor series available. For the sake of understanding, more details are provided just in the sequel through a trivial example. To estimate the square root of a number using only simple arithmetic, the Taylor series of the square root function provides a convenient method. Namely, the Taylor expansion around a^2 is given by:

$$\sqrt{a^2 + x} = \sum_{n=0}^{\infty} \frac{(-1)^n (2n)! x^n}{(1-2n)n!^2 4^n a^{2n-1}}. \tag{2.53}$$

In practice, this provides an efficient estimate of a number's square root. In particular, a 5^{th} order Taylor series is widely considered, which requires approximately 32 real multiplications.

The basic operations are summarized in Table 2.1, where $\{\cdot\}_{\mathrm{RR}}$, $\{\cdot\}_{\mathrm{RC}}$ and $\{\cdot\}_{\mathrm{CC}}$ denote real/real, real/complex and complex-complex operations, respectively.

Various receivers are presented in the present work. In accordance with the aforementioned assumptions, their computational complexities are introduced - unless otherwise specified - as a function of real multiplication equivalence. Also and for the sake of comparability, the $\mathcal{O}\{\cdot\}$ notation will only be used for discussion.

In particular and by referring to Section 2.7.1, the computational complexity of the MLD is known to be exponential in the modulation set size $|\xi|$. The computational complexity of LDs (see Section 2.7.2) is polynomial in n_T.

Complex operations	Real operations	MUL
1 ADD_{CC}	2 ADD_{RR}	0 MUL_{RR}
1 ADD_{RC}	1 ADD_{RR}	0 MUL_{RR}
1 ADD_{RR}	1 ADD_{RR}	0 MUL_{RR}
1 MUL_{CC}	4 MUL_{RR}	4 MUL_{RR}
1 MUL_{RC}	2 MUL_{RR}	2 MUL_{RR}
1 MUL_{RR}	1 MUL_{RR}	1 MUL_{RR}
1 DIV_{CC}	6 $MUL_{RR} + 2$ DIV_{RR}	38 MUL_{RR}
1 DIV_{RC}	2 DIV_{RR}	32 MUL_{RR}
1 DIV_{RR}	1 DIV_{RR}	16 MUL_{RR}
1 $SQRT_{RR}$	1 $SQRT_{RR}$	32 MUL_{RR}

Table 2.1: Computational complexities equivalences.

Neither the MLD - computationally infeasible - nor LDs - that offer poor performance - are retained for implementation. Anyway, they are considered as reference detectors in the sequel. In the following chapter, we review the conventional (sub-)optimal detection algorithms [Wan05], and analyse their advantages and inconveniences.

Chapter 3

Hard-Decision Near Maximum-Likelihood detectors

Contents

3.1 Decision-Feedback Detector

Although linear detection approaches are attractive in terms of computational complexity, they lead to degradation in BER performance due to the independent detection of $\mathbf{x}$ components.

Superior performance can be obtained if pseudo-linear approaches are employed, as in the Decision-Feedback Detection (DFD) algorithms. Their general principle relies on successive detection of symbols, where already-detected components of $\mathbf{x}$ are subtracted from the received vector. This leads to a system with less interferences. In the following two sections, we introduce two categories of DFD algorithms.

3.1.1 Vertical-Bell Labs Layered Space-Time Transmission

In V-BLAST, symbols are detected successively using the aforementioned linear detection approaches. At the end of each iteration, the already-detected component of $\mathbf{x}$ is subtracted from the received vector [Wol98, Hay05]. Also, the corresponding column of the matrix $\mathbf{H}$ is removed. When decision-feedback approach is used, error propagation becomes a challenging issue. Therefore, the order in which symbols are detected has a great impact on the system performance.
The idea behind the ZF-based V-BLAST (ZF-VB) algorithm is to detect first the components of $\mathbf{x}$ that suffer the least noise amplification. For the first decision, the pseudo-inverse - *i.e.* $\mathbf{G}$ equals $\mathbf{H}^{\dagger}$ (see Equation 2.46) - of the matrix $\mathbf{H}$ is obtained. By assuming that the noise components are i.i.d. and that noise is independent of $\mathbf{x}$, then the row of $\mathbf{G}$ with the least Euclidean norm corresponds to the required component of $\mathbf{x}$. That is:

$$k_1 = \arg\min_j \left(\|\mathbf{G}_{j,:}\|^2\right) \text{ and } \tilde{\mathbf{x}}_{k_1} = \mathbf{G}_{k_1,:}\mathbf{y}^{(1)}, \tag{3.1}$$

where $\mathbf{y}^{(1)} = \mathbf{y}$. The superscript indicates the iteration number and $\hat{\mathbf{x}}_{k_1} = \mathcal{Q}_{\xi}\left\{\tilde{\mathbf{x}}_{k_1}\right\}$ is the decision for the k_1-th component of $\mathbf{x}$, where $\mathcal{Q}_{\xi}\left\{\cdot\right\}$ is the quantification operator to the nearest constellation symbol. The interference due to the k_1-th symbol is then cancelled out as follows:

$$\mathbf{y}^{(2)} = \mathbf{y}^{(1)} - \hat{\mathbf{x}}_{k_1}\mathbf{H}_{:,k_1} \text{ and } \mathbf{H}^{(2)} = \left[\cdots, \mathbf{H}_{:,k_1-1}, \mathbf{H}_{:,k_1+1}, \cdots\right]. \tag{3.2}$$

This strategy is repeated up to the last component of $\mathbf{x}$.

In analogy with the linear detection approaches, MMSE-based V-BLAST (MMSE-VB) improves the BER performance, by alleviating the noise enhancement problem. Therefore, the filtering matrix $\mathbf{G}^{(i)}$ at the i-th iteration is given by:

$$\mathbf{G}^{(i)} = \left(\left(\mathbf{H}^{(i)}\right)^H \mathbf{H}^{(i)} + \frac{\sigma_n^2}{\sigma_x^2}\mathbf{I}_{n_T}\right)^{-1} \left(\mathbf{H}^{(i)}\right)^H, \tag{3.3}$$

rather than $\left(\mathbf{H}^{(i)}\right)^{\dagger}$ in the case of ZF-VB.

Figure 3.1 shows the uncoded BER performance of the different V-BLAST detection algorithms. In the assorted V-BLAST schemes, the symbols are detected in an ascending order - *i.e.* $\mathbf{x}_1, \mathbf{x}_2, \cdots, \mathbf{x}_{n_T}$ - without considering their noise conditions. Obviously, signal ordering leads to improvements for both the ZF-VB and MMSE-VB algorithms, and the improvement is larger in the case of the MMSE-VB algorithm. This point will be detailed in Section 3.1.3. Despite its performance advantage over ZF-VB, neither of them achieve a diversity order that is larger than 1. This indicates less error propagation in the case of MMSE-VB, compared to other V-BLAST detection algorithms.

The computational complexity of the BLAST detection algorithm - both ZF-VB and MMSE-VB - is $\mathcal{O}(n_T^4)$ [Has00], which is infeasible due to power and latency limitations of the mobile communication systems. Even though several techniques are proposed to reduce the complexity of the BLAST detection algorithm, it is still complex [Has00, Ben03, Zhu04].

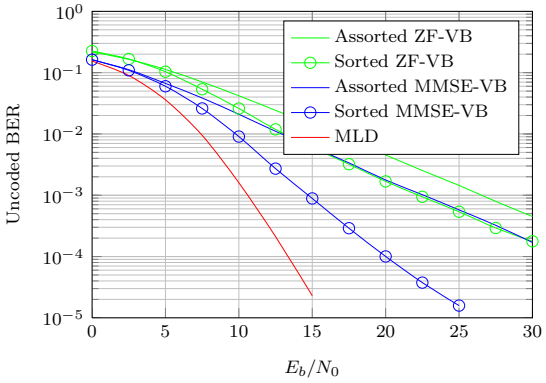

Figure 3.1: Uncoded BER as a function of E_b/N_0, Complex Rayleigh 4×4 SM-MIMO-SC system, Assorted ZF-VB, Sorted ZF-VB, Assorted MMSE-VB, Sorted MMSE-VB and ML detectors, 4-QAM modulations at each layer.

3.1.2 QR Decomposition-based Detectors

Generally, the main idea relies on splitting the detector's computational complexity into a preprocessing step - that depends on the channel only - and the detection step itself - that depends on data. That is why the preprocessing cost is not considered in the detection process since it is subject to large computational complexity reductions, due to the coherence bandwidth and to practical requirements.

The channel matrix $\mathbf{H}$ is first decomposed using the QR Decomposition (QRD) method. Hence, it is decomposed into the multiplication of a unitary matrix $\mathbf{Q} \in \mathbb{C}^{n_R \times n_T}$, *i.e.* $\mathbf{Q}$ has orthonormal columns or equivalently $\mathbf{Q}^H\mathbf{Q} = \mathbf{I}_{n_T}$, and an upper-triangular matrix $\mathbf{R} \in \mathbb{C}^{n_T \times n_T}$; that is $\mathbf{H} = \mathbf{QR}$. Then, the received symbol vector $\mathbf{y}$ is multiplied with $\mathbf{Q}^H$ prior to the symbol detection step, and Equation (2.41) - $\mathbf{y} = \mathbf{Hx} + \mathbf{n}$ - reads:

$$\mathbf{Q}^H\mathbf{y} = \mathbf{Q}^H\mathbf{QRx} + \mathbf{Q}^H\mathbf{n} = \mathbf{Rx} + \mathbf{Q}^H\mathbf{n}, \tag{3.4}$$

which rewrites:

$$\tilde{\mathbf{y}} = \mathbf{Rx} + \tilde{\mathbf{n}}, \tag{3.5}$$

where $\tilde{\mathbf{y}} = \mathbf{Q}^H\mathbf{y}$ and $\tilde{\mathbf{n}} = \mathbf{Q}^H\mathbf{n}$. The matrix $\mathbf{Q}$ is unitary, which remains the expectation and the covariance of the noise unaffected.
The matrix $\mathbf{R}$ structure being upper triangular, the transmitted symbol vector $\mathbf{x}$ could be estimated from the vector $\tilde{\mathbf{y}}$ and the matrix $\mathbf{R}$ by employing the Gauss elimination algorithm [Hig02]. In particular and due to the upper triangular structure of $\mathbf{R}$, $\tilde{\mathbf{y}}_{n_T}$ is ILI-free. Thus it is used to estimate $\hat{\mathbf{x}}_{n_T}$. By assuming correct previous decisions, the interference can be perfectly cancelled in each step.

Multiple classical QRD algorithms may be used and offer variable implementation advantages.
The Gram-Schmidt (GS) orthogonalization is frequently used in communication systems. The GS-based QRD algorithm consists of two steps, namely orthogonalization and normalization. In the orthogonalization step, a normal vector of the matrix $\mathbf{Q}$ that is already normalized (in the normalization step) is obtained and the remaining columns of $\mathbf{Q}$ are orthogonalized to the obtained column. Note that the matrix $\mathbf{Q}$ is initiated to $\mathbf{H}$. Therefore, the corresponding row of the matrix $\mathbf{R}$ is obtained from $\mathbf{Q}$ [Aub10]. The stable GS algorithm has been introduced through a minor update of the classical GS algorithm [Hig02].

The HouseHolder (HH) triangularization constitutes another classical QRD technique used to obtain the upper triangular matrix $\mathbf{R}$, from which the matrix $\mathbf{Q}$ can be obtained if required. The idea behind the HH technique is to obtain the matrix $\mathbf{R}$ using a reflection matrix. This reflection matrix, also known as Householder matrix, is used to cancel all the elements of a vector except its first element that is assigned as the norm of the vector. Therefore, the columns of the matrix $\mathbf{H}$ are treated iteratively to obtain the $\mathbf{R}$ matrix [Aub10].

The Givens Rotations (GR) can also be employed to factorize the matrix $\mathbf{H}$ [Hog07]. This technique is usually used in embedded systems because of its numerical stability [Lue07] and its well-suited implementation [Goe91]. The general principle of this technique is to cancel the elements of the matrix $\mathbf{H}$ so that a triangular form is obtained. Therefore, the GR technique is the only technique that is not iterative and, hence, has a parallelism capability that is explored in the sequel.

The Parallel Givens Rotations (PGR) technique allows independent operations in the QRD process so that the processing speed is increased [Aub10]. An example of the PGR is explained in the case of a 4×4 real matrix. The conventional GR technique obtains the following matrix:

$$\mathbf{R} = \begin{bmatrix} \mathbf{R}_{1,1} & \mathbf{R}_{1,2} & \mathbf{R}_{3,1} & \mathbf{R}_{4,1} \\ 0_1 & \mathbf{R}_{2,2} & \mathbf{R}_{3,2} & \mathbf{R}_{4,2} \\ 0_2 & 0_4 & \mathbf{R}_{3,3} & \mathbf{R}_{4,3} \\ 0_3 & 0_5 & 0_6 & \mathbf{R}_{4,4} \end{bmatrix}, \tag{3.6}$$

where the entries $\mathbf{R}_{i,j}$ represent the elements of $\mathbf{H}$ that are modified during the QRD. The notation 0_k represents the order k in which the corresponding elements of the matrix $\mathbf{H}$ are cancelled out and such that $\{\mathbf{R}_{i,j} \mid 1 \leq i \neq j \leq n_T\} \subset \mathbb{C}$ and $\{\mathbf{R}_{i,i} \mid 1 \leq i \leq n_T\} \subset \mathbb{R}$. Hence, it should be noted that 6 sequential and dependent steps are necessary for the cancellation stage of a 4×4 real matrix. Equation (3.7) illustrates the PGR technique to obtain the triangular matrix $\mathbf{R}$ from $\mathbf{H}$:

$$\mathbf{R} = \begin{bmatrix} \mathbf{R}_{1,1} & \mathbf{R}_{1,2} & \mathbf{R}_{3,1} & \mathbf{R}_{4,1} \\ 0_1 & \mathbf{R}_{2,2} & \mathbf{R}_{3,2} & \mathbf{R}_{4,2} \\ 0_2 & 0_3 & \mathbf{R}_{3,3} & \mathbf{R}_{4,3} \\ 0_3 & 0_4 & 0_5 & \mathbf{R}_{4,4} \end{bmatrix}, \tag{3.7}$$

where two elements are simultaneously cancelled at the third step due to their independence. Hence, a parallelization gain is obtained, which increases with the size of the matrix $\mathbf{H}$.

It is also shown in [Aub10] that the matrix $\mathbf{Q}$ does not need to be explicitly obtained, thus offering a significant computational complexity reduction with no performance loss. The corresponding lemma and its proof are recalled here.

Lemma 1. *Consider a modified $n_R \times (n_T+1)$ input matrix constructed as $[\mathbf{H}\ \mathbf{y}]$ and with $n_R \geq n_T$, the QRD process on first n_T rows results in a $n_T \times (n_T+1)$ triangular matrix corresponding to $[\mathbf{R}\ \tilde{\mathbf{y}}]$, with $\tilde{\mathbf{y}} = \mathbf{Q}^H\mathbf{y}$.*

Proof. Let us consider the initialization step of the QRD algorithm by introducing the $n_R \times (n_T+1)$ matrix:

$$\underline{\mathbf{Q}} = [\mathbf{H}\ \mathbf{y}] \tag{3.8}$$

and the $(n_T+1) \times (n_T+1)$ matrix:

$$\underline{\mathbf{R}} = \mathbf{I}_{n_T+1}. \tag{3.9}$$

For the sake of simplicity and without loss of generality, let us consider the common GS technique. By processing the QRD from columns 1 to n_T, the following results are obtained:

$$\underline{\mathbf{Q}} = [\mathbf{Q}\ \mathbf{y}] \text{ and } \underline{\mathbf{R}} = \left[\begin{array}{c|c} \mathbf{R} & \mathbf{0} \\ \hline \mathbf{0} & \mathbf{1} \end{array}\right]. \tag{3.10}$$

The QRD processing final step is realized at the n_T+1 column. By considering the GS technique, the $\underline{\mathbf{R}}$ coefficients are obtained with the expression $\underline{\mathbf{R}}_{i,j} = (\underline{\mathbf{Q}}_{:,i})^H \underline{\mathbf{Q}}_{:,j}$, $\forall i \in [\![1, n_T]\!]$, $\forall j \in [\![1, n_T+1]\!]$. Hence $\underline{\mathbf{R}}_{i,n_T+1} = (\underline{\mathbf{Q}}_{:,i})^H \underline{\mathbf{Q}}_{:,n_T+1} = (\underline{\mathbf{Q}}_{:,i})^H \mathbf{y}$ at this step of the algorithm process. From Equation (3.10): $\underline{\mathbf{Q}}_{:,i} = \mathbf{Q}_{:,i}$, $\forall i \in [\![1, n_T]\!]$. Consequently $\underline{\mathbf{R}}_{i,n_T+1} = \mathbf{Q}_{:,i}^H \mathbf{y}$ and $\underline{\mathbf{R}}_{1:n_T,n_T+1} = [\mathbf{R}\ \tilde{\mathbf{y}}]$. □

Lemma 1 implies the input of the detection stage - *i.e.* $\tilde{\mathbf{y}}$ and $\mathbf{R}$ - are obtained without explicitly calculating the unitary matrix $\mathbf{Q}$, thus leading to considerably reduced computational complexity as shown in [Aub10].

By assuming that $n_R = n_T = n$, the computational complexity of the aforementioned QRD algorithms is $\mathcal{O}(n^3)$ [Aub10], which is feasible in practice.

3.1.3 Layers re-Ordering

Until now, the QRD-based DFD were assumed without considering signal ordering, *i.e.* the transmitted signal was detected from the n_T-th symbol to the first one. However, this order is not unique and any detection order - among the $n_T!$ distinct possibilities - can be chosen. It can be modified by permuting elements of $\mathbf{x}$ and the corresponding columns of $\mathbf{H}$ prior to the QRD through the introduction of the - orthonormal [Boe06] - permutation matrix $\mathbf{P}$, leading to the system model being rewritten as:

$$\mathbf{y} = \mathbf{H}\mathbf{x} + \mathbf{n} = \mathbf{H}\mathbf{P}\mathbf{P}^{-1}\mathbf{x} + \mathbf{n} = \mathbf{H}_\mathrm{P}\mathbf{x}_\mathrm{P} + \mathbf{n}. \tag{3.11}$$

A well-suited ordering would combat error propagation - that induces a loss of diversity -, thus leading to a significant performance improvement. The corresponding detector is denoted as Ordered Decision-Feedback Detector (ODFD). While the brute force solution lies in evaluating $n_T!$ QRDs, this may be accomplished in a straightforward way by performing $\approx n_T^2/2$ QRDs of permutations of $\mathbf{H}$ through the myopic optimization [Fos99]. Obviously, this solution is not retained.

Wübben *et al.* propose a heuristic approach - denoted as ZF-SQRD - that only depends on the channel realization [Wue03]. While it does not ensure the optimal order and therefore the BLAST performance [Dam03], it only requires a fraction of its computational complexity [Wue01]. Assuming correct decisions in all previous detection steps and unit expected average power of the transmitted symbols, the SNR at the k-th layer (see Section 2.4.3) is given by [Boe06]:

$$SNR_k = \frac{\mathbf{R}_{k,k}}{\sigma_n^2}. \tag{3.12}$$

It is shown in [Fos99] that the minimum SNR - among all transmitted streams - is maximized by selecting the next best - the least subject to leading to incorrect estimation - layer to be detected. This criterion is also employed by the efficient ordering algorithm proposed in [Wue01], denoted as ZF-SQRD in the present work. In particular, the diagonal elements $\mathbf{R}_{k,k}^2$ are minimized in the order they are calculated during the orthogonalization process, instead of being maximized in the opposite order of detection. It is proposed in [Wue01] to find the permutation of $\mathbf{H}$ that minimizes

each $\mathbf{R}_{k,k}^2$ - with k running from 1 to n_T -, leaving all $\mathbf{R}_{1:k-1,1:k-1}$ unchanged. This minimizes the diagonal elements in every decomposition steps and thereby keeps maximal diagonal elements $\mathbf{R}_{k+1:n_T,k+1:n_T}^2$ in the following steps.

For more than two transmit antennas, this approach is no longer guaranteed to be optimal [Boe06]. In particular and since less interference needs to be suppressed by the linear MMSE filter in the first step, it may already be said that the impact of sorting is much more pronounced for MMSE-DFD [Boe06]. Thus, the efficiency of the ordering has been further improved through the extension of the ZF-SQRD to the MMSE criterion, which is proposed in [Wue03]. It is denoted as MMSE-SQRD in the present work.
By introducing the extended system model [Has00]:

$$\mathbf{H}_{\text{ext}} = \begin{bmatrix} \mathbf{H} \\ \sigma_n \mathbf{I}_{n_T} \end{bmatrix} \text{ and } \mathbf{y}_{\text{ext}} = \begin{bmatrix} \mathbf{y} \\ \mathbf{0}_{n_T} \end{bmatrix}, \tag{3.13}$$

the link with the ZF-SQRD is made obvious through the relation:

$$\mathbf{G}_{\text{ext,ZF}}\mathbf{y}_{\text{ext}} = \left(\mathbf{H}_{\text{ext}}^H \mathbf{H}_{\text{ext}}\right)^{-1} \mathbf{H}_{\text{ext}}^H \mathbf{y}_{\text{ext}} = \left(\mathbf{H}^H\mathbf{H} + \sigma_n^2 \mathbf{I}_{n_T}\right)^{-1} \mathbf{H}^H\mathbf{y} = \mathbf{G}_{\text{MMSE}}\mathbf{y}, \tag{3.14}$$

where the ZF equalization onto the extended channel matrix equals the classical MMSE equalization. By applying the ZF-SQRD onto the extended channel, it reads:

$$\mathbf{H}_{\text{ext}} = \mathbf{Q}_{\text{ext}}\mathbf{R}_{\text{ext}} = \begin{bmatrix} \mathbf{Q}_1 \\ \mathbf{Q}_2 \end{bmatrix} \mathbf{R}_{\text{ext}}, \tag{3.15}$$

where the $(n_T + n_R) \times n_T$ matrix $\mathbf{Q}_{\text{ext}}$ with orthonormal columns is partitioned into the $n_R \times n_T$ - non-orthonormal - matrix $\mathbf{Q}_1$ and the $n_T \times n_T$ upper trianguler matrix $\mathbf{Q}_2$ [Wue03].

Assuming correct decisions in all previous detection steps, the SINR of the k-th layer is given by [Boe06]:

$$SINR_k = \frac{(\mathbf{R}_{\text{ext}})_{k,k}^2}{\sigma_n^2} - 1. \tag{3.16}$$

The permutation must be chosen such that the corresponding SINR is maximized. In particular, the diagonal elements $(\mathbf{R}_{\text{ext}})_{k,k}^2$ are minimized in the order they are calculated during the orthogonalization process instead of being maximized in the opposite order of detection. In [Wue03], it is proposed to find the permutation of $\mathbf{H}$ that minimizes each $(\mathbf{R}_{\text{ext}})_{k,k}^2$ - with k running from 1 to n_T -, leaving all $(\mathbf{R}_{\text{ext}})_{1:k-1,1:k-1}$ unchanged. This minimizes the diagonal elements in every decomposition step and thereby keeps maximal diagonal elements $(\mathbf{R}_{\text{ext}})_{k+1:n_T,k+1:n_T}^2$ in the following steps.

While MMSE-SQRD offers a low-complexity solution [Wue03], the optimal ordering - thus the optimal performance - is not necessarily reached. Subsequently, the Post-Sorting-Algorithm (PSA) is introduced in [Wue03]. It ensures the optimal sorting - and therefore the BLAST performance [Dam03].
Clearly from Equations (3.13) and (3.15), the relation $\sigma_n \mathbf{I}_{n_T} = \mathbf{Q}_2\mathbf{R}_{\text{ext}}$ arises and rewrites:

$$\mathbf{R}_{\text{ext}}^{-1} = \frac{1}{\sigma_n}\mathbf{Q}_2. \tag{3.17}$$

Thus, it induces the following expression of the error covariance matrix:

$$\Phi = \sigma_n^2 \left(\mathbf{H}_{\text{ext}}^H \mathbf{H}_{\text{ext}}\right)^{-1} = \sigma_n^2 \mathbf{R}_{\text{ext}}^{-1}\mathbf{R}_{\text{ext}}^{-H} = \mathbf{Q}_2\mathbf{Q}_2^H. \tag{3.18}$$

Since $\mathbf{Q}_2$ is upper triangular, the k-th diagonal element of Φ reads:

$$\Phi_{k,k} \propto \left\| \left(\mathbf{Q}_2\right)_{k,:} \right\|^2 . \tag{3.19}$$

Consequently, if the optimum ordering has been achieved through the MMSE-SQRD, the last row of $\mathbf{Q}_2$ must necessarily have the minimum norm of all rows. Otherwise and within the considered sub-matrix, the row with the minimum norm is exchanged with the last row - as well as within $\mathbf{y}$ -, thus destroying the upper triangular structure of $\mathbf{Q}_2$. Finally, it is made triangular again through any QRD technique [Wue03, Lue07], which induce modifications of $\mathbf{Q}_1$.

The optimal ordering is given by MMSE ordering then PSA. The computational complexity of both of the QRD, the SQRD and the PSA algorithms is cubic in the number of antennas [Wue03, Bar08c]. However, the coefficient of the most significant term - w.r.t. assumptions in [Wue03] - in the PSA computational complexity is large. Consequently and due to its small performance gain [Mic05] - in particular in coded systems -, the PSA is discarded.

3.1.4 QR Decomposition-based Decision-Feedback Detector

The DFD scheme, that relies on the QRD of the channel matrix [Aub09], requires only a fraction of the computational efforts required by the V-BLAST detection algorithm [Shi99]. This is why QRD-based DFD is preferable for power and latency limited wireless communication systems. Equation (3.5) also rewrites:

$$\tilde{\mathbf{y}} = (\mathbf{D} + \mathbf{U})\,\mathbf{x} + \tilde{\mathbf{n}}, \tag{3.20}$$

where the matrix $\mathbf{D}$ is a diagonal matrix whose diagonal elements are also those of $\mathbf{R}$, and $\mathbf{U}$ is strictly an upper triangular matrix. As a consequence, the MIMO system becomes spatially causal, which implies that:

$$\mathbf{y}_k = \mathbf{R}_{k,k}\tilde{\mathbf{x}}_k + \sum_{i=k+1}^{n_T} \mathbf{R}_{k,i}\hat{\mathbf{x}}_i = \mathbf{D}_{k,k}\tilde{\mathbf{x}}_k + \sum_{i=k+1}^{n_T} \mathbf{U}_{k,i}\hat{\mathbf{x}}_i, \tag{3.21}$$

where $\tilde{\mathbf{x}}_k$ is a candidate symbol and $\hat{\mathbf{x}}_k$ is the estimate, both for the $k-$th component of $\mathbf{x}$. Therefore:

$$\hat{\mathbf{x}}_k = \mathcal{Q}_\xi \left\{ \frac{\tilde{\mathbf{y}}_k - \sum_{i=k+1}^{n_T} \mathbf{R}_{k,i}\hat{\mathbf{x}}_i}{\mathbf{R}_{k,k}} \right\} = \mathcal{Q}_\xi \left\{ \frac{\tilde{\mathbf{y}}_k - \sum_{i=k+1}^{n_T} \mathbf{U}_{k,i}\hat{\mathbf{x}}_i}{\mathbf{D}_{k,k}} \right\}, \tag{3.22}$$

where $\mathcal{Q}_\xi\{\cdot\}$ denotes the quantization operation to the nearest constellation symbol ξ.

The QRD-based detection algorithm is depicted in Figure 3.2, and is denoted as ZF-QRD DFD. Note that the feedback loop is equivalent to $(\mathbf{D} + \mathbf{U})^{-1} = \mathbf{R}^{-1}$. Due to the structure of the matrix $\mathbf{R}$, the last component of $\mathbf{x}$ - *i.e.* x_{n_T} - is ILI-free. Hence, it can be detected first. The already-detected component of $\mathbf{x}$ is cancelled out to detect the following component. This technique is repeated up to the first component of $\mathbf{x}$, *i.e.* $\mathbf{x}_1$ [Wue01, Wue03, Moh09a]. Figure 3.3 depicts the uncoded BER performance of the the QRD-based DFD algorithms. The MMSE-SQRD DFD algorithm has the best performance but its diversity order converges to unity for high E_b/N_0 values.

The computational complexity of the detection step itself - in the (S)QRD-based DFD - is square in the number of antennas. Thus, the SQRD-based scheme has much lower computational complexity than the V-BLAST algorithm and with tolerable degradation in the bit error performance. It will be considered as a basis for discussion in the present work.

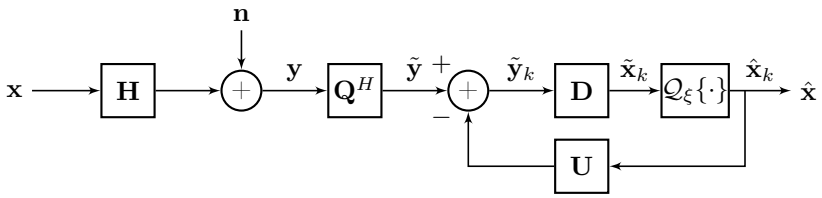

Figure 3.2: Block diagram of the QRD-based DFD algorithm.

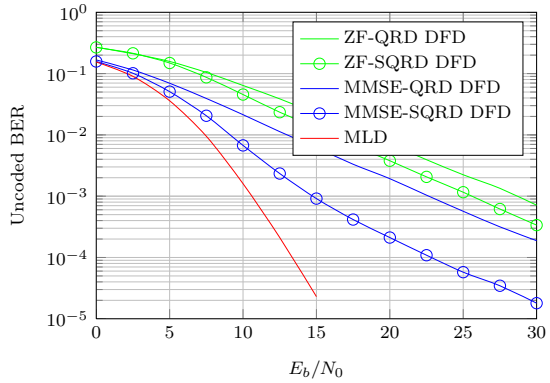

Figure 3.3: Uncoded BER as a function of E_b/N_0, Complex Rayleigh 4×4 SM-MIMO-SC system, ZF-QRD DFD, ZF-SQRD DFD, MMSE-QRD DFD, MMSE-SQRD DFD and ML detectors, 4-QAM modulations at each layer.

3.2 Sphere Decoder Techniques

Several tree-search detection algorithms that are proposed in the literature achieve quasi-ML performance while requiring lower computational complexity. In these techniques, the lattice search problem is presented as a tree where nodes represent the symbols' candidates [Agr02]. In this section, we introduce two tree-search algorithms and discuss their advantages and drawbacks.

3.2.1 Depth-First Search

The Sphere Decoder (SD) was proposed in the literature to solve several lattice search problems [Bou03]. Based on Hassibi and Vikalo analysis, the SD achieves quasi-ML performance with polynomial average computational complexity for a large range of SNR [Has01]. Hence, instead of testing all the hypotheses of the transmitted vector, the SD restricts the search in Equation (2.42) to the lattice points that lie in the hypersphere of radius d and that is implicitly centred around the unconstrained ZF estimate. Therefore by introducing the QRD:

$$\hat{\mathbf{x}}_{\text{SD}} = \underset{\mathbf{x}\in\xi^{n_T}}{\arg\min} \left\{ \|\mathbf{y} - \mathbf{H}\mathbf{x}\|^2 \leq d^2 \right\} = \underset{\mathbf{x}\in\xi^{n_T}}{\arg\min} \left\{ \|\tilde{\mathbf{y}} - \mathbf{R}\mathbf{x}\|^2 \leq d^2 \right\}. \tag{3.23}$$

The depth-first search strategy aims at considering a single node, that is then extended while the corresponding accumulated metric lies inside the sphere radius. The tree search starts at the top-level of the tree with the first child node. This node corresponds to the symbol transmitted by the n_T-th antenna. The accumulative metric in Equation (3.23) is then calculated partially and successively, where the Cumulated Euclidean Distance (CED) δ_{n_T} at the n_T-th detection level is

given by [Vik04]:

$$\delta_{n_T} = |\mathbf{y}_{n_T} - \mathbf{R}_{n_T,n_T}\tilde{\mathbf{x}}_{n_T}|^2 , \tag{3.24}$$

where $\tilde{\mathbf{x}}_{n_T}$ denotes the candidate at level n_T. The accumulative metric at the k-th detection level is given as follows:

$$\delta_k = \delta_{k+1} + \left| \tilde{\mathbf{y}}_k - \sum_{i=k+1}^{n_T} \mathbf{R}_{k,i}\hat{\mathbf{x}}_i - \mathbf{R}_{k,k}\tilde{\mathbf{x}}_k \right|^2 , \tag{3.25}$$

where $\hat{\mathbf{x}}_i$ denotes the considered estimate at previous levels. The respect of the sphere constraint by the explored symbols is then tested. The scan continues by trying the next possible symbol and progressively stepping down the tree [Aub09]. At the bottom level of the tree, the last remaining element has to be chosen and is denoted as the Babai Point (BP). Consequently, the BP is the first point found with a depth-first search SD and its formal definition is provided in [Agr02]. Actually, this solution is referred to QRD-based DFD in the communication theory [Dam03]. If $\delta_1 \leq d^2$ still holds then a complete candidate symbol vector has been found and meets the sphere constraint. Subsequently, the tree exploration continues by back-tracking to previously considered symbols and scanning in a different direction.

One important drawback in this kind of the SD algorithm - comprising the Viterbo and Boutros algorithm [Vit99] - is the choice of the initial value of the search radius. If this radius is chosen too small, there may be no solution for the algorithm (no point inside the hypersphere) and if the radius is chosen too large, the number of explored points may be very high and the algorithm will be inefficient, acting like the ML algorithm. Although there are some methods for deciding on the initial value of the radius [Has01, Hoc03], there is not yet any one method that works well in all different applications. In all algorithms that rely on a fixed radius, it is still possible that no valid point is found inside the hypersphere. In those cases, the search procedure must be repeated with a larger radius. This reiteration dramatically increases the detector latency. In fading channels, the choice of this radius is even more difficult [Vit99] because of the rapid changes in the channel condition. Thus, the initial value of this radius must be determined more frequently.

3.2.2 Symbols re-Ordering

The order in which hypotheses are tested at each detection level is defined by the employed search strategy, namely Fincke-Pohst (FP) [Fin85] or Schnorr-Euchner (SE) [Sch94]. By introducing the unconstrained ILI-free signal $\tilde{\mathbf{x}}_k$ at layer k - that corresponds to the BP after quantization to the nearest constellation symbol:

$$\tilde{\mathbf{x}}_k = \frac{\tilde{\mathbf{y}}_k - \sum_{i=k+1}^{n_T} \mathbf{R}_{k,i}\hat{\mathbf{x}}_i}{\mathbf{R}_{k,k}}, \tag{3.26}$$

the SE strategy orders the hypotheses based on their Euclidean distance from $\tilde{\mathbf{x}}_k$ at each layer; closer hypothesis being tested first. On the other hand, the FP strategy tests the hypotheses at each layer without considering the distance from $\tilde{\mathbf{x}}_k$.
Figure 3.4 shows the details of these two strategies for a 6-PAM constellation where the numbers inside the constellation points represent the order in which hypotheses are tested.

The advantage of the SE-based SD [Agr02, Dam03, Bur05, Guo06, Bar06b] over the FP-based SD [Dam00, Has01, Has05] has been widely presented. In particular, it is clear that employing the SE strategy leads to reduction in the computational complexity - which turns out to be independent of radius d - since the most probable hypothesis for any considered layer - independently of others - is tested first. This aspect is addressed in the next section.

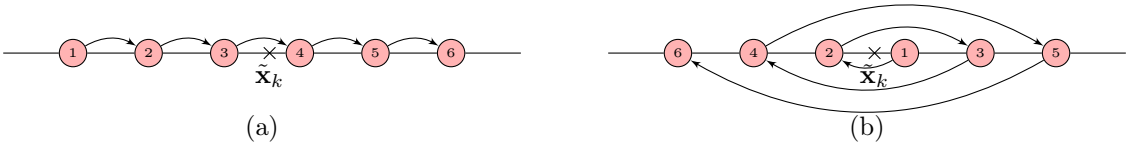

Figure 3.4: Search strategies employed by the SD, FP strategy (a) and SE strategy (b).

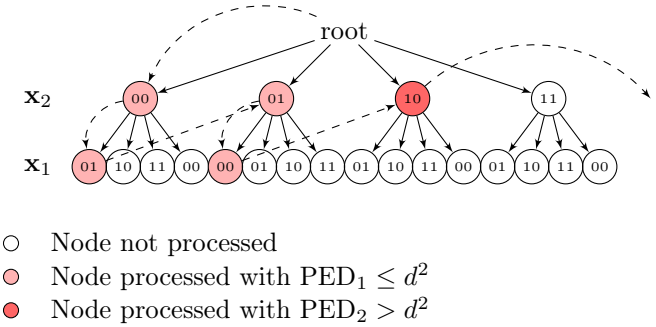

Figure 3.5: An example of the tree representation of the SD in a 2×2 system for $|\xi| = 4$ and using the SE strategy.

3.2.3 Adaptative Radius and Tree Pruning

The search optimization - for a depth-first search tree exploration - is presented and aims at decreasing the average number of visited nodes during the detection process. This step takes advantage of the degrees of freedom that are given to construct the tree.
An efficient way of solving the initial radius choice issue - discussed in Section 3.2.1 - relies on the use of an adaptative radius. Therefore, setting a proper initial radius becomes useless. At the beginning of the tree search, d^2 is initiated to infinity and the sphere constraint is shrunk through the tree exploration. In particular, it is at least updated to the accumulative metric of the first-found lattice point (the BP).
By using the SE strategy, child nodes are ordered by their Partial Euclidean Distances (PED) ascendantly. Thus, the search can be terminated as soon as a node's CED exceeds the current sphere constraint since the next ordered node at top level would exceed the last CED. They are denoted as pruned. In this way and after each iteration of the SD the search, the square radius can be tightened to exclude unnecessary nodes [Aub09], thus expediting the tree search with no performance degradation.

An example of the tree representation of the SD for $n_T = n_R = 2$ is provided in Figure 3.5, where the dashed lines represent the scanned nodes. The use of the SE enumeration method in the search phase reduces the number of visited nodes, which in turn reduces the computational complexity of the processing. The early termination condition is also pictured. The SD is terminated when no more lattice points can be obtained with an accumulative metric smaller than that of the already-found one.

3.2.4 Average and Worst-Case Computational Complexity

It could be shown that the BER performance of the SD coincides with that of the optimum detector. However, some drawbacks remain. In particular, its computational complexity is variable

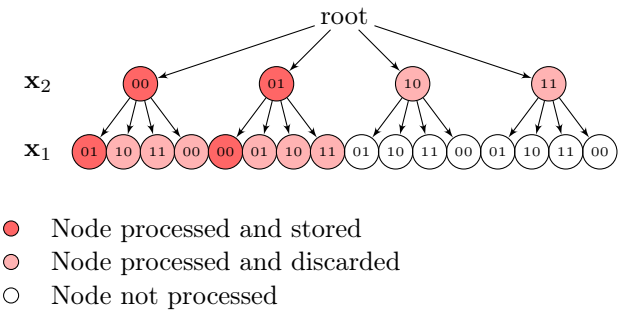

Figure 3.6: An example of the tree representation of the K-Best in a 2×2 system for $|\xi| = 4$ and using the SE strategy.

and depends on both the conditionality of the channel matrix and the noise variance, where the worst-case computational complexity of the SD is consequently comparable with that of MLD that is exponential. The worst-case complexity of the SD is therefore exponential which is infeasible in computational power limited communication systems [Dai05]. In fact, Jaldén and Otterson show in [Jal05] that even the average complexity of the SD is exponential for a fixed SNR value.
Also, the SD has a sequential nature because it requires the update of the search radius every time a new lattice point with smaller accumulative metric is found. This limits the possibility of parallel processing and hence reduces the detection throughput, *i.e.* increases the detection latency.
To set a fixed computational complexity at the detection stage and allow a parallel processing [Gra95], the K-Best algorithm - also equivalently denoted as QRD with M-algorithm [And84] - was proposed first for implementation in [Won02]. The K-Best algorithm is a general solution for implementation, and several related complexity reduction techniques are introduced in the following sections.

3.2.5 Fixed Computational Complexity

In the K-Best detection algorithm, only a fixed number K of symbol candidates is retained at each detection level [And84, Kim05]. Such a tree search strategy is denoted as a breadth first search - which is different from a metric first search - and the tree is constructed layer by layer. An example of the tree representation of the SD for $n_T = n_R = 2$ is provided in Figure 3.6. At the first detection level, the root node is extended to all the possible candidates of $\mathbf{x}_{n_T}$ - thus $\mathbf{x}_2$ -, the accumulative metrics of the resulting branches are calculated and the best K candidates with the smallest metrics are retained for the next detection level. In the example, $K = 2$. At the second detection level, the retained K candidates at the previous level are extended to all possible candidates. The resulting $K|\xi|$ - 8 in the example - branches are sorted according to their accumulative metrics where the K branches with the smallest accumulative metrics are retained for the next detection level. This strategy is repeated down to the last detection level.

By employing the K-Best algorithm, near-ML BER performance are reached for a sufficient K value, as depicted in Figure 3.7. Simultaneously, the computational complexity of the detection algorithm becomes fixed and dependent only on the size of the modulation set $|\xi|$ and the number of transmit antennas n_T. It also makes a parallel implementation possible. Note that the overall number of visited nodes by the K-Best algorithm is $|\xi| + (n_T - 1)K|\xi|$.

Although the conventional K-Best has an advantageous fixed complexity, it does not take into

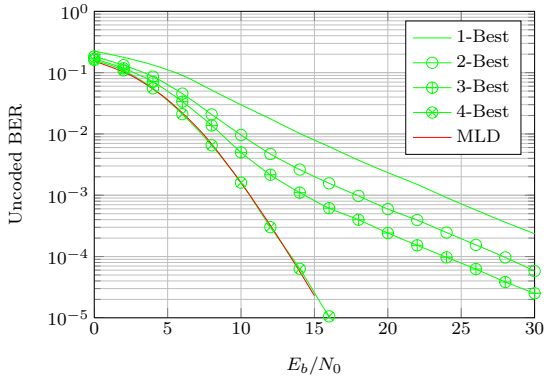

Figure 3.7: Uncoded BER as a function of E_b/N_0, Complex Rayleigh 4×4 SM-MIMO-SC system, K-Best algorithm for multiple K values and ML detectors, 4-QAM modulations at each layer.

consideration the noise and channel conditions. Thus, unnecessary computations are usually done when the channel is well-conditioned and the signal to noise ratio is high. Also, for high $|\xi|$ and n_T, the computational complexity of the K-Best algorithm becomes high.

3.2.6 Adaptive Computational Complexity

While it was not introduced in Section 3.1.3, (ZF/MMSE-)SQRD has also been shown to have a significant impact of the tree search construction. In particular, the SD structure can be advantageously modified in order to avoid unnecessary visited nodes, thus leading to an efficient performance versus computational complexity trade-off.
Several algorithms are proposed in the literature to resolve this. A solution that lies on applying a variable K has been widely studied and is denoted as the dynamic K-Best algorithm [Li 08, Rog09]. It offers promising performance results in the case of a SQRD preprocessing step. These algorithms reduce the number of retained candidates at each detection level with tolerable degradation in the performance [Kaw06, Jeo06, Moh10] and references therein. In [Moh09c], two algorithms are proposed. In addition to reducing the computational complexity of the K-Best algorithm, they either reduce the processing delay by parallelizing the detection stage or reduce the hardware requirements by iteratively processing the K-Best algorithm. While a variable K also implies a variable computational complexity, a particular case has to be introduced.

The Fixed-complexity Sphere Decoder (FSD) is proposed by Barbero *et al.* to overcome the aforementioned drawbacks of SDs. The FSD achieves a quasi-ML performance by performing the following two-stage tree search [Bar08b, Bar08a]:
– Full expansion: In the first p levels, a full expansion is performed, where all symbol replica candidates are retained to the following levels;
– Single expansion: A single expansion of each retained branch is done in the remaining $(n_T - p)$ levels, where only the symbol replica candidate with the lowest accumulative metric is considered for next levels.

Because all possible symbol candidates are retained in the first p levels, the reliability of the signals detected in these levels does not affect the final detection performance compared to MLD. Therefore, signals with the least robustness are detected in the full expansion stage. On the other hand, in the remaining $(n_T - p)$ levels, signals are sorted based on their reliability, where signals with the least noise amplification are detected first. In the conventional FSD, the V-BLAST algorithm is employed to obtain the required signal ordering by the FSD.

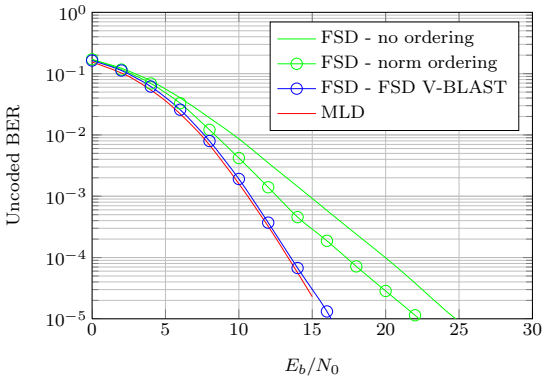

Figure 3.8: Uncoded BER as a function of E_b/N_0, Complex Rayleigh 4×4 SM-MIMO-SC system, FSD algorithms with $p = 1$ and ML detectors, 4-QAM modulations at each layer.

Figure 3.8 depicts the uncoded BER performance of the FSD for $p = 1$ in 4×4 SM-MIMO-SC system using 4-QAM. Results show that the ordering has a crucial effect on the the performance of the FSD. For instance, both the performance and the attained diversity order are degraded when the ordering stage is skipped or when a non-optimal signal ordering is used. A low complexity FSD ordering scheme that requires a fraction of the computations of the V-BLAST scheme is proposed in [Moh09a], where a close to optimum performance was achieved by embedding the sorting stage in the QR factorization of the channel matrix.

The FSD is retained by ST-E for 2×2 systems that are supported by the LTE standard. It is also claimed by Barbero *et al.* to be efficient for 4×4 systems that are supported by the LTE-A standard. However, FSDs offer limited performance in front of ill-conditioned channels. Also, its computational complexity depends on the constellation size, thus leading to a significant worst-case - with 64-QAM constellations - computational complexity (see Section 5.3.3).

Nevertheless, it is a separate improvement in the SD's computational complexity that is not sufficient while it is efficient. It is not discarded since it can be applied to the - also general - solution that is proposed in the present work. All the aforementioned SD-like techniques - including the FSD [Bar06b] - are subject to a smart optimization that is introduced in the sequel.

3.2.7 Equivalent Formula Leading to Minimum-Mean Square Error-Centred Sphere Decoder

The SD principle can be advantageously extended. By introducing the BP definition [Agr02], it corresponds to - in the case of a depth-first search algorithm - the first solution offered by the algorithm. The induced BP with the aforementioned techniques is thus - implicitly - a ZF-(S)QRD DFD. Clearly with a breadth first search algorithm, the BP corresponds to the solution that would be directly reached, without neighbourhood study. Another useful notation that has to be introduced is the equation of an $(n_T - 1)-$ sphere centred on $\mathbf{x}_C$ and of radius d. Any signal that lies inside of this sphere is such that $\|\mathbf{x}_C - \mathbf{x}\|^2 \leq d^2$, where $\mathbf{x}$ is any possible hypothesis. Generally, the SD formula is centred on the unconstrained ZF solution and the corresponding detector is denoted in the sequel as the naïve SD. Consequently, a fundamental optimization may be considered by introducing an efficient search center that results in an already close-to-optimal

BP. In other words, a solution that is already close to the ML solution is obtained. This way, it is clear that the size of the neighbourhood study can be decreased without affecting the outcome of the search process. In the case of the K-Best algorithm where the neighbourhood size is fixed, it will induce a performance improvement for a given K or a reduction of K for a given target BER. The classical SD expression Equation (3.23) can be re-arranged, leading to an exact formula that was first proposed by Wong *et al.*, aiming at optimizations for a VLSI implementation through an efficient PED expression and early pruned nodes [Won02]:

$$\mathbf{x}_{\text{ZF-(S)QRD SD}} = \underset{\mathbf{x}\in\xi^{n_T}}{\arg\min} \|\mathbf{R}\mathbf{e}_{\text{ZF}}\|^2, \tag{3.27}$$

where $\mathbf{e}_{\text{ZF}} = \tilde{\mathbf{x}}_{\text{ZF}} - \mathbf{x}$ and $\tilde{\mathbf{x}}_{\text{ZF}} = (\mathbf{H}^H\mathbf{H})^{-1}\mathbf{H}^H\mathbf{y}$. Equation (3.27) clearly exhibits the point that the naïve SD is unconstrained ZF-centred and implicitly corresponds to a ZF-(S)QRD DFD procedure with a neighbourhood study at each layer.
The main idea proposed by [Hoc03, Cui05, Wan08] is to choose a closer-to-ML BP than the ZF-(S)QRD, which is the case of the MMSE-(S)QRD solution. For the sake of clearness with definitions, we say that two ML equations are equivalent if the lattice points argument output of the minimum distance are the same, even in the case of different metrics. Two ML equations are equivalent iff:

$$\underset{\mathbf{x}\in\xi^{n_T}}{\arg\min}\{\|\mathbf{y}-\mathbf{H}\mathbf{x}\|^2\} = \underset{\mathbf{x}\in\xi^{n_T}}{\arg\min}\{\|\mathbf{y}-\mathbf{H}\mathbf{x}\|^2 + c\}, \tag{3.28}$$

where c is a constant.
In particular, Cui *et al.* [Cui05] propose a general equivalent minimization problem: $\hat{\mathbf{x}}_{\text{ML}} = \underset{\mathbf{x}\in\xi^{n_T}}{\arg\min}\{\|\mathbf{y}-\mathbf{H}\mathbf{x}\|^2 + \alpha\mathbf{x}^H\mathbf{x}\}$, by assuming that $\mathbf{x}$ are constant-modulus signals. This assumption holds true in the case of 4-QAM modulation and is not directly applicable to 16-QAM and 64-QAM modulations, even if this assumption is not limiting since a QAM constellation can be considered as a linear sum of 4-QAM points [Cui05].

This expression has been applied to the K-Best algorithm by Wang *et al.* in the case of the unconstrained MMSE-centre, which leads to an MMSE-(S)QRD procedure with a neighbourhood study at each layer [Wan08]. In this case, the equivalent ML equation is rewritten as:

$$\hat{\mathbf{x}}_{\text{ML}} = \underset{\mathbf{x}\in\xi^{n_T}}{\arg\min}\ (\mathbf{x}_C - \mathbf{x})^H \left(\mathbf{H}^H\mathbf{H} + \sigma_n^2\mathbf{I}_{n_T}\right)(\mathbf{x}_C - \mathbf{x}). \tag{3.29}$$

Finally and through the use of the Cholesky Factorization (CF) of $\mathbf{H}^H\mathbf{H} + \sigma_n^2\mathbf{I}_{n_T}$ - that simultaneously reads $\mathbf{U}^H\mathbf{U}$ - in the MMSE case ($\mathbf{H}^H\mathbf{H}$ in the ZF case), the ML expression is equivalently rewritten as:

$$\hat{\mathbf{x}}_{\text{LD SD}} = \underset{\mathbf{x}\in\xi_{\mathbb{C}}^{n_T}}{\arg\min}\left\{\left\|\tilde{\mathbf{U}}(\tilde{\mathbf{x}} - \mathbf{x})\right\|^2\right\},$$

where

$$\mathbf{U}^H\mathbf{U} = \begin{cases}\mathbf{H}^H\mathbf{H} & \text{in the ZF case,}\\ \mathbf{H}^H\mathbf{H} + \sigma_n^2\mathbf{I}_{n_T} & \text{in the MMSE case,}\end{cases} \tag{3.30}$$

and by noting that $\mathbf{U}$ is upper triangular with real diagonal elements and $\tilde{\mathbf{x}}$ is any - consistently with the $\mathbf{U}$ expression - LD unconstrained linear estimate.

While the introduced definition is strictly correct with constant-modulus signals only, it can be shown - consistently with what is proposed in [Cui05] - that the assumption can be advantageously soften. In particular, by considering that it is respected in mean for a large n_T - which is done in [Cui05] and in the sequel - convenient results are achieved, namely a tolerable degradation arise in the bit error performance. Consequently and in the present solution, only the metric expression has been modified compared to the classical K-Best. Consequently, there is no impact on computational complexity and conclusions provided in Section 3.2.5 still hold.

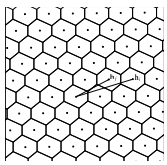

Figure 3.9: (a)

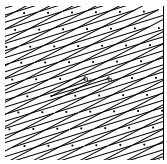

Figure 3.10: (b)

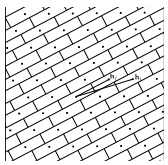

Figure 3.11: (c)

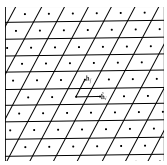

Figure 3.12: (d)

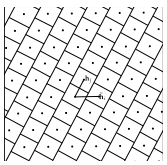

Figure 3.13: (e)

Figure 3.14: Undisturbed received signals and decision areas of (a) MLD, (b) LD, (c) DFD, (d) LRA-LD and (e) LRA-DFD [Wue04].

3.3 Lattice-Reduction-Aided Techniques

For higher dimensions, a close-to-ML estimate can be correctly provided with a reasonable complexity using a Lattice-Reduction-Aided (LRA) detection technique.

3.3.1 Problem Statement and Summary

As proposed in [Yao02], LRA techniques are used to transform any MIMO channel into a better-conditioned (short basis vectors norms and roughly orthogonal) equivalent MIMO channel, namely generating the same lattice points. Although classical low-complexity DLs - and even (O)DFD - fail to achieve full diversity as depicted in [Wue04], they can be applied to this equivalent (the exact definition will be introduced thereafter) channel and *significantly improve performance* [Win03a]. In particular, it has been shown that LRA detectors achieve the full diversity [Tah05, Lin06, Gan09]. By assuming $i < j$, Figure 3.14 depicts the decision regions in a trivial two-dimensional case and demonstrate to the reader the reason why LRA detection algorithms offer better performance by approaching the optimal ML decision areas [Wue04]. From a singular value theory point of view, when the lattice basis is reduced, its singular values becomes much closer to others with equal singular values for orthogonal basis. Therefore, the power of the system will be distributed almost equally on the singular values and the system becomes more immune against the noise enhancement problem when the singular values are inverted during the equalization process.

To this end, various reduction algorithms, namely the optimal (the orthogonality is maximized) but NP-hard Minkowski [Lam91], Korkine-Zolotareff [Lam91] algorithms [Agr02], the well-known LLL reduction [Len82], and Seysen's [Sey93, Lam91] Lattice-Reduction (LR) algorithm are proposed.

3.3.2 Lattice Reduction

By interpreting the columns $\mathbf{H}_{:,i}$ of $\mathbf{H}$ as a *generator basis*, note that $\mathbf{H}$ is also known as the lattice basis whose columns are referred to as "basis vectors", the lattice $\Lambda(\mathbf{H})$ is defined as all the complex integer combinations of $\mathbf{H}_{:,i}$, *i.e.*:

$$\Lambda(\mathbf{H}) \triangleq \left\{ \sum_{i=1}^{n_T} a_i \mathbf{H}_{:,i} \mid a_i \in \mathbb{Z}_{\mathbb{C}} \right\}, \tag{3.31}$$

where $\mathbb{Z}_{\mathbb{C}}$ is the set of complex integers that reads: $\mathbb{Z}_{\mathbb{C}} = \mathbb{Z} + j\mathbb{Z}$, $j^2 = -1$.
The lattice $\Lambda(\tilde{\mathbf{H}})$ generated by the matrix $\tilde{\mathbf{H}}$ and the lattice generated by the matrix $\mathbf{H}$ are *identical*

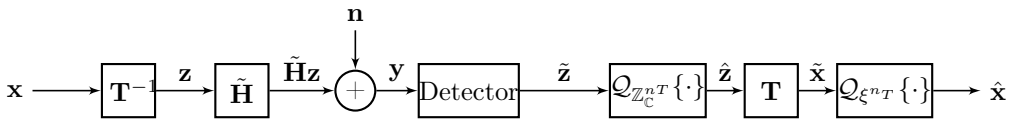

Figure 3.15: LRA detector bloc scheme.

iff all the lattice points are the same. The two aforementioned bases generate an identical lattices iff $\tilde{\mathbf{H}} = \mathbf{HT}$, where the $n_T \times n_T$ transformation matrix is *unimodular* [Agr02], *i.e.* $\mathbf{T} \in \mathbb{Z}_{\mathbb{C}}^{n_T \times n_T}$ and such that $|\det(\mathbf{T})| = 1$.
Using the reduced channel basis $\tilde{\mathbf{H}} = \mathbf{HT}$ and introducing $\mathbf{z} = \mathbf{T}^{-1}\mathbf{x}$, the system model given in Equation (5.5) can be rewritten as [Wue04]:

$$\mathbf{y} = \tilde{\mathbf{H}}\mathbf{z} + \mathbf{n}. \tag{3.32}$$

The idea behind LRA equalizers and detectors relies on the identical system model given above. The detection is then performed with respect to the reduced channel matrix ($\tilde{\mathbf{H}}$), which is now roughly orthogonal by definition, and to the equivalent transmitted signal that still belongs to an integer lattice since $\mathbf{T}$ is unimodular [Wue04]. Finally, the estimated $\hat{\mathbf{x}}$ in the original problem is computed with the relationship $\tilde{\mathbf{x}} = \mathbf{T}\hat{\mathbf{z}}$ and by hard-limiting $\tilde{\mathbf{x}}$ to a valid symbol vector. These steps are summarized in the block scheme in Figure 3.15.
In the sequel, the main aspects of the LLL Algorithm (LA) and the Seysen's Algorithm (SA) are briefly described and compared.

3.3.2.1 LLL Algorithm

The LA is a local approach that transforms an input basis $\mathbf{H}$ into an LLL-reduced basis $\tilde{\mathbf{H}}$ that satisfies both of the orthogonality and norm reduction conditions, respectively:

$$|\Re\{\mu_{i,j}\}|,\ |\Im\{\mu_{i,j}\}| \leq \tfrac{1}{2},\ \forall\ 1 \leq j < i \leq n_T, \tag{3.33}$$

where $\mu_{i,j} \triangleq \frac{<\mathbf{H}_{:,i},\ \tilde{\mathbf{H}}_{:,j}>}{\|\tilde{\mathbf{H}}_{:,j}\|^2}$, and

$$\|\tilde{\mathbf{H}}_{:,i}\|^2 = (\delta - |\mu_{i,i-1}|^2)\|\tilde{\mathbf{H}}_{:,i-1}\|^2,\ \forall\ 1 < i \leq n_T, \tag{3.34}$$

where δ, with $\frac{1}{2} < \delta < 1$, is a factor selected to achieve a good quality-complexity trade-off [Len82]. In the present work, δ is assumed to be $\delta = \frac{3}{4}$, as commonly suggested, and $\tilde{\mathbf{H}}_{:,i} = \tilde{\mathbf{H}}_{:,i} - \sum_{j=1}^{i-2}\{\lceil\mu_{i,j}\rfloor\mathbf{H}_{:,j}\}$. Another classical result consists in directly considering the Complex LA (CLA) that saves an average of nearly 50% in computational complexity compared to the straightforward real model system extension and with negligible performance degradation [Gan09].
It is shown in [Wue04] that the QRD output of $\mathbf{H}$ - $\mathbf{Q}$ and $\mathbf{R}$ - is a possible starting point for the LA, and it has been introduced [Bar08c] that the SQRD provides a better starting point since it finally leads to a significant reduction in the expected computational complexity [Wue04] and in the corresponding variance [Ges08].
By denoting the latter algorithm as the Sorted QRD-based LA (SLA), two points are depicted in Figure 3.16 (a-c) under DSP implementation-oriented assumptions on computational complexities (see [Aub10] for details).
Instead of applying the LA to only the basis $\mathbf{H}$, a simultaneous reduction of the basis $\mathbf{H}$ and the dual basis $\mathbf{H}^{\#} = \mathbf{H}(\mathbf{H}^H\mathbf{H})^{-1}$ [Wue07] may be processed.

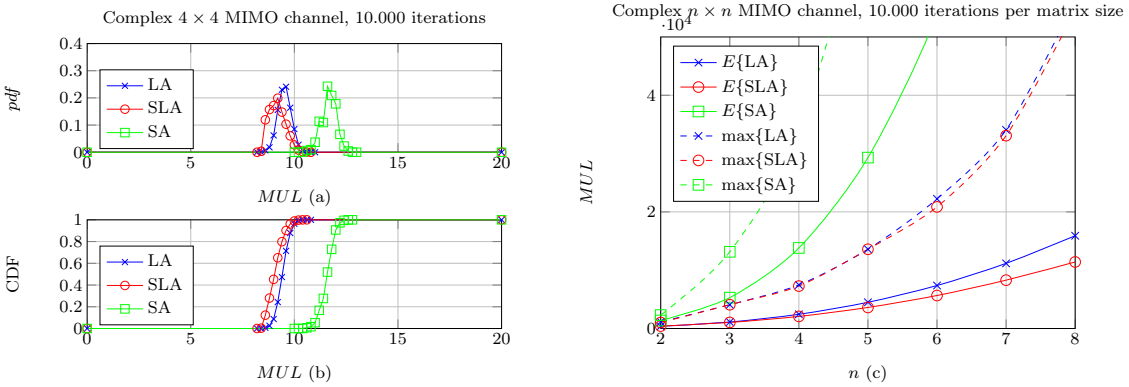

Figure 3.16: PDF (a) and CDF (b) of $\ln\{MUL\}$ for the LA, SLA and SA, and average and maximum total number of MUL for the LA, SLA and SA as a function of the number of antennas n (c).

3.3.2.2 Seysen's Algorithm

To start, let us introduce the *Seysen's orthogonality measure* [Sey93]:

$$\mathcal{S}(\tilde{\mathbf{H}}) \triangleq \sum_{i=1}^{n_T} \left\|\tilde{\mathbf{H}}_{:,i}\right\|^2 \left\|\tilde{\mathbf{H}}^{\#}_{:,i}\right\|^2, \tag{3.35}$$

where $\tilde{\mathbf{H}}^{\#}_{:,i}$ is the i-th basis vector of the dual lattice, *i.e.* $\tilde{\mathbf{H}}^{\#H}\tilde{\mathbf{H}} = \mathbf{I}_{n_T}$.
The SA is a global approach that transforms an input basis $\mathbf{H}$ (and its dual basis $\mathbf{H}^{\#}$) into a Seysen-reduced basis $\tilde{\mathbf{H}}$ that (locally) minimizes $\mathcal{S}$ and that satisfies, $\forall\, 1 \leq i \neq j \leq n_T$ [See07]:

$$\lambda_{i,j} \triangleq \left\lfloor \frac{1}{2} \left(\frac{\tilde{\mathbf{H}}^{\#H}_{:,j}\tilde{\mathbf{H}}^{\#}_{:,i}}{\|\tilde{\mathbf{H}}^{\#}_{:,i}\|^2} - \frac{\tilde{\mathbf{H}}^{H}_{:,j}\tilde{\mathbf{H}}_{:,i}}{\|\tilde{\mathbf{H}}^{\#}_{:,j}\|^2} \right) \right\rceil = 0. \tag{3.36}$$

By denoting $E\{\cdot\}$ and $\max\{\cdot\}$ as the expectation and the maximum opertors, respectively, the SA's computational complexity is depicted in Figure 3.16 (a-c) as a function of MUL (see Section 2.7.3), which allows for some discussion.

3.3.2.3 Concluding Remarks

The aforementioned LR techniques have been presented and both their performances (orthogonality of the obtained lattice) [Wue07] and computational complexities [Bar08c] have been compared when applied to MIMO detection in the Open-Loop (OL) case. In Figure 3.17 (a-f), the orthogonal deficiency (see Equation (2.39)), conditioning number (see Equation (2.40)) and Seysen's orthogonality measure (see Equation (3.36)) of the reduced basis provided by the SA compared to the LA and SLA are depicted. These are known to be popular measures of the quality of a basis for data detection [Win03a]. However, this orthogonality gain is obtained at the expense of a higher computational complexity, in particular compared to the SLA. Moreover, it has been shown that an uncoded BER performance improvement is gained in the case of LRA-LD only [Wue07]. In particular, in the case of LRA-DFD detectors, both LA and SA yield almost the same performance [Bar08c].

According to the curves depicted in Figure 3.16 (c), the mean computational complexities of

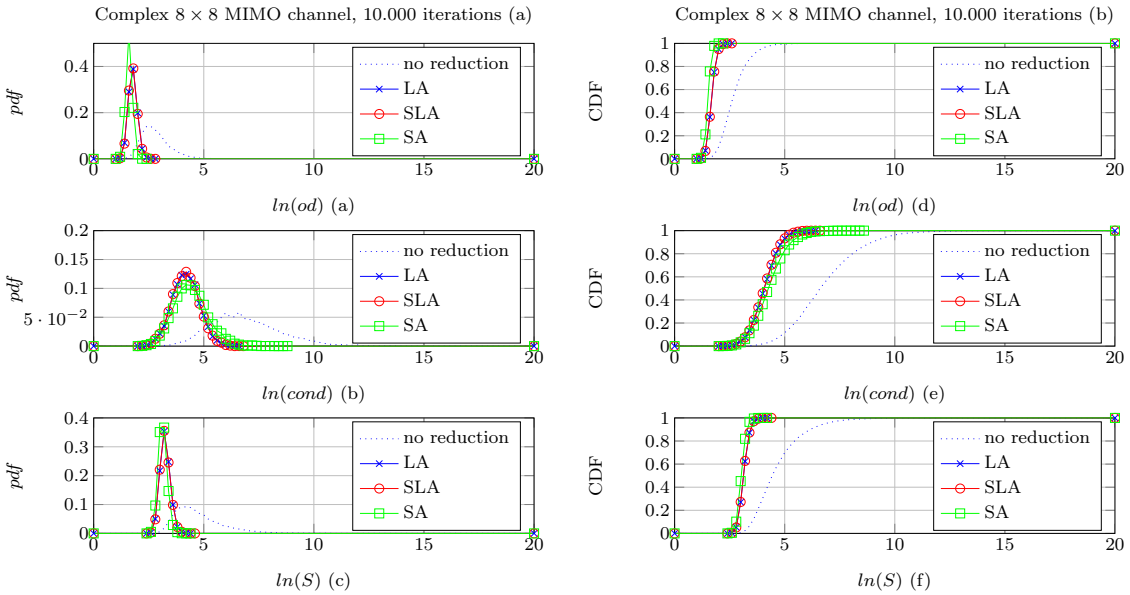

Figure 3.17: PDF (a-c) and CDF (d-f) of $ln(cond)$ (a, d), $ln(od)$ (b, e) and $ln(S)$ (c, f) by application of the LA, SLA and SA and compared to the original basis.

LA, SLA and SA are $1.6 \cdot 10^4$, $1.1 \cdot 10^4$ and $1.4 \cdot 10^5$ respectively in the case of a 4×4 complex matrix. The computed variance of the computational complexities of LA, SLA and SA are $3 \cdot 10^7$, $2.3 \cdot 10^7$ and $2.4 \cdot 10^9$ respectively, which illustrate the aforementioned reduction in the mean computational complexity and in the corresponding variance and consequently highlight the SLA advantage over other LR techniques. Also and interestingly, it is proven in [Jal08] that the computational complexity of the LA - whether it is QRD or SQRD based - decreases exponentially, which is clear from Figure 3.16 and advantageous in the algorithm calibration.

In Figure 3.17, the Probability Density Function (PDF) and Cumulative Density Function (CDF) of $ln(OD)$, $ln(\kappa)$ and $ln(S)$ for LA, SLA and SA are depicted and compared to the performance without LR. It can be observed that both LA and SLA offer exactly the same performance, with the only difference being their computational complexities. Also, there is a tiny improvement in the OD when SA is used as compared to (S)LA. This point will be discussed in the sequel.

The LRA algorithm preprocessing step has been exposed and implies some minor modifications in the detection step.

3.3.3 Lattice-Reduction-Aided Detectors

The key idea behind LRA detection schemes is understanding that the finite set of transmitted symbols ξ^{n_T} can be interpreted as the De-normalized, Shifted then Scaled (DSS) version of the infinite integer subset $\mathcal{Z}_{\mathbb{C}}^{n_T} \subset \mathbb{Z}_{\mathbb{C}}^{n_T}$ [Win03a], *i.e.*:

$$\xi^{n_T} = 2a\left(\mathcal{Z}_{\mathbb{C}}^{n_T} + \tfrac{1}{2}\mathbf{T}^{-1}\mathbf{1}_{\mathbb{C}}^{n_T}\right), \tag{3.37}$$

and reciprocally as the re-Scaled, re-Shifted then Normalized (SSN) version of the set of transmitted symbols:

$$\mathcal{Z}_{\mathbb{C}}^{n_T} = \tfrac{1}{2a}\xi^{n_T} - \tfrac{1}{2}\mathbf{T}^{-1}\mathbf{1}_{\mathbb{C}}^{n_T}, \tag{3.38}$$

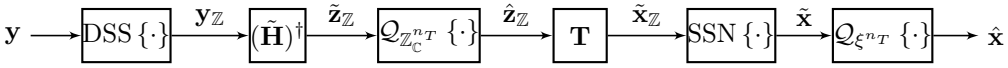

Figure 3.18: LRA-ZF detector block scheme.

where a is a power normalization coefficient (*i.e.* $1/\sqrt{2}$, $1/\sqrt{10}$ and $1/\sqrt{42}$ for 4-QAM, 16-QAM and 64-QAM constellations, respectively) and $\mathbf{1}_{\mathbb{C}}^{n_T} \in \mathbb{Z}_{\mathbb{C}}^{n_T}$ is a complex displacement vector (*i.e.* $\mathbf{1}_{\mathbb{C}}^{n_T} = [1+j,\ \cdots,\ 1+j]^T$ in the complex case).
Here a general notation is introduced. Starting from the system equation, it can be rewritten equivalently by de-normalizing, dividing by two and subtracting $\mathbf{H}\mathbf{1}_{\mathbb{C}}^{n_T}/2$ from both sides:

$$\frac{\mathbf{y}}{2a} - \frac{\mathbf{H}\mathbf{1}_{\mathbb{C}}^{n_T}}{2} = \frac{\mathbf{H}\mathbf{x}}{2a} + \frac{\mathbf{n}}{2a} - \frac{\mathbf{H}\mathbf{1}_{\mathbb{C}}^{n_T}}{2} \Leftrightarrow \frac{1}{2}\left(\frac{\mathbf{y}}{a} - \mathbf{H}\mathbf{1}_{\mathbb{C}}^{n_T}\right) = \mathbf{H}\frac{1}{2}\left(\frac{\mathbf{x}}{a} - \mathbf{1}_{\mathbb{C}}^{n_T}\right) + \frac{1}{2a}\mathbf{n}, \tag{3.39}$$

where $\mathbf{H}\mathbf{1}_{\mathbb{C}}^{n_T}$ is a simple matrix-vector product that is be computed for each channel realization. By introducing the DSS signals $\mathbf{y}_{\mathbb{Z}} = \frac{1}{2}\left(\frac{\mathbf{y}}{a} - \mathbf{H}\mathbf{1}_{\mathbb{C}}^{n_T}\right) = \mathrm{DSS}\{\mathbf{y}\}$ and $\mathbf{x}_{\mathbb{Z}} = \frac{1}{2}\left(\frac{\mathbf{x}}{a} - \mathbf{1}_{\mathbb{C}}^{n_T}\right) = \mathrm{DSS}\{\mathbf{x}\}$, which makes both belonging to $\mathbf{H}\mathcal{Z}_{\mathbb{C}}^{n_T}$ and $\mathcal{Z}_{\mathbb{C}}^{n_T}$, respectively, the expression reads:

$$\mathbf{y}_{\mathbb{Z}} = \mathbf{H}\mathbf{x}_{\mathbb{Z}} + \frac{\mathbf{n}}{2a}. \tag{3.40}$$

This intermediate step defines the symbols vector in the reduced transformed constellation through the relation $\mathbf{z}_{\mathbb{Z}} = \mathbf{T}^{-1}\mathbf{x}_{\mathbb{Z}} \in \mathbf{T}^{-1}\mathcal{Z}^{n_T} \subset \mathbb{Z}^{n_T}$. Finally, the lattice-reduced channel and reduced constellation expression can be introduced:

$$\mathbf{y}_{\mathbb{Z}} = \tilde{\mathbf{H}}\mathbf{z}_{\mathbb{Z}} + \frac{\mathbf{n}}{2a}. \tag{3.41}$$

The LRA detection steps comprise the $\hat{\mathbf{z}}_{\mathbb{Z}}$ estimation of $\mathbf{z}_{\mathbb{Z}}$ with respect to $\mathbf{y}_{\mathbb{Z}}$ and the mapping of these estimates to the corresponding symbols belonging to the ξ^{n_T} constellation through the $\mathbf{T}$ matrix. In order to finally obtain the $\hat{\mathbf{x}}$ estimation of $\mathbf{x}$, the DSS $\tilde{\mathbf{x}}_{\mathbb{Z}}$ signal is obtained following the $\tilde{\mathbf{z}}_{\mathbb{Z}}$ quantization with respect to $\mathbb{Z}_{\mathbb{C}}^{n_T}$ and SSN again.
The estimation for the transmitted signal is $\hat{\mathbf{x}} = \mathcal{Q}_{\xi^{n_T}}\{\tilde{\mathbf{x}}\}$, as described in the block scheme in Figure 3.18 in the case of the LRA-ZF solution. It can be globally rewritten as:

$$\hat{\mathbf{x}} = \mathcal{Q}_{\xi^{n_T}}\left\{a\left(2\mathbf{T}\mathcal{Q}_{\mathbb{Z}_{\mathbb{C}}^{n_T}}\{\tilde{\mathbf{z}}_{\mathbb{Z}}\} + \mathbf{1}_{\mathbb{C}}^{n_T}\right)\right\}, \tag{3.42}$$

where $\mathcal{Q}_{\mathbb{Z}_{\mathbb{C}}^{n_T}}\{\cdot\}$ denotes the quantization operation of the n_T-th dimensional integer lattice, for which the per-component quantization is $\mathcal{Q}_{\mathbb{Z}_{\mathbb{C}}^{n_T}}\{\mathbf{x}\} = [\lfloor \mathbf{x}_1 \rceil,\ \cdots,\ \lfloor \mathbf{x}_{n_T} \rceil]^T$, where $\lfloor\cdot\rceil$ denotes the rounding to the nearest integer.

Due to its performance versus complexity, the LA is a widely used reduction algorithm. This is because SA requires a high amount of additional computations compared to the LA to achieve a small, even negligible, gain in the BER performance [Bar08c], as depicted in Figure 3.17. Based on this conjecture, LA will be considered as the chosen LR technique in the remaining part of the chapter.
Subsequently to the aforementioned points, the SLA computational complexity is shown in [Jal08] to be upper-bounded by distinguishing the SQRD preprocessing step and the two LA related conditions. In particular and while the SQRD offers a polynomial complexity, the key point of the SLA computational complexity estimation lies in the knowledge of the number of iterations for both conditions. Since the number of iterations depends on the condition number of the channel matrix, it is consequently unbounded [Jal08], which leads to the conclusion that the worst-case computational complexity of the LA in the OL case is exponential in the number of antennas.

Nevertheless, the mean number of iterations (and consequently the mean total computational complexity) has also been shown to be polynomial [Jal08] and, therefore, a thresholded-based version of the algorithm offers convenient results. That is, the algorithm is terminated when the number of iterations exceeds a pre-defined threshold.

In the case of LRA-LD, the quantization is performed on $\mathbf{z}$ instead of $\mathbf{x}$. The unconstrained LRA-ZF equalized signal $\tilde{\mathbf{z}}_{\text{LRA-ZF}}$ is denoted as:

$$(\tilde{\mathbf{H}}^H\tilde{\mathbf{H}})^{-1}\tilde{\mathbf{H}}^H\mathbf{y} \text{ and simultaneously reads } \mathbf{T}^{-1}\tilde{\mathbf{x}}_{\text{ZF}}, \tag{3.43}$$

Consequently, the constrained LRA-ZF estimate is:

$$\hat{\mathbf{x}} = \mathcal{Q}_{\xi^{n_T}}\{\mathbf{T}\mathcal{Q}_{\mathbb{Z}^{n_T}}\{\tilde{\mathbf{z}}_{\text{LRA-ZF}}\}\}. \tag{3.44}$$

Identically, the constrained LRA-MMSE estimate is:

$$\hat{\mathbf{x}} = \mathcal{Q}_{\xi^{n_T}}\{\mathbf{T}\mathcal{Q}_{\mathbb{Z}^{n_T}}\{\tilde{\mathbf{z}}_{\text{LRA-MMSE}}\}\}, \tag{3.45}$$

by denoting the unconstrained LRA-MMSE equalized signal as:

$$\tilde{\mathbf{z}}_{\text{LRA-MMSE}} = (\tilde{\mathbf{H}}^H\tilde{\mathbf{H}} + \sigma_n^2\mathbf{T}^H\mathbf{T})^{-1}\tilde{\mathbf{H}}^H\mathbf{y}. \tag{3.46}$$

It is shown in [Wue04] that the consideration of the MMSE criterion, by reducing the extended channel matrix $\mathbf{H}_{\text{ext}}$ - introduced in Section 3.1.3 that leads to $\tilde{\mathbf{H}}_{\text{ext}}$ - and considering the extended received vector $\mathbf{y}_{\text{ext}}$, offers both an important performance improvement and further reduction in the computational complexity compared to the straightforward solution. We remember that in this case, not only the $\tilde{\mathbf{H}}$ conditioning is considered but also the noise amplification, which is of particular interest in the case of the LRA-MMSE linear detector. In the sequel, this LRA-LD is denoted as an LRA-MMSE Extended (LRA-MMSEE) detector.

The imperfect orthogonality of the reduced channel matrix leads to the advantageous use of DFD techniques [Wue04], due to the remaining presence of ILI. By considering the QRD output of the SLA - $\tilde{\mathbf{Q}}$ and $\tilde{\mathbf{R}}$ - and in accordance with the operation described in Section 3.1.2, the modified received vector simultaneously reads:

$$\tilde{\mathbf{Q}}^H\mathbf{y} \text{ and } \tilde{\mathbf{R}}\mathbf{z} + \tilde{\mathbf{Q}}^H\mathbf{n}. \tag{3.47}$$

The DFD procedure can then be performed in order to iteratively obtain the $\hat{\mathbf{z}}$ estimate. In analogy with the LRA-LD, the extended system model can be considered. As a consequence, it leads to the LRA-MMSE-QRD estimate that can be obtained via rewriting simultaneously the modified received vector such that:

$$\tilde{\mathbf{Q}}_{\text{ext}}^H\mathbf{y}_{\text{ext}} \text{ and } \tilde{\mathbf{R}}_{\text{ext}}\mathbf{z} + \tilde{\mathbf{n}}, \tag{3.48}$$

where $\tilde{\mathbf{n}}$ is a noise term that also includes residual interferences.

Figure 3.19 shows the uncoded BER performance versus E_b/N_0 (in dB) of some well-established LRA-(pseudo) LDs, for a 4×4 SM-MIMO-SC system, using 4-QAM modulation (a, c) and 16-QAM (b, d) at each layer. The aforementioned results are compared to some reference results; namely, ZF, MMSE, ZF-QRD DFD, MMSE-QRD DFD and ML detectors. It has been shown that the (S)LA-based LRA-LDs achieve full diversity [Tah05] and consequently offer a strong improvement compared to the common LDs.

The advantages of LRA-(pseudo)LDs are numerous. First, they constitute efficient detectors

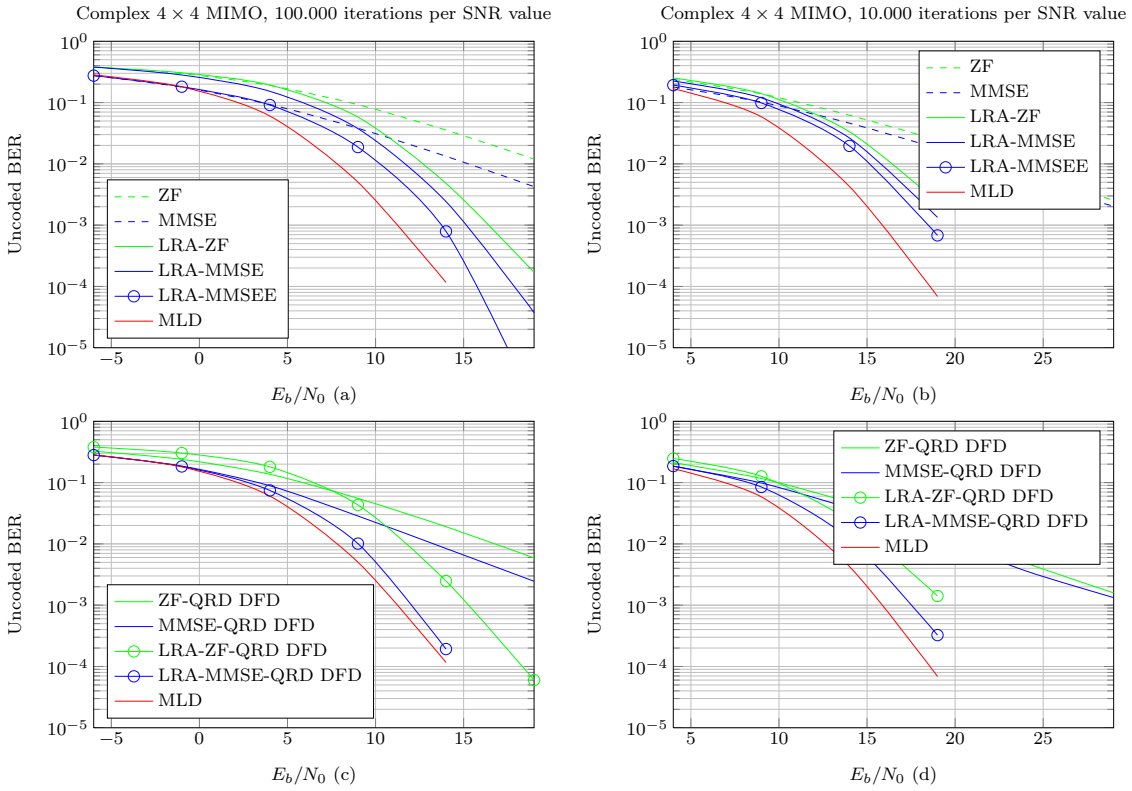

Figure 3.19: Uncoded BER as a function of E_b/N_0, Complex Rayleigh 4×4 SM-MIMO-SC system, ZF, MMSE, LRA-ZF, LRA-MMSE, LRA-MMSEE and ML detectors (a,b), ZF-QRD DFD, MMSE-QRD DFD, LRA-ZF-QRD DFD, LRA-MMSE-QRD DFD and ML detectors (c,d), 4-QAM modulations at each layer (a,c) and 16-QAM modulations at each layer (b,d).

in the sense of the high quality of their hard output - in particular, the ML diversity is reached within a constant offset - while offering a low overall computational complexity. In particular and despite the NP-hard nature of (S)LA (SA is not retained), its computational complexity is polynomial in mean and decreases exponentially, which is advantageous for implementation. These points are demonstrated in [Jal08]. Also and by noticing that the LR preprocessing step is data-independent, a promising aspect concerns the OFDM extension that would offer a significant computational complexity decrease due to the coherence bandwidth (see Section 2.6). This aspect is further addressed in Section 5.2.2.

However, there remain some important drawbacks. In particular, the aforementioned SNR offset is important in the case of high order modulations, namely 16-QAM and 64-QAM. Another is the sequential nature of the (S)LA due to its iterative running, which consequently limits the possibility of parallel processing.

For a reasonable K, a dramatic diversity loss is observed in Figure 3.7. For a low complexity solution such as LRA-(pseudo)LDs, a large SNR offset can eventually be observed in Figure 3.19. Consequently, the association of both to compensate for each of their drawbacks becomes obvious.

3.4 Lattice-Reduction-Aided Sphere Decoder

At this point and while it seems to be computationally expensive to cascade two NP-hard algorithms, the promising perspective of combining both a better-conditioned channel and a neighbourhood study arise. It relies on achieving the ML diversity through an LRA-(pseudo)LD and on reducing the remaining SNR offset through an additional SD technique. This idea senses that the neighbourhood size would be significantly reduced - compared to results presented in Section 3.2 - while reaching near-ML performance.

3.4.1 Problem Statement

Differently than LRA-LD and LRA-(O)DFD receivers - that only require a trivial quantization step at each layer -, the application of an SD detector that follows an LR technique is not straightforward. The main issue lies in the consideration of the set of all possibly transmitted symbol vectors in the reduced constellation. Unfortunately, it can not be predetermined since it does not depend on the considered constellation only, but also on the channel - actually the $\mathbf{T}^{-1}$ matrix. This aspect leads to two major drawbacks.

– First, the geometry of constellations in the reduced domain may be rather complex and even induce non-adjacent symbols, despite the regularity of QAM constellations. In particular and in presence of noise, some candidates may not map to any existing constellation points in the original domain [Qi 07];
– Second, the reduced domain does not regard the boundary region used for QAM constellations [Win03b], thus inducing no limitation in the neighbourhood size.

A brute-force solution to determine the set of all possibly transmitted vectors in the reduced domain - denoted as $\mathbf{Z} \ : \ \mathbf{Z}_{:,i} \in \mathcal{Z}_{\mathbb{C}}^{n_T}, \ \forall i \in [\![1, |\xi|^{n_T}]\!]$ - is to first get the set of all possibly transmitted vectors in the original domain - denoted as $\mathbf{X} \ : \ \mathbf{X}_{:,i} \in \xi^{n_T}, \ \forall i \in [\![1, |\xi|^{n_T}]\!]$ - and then apply the relation:

$$\mathbf{Z} = \mathbf{T}^{-1}\mathbf{X}, \tag{3.49}$$

for each channel realization. Clearly, this possibility is not feasible since it corresponds to the computational complexity of the ML detector. To avoid this problem, some solutions are offered in the literature, which are addressed in Section 3.4.3.

3.4.2 Lattice-Reduction-Aided Detection in the Reduced Domain

While the idea of combining both an LR and an SD was first proposed by Zhao *et al.* in [Zha06], Qi *et al.* [Qi 07] introduced in detail a novel scheme - denoted as LRA-SD algorithm - where a particular attention to neighbourhood exploration was paid. This algorithm was then enhanced by Roger *et al.* [Rog09] by - among others - associating both an LR and a K-Best, thus rendering it suitable for implementation.

In the case of a Reduced-Domain Neighbourhood (RDN) study, the equivalent channel matrix $\tilde{\mathbf{H}}$ is considered. In accordance with Section 3.3.3, it is remembered to be only roughly - and not exactly - orthogonal, thus not completely ILI-free. Consequently, neither LRA-LD nor LRA-(O)DFD detectors are optimal since the mutual influence of the transformed $\mathbf{z}$ signal is still present. This discussion exhibits the interest of SD-like techniques to still improve LRA detectors performance. Also and since $\tilde{\mathbf{H}}$ is nevertheless almost orthogonal, it is clear that to achieve the ML performance, an RDN study size would be smaller than an Original-Domain Neighbourhood (ODN) one.

First, the basic idea is reintroduced. It attempts to make the LR theory appropriate for application in complexity - and latency - limited communication systems. The normalize-shift-scale step, that has been previously introduced, will not be addressed again. Starting from Equation (3.41), both sides of the reduced channel and reduced constellation can be left-multiplied by $\tilde{\mathbf{Q}}^H$. Therefore, a new relation is obtained:

$$\tilde{\mathbf{Q}}^H \mathbf{y} = \tilde{\mathbf{R}}\mathbf{z} + \mathbf{n}, \tag{3.50}$$

which allows an SD scheme to be introduced, and eventually a K-Best. At this moment, the critical point of the neighbourhood generation in the reduced constellation has to be introduced in detail.

3.4.3 Reduced-Domain Neighbourhood Generation

As presented above, the geometry of constellations in the reduced domain is non-regular and infinite. In particular, the vicinity of a lattice point in the reduced constellation could be mapped - in the original domain - onto the same signal point, thus leading to the inefficient processing of useless solutions. While this simply induces some wasted resources, its unbounded nature is prohibitive and must be addressed. In particular, the expected computational complexity reduction of the SD may be lost, due to the complexity incurred by the much larger space that the decoder needs to cover [Dam03]. Thus, the neighbourhood study - and in particular its size reduction [Sha08, Rog09] - is a key point for implementation.

Zhao *et al.* offer a possible radius expression in the reduced lattice from the radius expression in the original constellation d through the Cauchy-Schwarz inequality [Zha06]:

$$(\mathbf{z}_i - \tilde{\mathbf{z}}_i)^2 \leq \|(\tilde{\mathbf{R}}^{-1})_{:,i}\|^2 \|\tilde{\mathbf{R}}\,(\mathbf{z} - \tilde{\mathbf{z}})\,\|^2 \leq \|(\tilde{\mathbf{R}}^{-1})_{:,i}\|^2 d^2. \tag{3.51}$$

This idea leads to an upper bound of the explored neighbourhood and accordingly a reduction in the number of tested candidates. However, this solution is not suitable for implementation. Again, the reason lies in the choice of the initial value of the search radius [Vit99], with dramatic consequence as well in the original and reduced domains.

Although it is simple, convenient boundaries control constraints are proposed by Roger *et al.*. By denoting boundaries in the original constellation $\mathbf{x}_{\min}$ and $\mathbf{x}_{\max}$, the reduced constellation boundaries can be obtained through the relation $\mathbf{z} = \mathbf{T}^{-1}\mathbf{x}$ that implies $\mathbf{z}_{\max,l} = \max\{(\mathbf{T}^{-1})_{l,:}\,\mathbf{x}\}$ for a given layer l. The exact solution for the real case is given in [Rog09] and can be extended to the complex case:

$$\mathbf{z}_{\max,l} = \mathbf{x}_{\max} \sum_{j \in P^l} \left(\mathbf{T}^{-1}\right)_{l,j} + \mathbf{x}_{\min} \sum_{j \in N^l} \left(\mathbf{T}^{-1}\right)_{l,j}, \tag{3.52}$$

$$\mathbf{z}_{\min\, l} = \mathbf{x}_{\min} \sum_{j \in P^l} \left(\mathbf{T}^{-1}\right)_{l,j} + \mathbf{x}_{\max} \sum_{j \in N^l} \left(\mathbf{T}^{-1}\right)_{l,j}, \tag{3.53}$$

where P^l and N^l stand for the set of indices j corresponding to positive and negative entries (l, j) of $\mathbf{T}^{-1}$, respectively. This solution is exact and does not induce performance degradation.

In accordance with the discussion in Section 3.2.2, an inside of bounds zig-zag strategy - even simplistic - is efficient and has been widely adopted [Zha06, Sha08, Rog09]. It is also the case in the present work. Starting from any - unconstrained - LRA-ZF solution, a neighbourhood is considered at each layer and leads to the RDN LRA-SD technique that corresponds to the LRA-DFD

BP. In particular, the RDN generation at each layer k is processed for a bounded number of N possibilities and in a SE manner - with an increasing distance from $\tilde{\mathbf{z}}_k$. This technique provides a set of displacements generating a neighbourhood, denoted as $\mathbf{Z}_{k,:}$, and such as:

$$\begin{aligned}\mathbf{Z}_{k,:} =& \mathcal{Q}_{\mathbb{Z}_{\mathbb{C}}^{n_T}}\left\{\tilde{\mathbf{z}}_k\right\},\\ & \mathcal{Q}_{\mathbb{Z}_{\mathbb{C}}^{n_T}}\left\{\tilde{\mathbf{z}}_k\right\}+1, \mathcal{Q}_{\mathbb{Z}_{\mathbb{C}}^{n_T}}\left\{\tilde{\mathbf{z}}_k\right\}+\ \ j, \mathcal{Q}_{\mathbb{Z}_{\mathbb{C}}^{n_T}}\left\{\tilde{\mathbf{z}}_k\right\}-1, \mathcal{Q}_{\mathbb{Z}_{\mathbb{C}}^{n_T}}\left\{\tilde{\mathbf{z}}_k\right\}-\ \ j,\\ & \mathcal{Q}_{\mathbb{Z}_{\mathbb{C}}^{n_T}}\left\{\tilde{\mathbf{z}}_k\right\}+2, \mathcal{Q}_{\mathbb{Z}_{\mathbb{C}}^{n_T}}\left\{\tilde{\mathbf{z}}_k\right\}+2j, \mathcal{Q}_{\mathbb{Z}_{\mathbb{C}}^{n_T}}\left\{\tilde{\mathbf{z}}_k\right\}-2, \mathcal{Q}_{\mathbb{Z}_{\mathbb{C}}^{n_T}}\left\{\tilde{\mathbf{z}}_k\right\}-2j,\\ & \cdots .\end{aligned} \tag{3.54}$$

The SE strategy reaches the correct decision early - leading to a safe early termination criterion. Thus it is advantageously retained in the present work.

3.4.4 Reduced-Domain Neighbourhood Lattice-Reduction-Aided Zero-Forcing-Centred Sphere Decoder

Now that the issue of RDN study has been addressed, a second aspect has to be highlighted. It has just been stated that the original LRA-SD is implicitly - unconstrained - LRA-ZF-centred, and leads to an LRA-DFD procedure with an RDN study at each layer. The exact formula has not been clearly provided but is implicitly used by any LRA-SD [Qi 07, Sha08, Rog09] and may even be considered as an incremental extension of Equation (3.27):

$$\hat{\mathbf{z}}_{\text{LRA-ZF SD}} = \underset{\mathbf{z}\in\mathbb{Z}_{\mathbb{C}}^{n_T}}{\arg\min} \left\|\tilde{\mathbf{R}}\mathbf{e}_{\text{LRA-ZF}}\right\|^2, \tag{3.55}$$

where $\mathbf{e}_{\text{LRA-ZF}} = \tilde{\mathbf{z}}_{\text{LRA-ZF}} - \mathbf{z}$ and $\tilde{\mathbf{z}}_{\text{LRA-ZF}} = \left(\tilde{\mathbf{H}}^H\tilde{\mathbf{H}}\right)^{-1}\tilde{\mathbf{H}}\mathbf{y}$.

The main advantage of the LRA-ZF-centred K-Best lies in its computational complexity that is independent of the constellation size $|\xi|$, which is not the case with the naïve K-Best presented in Section 3.2.5. This favourable aspect - in particular for required [3GP09d] high order constellations - arises while reaching the ML performance, as depicted in Figure 3.20. Also, LRA detectors performance - in the case of K-Best - are less sensitive to ill-conditioned channel matrices due to the LR effect while it is a dramatical aspect for classical K-Best [Rog08].
However, benefits are limited with the widely used 4-QAM modulation due to elimination of nearby lattice points during the quantization step [Zha06]. The reason lies in the aforementioned geometry of constellations in the reduced domain. In particular, many lattice points considered in the RDN would be associated with the same constellation point after quantization in the original constellation. Also, a large RDN size is still necessary for reaching the ML performance.

Thus, the present work has led to an original solution.

3.4.5 Reduced-Domain Neighbourhood Lattice-Reduction-Aided Minimum-Mean Square Error-Centred Sphere Decoder

The drawback presented above is expected to be bypassed through the consideration of - to the best of the author's knowledge - the most accurate (closest to optimum) BP, namely the LRA-MMSE DFD. No convincing formula has been proposed until now, even if Jaldén *et al.* propose an LRA-MMSE-centred solution through the relation [Jal09]:

$$\hat{\mathbf{z}}_{\alpha,\text{LRA-MMSE SD}} = \underset{\mathbf{z}\in\mathbb{Z}_{\mathbb{C}}^{n_T}}{\arg\min}\left\{\left\|\tilde{\mathbf{R}}^{-1}\mathbf{R}^{-\dagger}\mathbf{H}^{\dagger}\mathbf{y}-\mathbf{z}\right\|^2\right\} = \underset{\mathbf{z}\in\mathbb{Z}_{\mathbb{C}}^{n_T}}{\arg\min}\left\{\left\|\tilde{\mathbf{z}}_{\text{LRA-MMSE}}-\mathbf{z}\right\|^2\right\}, \tag{3.56}$$

for all regularization factor α, and in particular for $\alpha = \sigma_n^2$.
While it is true that such a detector consists in an RDN study around the unconstrained LRA-MMSE estimate, the provided solution will be the constrained LRA-MMSE DFD plus a list of candidates in its neighbourhood. The considered metric is non-equivalent to the ML expression and would not lead to a near-ML solution. In particular, the ML performance is not efficiently reached while the RDN size grows.

An efficient solution has been derived from Equation (3.30), under the assumption of using constant-modulus constellations. It consists in an unconstrained LRA-MMSE-centred search that leads to an LRA-MMSE DFD procedure with an RDN study at each layer. The equivalent ML equation reads:

$$\hat{\mathbf{z}}_{\text{LRA-LD SD}} = \underset{\mathbf{z}\in\mathbb{Z}_{\mathbb{C}}^{n_T}}{\arg\min} \left\{ \left\| \tilde{\mathbf{R}} \left(\tilde{\mathbf{z}} - \mathbf{z} \right) \right\|^2 \right\},$$

where

$$\tilde{\mathbf{R}}^H \tilde{\mathbf{R}} = \begin{cases} \tilde{\mathbf{H}}^H \tilde{\mathbf{H}} & \text{in the LRA-ZF case,} \\ \tilde{\mathbf{H}}^H \tilde{\mathbf{H}} + \sigma_n^2 \mathbf{T}^H \mathbf{T} & \text{in the LRA-MMSE case,} \end{cases} \tag{3.57}$$

and by noting that $\tilde{\mathbf{R}}$ is upper triangular with real diagonal elements and $\tilde{\mathbf{z}}$ is any - consistently with the $\tilde{\mathbf{R}}$ expression - LRA-LD unconstrained linear estimate.

Proof. Let us introduce any term $c^{'}$ s.t. $\left\| \mathbf{y} - \tilde{\mathbf{H}}\mathbf{z} \right\|^2 + c^{'} = \left\| \tilde{\mathbf{R}} \left(\tilde{\mathbf{z}} - \mathbf{z} \right) \right\|$, where $\tilde{\mathbf{z}}$ is any LRA-LD unconstrained linear estimate:

$$\begin{aligned}
c^{'} &= \left\| \tilde{\mathbf{R}} \left(\tilde{\mathbf{z}} - \mathbf{z} \right) \right\|^2 - \left\| \mathbf{y} - \tilde{\mathbf{H}}\mathbf{z} \right\|^2 \\
&= \left(\tilde{\mathbf{z}} - \mathbf{z} \right)^H \tilde{\mathbf{R}}^H \tilde{\mathbf{R}} \left(\tilde{\mathbf{z}} - \mathbf{z} \right) - \left(\mathbf{y} - \tilde{\mathbf{H}}\mathbf{z} \right)^H \left(\mathbf{y} - \tilde{\mathbf{H}}\mathbf{z} \right) \\
&\overset{(a)}{=} \tilde{\mathbf{z}}^H \tilde{\mathbf{G}} \tilde{\mathbf{z}} - \tilde{\mathbf{z}}^H \tilde{\mathbf{G}} \mathbf{z} - \mathbf{z}^H \tilde{\mathbf{G}} \tilde{\mathbf{z}} + \mathbf{z}^H \tilde{\mathbf{G}} \mathbf{z} - \mathbf{y}^H \mathbf{y} + \mathbf{y}^H \tilde{\mathbf{H}} \mathbf{z} + \mathbf{z}^H \tilde{\mathbf{H}}^H \mathbf{y} - \mathbf{z}^H \tilde{\mathbf{H}}^H \tilde{\mathbf{H}} \mathbf{z} \\
&\overset{(b)}{=} \mathbf{y}^H \tilde{\mathbf{H}} \tilde{\mathbf{G}}^{-1} \tilde{\mathbf{G}} \tilde{\mathbf{G}}^{-1} \tilde{\mathbf{H}}^H \mathbf{y} - \mathbf{y}^H \tilde{\mathbf{H}} \tilde{\mathbf{G}}^{-1} \tilde{\mathbf{G}} \mathbf{z} - \mathbf{z} \tilde{\mathbf{G}} \tilde{\mathbf{G}}^{-1} \tilde{\mathbf{H}}^H \mathbf{y} + \mathbf{z}^H \tilde{\mathbf{G}} \mathbf{z} - \mathbf{y}^H \mathbf{y} \\
&\qquad + \mathbf{y}^H \tilde{\mathbf{H}} \mathbf{z} + \mathbf{z}^H \tilde{\mathbf{H}}^H \mathbf{y} - \mathbf{z}^H \tilde{\mathbf{H}}^H \tilde{\mathbf{H}} \mathbf{z}, \\
&\overset{(c)}{=} \mathbf{y}^H \tilde{\mathbf{H}} \tilde{\mathbf{G}}^{-1} \tilde{\mathbf{H}}^H \mathbf{y} + \mathbf{z}^H \tilde{\mathbf{G}} \mathbf{z} - \mathbf{y}^H \mathbf{y} - \mathbf{z}^H \tilde{\mathbf{H}}^H \tilde{\mathbf{H}} \mathbf{z} \\
&= \mathbf{y}^H \tilde{\mathbf{H}} \tilde{\mathbf{G}}^{-1} \tilde{\mathbf{H}}^H \mathbf{y} + \mathbf{z}^H \left(\tilde{\mathbf{G}} - \tilde{\mathbf{H}}^H \tilde{\mathbf{H}} \right) \mathbf{z} - \mathbf{y}^H \mathbf{y},
\end{aligned} \tag{3.58}$$

where in (a), we substitute $\tilde{\mathbf{R}}^H \tilde{\mathbf{R}}$ and $\tilde{\mathbf{G}}$, in (b), we introduce $\tilde{\mathbf{z}} = \tilde{\mathbf{G}}^{-1} \tilde{\mathbf{H}}^H \mathbf{y}$ and $\tilde{\mathbf{z}}^H = \mathbf{y}^H \tilde{\mathbf{H}} \tilde{\mathbf{G}}^{-1}$ and where in (c):

$$\tilde{\mathbf{G}} = \begin{cases} \tilde{\mathbf{H}}^H \tilde{\mathbf{H}} & \text{in the LRA-ZF case,} \\ \tilde{\mathbf{H}}^H \tilde{\mathbf{H}} + \sigma_n^2 \mathbf{T}^H \mathbf{T} & \text{in the LRA-MMSE case.} \end{cases} \tag{3.59}$$

In the LRA-ZF case, $\tilde{\mathbf{H}} \tilde{\mathbf{G}}^{-1} \tilde{\mathbf{H}}^H = \tilde{\mathbf{H}} \tilde{\mathbf{H}}^{-1} (\tilde{\mathbf{H}}^H)^{-1} \tilde{\mathbf{H}}^H = \mathbf{I}_{n_R}$ and $\tilde{\mathbf{G}} - \tilde{\mathbf{H}}^H \tilde{\mathbf{H}} = \mathbf{0}$, consequently $c' = 0$.
In the LRA-MMSE case, $c' = \mathbf{y}^H (\tilde{\mathbf{H}} (\tilde{\mathbf{H}}^H \tilde{\mathbf{H}} + \sigma_n^2 \mathbf{T}^H \mathbf{T})^{-1} \tilde{\mathbf{H}}^H - \mathbf{I} n_R) \mathbf{y} + \sigma_n^2 \mathbf{z}^H \mathbf{T}^H \mathbf{T} \mathbf{z}$, which is a constant term in $\mathbf{x}$ iff the signal $\mathbf{x}$ entries are of constant modulus since $\sigma_n^2 \mathbf{z}^H \mathbf{T}^H \mathbf{T} \mathbf{z} = \sigma_n^2 \mathbf{x}^H \mathbf{x}$. □

The formula introduced in Equation (3.57) offers an equivalent metric, similarly to what is provided in Section 3.2.7. The difference - and in particular the interest in the LRA case - lies in the nature of the neighbourhood study.

As depicted in Figure 3.20, near-ML performance is achieved while the neighbourhood size is drastically reduced - as well as the corresponding scheme computational complexity - due to the prior calculation of a closer-to-ML solution. Thus, it results in a performance improvement for a fixed computational complexity. With 16-QAM modulations, a neighbourhood size processed with a 2-Best achieves very-near MLD performance with the RDN LRA-MMSEE method. It is not the case otherwise, in particular with ODN-based techniques unless with a 16-Best. Also and with the RDN LRA-ZF method, a 4-Best neighbourhood study is not enough for achieving near-MLD performance since an SNR offset remains.
Interestingly, it should be noted that its computational complexity is still independent of the constellation size. It is an important aspect that sets up the advantage of the RDN LRA-MMSEE K-Best hard-detector.

3.4.6 Original-Domain Neighbourhood Lattice-Reduction-Aided Minimum-Mean Square Error-Centred Sphere Decoder

Even if the issue of the RDN study has been addressed above, it relies on numerous intricate and sequential steps that have to be added in the receptor. As a consequence, the detector latency is increased and it does not offer a strong performance improvement in the 4-QAM case, due - as previously discussed - to wasted resource. Also, some particular system configurations - among others, well-conditioned channels and high SNR - do not require such a scheme.
Consequently, a bypassed solution is proposed and allow for the use of an efficient sphere centre, namely an LRA-ZF point, with an ODN study. The preprocessing step remain strictly the same and provided an unconstrained LRA-LD estimate. It consists in rearranging the ML expression such that:

$$\hat{\mathbf{x}}_{\text{LRA-ZF SD}} = \underset{\mathbf{x}\in\xi^{n_T}}{\arg\min} \left\| \tilde{\mathbf{R}}' \left(\mathbf{T}\tilde{\mathbf{z}}_{\text{LRA-ZF}} - \mathbf{x} \right) \right\|^2, \tag{3.60}$$

where $\tilde{\mathbf{R}}'$ is the CF - or equivalently [Zim07] the QRD output - of $\tilde{\mathbf{R}}\mathbf{T}^{-1}$, making an ODN study possible since the search is made in ξ^{n_T}. Also, since the unconstrained LRA-ZF estimate is considered, there is no quantization in the reduced domain either. This solution is denoted as ODN LRA-ZF K-Best.

Proof. By reconsidering Equation (3.57), the ML expression can be equivalently rearranged:

$$\begin{aligned}
\hat{\mathbf{x}}_{\text{LRA-ZF SD}} &= \underset{\mathbf{x}\in\xi^{n_T}}{\arg\min} \left\| \tilde{\mathbf{R}} \left(\tilde{\mathbf{z}}_{\text{LRA-ZF}} - \mathbf{z} \right) \right\|^2 \\
&= \underset{\mathbf{x}\in\xi^{n_T}}{\arg\min} \left\| \tilde{\mathbf{R}} \left(\mathbf{T}^{-1}\mathbf{T}\tilde{\mathbf{z}}_{\text{LRA-ZF}} - \mathbf{T}^{-1}\mathbf{x} \right) \right\|^2 \\
&= \underset{\mathbf{x}\in\xi^{n_T}}{\arg\min} \left\| \tilde{\mathbf{R}}\mathbf{T}^{-1} \left(\mathbf{T}\tilde{\mathbf{z}}_{\text{LRA-ZF}} - \mathbf{x} \right) \right\|^2.
\end{aligned} \tag{3.61}$$

The idea is now to make all the $\mathbf{x}$ entries iteratively independent - from previous layers - through the triangular shape induced by a CF/QRD output:

$$\hat{\mathbf{x}}_{\text{LRA-ZF SD}} = \underset{\mathbf{x}\in\xi^{n_T}}{\arg\min} \left\| \tilde{\mathbf{R}}' \left(\mathbf{T}\mathbf{z}_{\text{LRA-ZF}} - \mathbf{x} \right) \right\|^2 \tag{3.62}$$

where $\tilde{\mathbf{R}}'$ is the CF/QRD output of $\tilde{\mathbf{R}}\mathbf{T}^{-1}$. □

The cleverness of the presented technique comes from the slicing of the SD by bypassing the neighbourhood study in the reduced domain, if advantageous. Also and similarly to what has

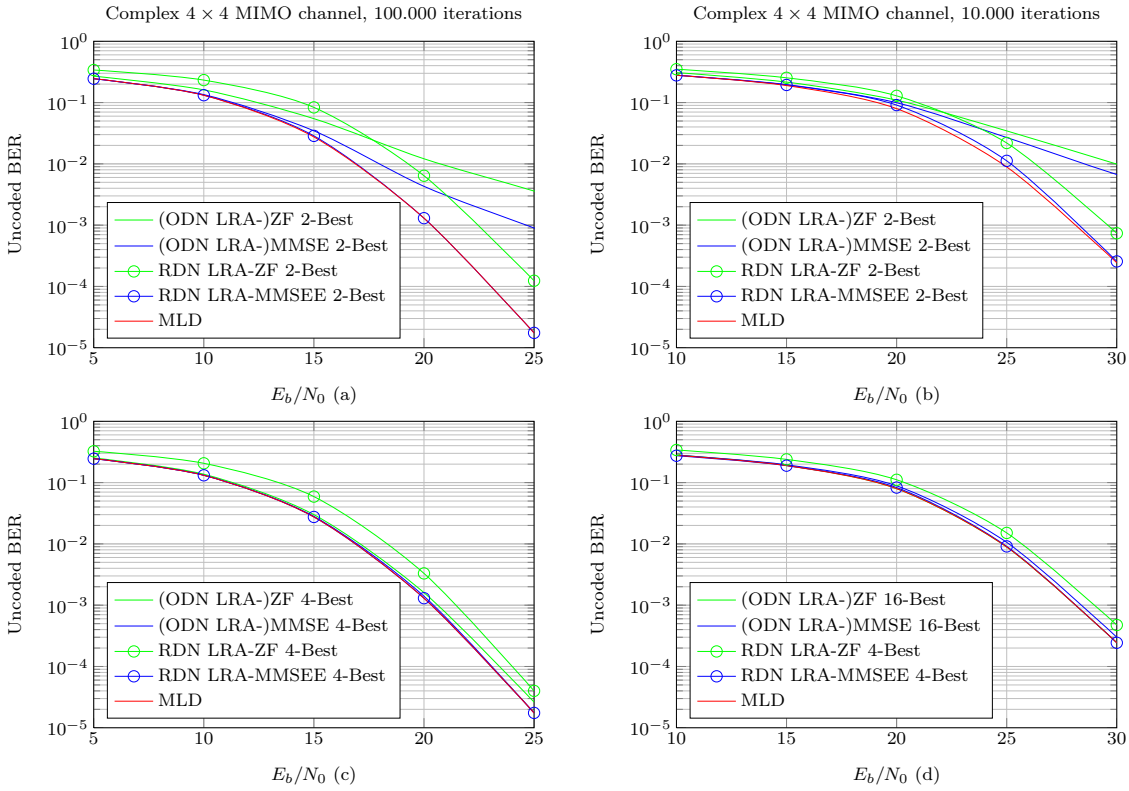

Figure 3.20: Uncoded BER as a function of E_b/N_0, Complex Rayleigh 4×4 SM-MIMO-SC system, (ODN LRA-)ZF 2/4(16)-Best, (ODN LRA-)MMSE 2/4(16)-Best, RDN LRA-ZF 2/4-Best, RDN LRA-MMSE 2/4-Best and ML detectors, 4-QAM modulations at each layer (a,c) and 16-QAM modulations at each layer (b,d).

been done in Section 3.4.5, a novel formula may be proposed, centred on an unconstrained LRA-MMSE solution. In general terms, the ML expression equivalently rewrites:

$$\hat{\mathbf{x}}_{\text{LRA-LD SD}} = \underset{\mathbf{x}\in\xi_{\mathbb{C}}^{n_T}}{\arg\min} \left\{ \left\| \tilde{\mathbf{R}}' \left(\mathbf{T}\tilde{\mathbf{z}} - \mathbf{x} \right) \right\|^2 \right\},$$

where

$$\tilde{\mathbf{R}}^H\tilde{\mathbf{R}} = \begin{cases} \tilde{\mathbf{H}}^H\tilde{\mathbf{H}} & \text{in the LRA-ZF case,} \\ \tilde{\mathbf{H}}^H\tilde{\mathbf{H}} + \sigma_n^2\mathbf{T}^H\mathbf{T} & \text{in the LRA-MMSE case,} \end{cases} \tag{3.63}$$

and

$$\left(\tilde{\mathbf{R}}'\right)^H \left(\tilde{\mathbf{R}}'\right) = \left(\mathbf{T}^{-1}\right)^H \tilde{\mathbf{R}}^H\tilde{\mathbf{R}}\mathbf{T}^{-1}, \tag{3.64}$$

by noting that $\tilde{\mathbf{R}}'$ is upper triangular with real diagonal elements and $\tilde{\mathbf{z}}$ is any - consistently with the $\tilde{\mathbf{R}}$ expression - LRA-LD unconstrained linear estimate.

By rearranging Equation (3.64), it is clear that it comes down on the classical SD expression with ODN study. Consequently, the performance of this detector - and thus its advantages and drawbacks - will be similar while the whole preprocessing step remains those of the efficient LRA-MMSEE K-Best. In particular, this solution outperforms the solution introduced in Section 3.4.5 in the 4-QAM case - and in the 4-QAM case only -, while reusing the computational

complexity of the preprocessing step, thus leading to an efficient re-use of available resources. Also, while it can be noted that the QRD computational complexity of a quasi-triangular matrix may be reduced compared to a classical QRD, it is not addressed in the present work.

At this step, the point of hard-decision detectors has been addressed. In the sequel, the soft-decision extension is eventually shown to be - relatively - straight-forward with some of the techniques introduced above. In the next chapter, each hard-decision detector is re-introduced by including the soft-decision aspect. In particular, the question is how to maintain in soft-decision the promising hard-decision performance of a detector.

Chapter 4

Soft-Decision Near Maximum-Likelihood detectors

Contents

In order to approach the channel capacity, redundancy and interleaving provide a practical way of processing. This is denoted as channel coding. In such schemes, soft-decisions, *i.e.* weighted decisions, of coded symbols are produced at the detector output. Consequently and compared to hard-decision, a performance improvement is induced [Ber93]. This aspect is a strong practical requirement and leads to considerations that are addressed in the present Chapter.

4.1 Log-Likelihood Ratios Generation

4.1.1 Log-Likelihood Ratio Definition

Soft-decisions of coded symbols are typically produced from the detector's output, plus any available side information, and passed on to the decoder in the form of bit-wise LLRs. In the latter, the sign represents the decision and the magnitude the reliability. In the classical considerations that are introduced below, the logical $\{0, 1\}$ bit patterns are respectively mapped onto the set of amplitude levels $\mathbb{B} = \{+1, -1\}$ - through an antipodal bit-to-symbol mapping, such as BPSK [3GP09b]

and due to the AWGN statistical properties [Bar03c] -, denoted as the channel's input. The BPSK modulation assumption has been made for the sake of simplicity and can be extended to any QAM constellation.

Before making an observation, the *a priori* probabilities for the bit $\mathbf{b}_k^l$ - related to the l-th transmitted symbol and to the k-th bit inside - read $\Pr\left\{\mathbf{b}_k^l = -1\right\}$ and $\Pr\left\{\mathbf{b}_k^l = +1\right\}$. The probability distribution of the random binary variable $\mathbf{b}_k^l$ is uniquely specified by the parameter $\Pr\left\{\mathbf{b}_k^l = -1\right\}$ since $\Pr\left\{\mathbf{b}_k^l = +1\right\} = 1 - \Pr\left\{\mathbf{b}_k^l = -1\right\}$. Thus, by introducing the conventional log ratio:

$$r = \log \frac{\Pr\left\{\mathbf{b}_k^l = -1\right\}}{\Pr\left\{\mathbf{b}_k^l = +1\right\}}, \tag{4.1}$$

its sign gives an estimate of the most likely bit value while its magnitude indicates the reliability of this estimate. Clearly from Equation (4.1):

$$r = \begin{cases} 0, & \mathbf{b}_k^l = -1 \text{ and } \mathbf{b}_k^l = +1 \text{ are equally likely,} \\ > 0, & \mathbf{b}_k^l = -1 \text{ is more likely than } \mathbf{b}_k^l = +1, \\ < 0, & \mathbf{b}_k^l = +1 \text{ is more likely than } \mathbf{b}_k^l = -1, \\ +\infty, & \mathbf{b}_k^l = -1, \\ -\infty, & \mathbf{b}_k^l = +1. \end{cases} \tag{4.2}$$

After making an observation, the *A Posteriori* Probability (APP) of $\mathbf{b}_k^l$ arises and is conditioned on the received signal $\mathbf{y}$. For the ML decoder - not for the MAP decoder since the whole bits sequence is not considered -, it is defined as:

$$\log \frac{\Pr\left\{\mathbf{b}_k^l = -1 \mid \mathbf{y}\right\}}{\Pr\left\{\mathbf{b}_k^l = +1 \mid \mathbf{y}\right\}}, \tag{4.3}$$

which - by denoting $f(\mathbf{y} \mid \mathbf{b}_k^l = i)$ *s.t.* $i \in \mathbb{B}$ as a *conditional PDF* [Bar03c] and through the Bayes' theory - rewrites:

$$\log \frac{f(\mathbf{y} \mid \mathbf{b}_k^l = -1) \Pr\left\{\mathbf{b}_k^l = -1\right\} / \Pr\left\{\mathbf{y}\right\}}{f(\mathbf{y} \mid \mathbf{b}_k^l = +1) \Pr\left\{\mathbf{b}_k^l = +1\right\} / \Pr\left\{\mathbf{y}\right\}}. \tag{4.4}$$

We assume that the a priori probabilities read $\Pr\left\{\mathbf{b}_k^l = -1\right\} = \Pr\left\{\mathbf{b}_k^l = +1\right\}$, which is true due to scrambling. Thus and through the logarithm introduction, Equation (4.4) simplifies to:

$$\log \frac{f(\mathbf{y} \mid \mathbf{b}_k^l = -1)}{f(\mathbf{y} \mid \mathbf{b}_k^l = +1)}. \tag{4.5}$$

The received vector can be modelled as a multivariate Gaussian random variable. Thus, similarly to Equation (2.44) and starting from Equation (4.5), the LLRs at the detector's output - also named channel observations in Section 2.2 and denoted here as $\Lambda(\mathbf{b}_k^l \mid \mathbf{y}, \mathbf{H})$ are fed to a turbo decoder - simplify to the expression:

$$\Lambda(\mathbf{b}_k^l \mid \mathbf{y}, \mathbf{H}) = \log \frac{\sum_{\mathbf{x} \in \mathbb{X}_{k,n}^{-1}} e^{\frac{1}{2}(\mathbf{y}-\mathbf{H}\mathbf{x})^H \Phi_{\mathbf{nn}}^{-1}(\mathbf{y}-\mathbf{H}\mathbf{x})}}{\sum_{\mathbf{x} \in \mathbb{X}_{k,n}^{+1}} e^{\frac{1}{2}(\mathbf{y}-\mathbf{H}\mathbf{x})^H \Phi_{\mathbf{nn}}^{-1}(\mathbf{y}-\mathbf{H}\mathbf{x})}}, \tag{4.6}$$

where $\mathbb{X}_{k,n}^i, i \in \mathbb{B}$ is the set of the $2^{n_T \log_2\{|\xi|\}-1}$ bit vectors $\mathbf{x}$ such that:

$$\begin{aligned} \mathbb{X}_{k,n}^{-1} &= \left\{\mathbf{x}, \mathbf{b}_k^l = -1\right\}, \\ \mathbb{X}_{k,n}^{+1} &= \left\{\mathbf{x}, \mathbf{b}_k^l = +1\right\}. \end{aligned} \tag{4.7}$$

Under the assumption of statistically independent code bits - also ensured by interleaving and which implies splitting up joint probabilities into products [Zim07] - the LLRs at the detector's output can be calculated through the well-known [Hoc03, Hag96] relation:

$$\Lambda(\mathbf{b}_k^l \mid \mathbf{y}, \mathbf{H}) = \log \frac{\sum_{\mathbf{x}\in\mathbb{X}_{k,n}^{-1}} e^{-\frac{1}{2\sigma_n^2}(\|\mathbf{y}-\mathbf{H}\mathbf{x}\|^2)}}{\sum_{\mathbf{x}\in\mathbb{X}_{k,n}^{+1}} e^{-\frac{1}{2\sigma_n^2}(\|\mathbf{y}-\mathbf{H}\mathbf{x}\|^2)}}, \tag{4.8}$$

where we recall (see Section 2.5) that σ_n^2 is the noise variance. Despite aforementioned complexity-reducing derivations, solving Equation (4.8) still requires an infeasible sum over $2^{n_T \log_2\{|\xi|\}-1}$ terms for both the numerator and denominator. As an answer, a classical further simplification is possible for implementation.

4.1.2 Max-Log Approximation

For the sake of DSP implementation, the max-log approximation of the extrinsic LLR is commonly considered. It relies on the Jacobian logarithm [Rob95] defined as:

$$\begin{aligned} jaclog\left\{d_1 + d_2\right\} &\triangleq \log\left\{e^{d_1} + e^{d_2}\right\} \\ &= \max\left\{d_1, d_2\right\} + \log\left\{1 + e^{-|d_1-d_2|}\right\} \\ &\approx \max\left\{d_1, d_2\right\}. \end{aligned} \tag{4.9}$$

While the term $\log\left\{1 + e^{-|d_1-d_2|}\right\}$ - denoted as the residual term - can be stored in an one-dimensional Look-Up Table (LUT), it is shown in [Rob95] that only a tiny performance degradation occurs. This result is extended to

$$\begin{aligned} \log\left\{\sum_{i=1}^{n} e^{-d_i^2}\right\} &= \log\left\{e^{\max\left\{-d_i^2\right\}}\right\} + \log\left\{e^{-|d_1^2-\max\left\{-d_i^2\right\}|} + \cdots + 1 + \cdots + e^{-|d_n^2-\max\left\{-d_i^2\right\}|}\right\} \\ &= \log\left\{e^{-\min\left\{d_i^2\right\}}\right\} + \log\left\{e^{-|d_1^2+\min\left\{d_i^2\right\}|} + \cdots + 1 + \cdots + e^{-|d_n^2+\min\left\{d_i^2\right\}|}\right\} \\ &\approx -\min\left\{d_i^2\right\}. \end{aligned} \tag{4.10}$$

In the present work, this approximation is considered. The APP in Equation (4.8) thus rewrites:

$$\Lambda(\mathbf{b}_k^l \mid \mathbf{y}, \mathbf{H}) \approx -\min_{\mathbf{x}\in\mathbb{X}_{k,n}^{-1}} \left\{\frac{1}{2\sigma_n^2}(\|\mathbf{y}-\mathbf{H}\mathbf{x}\|^2)\right\} + \min_{\mathbf{x}\in\mathbb{X}_{k,n}^{+1}} \left\{\frac{1}{2\sigma_n^2}(\|\mathbf{y}-\mathbf{H}\mathbf{x}\|^2)\right\}, \tag{4.11}$$

where the minimum element is obtained by successively applying the simple $\min\{\cdot\}$ operator - over two values.

4.2 Classical Algorithms Update

4.2.1 Maximum Likelihood

By noting that the max-log approximation is particularly appropriate in the high SNR range - that induces $\mathbf{y}$ to be very close to $\mathbf{H}\mathbf{x}$ in at least one case -, the optimal APP LLR of the bit $\mathbf{b}_k^l$ becomes advantageously approximated by:

$$\Lambda(\mathbf{b}_k^l \mid \mathbf{y}, \mathbf{H}) \approx -\frac{1}{2\sigma_n^2}\left(-\min_{\mathbf{x}\in\mathbb{X}_{k,n}^{-1}} \left\{\|\mathbf{y}-\mathbf{H}\mathbf{x}\|^2\right\} + \min_{\mathbf{x}\in\mathbb{X}_{k,n}^{+1}} \left\{\|\mathbf{y}-\mathbf{H}\mathbf{x}\|^2\right\}\right). \tag{4.12}$$

While it is not optimal, the soft-output MLD with the max-log approximation will be considered as the reference solution, according to a performance point of view.
However and despite the aforementioned simplifications, 4.12 is not feasible due to its exponential computational complexity. In particular and similarly to the discussion in Section 2.7, $|\xi|^{n_T}$ hypotheses have to be considered within each min term and for each bit sequence $\mathbf{b}_k^l$.

4.2.2 Linear Detectors

Aiming at suppressing ILI and in accordance with Section 2.7, LDs - including ZF and MMSE - decouple the whole MIMO detection step into a set of independent MISO detection steps, layer by layer. Following advantages and drawbacks of LDs by comparison to the MLD (see Section 2.7.2), both the ZF and MMSE approaches offer a low overall computational complexity. In particular, the $|\xi|\, n_T$ Euclidean distance computations - required in Equation 4.12 - are advantageously applied on scalars. Given a layer l and through [But04, Col04, See04, Fer08], the LLR approximates:

$$\Lambda(\mathbf{b}_k^l \mid \tilde{\mathbf{y}}_l, \mathbf{G}_{\text{LD}}) \approx -\frac{1}{2(\sigma_{LD})_l^2}\left(-\min_{\mathbf{x}_l \in \mathbb{X}_{k,l}^{-1}}\left\{\left|\tilde{\mathbf{y}}_l - \mathbf{x}_l\right|^2\right\} + \min_{\mathbf{x}_l \in \mathbb{X}_{k,l}^{+1}}\left\{\left|\tilde{\mathbf{y}}_l - \mathbf{x}_l\right|^2\right\}\right), \tag{4.13}$$

where $\tilde{\mathbf{y}} = \mathbf{G}_{\text{LD}}\mathbf{y}$ and, compared to Equation (4.12), norms have been replaced by absolute values. The LLR expression is a function of the equalization matrix, that is recalled to read:

$$\mathbf{G}_{\text{LD}} = \begin{cases} \mathbf{G}_{\text{ZF}} = \left(\mathbf{H}^H\mathbf{H}\right)^{-1}\mathbf{H}^H & \text{in the ZF case,} \\ \mathbf{G}_{\text{MMSE}} = \left(\mathbf{H}^H\mathbf{H} + \sigma_n^2\mathbf{I}_{n_T}\right)^{-1}\mathbf{H}^H & \text{in the MMSE case.} \end{cases} \tag{4.14}$$

In the MMSE case only and because $\mathbf{G}_{\text{MMSE}}\mathbf{H} \neq \mathbf{I}_{n_T}$, residual ILIs remain and - dually - diagonal elements of $\mathbf{G}_{\text{MMSE}}\mathbf{H}$ are not exactly one-valued. The latter aspect makes the MMSE detector biased, thus inducing - for its removal - the left-multiplication of $\mathbf{G}_{\text{MMSE}}$ by the diagonal matrix $\mathbf{B}$ such as its diagonal entries read [Col04]:

$$\mathbf{B}_{l,l} = \frac{\text{SINR}_l + 1}{\text{SINR}_l}, \tag{4.15}$$

where

$$\text{SINR}_l = \frac{1}{\sigma_n^2\left[\left(\mathbf{H}^H\mathbf{H} + \sigma_n^2\mathbf{I}_{n_T}\right)^{-1}\right]_{l,l}} - 1. \tag{4.16}$$

The unbiased expression of Equations (4.14) thus rewrites:

$$\mathbf{G}_{\text{LD}} = \begin{cases} \mathbf{G}_{\text{ZF}} = \left(\mathbf{H}^H\mathbf{H}\right)^{-1}\mathbf{H}^H & \text{in the ZF case,} \\ \mathbf{G}_{\text{MMSE}} = \mathbf{B}\left(\mathbf{H}^H\mathbf{H} + \sigma_n^2\mathbf{I}_{n_T}\right)^{-1}\mathbf{H}^H & \text{in the MMSE case.} \end{cases} \tag{4.17}$$

While the ZF detector is less complex than the MMSE due to the required computation - for each layer - of bias and SINR terms, the latter outperforms the ZF, which can be verified in Figure 4.1. In particular, this additional processing is negligible compared to the computation of $\mathbf{G}_{\text{LD}}$.

In both the ZF and MMSE cases, the AWGN $\mathbf{n}$ has been coloured [Fer08] such as it becomes $\mathbf{G}_{\text{LD}}\mathbf{n}$. In particular and for each layer l, the diagonal entries of their covariance matrices read [Col04]:

$$\begin{cases} (\sigma_{ZF})_l^2 = \sigma_n^2\sum_{i=1}^{n_T}\left|(\mathbf{G}_{ZF})_{l,i}\right|^2 & \text{in the ZF case,} \\ (\sigma_{MMSE})_l^2 = \left((\mathbf{G}_{MMSE})_{l,l} - 1\right)/\left(\mathbf{G}_{MMSE}\right)_{l,l} & \text{in the MMSE case.} \end{cases} \tag{4.18}$$

From an implementation point of view, the computational complexity of the ZF and MMSE metrics calculation can be further reduced by pointing out that:

$$|\tilde{\mathbf{y}}_l - \mathbf{x}_l|^2 = \Re\{\tilde{\mathbf{y}}_l - \mathbf{x}_l\}^2 + \Im\{\tilde{\mathbf{y}}_l - \mathbf{x}_l\}^2 . \tag{4.19}$$

On top of the separate - for each layer - LLR calculation, the considered QAM mapping properties induce that the metric can be separately computed through the in-phase and quadrature components, *i.e.* real and imaginary parts, respectively. Thus, it leads to the following expression of the LLR [Col04]:

$$\Lambda(\mathbf{b}_k^l \mid \tilde{\mathbf{y}}_l, \mathbf{G}_{\text{LD}}) \approx \frac{1}{2(\sigma_{LD})_l^2} \Delta\left(\mathbf{b}_k^l \mid \tilde{\mathbf{y}}_l\right), \tag{4.20}$$

where the term $\Delta\left(\mathbf{b}_k^l \mid \tilde{\mathbf{y}}_l\right)$ can be efficiently replaced by a linear equation [Col04]. The latter is a function of $\tilde{\mathbf{y}}_l$ and depends on the bit position only.
We consider the 16-QAM constellation introduced in Figure 2.1 and its corresponding QAM mapping. By considering the first bit position, its value indicates if the symbol is set in the right or left part of the plane. Thus, the imaginary part in the metric computation remains constant and finally cancels out in the LLR computation, according to Equation (4.13). By focusing on the in-phase component of $\tilde{\mathbf{y}}_l$ - related to bits 1 and 3 within a symbol -, three distinct cases must be considered per symbol. In particular, it leads to:

$$\Delta\left(\mathbf{b}_k^l \mid \tilde{\mathbf{y}}_l\right) = \begin{cases} 4\Re\{\tilde{\mathbf{y}}_l\} & \text{for } k = 1 \text{ and } |\Re\{\tilde{\mathbf{y}}_l\}| \leq 2, \\ 8\Re\{\tilde{\mathbf{y}}_l\} - 8sgn\{\Re\{\tilde{\mathbf{y}}_l\}\} & \text{for } k = 1 \text{ and } |\Re\{\tilde{\mathbf{y}}_l\}| \geq 2, \\ 8 - 4\Re\{\tilde{\mathbf{y}}_l\} & \text{for } k = 3 \text{ and } \forall\, \Re\{\tilde{\mathbf{y}}_l\}, \end{cases} \tag{4.21}$$

where $sgn(\cdot)$ is the signum function.

While this approximation has been applied to the present work, it is not addressed in detail since it is straight-forwardly applied from [Col04]. The only difference lies in the considered QAM mapping for the constellations that have been introduced in Figure 2.1. Thus, the set of linear equations for $\Delta\left(\mathbf{b}_k^l \mid \tilde{\mathbf{y}}_l\right)$ presented in [Col04] remains correct, only the bit position indexes have been updated.

In this chapter, the - coded - BER performance of multiple detectors is provided for a 4×4 SM-MIMO-SC system, for the two extreme 4-QAM and 64-QAM modulations. In the sequel and unless otherwise specified, our simulation conditions rely on settings that are specified here once and for all.
At the transmitter, data bits are first serial-to-parallel-converted into four data streams and are segmented into blocks containing a selected number of bits per packet frame, according to the employed MCS. Each information data sequence is independently turbo encoded, according to the considerations in Section 2.2. While the original coding rate is $R = \frac{1}{3}$, the sequences are then punctured, thus reaching the desired rate when the resultant encoded sequence is data-modulated. In particular and according to the Fixed Reference Channel (FRC) specified in 3GPP reference tests [3GP09d], the considered rates are $R = \frac{1}{2}$ and $R = \frac{3}{4}$ for 4-QAM and 64-QAM constellations, respectively. Blocks of information bits are fed to the channel encoder, and subsequently transmitted over a complex Rayleigh fading 4×4 MIMO channel, by forcing to 1026 the number of transmitted symbols per block, independently of the employed modulation. It presently corresponds to 1024 and 4608 transmitted bits per block, to within one rounding. By iterating 100 and 20 blocks with 4-QAM and 64-QAM constellations, respectively, approximatively 10^5 bits are considered for each SNR value. Thus, we consider that it is sufficient for obtaining smooth curves up to 10^{-3} BER. In a 4×4 SM-MIMO - SC or OFDM equally - system, there is a simple one-to-one mapping between layers and transmit antenna ports. Thus the layer mapping/demapping

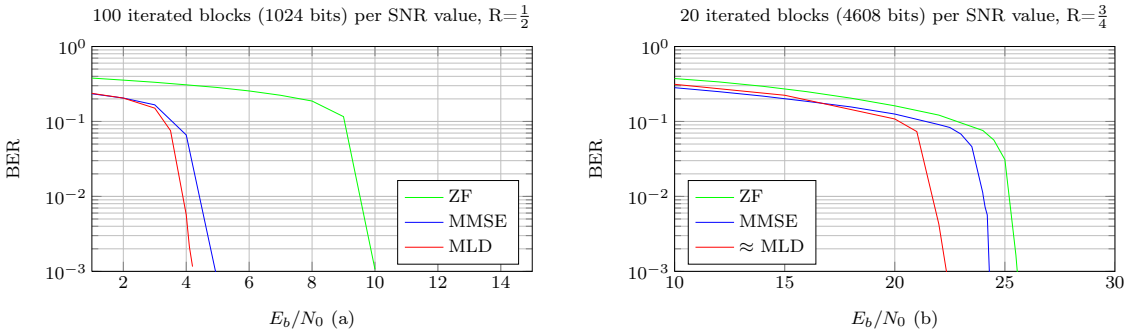

Figure 4.1: BER as a function of E_b/N_0, Complex Rayleigh 4×4 SM-MIMO-SC system, ZF, MMSE and ML detectors, 4-QAM modulations at each layer (a) and 64-QAM modulations at each layer (b).

blocks - introduced in Figure 2.6 - are transparent. Also, the OL mode is considered, thus no feedback loop is required. Then, SC transmissions only are simulated. There is no loss of generality on the performance results. The impact of an OFDM modulation on the overall computational complexity will be described in chapter 5. Last, for each block and according to the discussion in Section 2.2, 10 iterations within the turbo decoder are performed.

In Figure 4.1, the BER performance of the aforementioned LDs and of the MLD introduced in 4.2.1 are depicted and will be considered as references in the sequel. The performance gain compared to uncoded transmission in clear by comparison to Figure 2.10.
With the use of 64-QAM modulations in a 4×4 system, the MLD has been approximated by a ZF-SQRD-based 64-Best. Also, the max-log approximation in Equation (4.11) is employed when possible. Otherwise - this aspect will be introduced in Section 4.4.3 -, the LLR magnitudes are set to an arbitrary - and absolute - value of ± 3. This is shown in [Zim07] to almost achieve the MLD performance while being drastically faster to run. It is denoted in the present work as $\approx$ MLD.

As a conclusion, the presented solution for LDs is efficient for implementation in the sense of its very low complexity that has been further reduced since both the Euclidean distances computation and the minimization step have been skipped in Equation (4.14).
Nevertheless and while the approximation in Equation (4.20) only induces a tiny performance loss, the LDs performance is not sufficient. It is particularly true in presence of ill-conditioned channels, which arise with transmit and/or the receive spatial correlation. Thus, advanced techniques are necessary for achieving near-MLD performance.

4.2.3 Decision-Feedback Detector

The advantage of (O)DFDs over LDs for uncoded tranmissions has been stated in Section 3.1.4. We recall that their interest lies in reducing the main drawback of LDs, namely ILIs. Here, the soft interference cancellation is introduced but maintaining its advantage over soft-LDs is challenging.

Similarly to Section 3.1, the presented QRD-based detector allows an iterative computation of

LLRs. In particular, their expression reads [Zim07]:

$$\Lambda(\mathbf{b}_k^l \mid \tilde{\mathbf{y}}_l, \hat{\mathbf{x}}_{l+1:n_T}, \mathbf{R}) \approx -\frac{1}{2\sigma_n^2}\left(- \min_{\mathbf{x}_l \in \mathbb{X}_{k,l}^{+1}} \left\{ \left| \tilde{\mathbf{y}}_l - \mathbf{R}_{l,l}\mathbf{x}_l - \sum_{i=l+1}^{n_T} \mathbf{R}_{l,i}\hat{\mathbf{x}}_i \right|^2 \right\} + \min_{\mathbf{x}_l \in \mathbb{X}_{k,l}^{-1}} \left\{ \left| \tilde{\mathbf{y}}_l - \mathbf{R}_{l,l}\mathbf{x}_l - \sum_{i=l+1}^{n_T} \mathbf{R}_{l,i}\hat{\mathbf{x}}_i \right|^2 \right\} \right), \tag{4.22}$$

where $\tilde{\mathbf{y}} = \mathbf{Q}^H\mathbf{y}$. Also, the LLR is a function of $\mathbf{R}$ and of the previously detected symbol(s), from the layer $n+1$ to n_T. However, conclusions about the interest of (O)DFDs presented in Section 2.7 - in the hard-decision case - do not remain correct. It is for this reason that the LLR expression relies on previous hard-decision (in opposition to soft-decision) - which is clear from Equation (4.22) -, thus leading to a loss in the channel coding gain.

The issue presented above can be addressed - at great cost - by subtracting soft-estimates $\tilde{\mathbf{x}}$ while using their variance. In particular, the residual noise is considered. The initial idea is proposed in [Cho00] and further developed in [Bit06a]. The main steps are summarized in the sequel. Namely, the LLR preferably reads:

$$\Lambda(\mathbf{b}_k^l \mid \tilde{\mathbf{y}}_l, \tilde{\mathbf{x}}_{l+1:n_T}, \mathbf{R}) \approx -\frac{1}{2(\sigma_{DFD})_l^2}\left(- \min_{\mathbf{x}_l \in \mathbb{X}_{k,l}^{+1}} \left\{ \left| \tilde{\mathbf{y}}_l - \mathbf{R}_{l,l}\mathbf{x}_l - \sum_{i=l+1}^{n_T} \mathbf{R}_{l,i}\tilde{\mathbf{x}}_i \right|^2 \right\} + \min_{\mathbf{x}_l \in \mathbb{X}_{k,l}^{-1}} \left\{ \left| \tilde{\mathbf{y}}_l - \mathbf{R}_{l,l}\mathbf{x}_l - \sum_{i=l+1}^{n_T} \mathbf{R}_{l,i}\tilde{\mathbf{x}}_i \right|^2 \right\} \right), \tag{4.23}$$

where $\tilde{\mathbf{x}}_i$ denotes the expectation of $\mathbf{x}_i$ over the symbols in ξ, according to their a priori probability of occurrence. Also, ILIs are considered in the noise power, which subsequently reads:

$$(\sigma_{DFD})_l^2 = \sigma_n^2 + \sum_{i=l+1}^{n_T} \left\{ |\mathbf{R}_{l,i}|^2 \, var\left\{\mathbf{x}_i\right\} \right\}, \tag{4.24}$$

where $var\left\{\cdot\right\}$ denotes the variance of $\mathbf{x}_i$ over the symbols in ξ, according to their probability of occurrence.

In the - required - consideration of channel coding, (O)DFDs are very sub-optimal - in particular for high-order modulations - due, among others [Zim07], to error propagation. Occasionally, it is even worse than with MMSE [Zim06], in particular in the low SNR range. Moreover, this scheme is computationally costly [Bit06a]. Consequently, this solution is not retained in the rest of the present work.

4.3 Lattice-Reduction-Aided Linear Detectors

In the present section, a new step - that follows a hard-decision LRA detector - is introduced and aims at providing soft-output LRA detectors. It is important to highlight that these steps are completely separated, in particular for the comprehension of the techniques that are further introduced in Section 4.5.

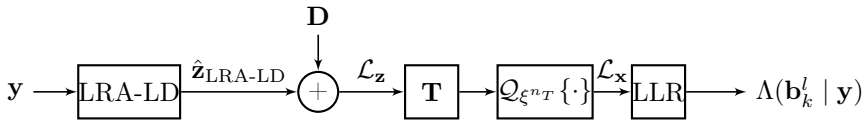

Figure 4.2: Perturbation matrix method for achieving soft-decision LRA-LD.

4.3.1 Perturbation Method

As mentioned in [Mil06, Pon07] and subsequently to a hard-decision LRA-LD, a set of candidates can be used to efficiently approximate the per-bit LLRs.
In particular, this list of possible solutions - unordered in the present case - is generated in the reduced domain, and can be considered as an additional neighbourhood. This neighbourhood is actually seen as a set of displacements $\mathbf{D}$ - determined off-line - that is denoted in [Mil06, Pon07] as a *fixed perturbation* matrix and that is applied jointly on the whole symbols vector. It should be noted that it is different to an SD technique, where the neighbourhood is generated layer by layer.
We denote a list $\mathcal{L}_{\mathbf{x}}$ of candidates that belong to the original domain and $\mathcal{L}_{\mathbf{z}}$ when they belong to the reduced domain. Also, $\mathcal{L}$ implicitly corresponds to $\mathcal{L}_{\mathbf{x}}$, unless otherwise specified. A neighbourhood in the reduced domain is generated by applying a pre-determined set of displacements - constituted of N n_T-dimensional column vectors - around a quantized LRA-LD hard-output $\hat{\mathbf{z}}_{\text{LRA-LD}}$. In particular, $N = 4n_T + 1$ and $\mathcal{L}_{\mathbf{z}}$ reads:

$$\begin{aligned}\mathcal{L}_{\mathbf{z}} &= \hat{\mathbf{z}}_{\text{LRA-LD}} + \begin{bmatrix} 0 & +1 & -1 & +j & -j & \cdots & 0 & 0 & 0 & 0 \\ 0 & 0 & 0 & 0 & 0 & \cdots & 0 & 0 & 0 & 0 \\ \cdots & \cdots & \cdots & \cdots & \cdots & \cdots & \cdots & \cdots & \cdots & \cdots \\ 0 & 0 & 0 & 0 & 0 & \cdots & 0 & 0 & 0 & 0 \\ 0 & 0 & 0 & 0 & 0 & \cdots & +1 & -1 & +j & -j \end{bmatrix} \\ &= \hat{\mathbf{z}}_{\text{LRA-LD}} + \mathbf{D}.\end{aligned} \tag{4.25}$$

In Figure 4.2, the structure of the solution is presented in a block-diagram manner. While an LRA-LD hard-estimate $\hat{\mathbf{z}}_{\text{LRA-LD}}$ is provided in the first block - in accordance to considerations in Section 3.3 - a list of neighbour candidates is produced according to the discussion above. Subsequently and similarly to Equation (3.44) or Equation (3.45), the list of candidates in the reduced domain is transformed to the original one - and denoted as $\mathcal{L}_{\mathbf{x}}$ - such as:

$$\mathcal{L}_{\mathbf{x}} = \mathcal{Q}_{\xi^{n_T}}\{\mathbf{T}\mathcal{L}_{\mathbf{z}}\}, \tag{4.26}$$

where the quantization step is necessary due to the presence of noise that induces that some candidates may not map to any existing constellation points in the original domain. Through $\mathcal{L}_{\mathbf{x}}$, it is then possible to compute the LLR magnitudes by using the max-log approximation-based Equation (4.11). However, this equation is not necessarily applicable. A classical solution consists in the use of a clipping value otherwise, which is clearly stated in [Pon07]. This key aspect is addressed in detail in Section 4.4.3. While it is proposed in [Mil06] to avoid repeated candidates within the list through an union-based solution - that induce anyway wasted resources -, it is not necessary for the LLR computation considered in the present work, namely with max-log approximation.

Due to its very low computational complexity, the perturbation method is efficient for implementation and can be applied to any LRA-LD hard-output. Moreover, a parallel implementation is clearly possible.

However, its performance remains limited [Mil06, Pon07]. Additionally and while the columns of $\mathbf{D}$ are ordered according to their increasing Euclidean norm [Mil06], the corresponding list output in the original constellation is not ordered. Thus it still induces additional computations for some of the smart techniques presented in Section 4.4 and does not necessarily reach the list of candidates that offer the highest probability of being transmitted.

4.3.2 Nearest Neighbour Method

While applying fixed perturbations - to the LRA-LD estimate - offers an efficient low complexity solution, the corresponding performance remains very sub-optimal. Even if a larger set of perturbation can be planned in order to reach the optimum, the presented solution outperforms the latter with a different approach.

Strictly speaking, Ponnampalam *et al.* are the first to propose a distance-based additional - subsequent to the LRA-LD step - neighbourhood study in the reduced domain to provide soft-estimates for LRA-LDs. In particular, it relies on the search algorithm proposed in [Rei05], which should be noted to be different to the LRA-ZF-centred SD introduced in Section 3.4. The algorithm has been made suitable following an LR step - namely adjusted to the reduced domain - by modifying the distance criterion, drawn from [Pon07]:

$$d_z\left(\tilde{\mathbf{z}}_{\text{LRA-LD}}, \mathbf{z}\right) = \sum_{i=1}^{n_T} \frac{\left\|\tilde{\mathbf{H}}_{:,i}\right\|^2}{\sigma_n^2} \left|(\tilde{\mathbf{z}}_{\text{LRA-LD}})_i - \mathbf{z}_i\right|^2. \tag{4.27}$$

This relation is obtained by assuming that the inverse of the covariance matrix of $\tilde{\mathbf{n}}$, that reads:

$$\mathbf{R}^{-1} = \frac{2}{\sigma_n^2}\tilde{\mathbf{H}}^H\tilde{\mathbf{H}}, \tag{4.28}$$

is diagonal, which is almost true since $\tilde{\mathbf{H}}$ is almost orthogonal.

For each call of the algorithm in [Rei05] and until a list output $\mathcal{L}_{\mathbf{x}}$ of size K is generated, the nearest neighbour in the reduced domain is produced. In particular, the algorithm considers a list of nodes in a tree search. The nearest neighbour is obtained w.r.t. Equation (4.27) and removed from the input/output list while another candidate has been added to the latter, thus maintaining a list of nodes. Clearly, the closest vector - that corresponds to the first nearest neighbour - to $\check{\mathbf{z}}$ is $\hat{\mathbf{z}}$.
Also and for each call of the algorithm as well, the candidate is checked if it belongs to the original constellation, and if so it is added to $\mathcal{L}_{\mathbf{x}}$. In [Pon07], repeated candidates within the list are not avoided.

Through the solution presented above, a significant performance improvement compared to Section 4.3.1 is achieved. Nevertheless, the remaining SNR offset compared to optimum is still large, even from 16-QAM constellations with complex 4×4 MIMO channels. In particular, the optimal performance is not reached for a large neighbourhood study [Pon07]. It is due to the expression 4.27 that has been provided with the assumption that the noise remains white after equalization. However, this assumption is not completely true.
While not reaching the optimum performance, the presented solution is computationally costly. In particular for large constellations that require numerous - up to 24 from 16-QAM constellations with complex 4×4 MIMO channels [Pon07] - nearest neighbours explorations to only approach it. Moreover and due to the iterative call of the nearest neighbour algorithm, such a solution does not even offer parallel implementation. Thus the high latency of this solution cannot be reduced.

4.3.3 Sphere-Decoder-based Neighbourhood Generation in the Original Domain

To calculate the reliability information, the idea introduced by Zhang *et al.* corresponds in reality to an additional neighbourhood study that is processed through an SD technique. In particular, it is centred around the unconstrained LRA-ZF solution, which is recalled (see Section 3.3.3) to be denoted as $\tilde{\mathbf{z}}_{\text{LRA-ZF}} = (\mathbf{H}^H\mathbf{H} + \sigma_n^2\mathbf{I}_{n_T})^{-1}\mathbf{H}^H\mathbf{y}$. This idea is extended to any LRA-LD solution. By discarding the classical issues of SD techniques, addressed in Section 2.7, we directly focus on the principle of the proposed solution. In particular, the main difference compared to the techniques presented in Sections 4.3.1 and 4.3.2 lies in the neighbourhood study that is processed in the original domain - while the demonstration starts by considering the reduced domain -, thus avoiding wasted resources.

By introducing a sphere constrain in the reduced domain d_z - necessary due to the infinite nature of the reduced lattice -, a list of neighbours $\mathcal{L}_{\mathbf{z}}$ centred around $\tilde{\mathbf{z}}_{\text{LRA-LD}}$ - $\tilde{\mathbf{z}}_{\text{LRA-ZF}}$ in [Zha07a] - is such as:

$$\mathcal{L}_{\mathbf{z}} = \left\{ \mathbf{z}, \left\| \mathbf{z} - \tilde{\mathbf{z}}_{\text{LRA-LD}} \right\|^2 < d_z^2 \right\}, \tag{4.29}$$

where $\mathbf{z}$ is a hypothetical value in the reduced domain. A direct estimation of $\mathcal{L}_{\mathbf{x}}$ can be obtained by left-multiplying each of the symbol to detect by correct rows of $\mathbf{T}^{-1}$. Clearly, Equation (4.29) is equivalent to the relation:

$$\mathcal{L}_{\mathbf{x}} = \left\{ \mathbf{x}, \left\| \mathbf{T}^{-1}\mathbf{x} - \tilde{\mathbf{z}}_{\text{LRA-LD}} \right\|^2 < d_z^2 \right\}, \tag{4.30}$$

where $\mathbf{x}$ is a hypothetical value in the original domain and where we note that the sphere constraint remains unchanged.
Similarly to the general issue of the neighbourhood generation in the reduced domain, addressed in the beginning of Section 3.4, $\mathcal{L}_{\mathbf{x}}$ cannot be determined straight-forwardly, unless jointly. Again, it is due to $\mathbf{T}^{-1}$ that mixes $\mathbf{x}$ entries. Thus, a reduced complexity approach is proposed in [Zha07a]. Namely, a possibility for solving Equation (4.30) layer by layer - by making the current detected symbol independent of the remaining to-detect symbols - relies on introducing the QRD of $\mathbf{T}^{-1}$. By denoting $\mathbf{T}^{-1} = (\mathbf{Q}_{\mathbf{T}^{-1}})(\mathbf{R}_{\mathbf{T}^{-1}})$, then the following relation is obtained:

$$\mathcal{L}_{\mathbf{x}} = \left\{ \mathbf{x}, \left\| (\mathbf{R}_{\mathbf{T}^{-1}})\,\mathbf{x} - (\mathbf{Q}_{\mathbf{T}^{-1}})^H\,\tilde{\mathbf{z}}_{\text{LRA-LD}} \right\|^2 \right\}. \tag{4.31}$$

Starting from the lowest layer, a classical tree-search method can be employed. In simulations, we decide to use the K-Best algorithm, which is strictly similar to the Fixed Point Algorithm introduced in [Zha07a]. For this reason and in order to insist on the separate neighbourhood study following the LR step, the present detector is denoted as LRA-ZF+K-Best. Also in [Zha07a], the hard decision candidate $\hat{\mathbf{z}}_{\text{LRA-ZF}}$ is added to the candidate list.

In Figure 4.3, the structure of the solution is presented in a block-diagram manner. The - unquantized - LRA-LD estimate and the QRD block's output are simultaneously fed to a K-Best detector that generates the list of solutions $\mathcal{L}_{\mathbf{x}}$ in the original domain. Similarly to Figure 4.2, the latter makes possible the computation of some of the LLR magnitudes.

In Figure 4.4, the BER performance of the LRA-ZF+K-Best, with K=2 and 4 in the 4-QAM case and K=4 and 16 in the 64-QAM case, are depicted and compared to the reference MLD. The max-log approximation in Equation (4.11) is employed when possible. Otherwise - this aspect will be introduced in Section 4.4.3 -, the LLR magnitudes are set to an arbitrary - and absolute - value of ± 3.

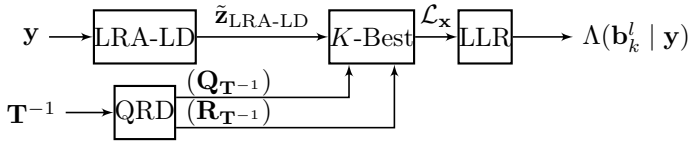

Figure 4.3: Additional neighbourhood study for achieving soft-decision LRA-LD.

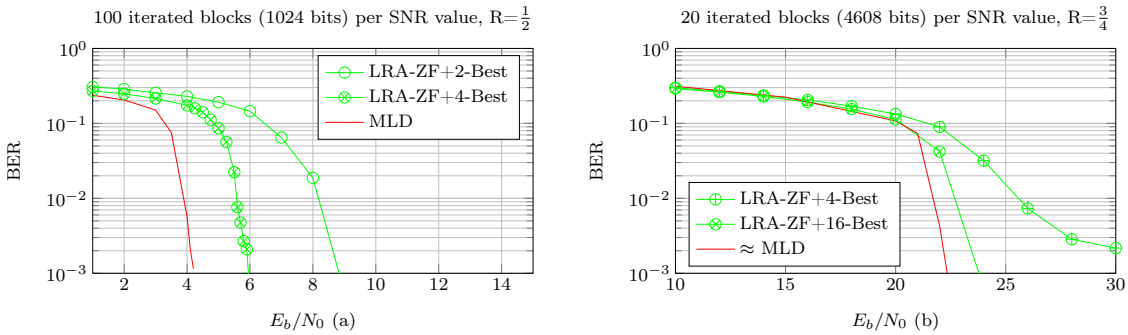

Figure 4.4: BER as a function of E_b/N_0, Complex Rayleigh 4×4 SM-MIMO-SC system, LRA-ZF+K-Best and ML detectors, 4-QAM modulations at each layer (a) and 64-QAM modulations at each layer (b).

While the solution introduced in [Zha07a] in the LRA-ZF case can be extended to any - actually not only LRA-ZF or LRA-MMSE - (sub-)optimal hard-solution, it only aims at generating a neighbourhood study for the sake of generating soft-output. It is different from the LRA-SD algorithm introduced in Section 2.7. In particular, the employed metrics are not even equivalent to the ML metric. Consequently and when K increases, there is no performance improvement in the sense of the quality of the hard-output detector: the only performance improvement lies in the LLR calculation that is thus made more frequently through the max-log approximation.
Concerning the computational complexity aspect, it should be noted that an additional QRD - of $\mathbf{T}^{-1}$ - is necessary. Nevertheless and since it is a part of the preprocessing step anyway, the inversion of $\mathbf{T}$ can be achieved with a very-low complexity by directly processing it within the LR algorithm [Rog10]. Moreover, the $\mathbf{T}^{-1}$ entries are all Gaussian. While this aspect has not been investigated, it will induce a decreased computational complexity compared to a classical QRD.

By summarizing the idea presented in the present section that aims at offering soft-output LRA techniques and while there are multiple means to this end, each presented solution consists in generating a neighbourhood set. Consequently, the direct association - not the LRA-LD+K-Best - of both the LR step and an SD technique is retained. This way, the advantages of their combination - presented in Section 2.7 - will anyway decrease an additional neighbourhood study size, this time aiming at generating soft-output.

4.4 List Sphere Decoder

While it has been claimed in Section 3.2 that the SD aims at reaching the ML hard-estimate only - thus offering the sign of the corresponding bits -, it is not sufficient from now on. Here, its purpose consists in solving the max-log approximation in Equation (4.11) for each bit, thus also

including the reliability of their sign.

With this aim in view, a straight-forward modification of the SD algorithm is sufficient. In particular, it relies on providing a list $\mathcal{L}_{\mathbf{x}}$ of $|\mathcal{L}_{\mathbf{x}}|$ solutions at the SD output. In the case of the K-Best algorithm, the latter is even directly available. Such an algorithm is denoted as a List SD (LSD) and the soft-output are generated from $\mathcal{L}_{\mathbf{x}}$. Namely, Equation (4.11) rewrites:

$$\Lambda(\mathbf{b}_k^l \mid \mathbf{y}, \mathbf{H}) \approx -\frac{1}{2\sigma_n^2}\left(-\min_{\mathbf{x}\in(\mathcal{L}_{\mathbf{x}})_{k,l}^{+1}}\left\{\|\mathbf{y}-\mathbf{H}\mathbf{x}\|^2\right\}+\min_{\mathbf{x}\in(\mathcal{L}_{\mathbf{x}})_{k,l}^{-1}}\left\{\|\mathbf{y}-\mathbf{H}\mathbf{x}\|^2\right\}\right), \tag{4.32}$$

where

$$\begin{aligned}(\mathcal{L}_{\mathbf{x}})_{k,l}^{+1} &= \left\{\mathbf{x}\in\mathcal{L}_{\mathbf{x}}, \mathbf{b}_k^l = +1\right\},\\ (\mathcal{L}_{\mathbf{x}})_{k,l}^{-1} &= \left\{\mathbf{x}\in\mathcal{L}_{\mathbf{x}}, \mathbf{b}_k^l = -1\right\}.\end{aligned} \tag{4.33}$$

Also, we denote here as an *hypothesis* the bit $\mathbf{b}_k^l$ that is mapped from the candidate estimate - within $\mathcal{L}_{\mathbf{x}}$ - that corresponds to the smallest Euclidean distance, namely the detector's hard-estimate. Since the list output of the K-Best LSD is ordered, thus $\mathbf{b}_k^l$ is mapped from $(\mathcal{L}_{\mathbf{x}})_{:,1}$. Similarly, a *counter-hypothesis* for each bit $\mathbf{b}_k^l$ is the symbol such as the bit sign is opposite - again within $\mathcal{L}_{\mathbf{x}}$. Clearly, $\mathcal{L}_{\mathbf{x}}$ contains at least an hypothesis for each bit and not necessarily its corresponding counter-hypothesis.
Thus and as previously mentioned is Sections 4.3.1 and 4.3.3, the max-log approximation is not always directly applicable. It is due to a certain number of missing counter-hypotheses, which depends on multiple parameters, clearly including $|\mathcal{L}_{\mathbf{x}}|$ as depicted in [Aub11a]. This key aspect will be theoretically introduced in Section 4.4.3.

In the sequel, multiple technical solutions with different approaches are introduced and discussed. In particular, the main trends rely on the list construction or on the management of the missing LLR magnitudes.

4.4.1 Bit Flipping

Certainly the most obvious idea lies in solving Equation (4.11) anyway for each bit position. For that, a solution for each missing counter-hypothesis is obtained.

This aspect was initially evaluated by Wang et. al in [Wan04]. With this aim in view, their straight-forward approach is to reverse the undetermined bit magnitudes in the ML hard-estimate. This operation is denoted as *bit flipping*. Subsequently, the Euclidean distance of the resulting counter-hypothesis can be obtained. Thus the max-log approximation in Equation (4.11) is applicable for all the received bit sequence.

However, this method is computationally demanding and low-quality counter-hypotheses are often provided [Mil08] since it relies on the independence of each bit within the sequence. Due to the coupling between layers, it is a strong assumption, which is highlighted in [Zim07]. Consequently, this approach overestimates the reliability of the bits due to the assumed orthogonality of the channel. Clearly, the performance loss will be decreased through a joint flipping of a certain number of bits, even if it leads to an exponential computational complexity in the number of bits. While the bit flipping solution is thus expected to work better with LRA detectors - due to significant reduction of ILIs (see Section 3.3.2) -, this possibility is not trivial since it requires to estimate the LLRs in the reduced domain. Consequently, this solution has not been retained in

accordance to conclusions in [Zim07].

In [Wat04], a similar approach lies in performing a separate tree search for each missing counter-hypothesis. It is denoted as *chase decoding*. It maintains the time complexity (see Section 2.7.3) due to the parallel processing of sub-detectors. In [Pak10], some improvements in the number of (depth first) tree search - thus the computational complexity - are proposed. Among others, it is based on the QAM constellations structure (see Section 2.1) and on a - specific in [Pak10] - layers re-ordering (see Section 3.1.3).

The present solution has been retained for current ST-E detectors for 2×2 systems supported by the LTE standard. One of the advantages of such an architecture lies in its flexibility, that allows devices to switch between the multiple wireless applications with no additional design [Pak10]. However and while it offers near-MLD performance, it requires an heavy complexity, even for 2×2 systems. While it claimed to be under investigation for up to 4×4 systems in [Pak10], different approaches will be shown in the present work to be more promising.

Despite their high level of likeness, the bit flipping solution is different from *bit-negating*- introduced in [Bar08d] from [Wan06] - that is generally seen as a candidate adding in the literature. With this aim in view, a counter-hypothesis is generated by taking the MAP estimate, flipping the concerned bit and calculating the Euclidean distance of the resulting hypothesis [Wan04]. This approach is specifically detailed in the next section.

4.4.2 Candidate Adding

Bäro *et al.* early encountered the problematic aspect of missing counter-hypotheses within $\mathcal{L}_{\mathbf{x}}$ on performance. As an answer, they propose to adapt the LSD by introducing a bit-wise approach in the tree construction. Thus, the reliability of the soft-output is highly impacted [Bar03b]. For the sake of consistency with the vocabulary in the literature, the term of path is employed and should not be confused with the notation in Section 2.6. Here, it simply denotes a branch in a tree search that connects a set of nodes, by starting from the root node. Clearly, it corresponds to a complete symbols vector when its size is the same as the total number of layers.

Along the tree construction, some nodes are disregarded due to the sphere constraint. As a consequence, some paths refer to symbols vectors that have been precociously - up to a layer that is lower than ν - terminated, and some counter-hypotheses will be missing within the detector's list output. Thus, the shortened paths are eventually extended, according to some assumptions that are introduced below. This extension is denoted as *path augmentation* and arises when the detector processes itself (not within a distinct step).

The aforementioned tree search extension is realized according to a distance criterion, with the knowledge of a soft-LD [Bar03b] - the soft-ZF in [Guo06] - and/or a priori information [Bar03b]. The decision to complete the exploration of an - incomplete - candidate is made possible by rewriting the APP LLR Λ as an additive metric [Bar03b]. This way and by assuming that a path of size n has been already explored, the path's metric up to this point reads [Bar03b]:

$$\Lambda(\mathbf{b}_k^l)_n = \sum_{l=n+1}^{n_T} \Lambda_l, \tag{4.34}$$

where

$$\Lambda_l = \left| \tilde{\mathbf{y}}_l - \mathbf{R}_{l,l}\mathbf{x}_l - \sum_{j=l+1}^{n_T} \mathbf{R}_{l,j}\tilde{\mathbf{x}}_j \right|^2 , \tag{4.35}$$

and where we recall - from Equation (4.14) - that the soft-LD reads $\tilde{\mathbf{x}} = \mathbf{G}_{\text{LD}}\mathbf{y}$.
The path augmentation solution proceeds iteratively. When the necessity of augmenting a path occurs at the first iteration, no a priori information is available. As an alternative, the augmentation is made through the - unconstrained [Bit06b, Guo06] - LD solution. Thus and by considering the extension of a path from the n^{th} layer - down to the first layer -, the metric increment reads [Bar03a]:

$$\Lambda(\mathbf{b}_k^l)_{n,\text{LD}} = \sum_{l=n+1}^{n_T} \left| \tilde{\mathbf{y}}_l - \mathbf{R}_{l,l}\mathbf{x}_l - \sum_{j=l+1}^{n_T} \mathbf{R}_{l,j}\tilde{\mathbf{x}}_j \right|^2 . \tag{4.36}$$

In the case of the a priori solution, the metric increment reads [Bar03a]:

$$\Lambda(\mathbf{b}_k^l)_{n,\text{a priori}} = \sum_{l=n+1}^{n_T} \left| \tilde{\mathbf{y}}_l - \mathbf{R}_{l,l}\left(\mathbf{x}_l + \bar{\mathbf{x}}_l\right) - \sum_{j=l+1}^{n_T} \mathbf{R}_{l,j}\tilde{\mathbf{x}}_j \right|^2 , \tag{4.37}$$

where we recall from Section 4.2.3 that $\bar{\mathbf{x}}_l$ corresponds to soft symbols - for the layer l - and denotes the expectation of $\mathbf{x}_l$ over the symbols in ξ [Bit06b], according to their a priori probability of occurrence.

Also, the application to the K-Best LSD or the FSD are considered in [Won05, Guo06] and [Bar08d], respectively. It is straight-forward, and smart implementation schemes are possible [Guo06].

Interestingly, the offered performance improvement is shown in [Bit06b] to be very attractive, even if it is not significant when no a priori information is available [Zim07].
However, this solution is very demanding, as claimed in [Won05, Bit06b] but only in a general discussion. Moreover, the path augmentation is made iteratively and, at the first iteration, the poor-performance soft-LD [Bar03a] can only be used. Consequently, despite contributive efforts in the computational complexity reduction and while a parallel implementation is possible [Guo06] - thus maintaining the latency of the hard-decision detector through major modifications -, this solution is not retained for implementation.

It is consistent with conclusions in [Zim07], where is larger K - in the K-Best LSD - is claimed to be preferable in order to reach a larger number of full-length paths. The remaining missing counter-hypotheses have to be treated. An efficient possibility is described in the sequel.

4.4.3 Log-Likelihood Ratio Clipping

A very low-cost while efficient solution lies in setting the - unknown - magnitude of the concerned bits to a predefined value. In accordance with the related state of the art, this strategy will be called in the sequel *LLR Clipping* (LC) to a value $\Lambda_{\text{clip}}(\mathbf{b}_k^l)$. As it is clearly stated in the latter symbol, the LC value only depends on the bit position, not on the received signal. In the present section, the significant impact of an accurate LC on performance is discussed.

Initially, it has been stated that the number of missing counter-hypotheses depends - among others - on $|\mathcal{L}_{\mathbf{x}}|$. Simultaneously, the accuracy of the LC value is also a function of the list size.

Beyond this consideration, a discussion is necessary.
Intuitively, we can consider that the soft-information about a bit $\mathbf{b}_k^l$ is mostly contained in $\mathcal{L}_\mathbf{x}$. Indeed, if there are many entries in $\mathcal{L}_\mathbf{x}$ such as $\mathbf{b}_k^l = +1$, then it can be concluded that the likely value for $\mathbf{b}_k^l$ is one with a large reliability. Whereas if there are few entries in $\mathcal{L}_\mathbf{x}$ with $\mathbf{b}_k^l = +1$, then the likely value is one with a small reliability. In particular when no counter-hypothesis arise in $\mathcal{L}_\mathbf{x}$ for a bit, Hochwald *et al.* propose a solution that consists in an extremely large LC [Hoc03] due to their high improbability.
Clearly in this scenario, the corresponding bit sign is particularly unreliable when a large $|\mathcal{L}_\mathbf{x}|$ has been processed. Indeed, its counter-hypothesis does not appear within the list, despite its large size. Thus it should be clipped to a large value. In the case of a small $|\mathcal{L}_\mathbf{x}|$, more counter-hypotheses are missing within the list input. Due to the partial nature of the study, the bit sign is not completely improbable, leading to choosing a small clipping value.

In order to address this aspect, numerous techniques have been proposed and studied. The main trends are introduced in the sequel.

4.4.3.1 Fixed Log-Likelihood Ratio Clipping

In accordance with the idea above, it has been widely proposed in the literature [Hoc03, de 05, Pon07, Qi 07, Myl07] to set the magnitude of the impacted bits to a fixed predefined value. This solution is denoted in the present work as *Fixed LC* (FLC).
In accordance with the aforementioned considerations on LC, extreme scenarii have been considered. Namely, Hochwald *et al.* first proposed a solution that solves their high improbability by setting $\Lambda_{\text{clip}}(\mathbf{b}_k^l)$ to an extremely large value [Hoc03]. $\Lambda_{\text{clip}}(\mathbf{b}_k^l) = \pm 128$ is considered as a reference. However, this solution is too agressive. In reality, there exists an optimal LC value that is a function of the list size. This aspect can be demonstrated in theory through the introduction of the *mutual information* $\mathcal{I}\{\mathbf{b}_k^l, \Lambda_{\text{clip}}(\mathbf{b}_k^l)\}$ of any bit amplitude and any corresponding LC value [de 05, Ravil]. By assuming that the bit sign in the LC is correct and $\Pr\{\mathbf{b}_k^l = +1\} = \Pr\{\mathbf{b}_k^l = -1\} = \frac{1}{2}$, the mutual information reads:

$$\mathcal{I}(\mathbf{b}_k^l, \Lambda_{\text{clip}}(\mathbf{b}_k^l)) = 1 - \tfrac{1}{2}\left(\log_2\left\{1 + e^{-\Lambda_{\text{clip}}(\mathbf{b}_k^l)}\right\} + \log_2\left\{1 + e^{\Lambda_{\text{clip}}(\mathbf{b}_k^l)}\right\}\right). \tag{4.38}$$

Subsequently, the impact of the clipping value choice can be observed. In particular, a solution for determining the LC setting relies on maximizing the mutual information.
Figure 4.5 plots the mutual information between $\mathbf{b}_k^l$ and the clipped detector output $\Lambda_{\text{clip}}(\mathbf{b}_k^l)$, versus the clipping value $\Lambda_{\text{clip}}(\mathbf{b}_k^l)$ and for different values of $\Pr\{\Lambda_{\text{clip}}(\mathbf{b}_k^l)\}$. Also, the maximal mutual information - for each $\Pr\{\Lambda_{\text{clip}}(\mathbf{b}_k^l)\}$ value - is pointed out by diamond marks and indicates the optimal clipping value and its evolution is plotted in a dashed style.

Consequently, it is clear that there exists an optimal value - the mutual information is maximized - that depends on $\Pr\{\Lambda_{\text{clip}}(\mathbf{b}_k^l)\}$. Of course in this trivial scenario, it depends only on the number of missing counter-hypotheses, which is clearly related to $|\mathcal{L}_\mathbf{x}|$. Also, while an efficient balance - that will be introduced in the sequel - can been found at intermediate clipping values, it has to be noticed that the FLC choice has a significant impact on the coded performance.
In particular and by referring again to Figure 4.5, choosing an exceedingly high (higher than its optimum) LC induces the decoder to assume a reliability that is too high for the bits with missing counter-hypotheses. In the case that this assumption is false, soft decisions on other bits must be compromised in order to meet the code constraints, leading to error propagation [de 05]. As a consequence, the performance is drastically decreased. This aspect will be corroborated by the performance curves in Figure 4.6 with $\Lambda_{\text{clip}}(\mathbf{b}_k^l) = \pm 128$.

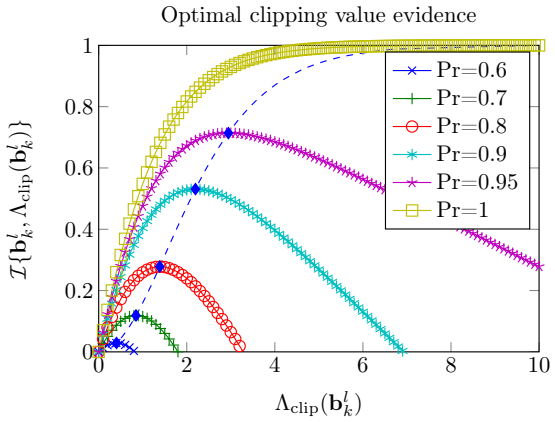

Figure 4.5: Mutual information versus clipping value $\Lambda_{\text{clip}}(\mathbf{b}_k^l)$ for multiple $\Pr\{\Lambda_{\text{clip}}(\mathbf{b}_k^l)\}$ values.

Reversly, setting the clipping level too low (lower than its optimum) limits the mutual information at the detector output. It can be seen as making the channel decoder largely ignore the clipped values [de 05]. Thus it prevents error correction at these bit positions and a part of the channel coding gain is lost.
Consequently, the optimal LC level strongly depends of the system configuration as well as the employed detector calibration.

Ideally, $\Lambda_{\text{clip}}(\mathbf{b}_k^l)$ should be different for each channel bit, such that the mutual information is maximized [de 05]. Nevertheless, a simple while robust proposal has been introduced [Hoc03, Qi 07]. Namely, the FLC is such as $\Lambda_{\text{clip}}(\mathbf{b}_k^l) = \pm 8$, based on the argument that a missing counter-hypothesis from the list of candidates makes the corresponding bit unlikely. As previously discussed, such a FLC value is efficient in the case of large $|\mathcal{L}_{\mathbf{x}}|$ only and it is even rather large according to Figure 4.5. This simple while efficient technique will be considered as a convenient - at least as a reference - solution [Myl07, Mil08].
Another reasonably balanced FLC is commonly employed. Namely, the FLC value can be chosen such as $\Lambda_{\text{clip}}(\mathbf{b}_k^l) = \pm 3$ and offers convenient performance [de 05]. Again, it has been previously discussed that such a FLC value is efficient in the case of small $|\mathcal{L}_{\mathbf{x}}|$ only.

In Figure 4.6, the BER performance of the K-Best LSD, with K=4 in the 4-QAM case and K=4 and 16 in the 64-QAM case, are depicted and compared to the reference MLD. The max-log approximation in Equation (4.11) is employed when possible. Otherwise, the employed FLC are ± 128, ± 8 and ± 3, respectively.

As it is depicted in Figure 4.6, improved performance are offered with $\Lambda_{\text{clip}}(\mathbf{b}_k^l) = \pm 8$ compared to $\Lambda_{\text{clip}}(\mathbf{b}_k^l) = \pm 3$, in particular when the study size $|\mathcal{L}_{\mathbf{x}}|$ increases. Nevertheless, when $|\mathcal{L}_{\mathbf{x}}|$ is large compared to the modulation order - namely $|\mathcal{L}_{\mathbf{x}}|$=4 and 16 for 4-QAM and 64-QAM modulations, respectively - few LLRs have to be clipped, thus limiting the impact on performance of the selected FLC. The extreme FLC - namely $\Lambda_{\text{clip}}(\mathbf{b}_k^l) = \pm 128$ is immediately discarded. Then $\Lambda_{\text{clip}}(\mathbf{b}_k^l) = \pm 8$ is retained - unless otherwise specified, according to the considered detector - in Section 5.3.2. This simple while efficient technique will be considered as a convenient - at least as a reference - solution in this work.

While the use of an appropriate FLC is very efficient in the sense of both the performance and computational complexity, a fine calibration of $\Lambda_{\text{clip}}(\mathbf{b}_k^l)$ is required. Otherwise, a performance

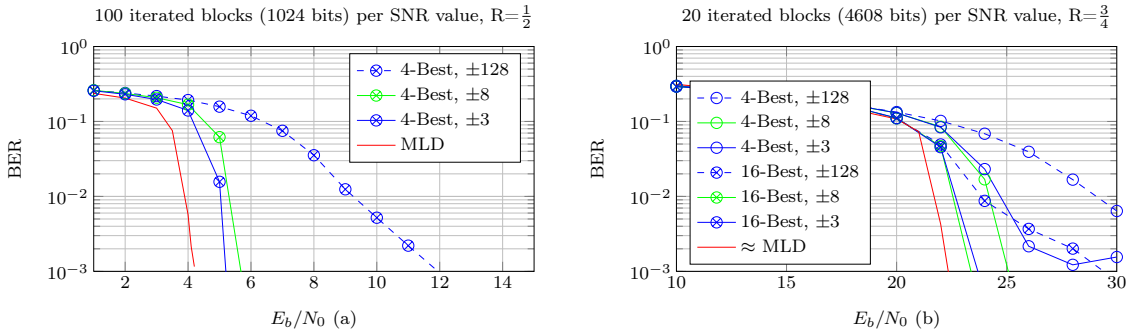

Figure 4.6: BER as a function of E_b/N_0, Complex Rayleigh 4×4 SM-MIMO-SC system, K-Best LSD detectors, 4-QAM modulations at each layer (a) and 64-QAM modulations at each layer (b).

loss occurs. Moreover, the FLC depends on the retained detector. Last but not least, it is an absolute value that varies according to the propagation condition - in particular the SNR. Thus, an enhanced solution is possible.
This is why the LC approach has been extended in order to take into consideration additional available information. The solutions introduced in the sequel are denoted as Empirical LC (ELC).

4.4.3.2 Empirical Log-Likelihood Ratio Clipping

While the idea was first expressed in [Hoc03], Widdup *et al.* were actually the first to clearly propose how to reuse important information available during the LSD processing, namely the sphere constraint.
In particular, since the distance of only the best $|\mathcal{L}_{\mathbf{x}}|$ solutions - regardless of their bit sign - are known, the missing LLRs can be advantageously estimated from the knowledge that the distance of the counter-hypotheses is at least as high as that of the worst known candidate [Wid04]. This cost is exactly the radius d in the case of a depth-first search SD.
This solution is also denoted as the Last List Entry (LLE) [Mil08] in the case of a K-Best LSD. In particular, the counter-hypothesis distance is replaced by the largest Euclidean distance within $\mathcal{L}_{\mathbf{x}}$. Thus and by assuming that the hypothesis concerns a bit sign set to one, Equation (4.11) is approximated by:

$$\Lambda(\mathbf{b}_k^l \mid \mathbf{y}, \mathbf{H}) \approx -\frac{1}{2\sigma_n^2}\left(-\min_{\mathbf{x}\in(\mathbb{L}_{\mathbf{x}})_{k,l}^{+1}}\left\{\|\mathbf{y}-\mathbf{H}\mathbf{x}\|^2\right\} + \|\mathbf{y}-\mathbf{H}(\mathcal{L}_{\mathbf{x}})_{:,K}\|^2\right), \tag{4.39}$$

where $(\mathcal{L}_{\mathbf{x}})_{:,K}$ denotes the last candidate within $\mathcal{L}_{\mathbf{x}}$.

Differently, Higuchi *et al.* introduced a *Likelihood Function Generation*(LFG) for selecting an appropriate clipping value [Hig04, Kaw04]. Briefly, this solution uses a statistical study of the minimal distance within the list and an empirical result. More details about the technique itself are given just below.
First of all and within $\mathcal{L}_{\mathbf{x}}$, the minimum Euclidean distance is reached for each bit. Their sign is considered. Thus, a minimal distance is obtained for each bit such as a total number of $n_T \log_2\{|\xi|\}$ distances are available from now on. At the same time and for each bit, the minimum distance - such as both its hypothesis and its counter-hypothesis are available within $\mathcal{L}_{\mathbf{x}}$ - is obtained. When it exists, it is larger than in the case with no distinction in the bit sign [Hig04, Kaw04]. Then, we

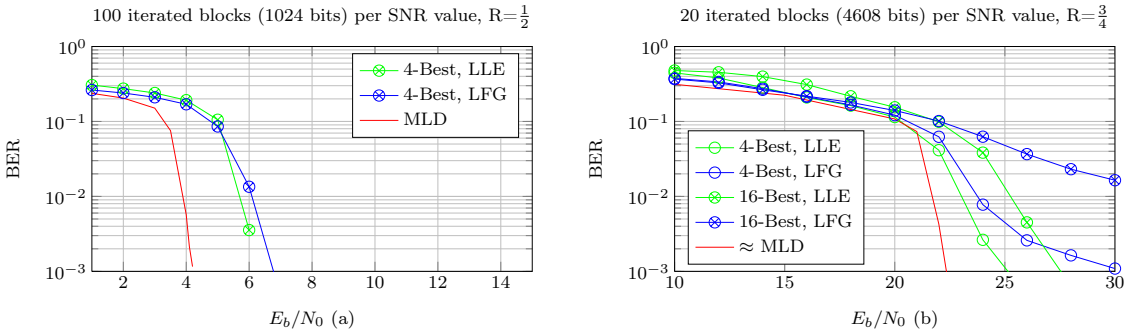

Figure 4.7: BER as a function of E_b/N_0, Complex Rayleigh 4×4 SM-MIMO-SC system, K-Best LSD detectors, 4-QAM modulations at each layer (a) and 64-QAM modulations at each layer (b).

calculate the expectation among the - available - previous minimum Euclidean distances. Subsequently, this result is further averaged over multiple symbols, while it is not taken into account in our simulations due to the lack of details in [Hig04, Kaw04].
Finally, this value is boosted by 50% [Hig04] or 100% [Kaw04] in order to increase its weight. This exhibits the weakness of the solution, and more generally the weakness of ELC solutions that do not rely on strong theoretical studies. Thus, the LFG-based ELC value is obtained.

In Figure 4.7, the BER performance of the K-Best LSD, with K=4 in the 4-QAM case and K=4 and 16 in the 64-QAM case, are depicted and compared to the reference MLD. The max-log approximation in Equation (4.11) is employed when possible. Otherwise, the employed ELC relies on LLE and LFG, respectively.

The LLE solution introduced above requires only few additional computational complexities compared to FLC techniques, which makes it interesting. Even if the largest Euclidean distance of the counter-hypothesis is considered, such a clipping is not important enough compared to the fact that the counter-hypothesis does not appear in $\mathcal{L}_{\mathbf{x}}$. It results in poor performance, as pictured in Figure 4.7. It is claimed in [Mil08] to be due to the employed bound that is generally rather small, causing a significant performance loss. By increasing the weight of the latter, the performance is indeed improved and we regress to an absolute threshold.

The LFG solution introduced above is not computationally expensive, but more complex compared to LLE. In particular and due to an averaging of statistical values over multiple symbols, a larger latency is required. Moreover and as pictured in Figure 4.7, this solution offers unsatisfying performance, in particular compared to FLC.

The solutions discussed in the present section lie in empirical results that do not rely on strong theoretical considerations. Moreover, the corresponding performance improvements are not convincing compared to the FLC while a - much - larger computational complexity is necessary. A smarter solution is provided in the sequel.

4.4.3.3 Signal-to-Noise Ratio Aware Log-Likelihood Ratio Clipping

A smarter solution has been introduced by Milliner *et al.*. Interestingly and while both the FLC and ELC solutions lie in empirical results, the *SNR-aware LC* (SLC) outperforms them by starting from theoretical considerations while offering convincing performance.

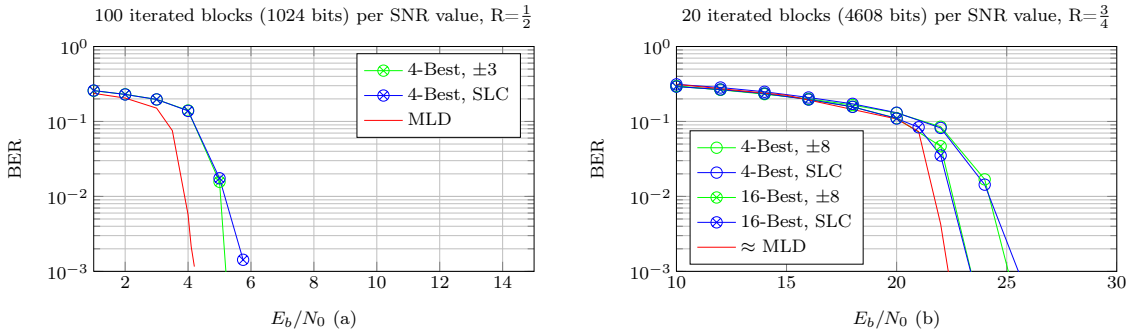

Figure 4.8: BER as a function of E_b/N_0, Complex Rayleigh 4×4 SM-MIMO-SC system, K-Best LSD detectors, 4-QAM modulations at each layer (a) and 64-QAM modulations at each layer (b).

As previously mentioned, it appeared that an accurate - even optimal in the sense of the mutual information maximization - LC depends on various parameters. Based on our experience and multiple publications [Mil08, Zim08, Aub11a], the LC value depends on the SNR, on $|\mathcal{L}_{\mathbf{x}}|$ and on the modulation scheme (not of the code rate, as clearly discussed in [Zim08]). However, the main issue relies on how to take these factors into account.
Milliner *et al.* recently proposed an analytical expression - especially detailed in [Zim08] in the particular case of BPSK - that is claimed to provide the optimal clipping value in the AWGN case with BPSK modulations and for any arbitrary code rate. Starting from the exact LLR definition - introduced in Equation (4.3) -, an approximation is proposed by assuming that $\mathbf{y}$ is independent of $\mathbf{H}$ in mean [Mil08], thus introducing the BER - at the detector output - of a bit to be $+1$ and -1.
In the SISO AWGN case, the exact SER expression for a $\sqrt{|\xi|}$-PAM - introduced in Equation (2.7) - has been revisited by considering an *effective SNR* γ_i [Mil08]:

$$P_S^{\sqrt{|\xi|}\text{-PAM}}(|\mathcal{L}_{\mathbf{x}}|, \gamma_i) = 2\left(1 - \frac{1}{\sqrt{|\xi|}}\right) Q\left(\sqrt{\frac{3}{|\xi| - 1}\sqrt{|\mathcal{L}_{\mathbf{x}}|}\gamma_i}\right), \tag{4.40}$$

where the Q-function has been previously defined in Equation (2.8) and

$$\gamma_i = \mathbf{R}_{i,i}^2 \frac{E_S}{N_0}, \tag{4.41}$$

is the instantaneous SNR for the i-th detection layer (i-th component of the received signal). Similarly to Section 2.1, the QAM SER is deduced from the PAM SER, from which the QAM BER expression can be easily obtained. The predicted error probability $P_B(|\mathcal{L}_{\mathbf{x}}|, \gamma_i)$ then yields the SLC value for bits in the i-th detection layer:

$$\Lambda_{clip,i}(\mathbf{b}_k^l) \approx -\ln P_B^{|\xi|\text{-QAM}}(|\mathcal{L}_{\mathbf{x}}|, \gamma_i). \tag{4.42}$$

In Figure 4.8, the BER performance of the K-Best LSD, with K=4 in the 4-QAM case and K=4 and 16 in the 64-QAM case, are depicted and compared to the reference MLD. The max-log approximation in Equation (4.11) is employed when possible. Otherwise, the SLC introduced above is employed.

This solution offers very convenient performance results compared to the solutions presented above. In particular, it is very similar to the best FLC - between ± 3 and ± 8 - and it outperforms any ELC solutions. However, it requires a non-negligible additional computational complexity.

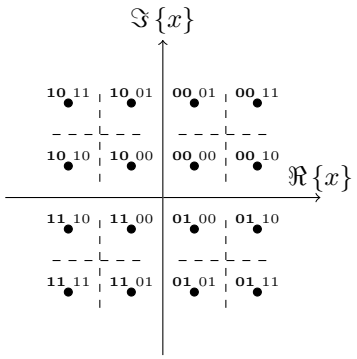

Figure 4.9: 16-QAM modulation constellations for LTE(-A) downlink [3GP09c].

Namely and as clearly stated in [Mil08], the computation of Equation (4.42) involves the use of the ln and of the Q-functions - while they can be approximated by LUTs - and of various basic operations that represent a demanding - while linear (147 MUL (see Section 2.7.3)) in the number of layers - computational complexity.
Still another drawback remains. Due to the AWGN channel assumption, the technique is no longer optimal with neither a Rayleigh nor a realistic channel. This explains the SNR offset observed in Figure 4.8.

Also, the whole bit sequence is considered. In particular, the additional knowledge about the bit position is not taken into account, which is shown to be advantageous in the sequel.

4.4.3.4 Multi-level Log-Likelihood Ratio Clipping

An original approach lies in taking into account the - multi-level bits-to-symbol mapping - nature of QAM constellations and is denoted as Multi-level LC (MLC).

As stated at the end of Section 2.1, this multi-level bit mapping aspect induces different symbols to be characterized by different mean Euclidean distances. Hence, different levels of protection against noise and amplitude impairments - depending on their position within the bit sequence - arise. In Figure 4.9, the 16-QAM example - introduced first in Figure 2.1 - is recalled. In particular for this case, two levels exist comprising Most Significant Bits (MSB) - with a bold representation - and Least Significant Bits (LSB) for each signal point.

For 64-QAM constellations, three levels of protection exist while only one exists for 4-QAM constellations. The latter not actually being multi-level mapping since the protection level is the same among the codeword. In the sequel, for the sake of simplicity and without loss of generality, the 16-QAM case will only be considered.
In the specific LTE(-A) downlink case [3GP09c], QAM constellations with a multi-level Gray mapping can be partitioned into square subsets with minimum mean intra-subset Euclidean distances. Namely and as depicted in Figure 4.9, the MSBs of a signal point determine in which subset it is located.
In [de 05], the multi-level bit mapping had already been considered in order to reduce the detector's computational complexity, which becomes nearly independent of the signal constellation size. Nevertheless, there is no link with the LLR calculation, and in particular with the LC. The idea of applying a distinct LC according to the bit position is novel in this context. It is justified in the sequel and will be shown to offer improved performance.

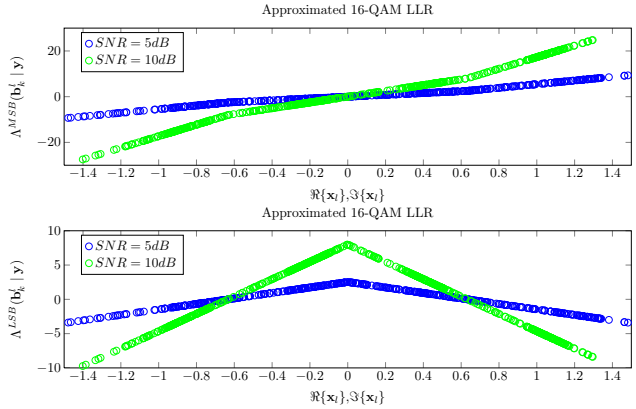

Figure 4.10: Separated $\Lambda^{LSB}(\mathbf{b}_k^l \mid \mathbf{y})$ and $\Lambda^{MSB}(\mathbf{b}_k^l \mid \mathbf{y})$ representation of $\Lambda(\mathbf{b}_k^l \mid \mathbf{y})$ as a function of both the real and imaginary parts of any transmitted symbol, for multiple SNR values, 4×4 AWGN MIMO system, 16-QAM modulation on each layer, 800 distinct values per bit weight.

This idea has been inspired from the point that the distribution of the MSBs and LSBs is different and even particularly advantageous. While analytical expressions are introduced in [Wan02], Figure 4.10 directly depicts the multi-level impact on the LLRs distribution. The trivial example of a 4×4 AWGN MIMO channel is considered, with 16-QAM modulations on each layer. The simulation results are provided from a soft-output MLD with the max-log approximation.

As shown in Figure 4.10 and theoretically confirmed in [Wan02], the LLRs present a distinct behaviour according to their bit index and the SNR. Namely there is no maximal value for MSBs, while - importantly - there is a maximal value for positive LSBs. Also and consistently with previous discussions in Section 4.4.3.3, this maximal value is different according to the SNR. The idea presented here consists in taking advantage of this additional knowledge in order to apply different LC - according to the level of protection of the concerned bits - to generate lower-distortion approximated LLR.

Through a SNR normalization, the positive LSBs are shown in [Aub11a] to still be upper bounded by a constant value in the Rayleigh channel case. Thus and similarly to [Mil08], the MLC technique is SNR-aware and also considers the modulation order - in the sense of its particular multi-level bit mapping. It does not consider the list size and offers an optimization by only taking into account the additional knowledge about the position of the concerned bits.
In particular, the positive LSB-positioned LLRs have been shown to offer a constant maximal magnitude, through a SNR normalization step. Concerning the negative LSBs and the MSBs, the LLRs still depend on the SNR. This point is illustrated in Figure 4.11, where the maximum normalized LLRs from the soft-decision MLD output are plotted as a function of SNR, for different bit positions.

From Figure 4.11, an efficient $\Lambda_{\text{clip}}^{LSB^+}(\mathbf{b}_k^l)$ is obtained. Also, it is highlighted in [Aub11a] that it is constant over the SNR range and independent of the number of to-be-clipped bits. This is not the case for the other bit positions that depend on the SNR and on the number of to-be-clipped bits. Nevertheless, it should be noted that from Figure 4.11 the absolute LC for MSBs is approximated as:

$$\Lambda_{\text{clip}}^{MSB^-}(\mathbf{b}_k^l) \approx -\Lambda_{\text{clip}}^{MSB^+}(\mathbf{b}_k^l). \tag{4.43}$$

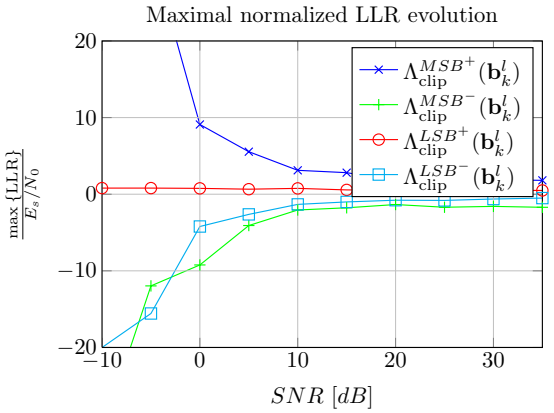

Figure 4.11: Maximal normalized LLR evolution as a function of SNR, 4×4 MIMO Rayleigh channel, $\frac{1000|\xi|\nu}{2}$ simulations per bit weight and per SNR value.

In Figure 4.12, the BER performance of the K-Best LSD, with K=4 and 16 in the 16-QAM case is depicted and compared to the reference MLD. The max-log approximation in Equation (4.11) is employed when possible. Otherwise, the MLC introduced above is employed. In order to simply illustrate the performance improvement in the choice of distinct LCs, we consider two distinct FLCs. Namely, FLCs of ± 2 and ± 3 are considered for LSBs and MSBs, respectively. These are compared to the reference FLC of ± 3 for all the bit positions.

In the same vein as Section 4.4.3.1, the use of an appropriate FLC is very efficient in the sense of both the performance and computational complexity even though a fine calibration of $\Lambda_{\text{clip}}(\mathbf{b}_k^l)$ is required. Although its performance improvement remains lower than that of SLC, the latter does not vindicate the corresponding additional computation complexity. Further details on how to enhance the MLC technique are introduced in [Aub11a].

Thus, the solution presented above is retained for implementation. Moreover, there is no loss of generality in its use. Namely, the MLC does not preclude its combination with any more advanced technique.

4.5 Lattice-Reduction-Aided Sphere Decoder

In the present section, a new step is introduced and aims to provide soft-output LRA detectors. Contrary to Section 4.3 the LRA detector and the soft-decision generation are processed simultaneously.

4.5.1 Randomized Lattice Decoding

Even if it is not specifically intended for this purpose, the *randomized lattice decoding* [Liu10] - first proposed in [Rag87] and extended to the closest vector problem in Klein's works [Kle00] - allows for soft-decision by generating a neighbourhood around the LRA-DFD solution. Namely, the quantization operation is randomized at each layer within the DFD processing. In particular, the quantization to the nearest symbol in the reduced domain - which is a rounding operation - is replaced by the quantization to a random Gaussian integer.

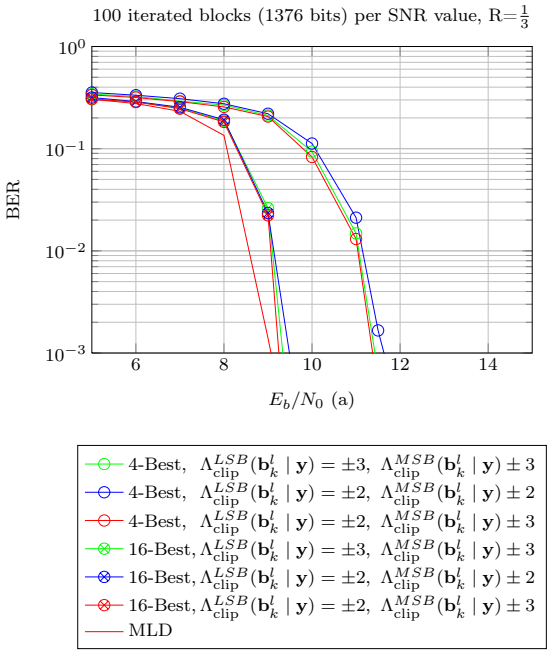

Figure 4.12: BER as a function of E_b/N_0, Complex Rayleigh 4×4 SM-MIMO-SC system, K-Best LSD detectors, 16-QAM modulations at each layer.

We introduce the discrete random variable Z that belongs to $\mathbb{Z}_{\mathbb{C}}$ and the complex floor and ceiling operators - the real and imaginary parts are rounded independently - $\lfloor \cdot \rfloor$ and $\lceil \cdot \rceil$, respectively. The random quantization $\hat{z}$ of $\tilde{z}$ - thus not necessarily $\mathcal{Q}_{\mathbb{Z}_{\mathbb{C}}}\{\tilde{z}\}$ - is made through the discrete Gaussian distribution [Kle00]:

$$\begin{cases} \Pr\{Z = \lfloor \tilde{z} \rfloor - i\} & = \frac{1}{s} e^{-\frac{1}{\sigma^2}(\tilde{z} - \lfloor \tilde{z} \rfloor + i)^2}, \\ \Pr\{Z = \lceil \tilde{z} \rceil + i\} & = \frac{1}{s} e^{-\frac{1}{\sigma^2}(\lceil \tilde{z} \rceil - \tilde{z} + i)^2}, \end{cases} \tag{4.44}$$

where $i \in \mathbb{N}_{\mathbb{C}}$ - by denoting $\mathbb{N}_{\mathbb{C}}$ as the set of complex natural integers that reads $\mathbb{N}_{\mathbb{C}} = \mathbb{N} + j\mathbb{N}$ - and σ^2 is a parameter that controls the variance of the resulting discrete and complex Gaussian distribution. Also, it is normalized such as:

$$s = \sum_{i \in \mathbb{N}_{\mathbb{C}}} \{e^{-\frac{1}{\sigma^2}(\tilde{z} - \lfloor \tilde{z} \rfloor + i)^2}\} + \sum_{i \in \mathbb{N}_{\mathbb{C}}} \{e^{-\frac{1}{\sigma^2}(\lceil \tilde{z} \rceil - \tilde{z} + i)^2}\}. \tag{4.45}$$

Thus and as it is remarked in [Liu10], a large σ^2 induces a large neighbourhood study, while a small σ^2 induces a small neighbourhood study, up to the classical quantization to the nearest Gaussian when it is zeros-valued.

The presented solution is an interesting and original theoretical tool. In particular, theoretical expressions of both its performance and computational complexity can be expressed [Liu10], which offers an academic interest.
However, how to choose an accurate - verily optimal - σ^2 is an important drawback. In reality, this issue is similar to the selection of the radius of classical SDs, which has been addressed in Section 3.2. Even by assuming that the optimal variance can be correctly reached, the latter depends on the propagation conditions, thus implying a variable computational complexity. We recall that it is an important issue for implementation.
Also and while both the QRD and LR steps are proceed only once, N distinct DFDs are processed

according to the rounding operation introduced in Equation (4.44) [Liu10]. Thus, the corresponding computational complexity is $\mathcal{O}(4Nn^2)$, when considering the processing step only. On top of that, the random aspect leads to duplicate solutions that induce wasted resources. Namely, N distinct DFDs will offer $N^{'}$ distinct candidates, where $N^{'} \leq N$. In particular in simulations and with $N = 25$, $N^{'} \approx 10$ in mean. While non completely removing this aspect, a solution lies in increasing the variance σ^2.
From the performance point of view and differently from [Kle00], an optimal σ^2 is given in [Liu10] according to the list size N. It offers near-optimum performance in the uncoded case, even for large dimensional systems and high order modulations.

However and - again - while such a detector offers an academic interest, we decided not to retain it for practical applications. This is due to the aforementioned random computational complexity and wasted resources, even if a parallel implementation is clearly possible.
Also, in order to retain the quality of the hard-output of the LRA detector in the case of soft decision, a very high computational complexity is needed.

4.5.2 Sphere-Decoder-based Neighbourhood Generation in the Reduced Domain

The size of the stored list has been shown to impact the LLR choice. In particular in the case of LRA-SD techniques, the neighbourhood size has been drastically decreased due to the LR step. Consequently, a large part of information is not available from now on. That is why some additional information, aiming at more efficiently clipping missing LLRs, has been reached within the LR step. However, this novel solution has not been protected for the moment, thus inducing the non-disclosure of this idea.

It was shown in the present chapter that the extension to soft-decision of LRA only - with no neighbourhood study - detectors is inefficient or at least very intricate. However, this chapter relies on general studies. The interest of the technical choices that are proposed in the present work are further detailed in the next chapter. In particular, the computational complexity results are detailed with practical considerations.

Chapter 5

Practical considerations and implementation aspects

Contents

5.1 LTE(-A) Downlink Standard

5.1.1 Practical Requirements of MIMO Channel Models

As partially evoked in Section 2.5 and according to the 3GPP LTE(-A) standard [3GP09d], a grid-represented RB is transmitted through the entire channel bandwidth that varies in both the frequency and time domains. Thus, the transmission is impacted by the coherence bandwidth and coherence time, respectively. These phenomena are induced by multi-path propagation and Doppler effect, respectively, as introduced in Section 2.6. A small coherence bandwidth or time corresponds to a strong fading, which imply a reduction of the *correlation* between two channel matrices associated to *adjacent* REs, namely neighbour REs within the RB. With an abuse of notation for the sake of simplicity, the channel that is associated to an adjacent RE will be denoted as *adjacent channel* in the sequel. Also, we define the correlation between two matrices as the measure of dependence between these two matrices, namely by dividing their covariance by the product of their own variances.

Due to reflection and scattering in the environment - as theoretically introduced in 2.6 -, channel responses are commonly approximated by a finite number of distinct paths. Paths of similar amplitudes interfere constructively and destructively, thus inducing frequency fading.
In the present work, the simulation results are provided according to 3GPP LTE(-A) channel

Excess tap delay [ns]	0	30	70	90	110	190	410		
Relative power [dB]	0.0	-1.0	-2.0	-3.0	-8.0	-17.2	-20.8		
Excess tap delay [ns]	0	30	150	310	370	710	1090	1730	2510
Relative power [dB]	0.0	-1.5	-1.4	-3.6	-0.6	-9.1	-7.0	-12.0	-16.9
Excess tap delay [ns]	0	50	120	200	230	500	1600	2300	5000
Relative power [dB]	-1.0	-1.0	-1.0	0.0	0.0	0.0	-3.0	-5.0	-7.0

Table 5.1: EPA, EVA and ETU tapped delay line model details.

models [3GP09d] that have been chosen as simplifications or typical realisations of the COST 259 model [Cor01]. The evaluation of LTE(-A) detectors requires channel modelling with increased bandwidth - compared to general UMTS models - due to the radio channel frequency response which depends on the delay resolution of the receiver. In 3GPP, the 20 MHz LTE(-A) channel models were based on a synthesis of existing models such as the ITU and 3GPP models. Subsequently, extended wideband models with low, medium, and large delay spread values could be identified.
The low delay spread gives an Extended Pedestrian A (EPA) model which is employed in an urban environment with fairly small cell sizes ($\tau_{\text{RMS}} = 43$ ns). The medium delay spread gives an Extended Vehicular A (EVA) model which corresponds to a medium delay spread environnement ($\tau_{\text{RMS}} = 357$ ns). The large delay spread gives an Extended Typical Urban (ETU) model which has a large maximum excess delay and applies to some extreme urban, suburban, and rural cases. While it seldom occurs, it remains important in evaluating LTE(-A) performance in the most challenging environments ($\tau_{\text{RMS}} = 991$ ns). The tapped delay line model is characterized in Table 5.1.

As specified in [3GP09a], the models introduced in Table 5.1 can be specifically simplified to allow for more efficient and less complex simulations and testing. The simplification should be done with a specific time resolution ΔT, with

$$\Delta T = \frac{1}{f_S}, \tag{5.1}$$

where f_S is one sub-carrier bandwidth in the OFDM symbol, namely $1/(NT_U)$ (see Section 2.3). In order to avoid confusion and in accordance to 3GPP standard rules, we clearly state that the channel profiles are re-sampled at delays $\{0,\ \Delta T,\ 2\Delta T,\ 3\Delta T\}$.
This sampling is accomplished such that all taps belonging to the interval:

$$\left]\left(i-\frac{1}{2}\right)\Delta T;\left(i+\frac{1}{2}\right)\Delta T\right], \tag{5.2}$$

would be sampled into the tap positioned at delay $i\Delta T$ for all non-negative integers i [3GP09a]. Only the taps that correspond to a power within 25 dB of the strongest are retained [3GP09a]. Tap powers should be normalized so that the sum of all tap powers is equal to 1 [3GP09a]. All taps should have a classical Doppler spectrum and no direct path Doppler spectrum, thus resulting in Rayleigh fading - in opposition to Rician fading.
Also, for a frequency hopping or multi-carrier system and to take into account the frequency correlation of the channel model, the ΔT should be set in order to be compatible with a sampling frequency of 30.72 MHz [Ses09], which is the entire channel bandwidth. Namely, $\Delta T = 32.6$ ns for the maximum allowed number of sub-carriers. Also, it remains compatible with UMTS where the sampling frequency of 3.84 MHz is one eighth of the LTE(-A) sampling frequency.

EPA	$f_{\mathrm{d,max}}$=5 Hz
EVA	$f_{\mathrm{d,max}}$=70 Hz
ETU	$f_{\mathrm{d,max}}$=300 Hz

Table 5.2: Channel model parameters.

Simultaneously and as theoretically introduced in 2.6, a motion of the receiver causes a Doppler shift inducing time fading.
In the present work, the simulation results are provided according to 3GPP LTE(-A) channel models [3GP09d]. The propagation conditions are obtained for low, medium, and high maximal Doppler frequencies, namely 5 Hz, 70 Hz and 300 Hz [3GP09d]. According to Equation (2.35) and at a carrier frequency of 2.5 GHz, the corresponding mobile speeds are 2, 30 and 130 km/h, respectively. The maximum Doppler frequencies $f_{\mathrm{d,max}}$ are summarized in Table 5.2.

The MIMO minimum performance requirement is specified in [3GP09d]. It provides - with 64-QAM constellations - the consideration of up to a 70 Hz maximal Doppler frequency. Consequently in the present work, the worst-case simulations would rely on a 70 Hz maximal Doppler frequency.

Spatial correlation arises due to spatial scattering conditions, as theoretically introduced in 2.6.
In the present work, the simulation results are provided according to 3GPP LTE(-A) channel models [3GP09d]. Namely, the Kronecker model is considered. It is a correlation-based analytical model where correlation at the transmitter and at the receiver can be separated. The correlation matrices are clearly stated in [3GP09d] in the 4×4 MIMO case. Consistent with the expressions introduced in Equation (2.38), the eNodeB (eNB) - equivalent in UMTS to the Base Station (BS) - and the UE correlation matrices, respectively, are defined as follows:

$$\mathbf{R}_{\mathrm{eNB}} = \begin{bmatrix} 1 & \alpha^{\frac{1}{9}} & \alpha^{\frac{4}{9}} & \alpha \\ \left(\alpha^{\frac{1}{9}}\right)^* & 1 & \alpha^{\frac{1}{9}} & \alpha^{\frac{4}{9}} \\ \left(\alpha^{\frac{4}{9}}\right)^* & \left(\alpha^{\frac{1}{9}}\right)^* & 1 & \alpha^{\frac{1}{9}} \\ \alpha^* & \left(\alpha^{\frac{4}{9}}\right)^* & \left(\alpha^{\frac{1}{9}}\right)^* & 1 \end{bmatrix}, \mathbf{R}_{\mathrm{UE}} = \begin{bmatrix} 1 & \beta^{\frac{1}{9}} & \beta^{\frac{4}{9}} & \beta \\ \left(\beta^{\frac{1}{9}}\right)^* & 1 & \beta^{\frac{1}{9}} & \beta^{\frac{4}{9}} \\ \left(\beta^{\frac{4}{9}}\right)^* & \left(\beta^{\frac{1}{9}}\right)^* & 1 & \beta^{\frac{1}{9}} \\ \beta^* & \left(\beta^{\frac{4}{9}}\right)^* & \left(\beta^{\frac{1}{9}}\right)^* & 1 \end{bmatrix}. \quad (5.3)$$

Subsequently and accordingly to [3GP09d], the spatial correlation is defined as:

$$\mathbf{R}_{\mathrm{spat}} = \mathbf{R}_{\mathrm{eNB}} \otimes \mathbf{R}_{\mathrm{UE}}, \quad (5.4)$$

where $\otimes$ is the Kronecker product.
The low correlation case actually represents a case where the antennas are fully uncorrelated. The medium correlation is achieved by means of orthogonal polarization. The high correlation case the eNB and UE antenna arrays are co-polarized and have small inter-antenna distances of 1.5 and 0.5 wavelengths respectively [Ses09]. The α and β coefficients - that are employed in the low, medium and high correlation cases - are summarized in Table 5.3 from [3GP09d].

The entire channel bandwidth - associated to the whole grid-represented RB - induces multiple channel matrices. By considering a channel matrix at the position (k, l) - that is associated to the (k, l)-th RE -, it is denoted as $\mathbf{H}_{k,l}$ as in Equation (2.28). Consequently, a channel matrix $\mathbf{H}_{k',l'}$ varies more or less - in both the time and frequency domains - compared to an adjacent channel $\mathbf{H}_{k,l}$. Thus, its corresponding level of correlation with $\mathbf{H}_{k,l}$ is more or less important.

Low correlation	α=0	β=0
Medium correlation	α=0.3	β=0.9
High correlation	α=0.9	β=0.9

Table 5.3: Spatial correlation between the antennas at the eNB and the UE.

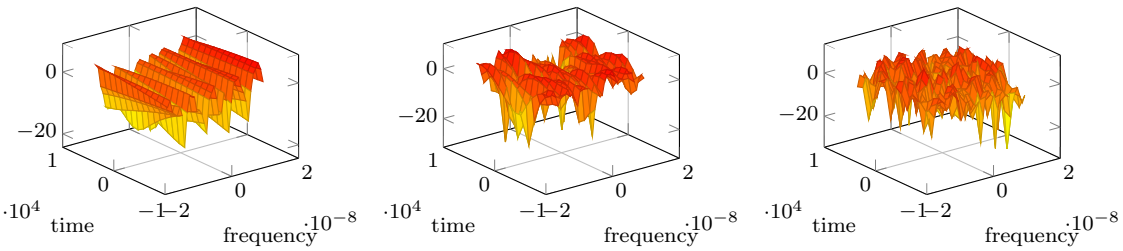

Figure 5.1: Mobile multipath channel gain in dB, EPA model, FFT size of 2048.

In Figure 5.1, the absolute values in dB of an entire SISO LTE(-A) channel are plotted. The EVA model and an FFT size of 2048 are considered for all the three figures. Also, multiple maximal Doppler frequencies - namely of 5 Hz, 70 Hz and 300 Hz, respectively - are depicted. Consistently the introductive discussion of this section, a low maximal Doppler frequency leads to a quasi-constant channel matrix in time while strong fading in time occurs with a large maximal Doppler frequency.
Clearly from Figure 5.1, there exist different possibilities for selecting an adjacent channel. Namely an RE can be adjacent in frequency, in time or even in both. This aspect will be further developed in Sections 5.2.1 and 5.2.2.

It is important to specify realistic propagation conditions for the evaluation of LTE(-A) performance. Nevertheless, it is mainly provided here with the aim to provide - in particular in Sections 5.2.1 and 5.2.2 - a contributive computational complexity decrease at the preprocessing step, with practical considerations.

5.1.2 Downlink LTE(-A) Resource Allocation

In the LTE(-A) DL and following Section 5.1.1, OFDM transmissions - theoretically introduced in Section 2.3 - can be described by a two-dimensional - in time and frequency - grid of REs. The whole grid is denoted as an RB and we consider that the channel is flat-fading within each RE. This particular structure aims at simplifying the multiplexing of the Reference Signals (RS) [Ses09], which are employed for the MIMO channel estimation through additional interpolation.

In the present work and according to the 3GPP LTE(-A) standard [3GP09d], the entire channel bandwidth, *i.e.* 30.72 MHz, can be divided in up to 2048 sub-channels. A set of sub-channels on each end is used as a guard tone, and the rest - 1200 tones in the case of an FFT size N of 2048 - are used to transmit data and are thus denoted as data sub-carriers or tones equally. The FFT size N and the number of data sub-carriers N_U - according to the bandwidth - are summarized in Table 5.4 from [3GP07]. Notations were introduced in Section 2.3. These choices rely on the simplification of the Radio Frequency (RF) chain commonly used for UMTS and LTE(-A). As an example, the sampling frequency is 30.72 MHz $= 8 \cdot 3.84$ MHz, thus it corresponds to eight times the sampling frequency of UMTS.

Transmission bandwidth (MHz)	1.4	3	5	10	20
Sub-frame duration			0.5 ms		
Sub-carrier spacing			15 kHz		
N	128	256	512	1024	2048
N_U	72	180	300	600	1200

Table 5.4: DL OFDM modulation parameters.

Data sub-carriers	72	180	300	600	1200
RBs per slot	6	15	25	50	100

Table 5.5: Number of RBs per slot range.

By taking into account the aspect that one slot duration is 0.5 ms and corresponds to 7 OFDM symbols, the symbol duration T_U is chosen as 71.43 μs. An additional guard interval is not considered in the present case. The allocation base unit in an RB is 1 ms per 180 kHz, thus sub-carriers are grouped by 12 - 12 sub-carriers times 15 kHz - within an RB. Consequently, the number of RBs per slot is comprised between 6 - with a 1.4 MHz transmission bandwidth - and 100 - with a 20 MHz transmission bandwidth -, as it is summarized in Table 5.5.

According to [3GP07] and by denoting R_n as the RE that is used for transmitting an RS at the antenna port n, Figure 5.2 illustrates their specific mapping. When an RE is used to transmit an RS at one antenna port n and at the position (k, l), the corresponding RE - thus also at the position (k, l) - on the other antenna ports is set to zero, thus inducing orthogonal received RSs and consequently avoiding interference. It is depicted by dashed REs. Also, Figure 5.2 illustrates the - previously introduced - RB allocation that we recall to be constituted of 14 OFDM symbols - in time - and of 12 data sub-carriers - in frequency.

The DL RB in LTE(-A) possesses dimensions - in more than space - of frequency and time. The two-dimensional grid bandwidth - 180 kHz - and duration - 1 ms - allow for challenging a system's sensitivity to frequency fading and Doppler, respectively. Simultaneously and in Section 5.2, it will allow us to address the decrease in the computational complexity due to coherence bandwidth or time. In the next section, another LTE(-A) standard requirement induces further decreases in computational complexity and some basic concepts are introduced.

5.1.3 Closed-Loop Mode for Spatial Multiplexing

Consistently with Section 2.5, consider a n_T-transmit and n_R-receive $n_T \times n_R$ SM-MIMO-SC system. The transmitted signal $\mathbf{x}$ is pre-multiplied by a $n_T \times \nu$ matrix $\mathbf{W}$, by having previously introduced (see Section 2.4.3) the number of layers ν. It is denoted as the precoding matrix. It is chosen from a finite set of possible matrices $\mathcal{W} = \{\mathbf{W}_1, \cdots, \mathbf{W}_l\}$. The corresponding index of the chosen precoding matrix is then send back to the transmitter using $\lceil \log_2\{l\} \rceil$ bits of feedback through an assumed zero-delay link, where $\lceil \cdot \rceil$ denotes the rounding toward plus infinity. As a consequence, the equivalent system model reads:

$$\mathbf{y} = \mathbf{HWx} + \mathbf{n}, \tag{5.5}$$

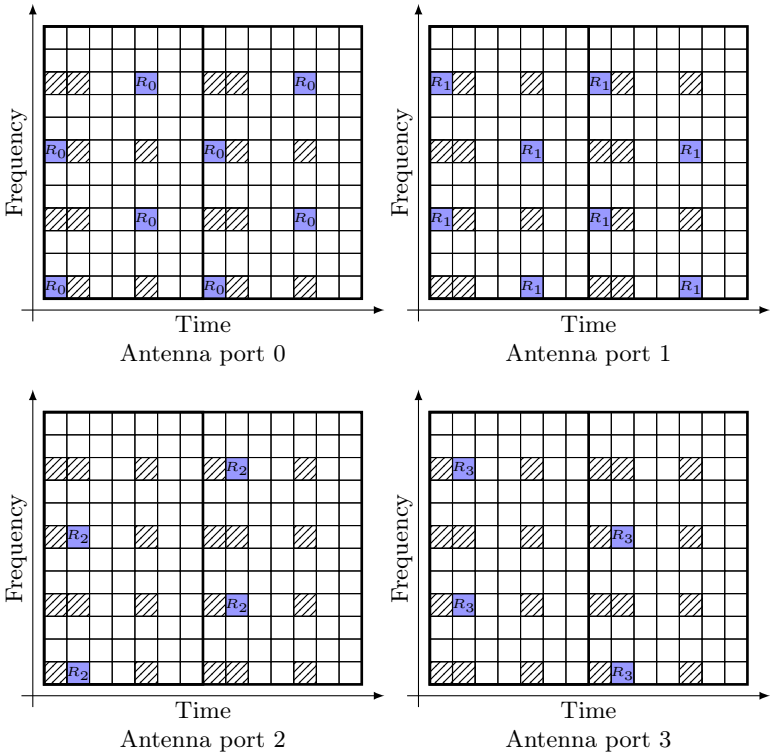

Figure 5.2: Time-frequency RB with RS positions according to the antenna port, case of four antenna ports.

where the notations remain those introduced in Equation (2.28).
By considering the system model introduced in Equation (5.5), two main issues arise. The first is how to design the set $\mathcal{W}$. Due to its setting by the 3GPP LTE(-A) standard [3GP07] - as introduced in the sequel -, it is not addressed in the present work and the codebooks from the standard are directly introduced. Anyway, it relies on general considerations provided in [Lov05b]. The second is the selection of an accurate precoding matrix from a - finite - codebook of matrices $\mathcal{W}$.

In the LTE(-A) standard, precoding for SM is only used in combination with layer mapping that supports two or four antenna ports [3GP07].
In the case of a transmission on two antenna ports, the precoding matrix $\mathbf{W}$ shall be selected from Table 5.6 configured in both the eNB and the UE [3GP07]. Briefly, it should be noted that this table is designed such as to yield codebooks with large minimum distances, by considering them with a rotated DFT form [Lov05a].

For transmission on four antenna ports, the precoding matrix $\mathbf{W}$ shall be similarly selected from a table available in [3GP07]. The quantity $\mathbf{W}_n^{\{s\}}$ denotes the matrix defined by the columns given by the set $\{s\}$ from the expression:

$$\mathbf{W}_n^{\{s\}} = \mathbf{I}_4 - 2\frac{\mathbf{U}_{:,n}(\mathbf{U}_{:,n})^H}{(\mathbf{U}_{:,n})^H\mathbf{U}_{:,n}}, \tag{5.6}$$

where the vector $\mathbf{U}_{:,n}$ is given by a table available in [3GP07] that is not recalled in the present work.

Codebook index	Number of layers	
	1	2
0	$\begin{bmatrix}1\\0\end{bmatrix}$	$\frac{1}{\sqrt{2}}\begin{bmatrix}1 & 0\\0 & 1\end{bmatrix}$
1	$\begin{bmatrix}0\\1\end{bmatrix}$	$\frac{1}{2}\begin{bmatrix}1 & 1\\1 & -1\end{bmatrix}$
2	$\frac{1}{\sqrt{2}}\begin{bmatrix}1\\1\end{bmatrix}$	$\frac{1}{2}\begin{bmatrix}1 & 1\\j & -j\end{bmatrix}$
3	$\frac{1}{\sqrt{2}}\begin{bmatrix}1\\-1\end{bmatrix}$	-
4	$\frac{1}{\sqrt{2}}\begin{bmatrix}1\\j\end{bmatrix}$	-
5	$\frac{1}{\sqrt{2}}\begin{bmatrix}1\\-j\end{bmatrix}$	-

Table 5.6: SM precoding codebooks for 2 transmit antennas.

As previously evoked, the efficiency - from a performance point of view - of the selection criterion depends on the receiver. In this section, two different receivers are briefly considered, namely the MLD and the MMSE LD.
To the best of the author's knowledge, no analytical expression of the probability of error is available for the MLD. Nevertheless, a high SNR upper bound can be obtained through the introduction of the received minimum squared distance $d^2_{\min}$ of the multidimensional constellation ξ^{n_T}. It reads:

$$d^2_{\min} = \min_{\substack{\mathbf{x}_1,\mathbf{x}_2\in\xi^{n_T}\\ \mathbf{x}_1\neq\mathbf{x}_2}} \|\mathbf{HW}(\mathbf{x}_1-\mathbf{x}_2)\|^2. \tag{5.7}$$

The *ML-Selection Criterion* (ML-SC) [Lov05b] consists in choosing $\mathbf{W}$ such that:

$$\mathbf{W} = \arg\max_{\mathbf{W}_i\in\mathcal{W}} \left\{d^2_{\min}\right\}. \tag{5.8}$$

In the case of a MMSE LD, the selection criterion is based on the capacity (or mutual information $\mathcal{I}$) maximization. The mutual information reads:

$$\mathcal{I}(\mathbf{W}) = \log_2\left\{\det\left(\sigma_n^2\mathbf{I}_{n_T} + (\mathbf{HW})^H\mathbf{HW}\right)\right\}. \tag{5.9}$$

The *Capacity-Selection Criterion* (C-SC) [Lov05b] consists in choosing $\mathbf{W}$ such that:

$$\mathbf{W} = \arg\max_{\mathbf{W}_i\in\mathcal{W}} \left\{\mathcal{I}(\mathbf{W}_i)\right\}. \tag{5.10}$$

Exceptionally in the present work, the discussion offers a distinct - from the 4×4 MIMO system - study that aims at exhibiting the behaviour of the LR step - in particular the (S)LA - in the Closed-Loop (CL) mode. It is due to the fact that precoding for SM is only used in combination with layer mapping that supports two or four antenna ports in the LTE(-A) standard [3GP07], consistently with the codebooks previously introduced. Thus, only the 2×2 and 4×2-dimensional MIMO systems have been considered at the present date of publication.

As introduced in [Zha07b], the performance gain of LDs can be estimated through the OD measurement - introduced in Equation (2.39) - of the effective channel matrix. In Figure 5.3, the CDF

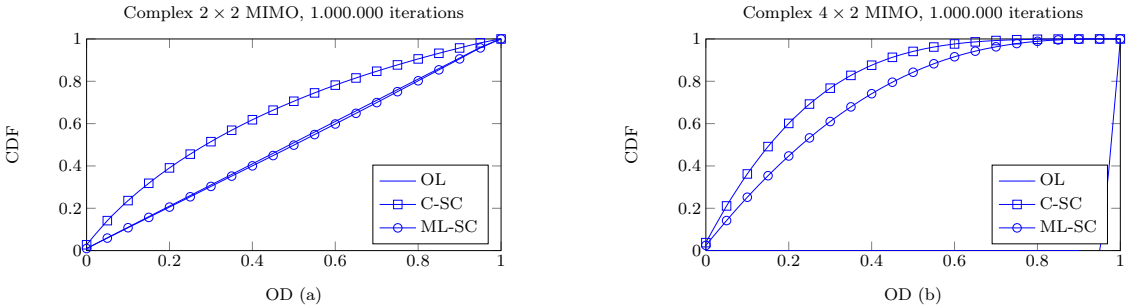

Figure 5.3: CDF of the OD, for a 2×2 MIMO (a) and a 4×2 MIMO (b) precoding schemes.

of the OD of **HW** is depicted for the ML-SC and C-SC CL modes. It should be noted that it is independent of SNR. It is compared to the reference OL mode, namely the OD of **H**.

Clearly from Figure 5.3, an appropriate precoding bounds the OD of the effective channel **HW** - this aspect is demonstrated in [Tep04] - with a 4×2 MIMO system. Also, the bounding limit depends on the employed codebook and criterion.

The proposed LRA-MMSEE K-Best detector is still straightforwardly applied in the CL mode, in particular the LR step. Nevertheless and interestingly, this particular mode will induce a computational complexity decrease, as clearly stated in Section 5.2.3.

5.2 Computational Complexity Reduction

Until now, the data-dependent LSD's computational complexity has been reduced to its maximum. In particular, a large part of the detector's computational complexity has been shifted to the preprocessing step. The arising coherence bandwidth or time induce correlations between adjacent channels in frequency or time, respectively. Consequently, the preprocessing step is subject to a significant computational complexity decrease, by considering this additional available information. The concerned steps are the (S)QRD and the LR. Contributive solutions providing computational complexity decrease have been proposed and are summarized in the following sections.

5.2.1 QR Decomposition Preprocessing

In the present section, the advantage of shifting the detector's computational complexity to the preprocessing step is addressed for the (S)QRD.
While in the literature - and as strongly recalled in Section 3.1.2 - some classical (S)QRD algorithms have been widely considered, the straightforward mono-carrier to multi-carriers extension is not satisfying. Namely, it leads to a dramatic overall - over a whole RB - computational complexity since the full-(S)QRD remains a demanding step [Aub10] that must be done N_U times for each time slot. As evoked in Sections 2.6 and 5.1.1, adjacent channel matrices are subject to correlation in time, frequency or both.
Consequently in practical applications, a solution that provides the $\mathbf{Q}_{k',l'}$ and $\mathbf{R}_{k',l'}$ output, from any correlated $\mathbf{Q}_{k,l}$ and $\mathbf{R}_{k,l}$ input and from the channel variation $\Delta_H = \mathbf{H}_{k',l'} - \mathbf{H}_{k,l}$, would be computationally advantageous. In particular, if it maintains the performance. The interest is

even obvious if we consider the trivial case of a channel - thus its (S)QRD output - as constant over a certain number of REs. With this aim in view and to the best of the authors' knowledge, two main trends have been explored in the literature, by discarding the solution that consists in considering the QRD output as constant within the coherence bandwidth or time.

Cescato *et al.* were interested in such a consideration early on. The technical solution that they propose lies in the interpolation of full-QRDs - processed for only a limited number of REs - through the Laurent Polynomial [CDA05, Wue06]. A smart additional and invertible mapping makes this kind of interpolation applicable in [CDA05]. In [Wue06], this technique has been extended to the SQRD. Little success is offered, unless at the cost of a computationally expensive calibration [CDA05, Wue06]. Otherwise, a performance floor is observed in the high SNR range.
Gor *et al.* [Gor06] propose another solution that lies in a direct tracking of the matrix $\mathbf{R}_{k,l}$ - instead of classically tracking the channel matrix $\mathbf{H}_{k,l}$ at each RS position. Subsequently, the QRD at each RE position is obtained from a full-QRD at each RS position. This solution is by nature different since it consists in bypassing the QRD computation that is addressed in the present section. Moreover, this absolute threshold-based solution involves a specific system configuration, leading to implementation issues and in particular a weak robustness.
In the sequel, a novel approach is considered. It constitutes the first theoretical expression for answering the aforementioned aspect. In particular, it relies on the matrix perturbation theory, that is a field of linear algebra. It focuses on the extension of known results of perturbed matrices, initiated by Kato in [Kat70]. We are interested in additively perturbed matrices, *i.e.* of the form $\tilde{\mathbf{H}} = \mathbf{H} + \Delta_H$. Stewart [Ste92] studied the series expansion of perturbations of the identity matrix, and showed how to extend this result to perturbations of arbitrary matrices for Lower-Upper (LU), Cholesky and QR factorizations. In this section, we focus on QR perturbation theory.

Dopico and Molera [Dop06] have stated that the series expansion of Cholesky factors can be recursively defined as follows. We recall this result and provide a proof.

Theorem 5.2.1 (CF series expansion)**.** *We denote $\mathbf{H} \in \mathbb{C}^{n_T \times n_T}$ - thus square - an Hermitian positive definite matrix (*i.e. *symmetric with real positive eigenvalues) with CF $\mathbf{H} = \mathbf{U}^H\mathbf{U}$, and $\mathbf{E}_H$ another Hermitian matrix, called* perturbation*. We consider the Hermitian matrix $\tilde{\mathbf{H}} = \mathbf{H} + \mathbf{E}_H$ and set $\mathbf{F} = \mathbf{U}^{-H}\mathbf{E}_H\mathbf{U}^{-1}$. Given any matrix $\mathbf{A}$, we define $\mathbf{A}_{\hat{U}}$ as the matrix:*

$$\mathbf{A}_{ij} = \begin{cases} \frac{1}{2}\mathbf{A}_{ii}, & \forall i = j \\ \mathbf{A}_{ij}, & \forall i < j \\ 0, & \forall i > j. \end{cases} \tag{5.11}$$

We denote $|\mathbf{F}|$ as the matrix that has $\{|\mathbf{F}_{ij}|\}_{i,j}$ as coefficients. If its spectral radius - i.e. *its maximal eigenvalue - $\rho(|\mathbf{F}|) < 1$, then $\tilde{\mathbf{H}}$ is positive definite and has a CF $\tilde{\mathbf{H}} = \tilde{\mathbf{U}}^H\tilde{\mathbf{U}}$, with*

$$\tilde{\mathbf{U}} = \left(\mathbf{I}_{n_T} + \sum_{i=1}^{\infty} \mathbf{U}_i\right)\mathbf{U}, \tag{5.12}$$

and the following upper triangular matrices:

$$\begin{cases} \mathbf{U}_1 &= \mathbf{F}_{\hat{U}} \\ \mathbf{U}_i &= (-\mathbf{U}_1^H\mathbf{U}_{i-1} - \mathbf{U}_2^H\mathbf{U}_{i-2} - \cdots - \mathbf{U}_{i-1}^H\mathbf{U}_1)_{\hat{U}} \text{ for } i \geq 2. \end{cases} \tag{5.13}$$

The existence of this CF is proven in [Dop06]. In the following proof and in addition to [Dop06], the details of how $\tilde{\mathbf{U}}$ is computed are given. To the best of the author's knowledge, these have not been previously given in the literature until [Aub11b].

Proof. We denote $\mathbf{H}$ as a square and non-singular ($\det\{\mathbf{H}\} \neq 0$) complex matrix, such that $\mathbf{H} = \mathbf{U}^H\mathbf{U}$ is a CF. Also, we denote $||.||$ as any consistent matrix norm. Namely, it should verify that if $|\mathbf{H}| < |\mathbf{B}|$, then $||\mathbf{H}|| < ||\mathbf{B}||$ and $||\mathbf{HB}|| < ||\mathbf{H}||||\mathbf{B}||$. As an example, the Frobenius norm could be used while it is not the case in this demonstration in order to maintain the generality of the proposed solution.
We assume that $||\mathbf{F}|| < 1$. Dopico and Molera show in [Dop06] that the perturbed identity $\mathbf{I}_{n_T} + \mathbf{F}$ is positive definite and has a CF: $\mathbf{I}_{n_T} + \mathbf{F} = (\mathbf{U}_I)^H\mathbf{U}_I$. This yields:

$$\tilde{\mathbf{H}} = \mathbf{U}^H(\mathbf{I}_{n_T} + \mathbf{U}^{-H}\mathbf{E}_H\mathbf{U}^{-1})\mathbf{U} = \mathbf{U}^H(\mathbf{U}_I)^H\mathbf{U}_I\mathbf{U} = \tilde{\mathbf{U}}^H\tilde{\mathbf{U}}, \tag{5.14}$$

which is a CF of $\tilde{\mathbf{H}}$ since $\mathbf{U}_I$ is upper-triangular.
Moreover, $\rho(|\mathbf{F}|) \leq ||\mathbf{F}||$. Note that in [Dop06], the spectral radius is used. It is valid for a wider set of matrices. However in practice, checking the condition with the Frobenius norm is low-computational while not affecting the proof. In the sequel, we will restrict to matrices verifying $||\mathbf{F}|| < 1$ for this norm.
Since $\tilde{\mathbf{H}} = \tilde{\mathbf{U}}^H\tilde{\mathbf{U}}$, we can focus on the basic CF of perturbations of the identity matrix $\mathbf{I}_{n_T} + \mathbf{F}$.

We multiply the perturbation matrix $\mathbf{F}$ by a complex factor $z \in \mathbb{C}$ to have some control on the amplitude of the perturbation. The introduction of this new variable z allows for some interesting complex analysis results. We compute the CF of the perturbation of identity:

$$\mathbf{I}_{n_T} + z\mathbf{F} = (\mathbf{U}_I)^H(z)\mathbf{U}_I(z), \tag{5.15}$$

where $\mathbf{U}_I(z)$ is a complex function of z, and $\mathbf{U}_I(1) = \mathbf{U}_I$. These factors exist when $\rho(|zF|) < 1$, *i.e.* inside the disc $D_{\mathbb{C}}^F = \{z \in \mathbb{C},\ |z| < \frac{1}{\rho(|F|)}\}$.
Moreover, it can be shown, by studying the CF algorithm, that $\mathbf{U}_I(z)$ is a rational function of z when $\rho(|F|) \neq 0$. Therefore, the coefficients of $\mathbf{U}_I(z)$ are analytic functions of z in $D_{\mathbb{C}}^F$, and the Taylor series of $\mathbf{U}_I(z)$ around 0 are power series in $D_{\mathbb{C}}^F$.

We write $\mathbf{U} = \sum_{i=0}^{\infty}\mathbf{U}_i z^i$, which leads - by using the power series multiplication rule - to:

$$\mathbf{I}_{n_T} + z\mathbf{F} = \mathbf{U}^H(z)\mathbf{U}(z) = (\sum_{i=0}^{\infty}(\mathbf{U}_i)^H z^i)(\sum_{j=0}^{\infty}\mathbf{U}_j z^j) = \sum_{i=0}^{\infty}(\sum_{j=0}^{i}(\mathbf{U}_j)^H\mathbf{U}_{i-j})z^i. \tag{5.16}$$

Subsequently and by matching the terms with the same power of z, we get:

$$\begin{cases} \mathbf{I}_{n_T} = (\mathbf{U}_0)^H\mathbf{U}_0, & (i=0) \\ \mathbf{F} = (\mathbf{U}_0)^H\mathbf{U}_1 + (\mathbf{U}_1)^H\mathbf{U}_0, & (i=1) \\ 0 = (\mathbf{U}_0)^H\mathbf{U}_i + (\mathbf{U}_1)^H\mathbf{U}_{i-1} + \ldots + (\mathbf{U}_{i-1})^H\mathbf{U}_1 + (\mathbf{U}_i)^H(\mathbf{U}_0)^H, & (i \geq 2) \end{cases} \tag{5.17}$$

All the $\mathbf{U}_i$'s are upper triangular and the previous equations lead to their definitions. In particular and for $i = 0$, we get $\mathbf{U}_0 = \mathbf{I}_{n_T}$. Next - for $i = 1$ -, $\mathbf{F} = \mathbf{U}_1 + (\mathbf{U}_1)^H$, and we get $\mathbf{U}_1 = \mathbf{F}_{\hat{U}}$, as defined in Theorem 5.2.1. Finally for $i \geq 2$, we get $\mathbf{U}_i + (\mathbf{U}_i)^H = -(\mathbf{U}_1)^H\mathbf{U}_{i-1} - \ldots - (\mathbf{U}_{i-1})^H\mathbf{U}_1$, and - similarly to the simpler case $k = 1$ - $\mathbf{U}_i = (-(\mathbf{U}_1)^H\mathbf{U}_{i-1} - \ldots - (\mathbf{U}_{i-1})^H\mathbf{U}_1)_{\hat{U}}$.
Finally, $\tilde{\mathbf{U}} = (\mathbf{I}_{n_T} + \sum_{i=1}^{\infty}\mathbf{U}_i)\mathbf{U}$ is obtained for $z = 1$. □

In this section, we now focus on the QRD. Namely, the perturbation of $\mathbf{H}$ - that can be seen as the $\mathbf{QR}$ product - is treated. The novelty lies in the extension of the previous result to the QRD. This way, it allows the acquisition of "perturbed" $\mathbf{Q}$ and $\mathbf{R}$ factors, thus taking advantage of the correlation between adjacent channels.
By introducing $\mathbf{B} = \mathbf{H}^H\mathbf{H}$ and $\tilde{\mathbf{B}} = \tilde{\mathbf{H}}^H\tilde{\mathbf{H}}$ with $\tilde{\mathbf{H}} = \mathbf{H} + \mathbf{E}_H$, we get:

$$\tilde{\mathbf{B}} = \mathbf{H}^H\mathbf{H} + \mathbf{H}^H\mathbf{E}_H + (\mathbf{E}_H)^H\mathbf{H} + (\mathbf{E}_H)^H\mathbf{E}_H \tag{5.18}$$

$$= \mathbf{H}^H\mathbf{H} + \mathbf{H}^H\mathbf{E}_H + (\mathbf{E}_H)^H\mathbf{H} + O(\|\mathbf{E}_H\|^2). \tag{5.19}$$

Since $\mathbf{H}$ is necessarily QR decomposable, it rewrites $\mathbf{H} = \mathbf{QR}$, with the notations introduced in Section 3.1.2. This yields $\mathbf{B} = \mathbf{H}^H\mathbf{H} = \mathbf{R}^H\mathbf{R}$, which can thus be considered as a CF of $\mathbf{B}$.
Now, we compute $\mathbf{R}^{-H}\tilde{\mathbf{B}}\mathbf{R}^{-1} = \mathbf{I}_{n_T} + \mathbf{R}^{-H}(\mathbf{H}^H\mathbf{E}_H + (\mathbf{E}_H)^H\mathbf{H} + \mathbf{E}_H^H\mathbf{E}_H)\mathbf{R}^{-1}$, and set $\mathbf{E_B} = \mathbf{H}^H\mathbf{E}_H + (\mathbf{E}_H)^H\mathbf{H} + \mathbf{E}_H^H\mathbf{E}_H$, which is also Hermitian. Theorem 5.2.1 can be applied to $\mathbf{B} + \mathbf{E}_B$ as soon as the condition $\rho(|\mathbf{F}_B|) < 1$ is satisfied for:

$$\mathbf{F}_B = \mathbf{R}^{-H}(\mathbf{H}^H\mathbf{E}_H + (\mathbf{E}_H)^H\mathbf{H} + (\mathbf{E}_H)^H\mathbf{E}_H)\mathbf{R}^{-1}. \tag{5.20}$$

Subsequently and for $\mathbf{F} = \mathbf{F}_B$, the key expression - for a QRD - arise from Equation (5.12) and reads:

$$\tilde{\mathbf{R}} = \left(\mathbf{I}_{n_T} + \sum_{i=1}^{\infty}\mathbf{R}_i\right)\mathbf{R}. \tag{5.21}$$

In particular, the first approximation orders of $\mathbf{R}$ factors read:

$$\begin{cases} \tilde{\mathbf{R}}_0 &= \mathbf{R} \\ \tilde{\mathbf{R}}_1 &= (\mathbf{I}_{n_T} + \mathbf{F}_{\hat{U}})\mathbf{R} \\ \tilde{\mathbf{R}}_2 &= (\mathbf{I}_{n_T} + \mathbf{F}_{\hat{U}} - (\mathbf{F}_{\hat{U}}^H\mathbf{F}_{\hat{U}})_{\hat{U}})\mathbf{R}. \end{cases} \tag{5.22}$$

Subsequently, $\tilde{\mathbf{Q}}$ may be obtained as $\tilde{\mathbf{H}}\tilde{\mathbf{R}}^{-1}$, and simplified by introducing some approximations [Ste92]. As an example with the first approximation order of $\mathbf{Q}$, we are able to compute $\tilde{\mathbf{Q}}_1$:

$$\begin{cases} \tilde{\mathbf{Q}}_1 &= \tilde{\mathbf{H}}\tilde{\mathbf{R}}_1^{-1} \\ &= (\mathbf{H} + \mathbf{E}_H)\mathbf{R}^{-1}(\mathbf{I}_{n_T} + \mathbf{F}_{\hat{U}})^{-1} \\ &= (\mathbf{Q} + \mathbf{E}_H\mathbf{R}^{-1})(\mathbf{I}_{n_T} - \mathbf{F}_{\hat{U}}) \\ &\approx \mathbf{Q}(\mathbf{I}_{n_T} - \mathbf{F}_{\hat{U}}) + \mathbf{E}_H\mathbf{R}^{-1}. \end{cases} \tag{5.23}$$

By considering the expression given above, it should be noted that - by neglecting the residual $(\mathbf{E}_H)^H\mathbf{E}_H = O(\|\mathbf{E}_H\|^2)$ - the first order formula corresponds to an existing result that is proposed by Stewart [Ste92]. How to obtain a convenient formulation about the expression of $\mathbf{Q}$ is not further addressed since its proposed application - namely the LSD - relies on $\tilde{\mathbf{R}}$ only.

The only required statement in Theorem 5.2.1 is that the spectral radius - that is recalled to be the maximal eigenvalue - of $|\mathbf{F}|$ is smaller than 1. It is not reasonable in practice to check this computationally expensive condition that is of the order of a full-QRD. Fortunately, Theorem 5.2.1 remains valid if the condition is replaced by $||\mathbf{F}|| < 1$ - under the condition that it is a consistent norm - which is a novel approach. The Frobenius norm is one of these norms. The Frobenius norm-based criterion is an efficient low-complexity tool - drastically cheaper to compute while providing a satisfying simplification of the algorithm - as further detailed.

Equation (5.21) is applicable to our context. At this point, it is convenient to make use of the notations specified in Section 2.5, in particular in Equation (2.28). While the expression is exact - namely it tends to the exact full-QRD $\mathbf{R}_{k',l'}$ output towards infinity - when the series converges, a dramatic accuracy loss is observed when the series diverges. Consequently, the convergence criterion has been considered in the solution proposed in [Aub11b]. As previously suggested in the formula's demonstration, the convergence criterion is advantageously replaced by the squared Frobenius norm $\|\mathbf{F}\|_{\mathcal{F}}^2 = Trace\{\mathbf{F}^H\mathbf{F}\}$ of $\mathbf{F}$, defined as:

$$\mathbf{F} = \mathbf{R}_{k,l}^{-H}(\mathbf{H}_{k,l}^H\mathbf{E}_H + (\mathbf{E}_H)^H\mathbf{H}_{k,l} + (\mathbf{E}_H)^H\mathbf{E}_H)\mathbf{R}_{k,l}^{-1}. \tag{5.24}$$

Thus, deciding whether the proposed formula should be applied or not can then be done in a low-computational way. Our solution introduces the variable choice of the n^{th} order of the series to be

	$\mathcal{C}$	$\mathcal{T}$
full-QRD [Aub10]	$4n^3 + 30n^2 + 32n$	$4n^3 + 30n^2 + 32n$
VIQRD	$cn^3 + 8n^2 + \frac{22}{3}n$	$\frac{2}{3}n^3 + 8n^2 + cn$

Table 5.7: $\mathcal{C}$ and $\mathcal{T}$ equivalence, expressed in MUL.

considered. It is set depending on whether the convergence criterion is respected or not. Namely, different series orders n_{dv} and n_{cv} are selected, according to the divergence or convergence of the series, respectively. We have:

$$\mathbf{R}_{k',l'} = \left(\mathbf{I}_{n_T} + \sum_{i=1}^{n_{end}} \mathbf{U}_i\right) \mathbf{R}_{k,l}, \tag{5.25}$$

with n_{end} chosen as n_{dv} or n_{cv}. The existence of an efficient couple (n_{dv}, n_{cv}) has been shown by simulations, in the practical case. It will be introduced in the sequel and the corresponding technique is denoted as the Variable Incremental QR Decomposition (VIQRD) [Aub11b].

The algorithm proposed in the previous section is generic and allows for the consideration of an adjacent channel in time or in both time and frequency domains. In the case of an adjacent RE in the frequency domain, additional memory for channel coefficients storage is not needed. That is why, without loss of generality, we focus on the frequency domain neighbourhood in this section.

The computational complexity of the GS-based full-QRD has been theoretically obtained [Aub10] and is displayed in Table 5.7. Herein, for the sake of readability in the computational complexity expressions, we consider $n_R = n_T = n$ and introduce the auxiliary constant $c = (74 + 6n_{cv}(n_{cv} - 1))/3$. While we recall - from Section 3.2.7 - that the $\mathbf{Q}$ calculation is unnecessary for the SD detector, it is necessary within any full-QRD algorithm. Thus the computational complexity that is summarized in [Aub10] cannot be reduced.
The computational complexity of the VIQRD algorithm can be split into the inversion of $\mathbf{R}_{k,l}$, the convergence criterion computation and comparison to 1 and finally the series calculation. By assuming that $n_{dv} \leq n_{cv}$, its maximal computational complexity $\mathcal{C}$ has been theoretically obtained and is introduced in Table 5.7.

It is clear from Table 5.7 that both the full-QRD and the VIQRD offer a $O(n^3)$ total computational complexity. Nevertheless, we introduce a comparison parameter in order to make a distinction between them, namely the time complexity $\mathcal{T}$. It has been strongly introduced in Section 2.7.3 and we recall that it is related to the number of processors available for implementation. According to the discussion introduced in Section 2.7.3 from [Li 99], the time/processor complexity trade-off is summarized. By considering a highly parallel DSP architecture allowing to operate on 16 16-bit words vectors - and since the LTE(-A) norm requires to provide up to 8×8 antennas in the DL - any matrix multiplication time complexity within the VIQRD algorithm becomes $O(n)$ (see Section 2.7.3). Thus, this discussion still holds true with an EVP (see Section 2.7.3).
This parallel architecture will significantly reduce the time complexity of the VIQRD since parallel calculations are allowed. It is not the case of the full-QRD [Aub10] due to the iterative nature of the related algorithms [Aub10]. The main part of the time complexity effort lies in the $\mathbf{R}_{k,l}$ matrix inversion, despite simplifications induced by real diagonal entries. Its maximal time complexity has been theoretically obtained and is given in Table 5.2. Thus it is clear that our algorithm implementation offers a reduced time complexity compared to full-QRD.

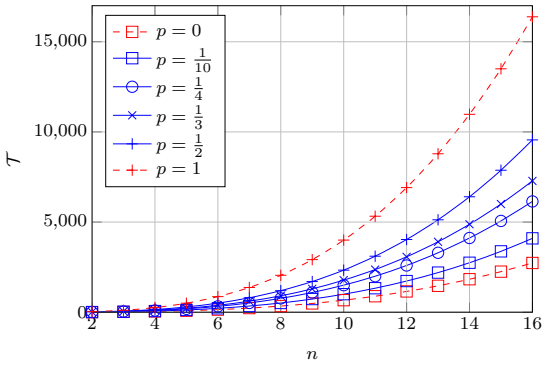

Figure 5.4: $\mathcal{T}$ as a function of the channel matrix size, for multiple VIQRD densities in an RB.

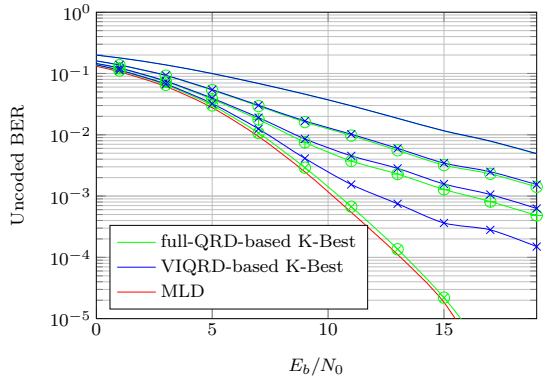

Figure 5.5: Uncoded BER as a function of E_b/N_0, Complex 4×4 SM-MIMO-SC system with an EVA filter, a speed of 50 km/h and 512 sub-carriers, K-Best and ML detectors, 4-QAM modulations at each layer.

From now on, the full-QRD/VIQRD mixing over a whole RB is presented. By considering p as the ratio of full-QRD processing within the RB, and dually $(1-p)$ the ratio of VIQRD processed, the total time complexity reads:

$$\mathcal{T}_{Mixed} = p(4n^3 + O(n^2)) + (1-p)(\frac{2}{3}n^3 + O(n^2)). \tag{5.26}$$

In Figure 5.4, the time complexity advantage of the proposed solution is highlighted through numerical evaluations. In particular, for p=1/2, the time complexity over an RB is significantly reduced, namely by a factor of 42%, independently of the channel matrix size.

In Figure 5.5, the uncoded BER performance of the QRD-based K-Best LSD is depicted with the use of 4-QAM modulations in a 4×4 system. The neighbourhood size K is set to 1, 2, 3 and 4, similarly to Figure 3.7. The full-QRD and the aforementioned - $(n_{dv}, n_{cv}) = (1, 2)$ and p=1/2 - mixed solution are considered and compared to the reference MLD. The simulation results are provided according to 3GPP LTE channel models. We focus on the EVA model - that corresponds to a medium delay spread environment - and on a mobile speed of 50 km/h with a carrier frequency of 2 GHz. The entire channel bandwidth has been divided into 512 sub-channels, which leads to 300 tones allocated to data transmission.

The performance in Figure 5.5 confirms the efficiency of the proposed solution technique. As

it is depicted - and with the aforementioned system configuration and VIQRD calibration - the 42% time complexity decrease is achieved at the price of a SNR loss compared to the reference full-QRD-based 4-Best, which is the closest-to-MLD. The - small - inaccuracy of the proposed solution impacts the performance of the SD when it is near-MLD. It is particularly clear in the high SNR range. It is due to the detector nature itself that is not robust to imperfect channel estimation - or computation. This sensitivity disappears with a smaller neighbourhood study. Also, the performance loss between reference and proposed solutions will be reduced through the fixed point step that will introduce quantification noise.

However, the proposed solution only offers a tiny performance improvement compared to a constant QRD over a certain number - that is required to be efficiently estimated - of REs. It is particularly true in the worst-case computational complexity configuration - the maximal number of sub-carriers - where the maximal correlation in frequency arises and thus the coherence bandwidth is large.

The occurring trade-off leads to a discussion about the accepted performance loss that depends on the system requirements. This idea is retained as a possible alternative. While this preprocessing step - as previously claimed - offers a possible time complexity decrease, more advantageous results are provided in the sequel.

5.2.2 Lattice-Reduction Preprocessing

In the present section, the advantage of shifting the detector's computational complexity to the preprocessing step is addressed for the LR.
Similarly to the section above, the full-(S)LA is not straightforwardly applied on each channel within the RB. Namely, the correlation between adjacent channels is exploited. To the best of the author's knowledge, only one main trend has been explored in the literature.

Precisely, we denote two adjacent channels $\mathbf{H}_1$ and $\mathbf{H}_2$. Consistently with Section 3.3.2, their reduced forms read $\tilde{\mathbf{H}}_1$ and $\tilde{\mathbf{H}}_2$ and their transformation matrices read $\mathbf{T}_1$ and $\mathbf{T}_2$, respectively. We apply the (S)LA on the *pre-reduced* matrix [Mur08, Mur09], which means that the (S)LA is applied on the matrix $\mathbf{H}_2\mathbf{T}_1$. Due to the lattice definition stated in Section 3.3.2, it is equivalent - it generates the same lattice points - to directly applying it on $\mathbf{H}_2$. This way, the accurate reduced matrix $\tilde{\mathbf{H}}_2$ is obtained through the transformation matrix $\mathbf{T}_2^{'}$ [Mur08, Mur09] - different from $\mathbf{T}_2$ - such that:

$$\mathbf{T}_2 = \mathbf{T}_2^{'}\mathbf{T}_1. \tag{5.27}$$

Advantageously when correlation arises, a large number of swapping and reduction inside the (S)LA have been previously - occasionally on the adjacent channel - done, thus inducing a decrease in the computational complexity [Mur08, Mur09]. The two additional matrix multiplications have been taken into account in the simulation results that are depicted in the sequel. It is important to note that this solution is exact and does not introduce performance loss.

In [Naj11], two different methods are discussed. The first is the exact technique proposed in [Mur08, Mur09] and introduced just above. Nevertheless, an additional theoretical study - through the 1^{st} order autoregressive model - is offered in [Naj11].
The second induces more savings in the computational complexity. However, it only relies on the use of the same matrix $\mathbf{T}$ over a certain number of adjacent channels [Naj11]. The accurate $\tilde{\mathbf{H}}$ is subsequently deduced from the relation $\tilde{\mathbf{H}} = \mathbf{HT}$. With this aim in view, the LR step is or is not applied according to a condition that relies on the OD criterion [Naj11]. However, such a solution

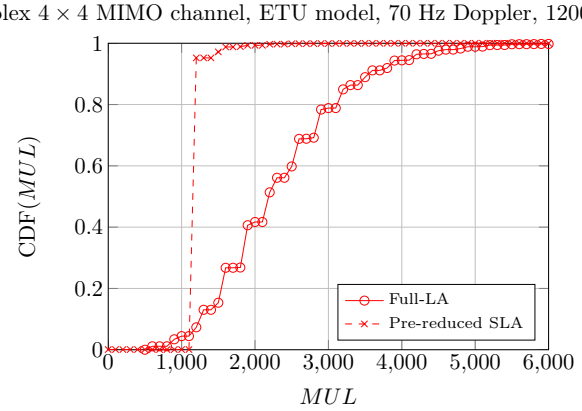

Figure 5.6: CDF of the number of equivalent MUL of the SLA with or without pre-reduction.

is suboptimal and it is only interesting in high-correlation scenarii.
Also, a mix of both these methods is discussed but is not satisfying either.

In Figure 5.6, the MMSE-SQRD-based (see Section 3.1.3) SLA (see Section 3.3.2.1) with pre-reduction is depicted. In the simulations, the pre-reduction aspect has been directly considered in time, the reason will become clear in the sequel. Consequently, each channel $\mathbf{H}_{k,l}$ - except for $k = 1$ -, is pre-reduced by the matrix $\mathbf{T}_{k-1,l}$ that corresponds to the SLA of the previous channel. It is compared to the reference - without pre-reduction - QRD-based LA, thus denoted as full-LA. The CDF of the number of equivalent MUL of the SLA is depicted. In the simulations, we consider the worst-case - that induces the least correlated $\mathbf{H}_1$ and $\mathbf{H}_2$ in time - maximal Doppler frequency, namely 70 Hz according to Section 5.1.1. Also, the worst-case - that induces the least correlated $\mathbf{H}_1$ and $\mathbf{H}_2$ in frequency - ETU channel model is employed. While it offers convenient correlation in frequency, an FFT size of 2048 is considered since it corresponds to the most demanding configuration, thus justifying further studies in the computational complexity decrease.

Clearly from Figure 5.6, the presented solution offers a significant computational complexity decrease in mean. Even the maximum computational complexity is reduced, while it is not theoretically stated neither in the present literature nor in this work. Consequently, the NP-hard nature of the (S)LA is still relevant and must be discussed for implementation. In particular, a thresholded variant of the (S)LA is required. Consistent with Section 3.3.2, the (S)LA's computational complexity decreases exponentially. By considering the pre-reduced solution, the computational complexity decreases more rapidly compared to the reference one. Thus, the pre-reduced SLA can be thresholded more efficiently, even if a tiny performance loss still occurs.
While taking advantage of correlation in frequency is efficient - namely, for 95% of SLA calls, a computational complexity decrease by a factor of 2.6 arises - simulations show that taking advantage of correlation in time leads to a higher computational complexity decrease. Namely and for 95% of SLA calls, a computational complexity decrease by a factor of 3.5 is obtained.
Nevertheless in this case and as claimed in Section 5.1.1, an additional memory cost is required. It consists in storing one additional $\mathbf{T}$ matrix - namely the previous one in time -, by interestingly noting that its entries are all Gaussian - complex, with real and imaginary integer parts - which induces to a reasonable cost. In particular with a 4×4 MIMO scheme, $\mathbf{T}$ is made of 16 entries that are signed integers. The maximal occurring - signed - value being lower to 8 (in absolute value), 4 bits are sufficient for each entry, thus inducing a - low - additional memory cost of 64 bits.

Further improvements are possible. In particular, a smart extension of this idea can be proposed and offers a further computational complexity decrease, again with no performance loss. However, this novel solution has not been protected for the moment, thus inducing the non-disclosure of this idea.
Also and depending on the environnement or the available resources, a more agressive threshold may be used. Thus, it leads to an important complexity decrease even if a performance loss occurs.

As a conclusion, this solution is retained and is considered to be of high interest. It leads to a promising - since this study remains an algorithmic study - detector for the 4×4 SM-MIMO-OFDM scheme with the LTE(-A) standard. In particular, the advantage of shifting the detector's computational complexity to the preprocessing step clearly arises here.

5.2.3 Lattice-Reduction Preprocessing in the Closed-Loop Mode

In the present section, the advantage of shifting the detector's computational complexity to the preprocessing step is addressed for the LR in the CL mode.
Similarly to the section above, a decrease in the computational complexity is expected due to practical requirements. But here, differently, it does not rely on correlation between adjacent channels. In particular, CL mode allows for precoding, which offers an advantageous aspect when set prior to the LR step. Namely, it makes the effective channel better conditioned, thus decreasing the computational complexity of the (S)LA.

It is due to the large part of likeness between the impact of the precoding and of the LR step on the equivalent channel. Nevertheless, it should be noted that this method is different since the LR step is processed in reception only, while the CL mode requires a feedback loop. In Figure 5.7, the idea of (S)LA applied with precoding is depicted in a block-scheme manner. It is constituted of a simplified version of Figure 3.15 - with the same notations - and the selection process of a precoding matrix $\mathbf{W}$ is added, consistently with Section 5.1.3.

As a consequence, the pre-multiplication by a precoding matrix $\mathbf{W}$ leads to a better conditioned -

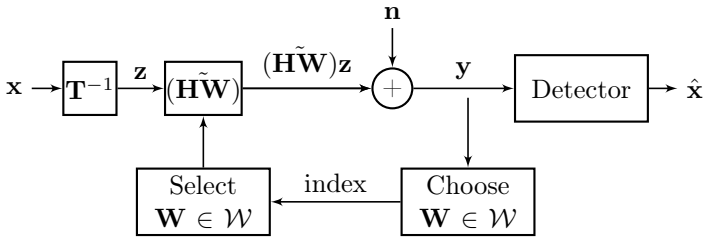

Figure 5.7: LRA detector bloc-scheme with precoding.

compared to $\mathbf{H}$ and according to the selected criterion (see Section 5.1.3) - effective channel matrix $\mathbf{HW}$. Consequently, a lower number of swapping and reduction inside of the (S)LA is required, thus leading to a computational complexity decrease to obtain the reduced channel matrix $(\tilde{\mathbf{HW}})$. Moreover, the (S)LA improves the conditioning of the reduced channel matrix compared to the precoding step alone, thus improving the corresponding detector's performance. It is due to the finiteness of the available codebooks, introduced in Section 5.1.3.
Both the performance and computational complexity aspects will be discussed through simulations in the sequel. Also, a particular attention will be paid to computational complexity bounds of both the SLA and SA, which is an essential aspect for implementation.

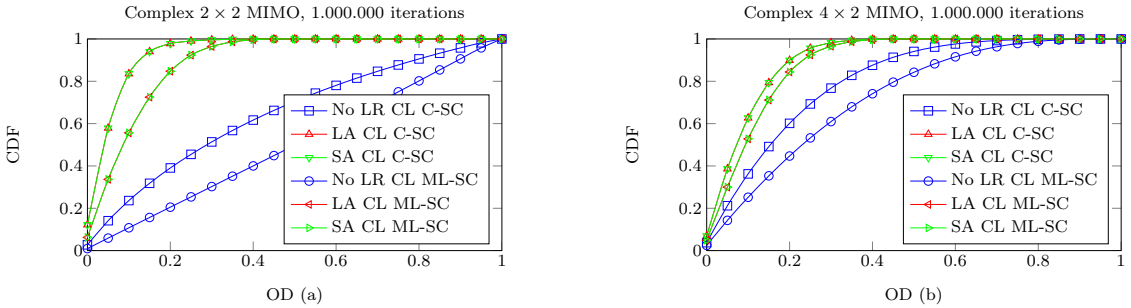

Figure 5.8: CDF of the OD, for a 2×2 MIMO (a) and a 4×2 MIMO (b) precoding schemes.

In Figure 5.8, the CDF of the computational complexity of the LA is depicted, with both the ML and capacity selection criteria. It is compared to the reference - with no LR - CL mode, also with both the introduced criteria. In addition, the SA has been depicted in order to eventually soften the choice of the (S)LA - versus SA - for the LR step, previously introduced in Section 3.3.2. In the simulations, the 2×2 and 4×2 - available - modes have been considered and 1.000.000 i.i.d. channel matrices have been drawn, which is large enough for providing relevant simulation result about - OD and computational complexity - upper bounds.

As depicted, the LR step following an appropriate precoding offers improved OD of the equivalent channel matrix. It should be noted that with both the 2×2 and the 4×2 systems, there is no gain - from an OD criterion point of view - with SA compared to (S)LA. It is due to the dimension of the study that consists in reducing only matrices made of two column vectors. Consequently, the most accurate - while most complex - SA does not offer improved performance.

In Figure 5.9, the CDF of the computational complexity of the LA and the SA is depicted, with both the ML and capacity selection criteria. It is compared to the reference - with no LR - CL mode, also with both the introduced criteria. In the simulations, the 2×2 and 4×2 - available - modes have been considered and 1.000.000 i.i.d. channel matrices have been drawn. The maximal number of MUL is pointed out by markers.

Obviously, the mean computational complexity is decreased in both the 2×2 and 4×2 MIMO systems, by assuming that the accurate selection criterion has been employed.
Last but not the least, while the upper bounded computational complexity of the (S)LA/SA does not change in 2×2 MIMO systems compared to the OL mode, it is decreased in 4×2 systems. It is due to the OD bound - away from 1 - in 4×2 MIMO systems, exhibited in Section 5.1.3. The link between the OD bound - made away from 1 - and the C-SC (see Figure 5.3) is demonstrated in [Ma 08]. This aspect vindicates that we expected the computational complexity of the LR step to be bounded also. To the best of the author's knowledge, this interesting aspect has not been theoretically shown in the literature nor in the present work.
Moreover, a better computational complexity decrease arises with LA compared to SA, thus endorsing the choice of the (S)LA at the LR step, as introduced in Section 3.3.2.

The aforementioned discussion about the mean and maximal computational complexities is clearly summarized in Tables 5.8 and 5.9, subsequently to Figure 5.9. The simulation setup remains unchanged.

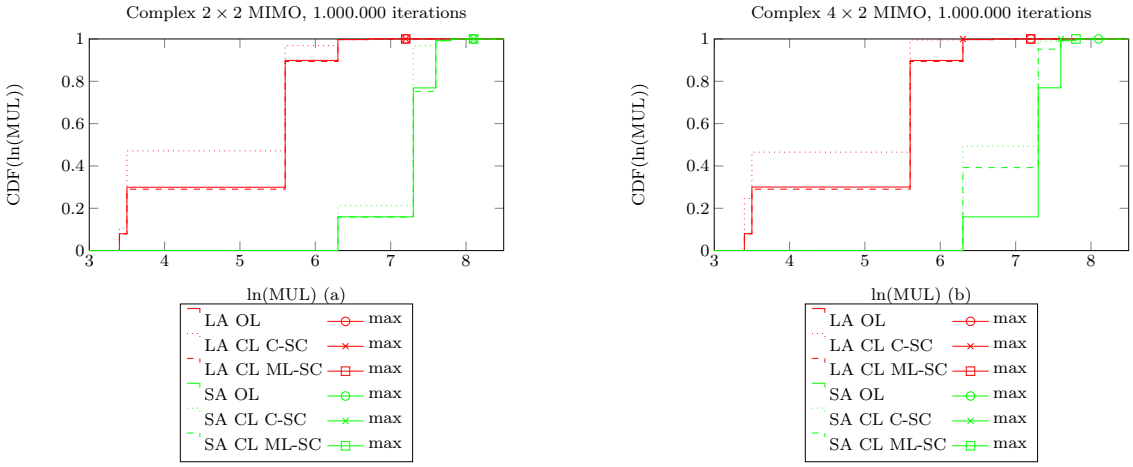

Figure 5.9: CDF of $ln(MUL)$ for LA-based and SA-based LR, for a 2×2 MIMO (a) and a 4×2 MIMO (b) precoding schemes.

	OL		CL C-SC		CL ML-SC	
	mean	max	mean	max	mean	max
LA	223	1225	165	1224	227	1226
SA	1373	3200	1233	3200	1381	3200

Table 5.8: Mean and maximum complexities in OL, CL C-SC and CL ML-SC cases, in Complex 2×2 MIMO case.

In 2×2 MIMO systems, a mean computational complexity decrease of up to 26% occurs for LA-based LR, by considering the C-SC. Simultaneously, the upper bound of the computational complexity remains unchanged.

In 4×2 MIMO systems, a mean computational complexity decrease of up to 58% occurs for LA-based LR, by considering the C-SC.
Simultaneously, the upper bound of the computational complexity is decreased, despite the finiteness aspect of the codebook required by the LTE(-A) standard. The decrease is significant, namely 39% for LA-based LR, by considering the C-SC.

The proposed LRA-MMSEE K-Best detector still straightforwardly applies in the CL mode, in particular the LR step. Nevertheless, this particular mode will induce a computational complexity decrease. Since the system calibration relies on the worst-case computational complexity - namely the 4×4 SM scheme and OL mode - and for a fixed clock rate, the CL mode will offer a reduced consumption in the LR step - according to the presented algorithmic choices. It should be further noted that, interestingly, the introduced results on the computational complexity are independent of SNR, consistently with the claimed advantages of shifting the computational complexity to the preprocessing step.

	OL		CL C-SC		CL ML-SC	
	mean	max	mean	max	mean	max
LA	223	1226	159	509	176	746
SA	1373	3200	971	1856	1079	2304

Table 5.9: Mean and maximum complexities in OL, CL C-SC and CL ML-SC cases, in Complex 4×2 MIMO case.

5.3 Performance and Computational Complexity Evaluation of the Proposed Solution

By aiming at assessing the conclusions brought by the previous sections, the performance and computational complexity of the proposed detector are evaluated and discussed.

5.3.1 Simulation Setup

With this aim in view and for the sake of comparability with the literature, the simulation setup of the provided scenario is clearly stated. While the general aspects are only recalled from previous sections, some particular - required or induced by the LTE(-A) standard - features are clearly established.

In this section, the simulation results are provided following the system overview that has been previously introduced in Figure 2.6. The general simulation setup remains unchanged compared to what is stated in Chapter 4 and in particular in Section 4.2.2. We recall here the most important ones.
The - coded - BER performance of the proposed LRA-MMSEE K-Best detector is provided for a 4×4 SM-MIMO-OFDM system, for the two extreme 4-QAM and 64-QAM modulations. Even at this final step, the academic Rayleigh fading MIMO channel is considered since it has been widely introduced - in Section 5.2 - that practical propagation environments do not impact the performance, although they lead to computational complexity decrease. Concerning the OFDM modulation, the worst-case configuration is considered. Namely, an FFT size of 2048 sub-carriers that leads to 1200 data sub-carriers (see Section 5.1.2).

Nevertheless, practical requirements and normative aspects from the LTE(-A) standard induce some special features.
At the transmitter, data bits are first serial-to-parallel-converted into four data streams. Each information data sequence is independently turbo encoded, according to the considerations in Section 2.2. While the original coding rate is $R = \frac{1}{3}$, the sequences are then punctured - through a Rate-Matching (RM) algorithm [3GP10] - to obtain the desired coding rate. Thus the desired rate is reached when the resultant encoded sequence is data-modulated. In particular, the RM algorithm selects certain bits for transmission. Since they are determined based on the available physical resources, the RM generates puncturing patterns of arbitrary rates. More details are provided in [3GP10]. In accordance to the standard [3GP09d], the considered rates are $R = \frac{1}{2}$ and $R = \frac{3}{4}$ for 4-QAM and 64-QAM constellations, respectively. It is recalled to be denoted as the MCS.
On top of channel coding, each block of data is further protected against transmission errors by adding a Cyclic Redundancy Check (CRC) [3GP10]. By relying on the CRC processing,

ACK/NACK responses are generated, thus indicating the correct or incorrect reception of a block, respectively.
In order to make the most of the system capacity and coverage - given a power of transmission - for each user, the information data rate is adapted according to the quality of the channel link, at the transmitter. In the LTE(-A) standard [3GP09b], the UE can be configured to report Channel Quality Indicators (CQI). The CQI reports are derived from the DL received signal quality, typically based on measurements of the DL RSs [Ses09]. Subsequently, it is possible for the eNodeB to play on an appropriate MCS for the DL transmissions, by means of a CQI value. It is stated in the standard [3GP09b] but not recalled here. This is commonly referred to as link adaptation and is typically based on Adaptive Modulation and Coding (AMC) [Ses09]. Also, this feature is not considered in the present simulation results. Thus at the transmitter, the four data streams are segmented into blocks containing a selected number of bits per packet frame, according to the aforementioned MCS.
In the presence of services tolerating higher transfer delays, the Hybrid-Automatic Repeat reQuest (HARQ) retransmission of packets may be configured [Ses09]. Subsequently and in response to DL data packets, two ACK/NACK bits are transmitted in case of a two codeword DL transmission. In the case of retransmission through the HARQ - due to the occurrence of an incorrectly received block -, LLR values of preceding receptions are combined with the current ones. By proceeding this way, the SNR in a code block is increased, thus improving the performance. This feature is not considered in the present simulation results.

According to the conclusions brought through the previous sections, the proposed solution is clearly stated. This detector is denoted as soft-decision RDN LRA-MMSEE K-Best. It incorporates numerous blocks that have been presented in detail in this work. In particular, the whole detector is split into four main distinct parts:

- The preprocessing step, which includes the MMSE-SQRD prior to SLA algorithms. It is recalled to exclusively depend on the channel $\mathbf{H}$ and - the noise σ_n^2 - that leads to an efficient detection by some re-arrangements (see Sections 3.1.3 and 3.3.2);
- The *loading* step, which aims at centring the search phase around an advantageous close-to-optimal solution, namely the LRA-MMSEE LD (see Section 3.3.3);
- The detection step, which depends - among others - on data. It consists in a K-Best - in the reduced domain - SD technique. Thus it is a neighbourhood search that generates a K-dimensional list of solutions (see Section 4.4);
- The LLR generation block, which strictly speaking constitutes the soft detection step (see Section 4.4.3.1).

In Figure 5.10, the complete description of the structure of the soft-decision RDN LRA-MMSE K-Best detector is depicted in a block-scheme manner. The detector's parameters are clearly stated. In particular, they are split into:

- The input: $\mathbf{y}$, $\mathbf{H}$ and σ_n^2;
- The output: $\Lambda(\mathbf{b}_k^l \mid \mathbf{y}, \mathbf{H})$;
- The parameters: K, which is the search size in the original neighbourhood; N, which is the search size in the reduced neighbourhood; ξ, which is the constellation set; $\Lambda_{\text{clip}}(\mathbf{b}_k^l)$, which is the clipping value for the LLRs that cannot be calculated explicitly.

Within the proposed solution, a particular attention has been paid to the detector's architecture. Namely, the detector's computational complexity has been shifted to the preprocessing step as much as possible, which clearly arises in its block-scheme in Figure 5.10. Such a strategic approach turns out to be relevant from both its computational complexity and performance point of view. This aspect is clearly stated in the next section.

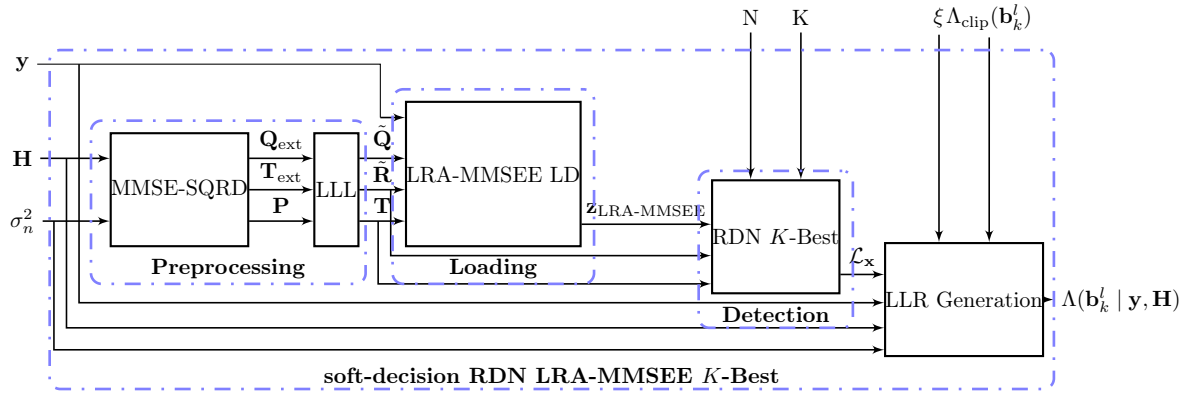

Figure 5.10: Proposed soft-decision RDN LRA-MMSEE K-Best.

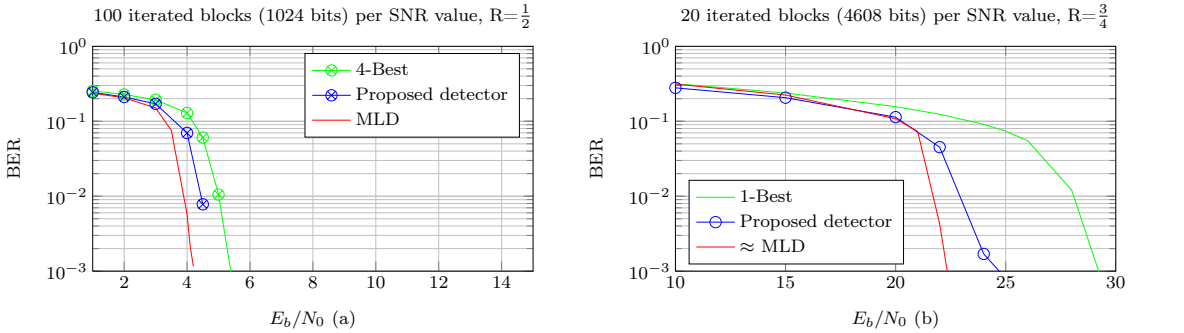

Figure 5.11: BER as a function of E_b/N_0, Complex Rayleigh 4×4 SM-MIMO-OFDM system, proposed soft-decision RDN LRA-MMSEE K-Best, classical K-Best and ML detectors, 4-QAM modulations at each layer (a) and 64-QAM modulations at each layer (b).

5.3.2 Parametric Study

We consider the simulation setup previously stated. The proposed detector is recalled - also from Section 5.3.1 - to depend on parameters. Clearly, their choice will impact both the performance and the computational complexity of the detector.

In Figure 5.11, the BER performance of the proposed soft-decision LRA-MMSEE K-Best detector is depicted with K set to 4. It is compared to the K-Best with K set to 4 and 1 with the 4-QAM and 64-QAM modulations, respectively. It is due to similar computational complexities, as stated in Table 5.10. Concerning only the proposed solution, the neighbourhood size in the reduced domain N is - as in Section 3.4.5 - set to 5. The max-log approximation in Equation (4.11) is employed when possible. Otherwise, the employed FLC is ± 8. Also, the reference MLD is depicted for the sake of comparison.

As it is depicted, the soft-decision RDN LRA-MMSEE K-Best performance is very close to the MLD, even with 64-QAM modulations. Namely, SNR offsets of 0.5 and 1.22 dB occur at a BER of 10^{-2} with 4-QAM and 64-QAM modulations, respectively. To the best of the author's knowledge and for the 4×4 SM-MIMO-OFDM scheme, the attained performance is very attractive compared to the techniques from the literature. Thus, it stands as an efficient solution in comparison with existing techniques. As a example, we consider a reference detector that offers

a similar computational complexity, namely the K-Best with an appropriate - of similar computational complexity - K. The proposed detector outperforms the K-Best. In particular with 64-QAM modulations, it offers about 5 dB of SNR improvement.

The presented performance has been obtained by setting the detector's parameters according to the following:
- K has been set to 4. It is relatively small compared to what is required for most of the K-Best LSD in order to approach the MLD performance. It is due to the LR preprocessing step that reduces the ILIs (see Section 3.3.3);
- N has been set to 5. It is relatively small compared to what is required for most of the naïve LRA K-Best LSDs in order to approach the MLD performance, in particular for high-order modulations. It is due to the LRA-MMSEE loading step that centres the neighbourhood search around a convenient - while suboptimal - solution (see Section 3.4.5);
- $\Lambda_{\text{clip}}(\mathbf{b}_k^l)$ has been set to ± 8. It is relatively large compared to what is required for most of the naïve K-Best LSD (see Section 4.4). It is due to the efficiency of the hard-detector, that aims at drastically reducing the neighbourhood search size. Namely, the latter is so small that the number of missing counter-hypothesis - thus of to-be-clipped LLRs - becomes large, thus becoming an issue for the soft-decision step. Consequently, the impact of an accurate clipping value increases. In the present work, a simple FLC is used and is chosen to be large due to the discussion in Section 4.4.3.1.

At this point, the required computational complexity of the proposed detector is provided. A realistic environnement is considered. Thus and as introduced in Section 5.2.2, the computational complexity decrease is taken into account. Namely the MMSE-SQRD-based SLA with pre-reduction in time is considered. The computational complexity decreases introduced in Sections 5.2.1 and 5.2.3 are not considered.
Since it aims at calibrating the receiver, their estimations are provided in the worst-case configuration. Similarly to Section 5.2.2, the ETU channel model, a 70 Hz maximal Doppler frequency and an FFT size of 2048 have been adopted. Also, the computational complexity of the preprocessing step has been computed over a whole RB, then it has been taken down to an RE. Consequently, the preprocessing step is achieved in 95% of the instances for a computational complexity of 1200 MUL (see Section 2.7.3).

The computational complexity of the RDN LRA-MMSEE K-Best detector can be provided in an analytical manner:

$$\begin{aligned} &2N\min\{K,N\}n_T^2 + 2\min\{K,N\}n_T^2 + 2\min\{K,N\}n_T n_R + 4n_T^3 + 8n_T^2 n_R \\ &+30\min\{K,N\}n_T - 4N\min\{K,N\} + 2\min\{K,N\}n_R + 4n_T n_R + 4n_T^2 \\ &+2N - 32\min\{K,N\} + 1200. \end{aligned} \tag{5.28}$$

In Table 5.10, the computational complexities of the proposed detector are summarized. Advantageously, a constant - in the constellation size - computational complexity is obtained. By considering the K-Best detector as a reference - which is common in the literature -, drastically improved performance occurs with the RDN LRA-MMSSE K-Best detector. The advantage is weaker for the 4-QAM modulation due to discussion is Section 3.4.4.

Consistently with discussion in Section 3.4, it possible to check in Table 5.10 that the computational complexity of the soft-decision RDN LRA-MMSEE K-Best detector does not depend on the constellation order $|\xi|$ (concerning the most significant terms). It is the key point of this advantageous solution over classical techniques for high order modulations. Also, it is independent of the SNR. As a consequence, the proposed solution offers a computational complexity decrease

MUL	4-QAM	16-QAM		64-QAM		
K	4	4	16	1	4	64
K-Best	1940	3840	11616	3904	11032	153592
RDN LRA-MMSEE K-Best	3466	3466	3806	2446	3466	3806

Table 5.10: Computational complexities equivalences.

by a factor of 3.4 for 16-QAM and - above all - 44.3 for 64-QAM modulations.
It has been decided by simulations that an efficient computational complexity/performance trade-off leads to setting the K to 4 and N to 5. It corresponds to a computational complexity of 3806 MUL for each call of the proposed solution, namely for each RE.

The computational complexity of the RDN LRA-MMSEE K-Best solution reaches a ceiling for K greater than 5 due to the $\min\{K, N\}$ term within Equation (5.28).
While the parameters N, K and $\Lambda_{\text{clip}}(\mathbf{b}_k^l)$ have been smartly - from simulations and for the purpose of an efficient computational complexity/performance trade-off - calibrated, they rely on a general 4×4 system. As an example, lower N and K are required in the CL mode. Anyway and while a small K - namely of 4 - has been chosen, it cannot be further reduced as is. According to the employed FLC and since starting from a quasi-ML - the LRA-MMSEE - hard-decision, the proposed solution offers a neighbourhood set output that is very concentrated around the hard-decision. Thus, the number of missing counter-hypothesis is very important and $\Lambda_{\text{clip}}(\mathbf{b}_k^l)$ must be chosen as small. However and due to the efficiency of the hard-decision, the missing counter-hypothesis are very unreliable and are set to ± 8. K is increased for this reason only, while a K set to 2 is sufficient in hard-decision for reaching the MLD performance, even with 64-QAM modulations.

In the next section, practical complexity measurements are provided in the LTE(-A) background.

5.3.3 Rate Estimation

The detection step is fully processed for each RE within the RB grid. As stated in Section 5.1.2, the number of occupied sub-carriers is up to 1200, thus the worst-case - the highest-computational - calibration requires the detection of 1200 REs per OFDM symbol. Also, we recall that the number of OFDM symbols within one 1 ms is 14.
Simultaneously, the number of OFDM symbols dedicated to Physical Downlink Control Channel (PDCCH) [3GP07] - that does not require detection - is comprised between 1 and 3. Thus, the worst-case configuration requires the detection of 13 OFDM symbols that are dedicated to data (and RSs). As depicted in Figure 5.2, the pattern of RSs is provided for four antenna ports that do not require detection, either. We do not reconsider the PDCCH symbol that also contains RSs. In the worst-case configuration, $5 * 1200/3 = 2000$ REs are not used for data transmission.
Consequently and by relying on the computational complexity from Section 5.3.2 with 64-QAM modulations, the upper bound rate - with no parallelism consideration, thus the number of Million of Operations Per Second (MOPS) equals the number of Million of Instructions Per Second (MIPS) - of the proposed solution is:

$$\mathcal{C}_{\text{Soft-decision RDN LRA-MMSEE } K\text{-Best}} = 52.578 \text{ GIPS}. \tag{5.29}$$

Within this rate and by considering the detector's block in Figure 5.10, 37% of the effort is required at the preprocessing step, 20% at the loading step, 22% for the neighbourhood search and

21% for the LLRs computation.

We claim that - to the best of the author's knowledge and at the present date of publication - the introduced computational complexity offers a very competitive performance-complexity trade-off, among the existing detectors in 4×4 SM-MIMO-OFDM systems and in the OL mode. Also, it positively answers the multiple implementation issues.
Even the promising FSD is gone over - in particular with 64-QAM constellation - since its computational complexity depends on the constellation size. By way of an indication and without specific simplifications through the implementation step, the FSD in 4×4 systems - calibrated with $K = \{1, 1, 1, |\xi|\}$ for all the layers in [Bar06a] - offers an upper bound rate of 95.091 GIPS.

Along the present work, a particular attention has been paid to the detector's architecture. Namely, the computational complexity has been shifted to the preprocessing step as much as possible, thus inducing an almost constant - in the constellation size (see Section 5.3.2) - computational complexity, while offering near-MLD performance. Such a strategic approach has been shown to be advantageous from both a computational complexity and performance point of view. Consequently, the soft-decision RDN LRA-MMSEE K-Best compares to existing 4×4 detectors as a very efficient solution.

Chapter 6

Conclusion & Future work

Contents

This thesis has addressed the challenge of demultiplexing the transmitted symbols via spatial multiplexing-MIMO techniques. Discussions and conclusions have been provided by focusing on 4×4 systems. The overall objective was to reach near-optimum performance at the detection step, while offering polynomial computational complexity. While providing a solution to this problem, careful consideration of implementation issues and an efficient performance/complexity trade-off within the LTE(-A) framework were considered.

6.1 Conclusion and contributions

Particular attention was paid to the detector's architecture. Namely, the computational complexity was shifted to the preprocessing step as much as possible. With this aim in view, the present work has led to numerous contributions throughout the previous chapters.

In Chapter 3, an inventory of the existing solutions was presented. Contributive results have then been provided at the preprocessing step.
Particular attention was paid to parallelism capabilities of the QR decomposition in [Aub10]. Also, a smart arrangement in the QR decomposition bypasses the explicit computation of $\mathbf{Q}$, thus leading to savings in the computational complexity [Aub10].
The results presented in the previous chapters have led to combining three distinct solutions, aiming at shifting a large part of the detector's computational complexity to the preprocessing step. In particular and through a neighbourhood search centred on an efficient lattice reduction-aided solution, an original hard-decision detector was introduced (see Section 3.4.5). It was shown to offer a promising computational complexity/performance trade-off.

In Chapter 4, an inventory of the existing solutions was presented. Contributive result were then provided at the log-likelihood ratio generation step.
By considering a multi-level log-likelihood ratio clipping - from 16-QAM -, a novel technique was proposed and allows for low distortion approximated log-likelihood ratio computation at the output of a soft-decision near-maximum-likelihood detector [Aub11a]. This low-computational and general optimization was shown to offer a significant performance gain.

In Chapter 5, an overview of the practical and normative requirements was presented. Con-

tributive results were then provided at the preprocessing step.
A novel solution that takes advantage of the channel correlation, by using the matrix perturbation theory applied to the QR decomposition, was proposed in [Aub11b]. It was shown to lead to time complexity savings while keeping close to the reference full-QR decomposition performance.
In Section 5.2.3, we investigated the impact of linear precoding prior to the classical lattice reduction algorithms. For a 4×2 scheme and under the capacity-selection criterion, the mean and maximal computational complexities of the LLL-based lattice reduction algorithm decrease by 28% and 58%, respectively. It is an advantageous implementation aspect.

Based on the results presented in the previous chapters, our choices in the detector's architecture have been shown to be a winning strategy for both computational complexity and performance. Namely, the proposed solution leads to an almost constant - in the constellation size (see Section 5.3.2), thus advantageous for high-order constellations - computational complexity, while offering near-maximum-likelihood performance. Consequently, the proposed soft-decision detector compares to existing 4×4 detectors as a very efficient solution. For achieving near-maximum-likelihood performance, it offers a computational complexity decrease by a factor of 44.3 for 64-QAM modulations compared to the K-Best.

Clearly, the advantage of one receiver compared to others comes from the - implementation oriented - study of its cost while meeting specific achievable throughput. We claim that the introduced computational complexity offers a very attractive performance-complexity trade-off, among the existing detectors in 4×4 spatial multiplexing-MIMO systems and in the open-loop mode.
In addition to the exhibited convenient performance/computational complexity trade-off, the proposed solution is adaptable to the closed-loop mode. With the same aim in view, it is a multi-standard application. Namely and due to the flexibility of the architecture, no additional effort in the design is required to target a specific mode or other wireless applications. Consequently, the proposed detector stands as an efficient solution in comparison with existing techniques.

A downside still remains in that the proposed solution is computationally demanding. Following the present work, the main goal remaining is to further decrease its computational complexity - through additional studies, optimisations and smarter techniques - while maintaining the present performance. The evoked additional decrease in the computational complexity could be reached through further studies, for which some ideas are stated in the sequel.

6.2 Future Work

It should be noted that the presented solution is very general and is subject to multiple optimizations, that have not been explored for the moment.

6.2.1 Algorithmic aspects

Preprocessing We focus on the preprocessing step:
- By considering the (sorted) QR decomposition step, Givens Rotations can be made square root and division free [Goe91], which is particularly convenient for implementation. Also, the QR decomposition introduced in Section 5.2.1 can be advantageously used within the coherence bandwidth or time, while it was not considered in the simulation results in Section 5.3.2;
- By considering the sorted QR decomposition step, a computational complexity decrease - with no performance degradation - is possible through the re-use of adjacent channel output $\mathbf{P}$

within the coherence bandwidth or time, similarly to what is done for the lattice reduction in Section 5.2.2;
– By considering the lattice reduction step, a computational complexity decrease with no performance degradation has been shown to be possible in Section 5.2.2. Nevertheless, further computational complexity decrease with no performance degradation is possible, as evoked in Section 5.2.2. Also, computational complexity decrease with performance degradation may be considered since the computational complexity of the (sorted)LLL algorithm's computational complexity decreases exponentially [Jal08], thus leading to a more aggressive trade-off.

Detection We focus on the detection step, and in particular the neighbourhood search.

– The Schnorr-Euchner enumeration allows for early termination of the tree search phase since child nodes are ordered according to their increasing partial Euclidean distances. Thus, the search can be terminated as soon as a node's cumulated Euclidean distance exceeds the current sphere constraint since the next ordered node at the top level would exceed the last cumulated Euclidean distance;
– Classically, the Schnorr-Euchner enumeration can be optimized through a look-up table while it introduces an additional computational complexity/performance study;
– A dynamic K choice is possible - and even necessary - and was not considered. In particular with the sorted QR decomposition ordering, a large computational complexity reduction is expected - with a very tiny performance loss - by judiciously calibrating the K parameter at each layer. It is especially true with a large number of layers. The extreme ($K = |\xi|$ at top layers, K=1 elsewhere) case of the famous fixed-complexity sphere decoder has been shown to be convenient for implementation [Bar06a]. However, it is not convenient with 64-QAM constellations. Also, it was not considered when associated to lattice reduction.

Log-Likelihood Ratio Generation We focus on the soft-decision extension step. While the near-maximum-likelihood detectors have been widely studied in the literature, hard-decision detectors have been generally addressed since it is a practical consideration. The most promising possible further improvements concern this block within the proposed detector. In particular in the present work, the soft-decision extension was neglected in the sense that the brute-force - while already efficient - fixed log-likelihood ratio clipping was considered. Anyway, some smart solutions is proposed in the literature:

– The search phase can be constructed to make possible the explicit calculation of each log-likelihood ratio, as stated in Sections 4.4.1 and 4.4.2. This way, the computational complexity of the neighbourhood search is recalled to increase, even if the performance is improved. While no convincing solution was provided until now, the consideration of a mixed method between log-likelihood ratio clipping and a bit-wise approach in the tree construction should be efficient. As a consequence and by assuming that the tree construction has been perfectly done, the neighbourhood size would be reduced to K=2;
– Additional knowledge in the log-likelihood ratio computation can be used. In particular, distances within the list of solutions could be considered. This way, the performance would be improved and the neighbourhood size would again be reduced;
– As stated in Section 4.5.2, some information aiming at clipping missing log-likelihood ratios more efficiently is available from the lattice reduction step. Thus, it makes some optimizations possible in the log-likelihood ratio clipping.

6.2.2 Implementation Aspects and Practical Considerations

Implementation Aspects Concerning the proposed detector's implementation phase, the architecture study and the estimation of the numbers of required gates are still necessary for a hardware implementation.
In particular, the proposed solution offers a potential parallelism, which induces a best-case reduction of the rate estimation (see Section 5.3.3) by a factor of 16 - by assuming 16-bit words - on an EVP (see Section 2.7.3). We summarize the presence or lack of parallel implementation within the proposed architecture:
– No potential parallelism arises within the sorted QR decomposition due to the ordering;
– No potential parallelism arises within the LLL algorithm due to its iterative nature;
– A large amount of potential parallelism arises from the tree exploration due to breadth first search that leads to the tree to be constructed layer by layer.

Practical Considerations From a global point of view, the K, N and $\Lambda_{\text{clip}}(\mathbf{b}_k^l)$ parameters (see Section 5.3.2) are subject to a judicious calibration, according to:
– The channel propagation condition, since - and among others - the preprocessing computational complexity depends on the coherence bandwidth or time;
– The system characteristics, since a different calibration is required between the open-loop and closed-loop modes.

The proposed solution is designed as a multi-standard detector that allows devices to switch between the wideband code-division multiple-access and the LTE(-A) standards, within the UMTS. In particular, its efficiency has been demonstrated and remains valid as soon as a MIMO scheme arises, even if it is still more attractive with the use of OFDM.
Interestingly, the presented results are worst-case computational complexities. In particular, the open-loop mode was considered. The presented analysis offers a worst-case result that would be significantly improved through the closed-loop mode consideration, as studied in Section 5.2.3.

The proposed detector can be extended to multi-user-MIMO systems, by assuming that additional knowledge - such as user received energies and transmission delays - is available.

Bibliography

[3GP07] 3GPP. Evolved Universal Terrestrial Radio Access; Physical Channels and Modulation, v8.0.0. TS 36.211, 3rd Gen. Partnership Project, 2007. 24, 90, 91, 92, 93, 109

[3GP09a] 3GPP. Evolved Universal Terrestrial Radio Access; Deployment aspects, v9.0.0. TS 25.943, 3rd Gen. Partnership Project, 2009. 26, 88

[3GP09b] 3GPP. Evolved Universal Terrestrial Radio Access; Physical layer procedures, v9.0.0. TS 36.213, 3rd Gen. Partnership Project, 2009. 63, 106

[3GP09c] 3GPP. Evolved Universal Terrestrial Radio Access; Spreading and modulation, v9.1.0. TS 25.213, 3rd Gen. Partnership Project, 2009. 14, 16, 82

[3GP09d] 3GPP. Evolved Universal Terrestrial Radio Access; User Equipment radio transmission and reception, v8.8.0. TS 36.101, 3rd Gen. Partnership Project, 2009. 27, 58, 67, 87, 88, 89, 90, 105

[3GP10] 3GPP. Evolved Universal Terrestrial Radio Access; Multiplexing and channel coding, v10.0.0. TS 36.212, 3rd Gen. Partnership Project, 2010. 17, 105

[Agr02] Agrell E., Eriksson T., Vardy A., and Zeger K. Closest point search in lattices. *Information Theory, IEEE Transactions on*, 48(8):2201–2214, Aug. 2002. 42, 43, 47, 49, 50

[Ala98] Alamouti S.M. A simple transmit diversity technique for wireless communications. *Selected Areas in Communications, IEEE Journal on*, 16(8):1451–1458, Oct. 1998. 23

[And84] Anderson J., and Mohan S. Sequential coding algorithms: a survey and cost analysis. *Communications, IEEE Transactions on*, 32(2):169–176, Feb. 1984. 45

[Aub09] Aubert S., Nouvel F., and Nafkha A. Complexity Gain of QR Decomposition Based Sphere Decoder in LTE Receivers. *Vehicular Technology Conference, IEEE*, pages 1–5, Sept. 2009. 41, 43, 44

[Aub10] Aubert S., Mohaisen M., Nouvel F., and Chang K.H. Parallel QR decomposition in LTE-A systems. *Signal Processing Advances in Wireless Communications, IEEE International Workshop on*, June 2010. 37, 38, 39, 50, 94, 98, 111

[Aub11a] Aubert S., Ancora A., and Nouvel F. Multi-Level Log-Likelihood Ratio Clipping in a Soft-Decision Near-Maximum Likelihood Detector. *International Conference on Digital Telecommunications*, pages 30–35, April 2011. 74, 81, 83, 84, 111

[Aub11b] Aubert S., Tournois J., and Nouvel F. On the Implementation of MIMO-OFDM Schemes Using Perturbation of the QR Decomposition: Application to 3GPP LTE-A Systems. *Acoustics, Speech and Signal Processing, IEEE International Conference on*, May 2011. 95, 97, 98, 112

[Bah74] Bahl L., Cocke J., Jelinek F., and Raviv J. Optimal decoding of linear codes for minimizing symbol error rate. *Information Theory, IEEE Transactions on*, 20(2):284–287, March 1974. 17

[Bar03a] Baro S. Turbo detection for MIMO systems using a list-sequential detector: Improved soft output by path augmentation. *Diskussionssitzung Angewandte Informationstheorie*, pages 66–68, June 2003. 76

[Bar03b] Baro S., Hagenauer J., and Witzke M. Iterative detection of MIMO transmission using a list-sequential (LISS) detector. *Communications, IEEE International Conference on*, 4:2653–2657, May 2003. 75

[Bar03c] Barry J.R., Lee E.A., and Messerschmidt D.G. *Digital Communication: Third Edition*. Kluwer Academic Publishers Norwell, 2003. 15, 18, 19, 64

[Bar06a] Barbero L.G., and Thompson J.S. A Fixed-Complexity MIMO Detector Based on the Complex Sphere Decoder. *Signal Processing Advances in Wireless Communications, IEEE International Workshop on*, pages 1–5, July 2006. 110, 113

[Bar06b] Barbero L.G., and Thompson J.S. Rapid Prototyping of a Fixed-Throughput Sphere Decoder for MIMO Systems. *Communications, IEEE International Conference on*, pages 3082–3087, June 2006. 43, 47

[Bar08a] Barbero L., and Thompson J. Extending a fixed-complexity sphere decoder to obtain likelihood information for turbo-MIMO systems. *Vehicular Technology, IEEE Transactions on*, 57(5):2804–2814, Sept. 2008. 46

[Bar08b] Barbero L., and Thompson J. Fixing the complexity of the sphere decoder for MIMO detection. *Wireless Communications, IEEE Transactions on*, 7(6):2131–2142, June 2008. 46

[Bar08c] Barbero L.G., Ratnarajah T., and Cowan C. A comparison of complex lattice reduction algorithms for MIMO detection. *Acoustics, Speech and Signal Processing, IEEE International Conference on*, pages 2705–2708, March 2008. 41, 50, 51, 53

[Bar08d] Barbero L.G., Ratnarajah T., and Cowan C. A low-complexity soft-MIMO detector based on the fixed-complexity sphere decoder. *Acoustics, Speech and Signal Processing, IEEE International Conference on*, pages 2669–2672, March 2008. 75, 76

[Bel63] Bello P.A. Characterization of randomly time-invariant linear channels. *Communications Systems, IEEE Transactions on*, (11):360–393, Dec. 1963. 26

[Ben98] Benedetto S., Divsalar D., Montorsi G., and Pollara F. Serial Concatenation of Interleaved Codes: Performance Analysis, Design, and Iterative Decoding. *Information Theory, IEEE Transactions on*, 44(3):909–926, May 1998. 24

[Ben02] Benvenuto N., and Tomasin S. On the comparison between OFDM and single carrier modulation with a DFE using a frequency-domain feedforward filter. *Communications, IEEE Transactions on*, 50(6):947–955, June 2002. 20

[Ben03] Benesty J., Huang Y., and Chen J. A fast recursive algorithm for optimum sequential signal detection in a BLAST system. *Signal Processing, IEEE Transactions on*, 51(7):1722–1730, July 2003. 36

[Ber93] Berrou C., Glavieux A., and Thitimajshima P. Near Shannon limit error-correcting coding and decoding: Turbo-codes. *Communications, IEEE International Conference on*, 2:1064–1070, May 1993. 16, 17, 18, 24, 28, 63

[Ber96] Berrou C., and Glavieux A. Near optimum error correcting coding and decoding: turbo-codes. *Communications, IEEE Transactions on*, 44(10):1261–1271, Oct. 1996. 17

[Bit06a] Bittner S., Zimmermann E., and Fettweis G. Low Complexity Soft Interference Cancellation for MIMO-Systems. *Vehicular Technology Conference, IEEE*, pages 1993–1997, May 2006. 69

[Bit06b] Bittner S., Zimmermann E., Rave W., and Fettweis G. List Sequential MIMO Detection: Noise Bias Term and Partial Path Augmentation. *Communications, IEEE International Conference on*, pages 1300–1305, June 2006. 76

[Boe06] Boehnke R., and Kammeyer K.D. SINR Analysis for V-BLAST with Ordered MMSE-SIC Detection. *Wireless Communications and Mobile Computing, International conference on*, pages 623–628, 2006. 39, 40

[Bou03] Boutros J., Gresset N., Brunel L., and Fossorier M. Soft-input soft-output lattice sphere decoder for linear channels. *Global Telecommunications Conference, IEEE*, pages 1583–1587, Dec. 2003. 42

[Bur91] Burrus C.S.S., and Parks T.W. *DFT/FFT and Convolution Algorithms: Theory and Implementation*. New York: John Wiley & Sons, Ltd/Inc., 1991. 21

[Bur05] Burg A., Borgmann M., Wenk M., Zellweger M., Fichtner W., and Bolcskei H. VLSI implementation of MIMO detection using the sphere decoding algorithm. *Solid-State Circuits, IEEE Journal of*, 40(7):1566–1577, July 2005. 43

[But04] Butler M.R.G., and Collings I.B. A zero-forcing approximate log-likelihood receiver for MIMO bit-interleaved coded modulation. *Communications Letters, IEEE*, 8(2):105–107, Feb. 2004. 66

[Cai98] Caire G., Taricco G., and Biglieri E. Bit-interleaved coded modulation. *Information Theory, IEEE Transactions on*, 44(3):927–946, May 1998. 23

[CDA05] Bölcskei H. Hansen J. Cescato D., Borgmann M. and Burg A. Interpolation-based QR decomposition in MIMO-OFDM systems. *Signal Processing Advances in Wireless Communications, IEEE International Workshop on*, pages 945–949, 2005. 95

[Cha66] Chang R. W. Synthesis of Band-Limited Orthogonal Signals for Multichannel Data Transmission. *Bell Systems Technical Journal*, 46:1775–1796, Dec. 1966. 19

[Cho00] Choi W.-J., Cheong K.-W., and Cioffi J.M. Iterative soft interference cancellation for multiple antenna systems. *Wireless Communications and Networking, IEEE Conference on*, 1:304–309, Sept. 2000. 69

[Col04] Collings I.B., Butler M.R.G., and McKay M. Low Complexity Receiver Design for MIMO Bit-Interleaved Coded Modulation. *Spread Spectrum Techniques and Applications, International Symposium on*, pages 12–16, Sep 2004. 66, 67

[Cor01] Correia L.M. *Wireless Flexible Personalized Communications: COST 259: European Co-operation in Mobile Radio Research*. New York: John Wiley & Sons, 2001. 88

[Cos98] Costello D.J. Jr., Hagenauer J., Imai H., and Wicker S.B. Applications of error-control coding. *Information Theory, IEEE Transactions on*, 44(6):2531–2560, Oct. 1998. 19

[Cos07] Costello D.J. Jr, and Forney G.D. Jr. Channel Coding: The Road to Channel Capacity. volume 95, pages 1150–1177, Feb. 2007. 17

[Cui05] Cui T., and Tellambura C. An efficient generalized sphere decoder for rank-deficient MIMO systems. *Communications Letters, IEEE*, 9(5):423–425, May 2005. 48

[Dai05] Dai Y., Sun S., and Lei Z. A comparative study of QRD-M detection and sphere decoding for MIMO-OFDM systems. *Personal, Indoor and Mobile Radio Communications, IEEE International Symposium on*, pages 186–190, Sept. 2005. 45

[Dam00] Damen O., Chkeif A., and Belfiore J.-C. Lattice code decoder for space-time codes. *Communications Letters, IEEE*, 4(5):161–163, May 2000. 43

[Dam03] Damen M.O., El Gamal H., and Caire G. On maximum-likelihood detection and the search for the closest lattice point. *Information Theory, IEEE Transactions on*, 49(10):2389–2402, Oct. 2003. 39, 40, 43, 57

[de 05] de Jong Y.L.C., and Willink T.J. Iterative Tree Search Detection for MIMO Wireless Systems. *Communications, IEEE Transactions on*, 53(6):930–935, June 2005. 77, 78, 82

[Dop06] Dopico F.M., and Molera J.M. Perturbation theory for factorizations of LU type through series expansions. *Journal on Matrix Analysis and Applications, SIAM*, 27(2):561–581, 2006. 95, 96

[Dur99] Durgin G.D., and Rappaport T.S. Effects of Multipath Angular Spread on the Spatial Cross-Correlation of Received Voltage Envelopes. *Vehicular Technology Conference, IEEE*, 2:996–1000, 1999. 27

[Eli55] Elias P. Coding for noisy channels. *International Convention Record, IRE*, 3(4):37–46, 1955. 17

[Fer08] Fertl P., Jalden J., and Matz G. Capacity-based performance comparison of MIMO-BICM demodulators. *Signal Processing Advances in Wireless Communications*, pages 166–170, July 2008. 66

[Fin85] Fincke U., and Pohst M. Improved methods for calculating vectors of short length in a lattice, including complexity analysis. *Mathematics of Computation*, 44(170):463–471, Apr. 1985. 43

[Fos96] Foschini G.J. Layered space-time architecture for wireless communication in a fading environment when using multi-element antennas. *Bell Labs Technical Journal*, 1(2):41–59, Summer 1996. 23

[Fos98] Foschini G.J., and Gans M.J. On Limits of Wireless Communications in a Fading Environment when Using Multiple Antennas. *Wireless Personal Communications*, 6(3):311–335, 1998. 22

[Fos99] Foschini G.J., Golden G.D., Valenzuela R.A., and Wolniansky P.W. Simplified processing for high spectral efficiency wireless communication employing multi-element arrays. *Selected Areas in Communications, IEEE Journal on*, 17(11):1841–1852, Nov. 1999. 39

[Gal62] Gallager R. Low-density parity-check codes. *Information Theory, IRE Transactions on*, 8(1):21–28, Jan. 1962. 17

[Gan09] Gan Y.H., Ling C., and Mow W.H. Complex Lattice Reduction Algorithm for Low-Complexity Full-Diversity MIMO Detection. *Signal Processing, IEEE Transactions on*, 57(7):2701–2710, july 2009. 49, 50

[Ges08] Gestner B., Zhang W., Ma X., and Anderson D.V. VLSI Implementation of a Lattice Reduction Algorithm for Low-Complexity Equalization. *Circuits and Systems for Communications, IEEE International Conference on*, pages 643–647, 2008. 50

[God97] Godara L.C. Application of antenna arrays to mobile communications. II. Beam-forming and direction-of-arrival considerations. *Proceedings of the IEEE*, 85(8):1195–1245, Aug. 1997. 22

[Goe91] Goetze J., and Schwiegelshohn U. A Square Root and Division Free Givens Rotation for Solving Least Squares Problems on Systolic Arrays. *Scientific and Statistical Computing, SIAM Journal on*, 12(4):800–807, 1991. 38, 112

[Gor06] Gor L. and Faulkner M. Power Reduction through Upper Triangular Matrix Tracking in QR Detection MIMO Receivers. *Vehicular Technology Conference, IEEE*, pages 1–5, 2006. 95

[Gra95] Grama A., and Kumar V. A Survey of Parallel Search Algorithms for Discrete Optimization Problems. *ORSA Journal of Computing*, 7(4):365–385, 1995. 45

[Guo06] Guo Z., and Nilsson P. Algorithm and implementation of the K-best sphere decoding for MIMO detection. *Selected Areas in Communications, IEEE Journal on*, 24(3):491–503, March 2006. 43, 75, 76

[Hag96] Hagenauer J., Offer E., and Papke L. Iterative decoding of binary block and convolutional codes. *Information Theory, IEEE Transactions on*, 42(2):429–445, March 1996. 65

[Ham50] Hamming R.W. Error detecting and error correcting codes. *The Bell System Technical Journal*, 29(2):147–160, Apr. 1950. 17

[Han04] Han S.H., and Lee J.H. PAPR reduction of OFDM signals using a reduced complexity PTS technique. *Signal Processing Letters, IEEE*, 11(11):887–890, Nov. 2004. 21

[Has00] Hassibi B. An efficient square-root algorithm for BLAST. *Acoustics, Speech, and Signal Processing, IEEE International Conference on*, pages 737–740, June 2000. 36, 40

[Has01] Hassibi B., and Vikalo H. On the expected complexity of sphere decoding. *Signals, Systems and Computers, Asilomar Conference on*, 2:1051–1055, Nov. 2001. 42, 43

[Has05] Hassibi B., and Vikalo H. On the sphere-decoding algorithm I. Expected complexity. *Signal Processing, IEEE Transactions on*, 53(8):2806–2818, Aug. 2005. 43

[Hay05] Haykin S., and Moher M. Modern Wireless Communications. *USA, NJ, Pearson Prentice Hall*, 2005. 36

[Hig02] Higham N.J. *Accuracy and Stability of Numerical Algorithms*. Siam, 2002. 37

[Hig04] Higuchi K., Kawai H., Maeda N., Sawahashi M., Itoh T., Kakura Y., Ushirokawa A., and Seki H. Likelihood function for QRM-MLD suitable for soft-decision turbo decoding and its performance for OFCDM MIMO multiplexing in multipath fading channel. *Personal, Indoor and Mobile Radio Communications, IEEE International Symposium on*, 2:1142–1148, Sep. 2004. 79, 80

[Hoc03] Hochwald B.M., and ten Brink S. Achieving Near-Capacity on a Multiple-Antenna Channel. *Communications, IEEE Transactions on*, 51(3):389–399, Mar. 2003. 25, 43, 48, 65, 77, 78, 79

[Hoe92] Hoeher, P. A statistical discrete-time model for the WSSUS multipath channel. *Vehicular Technology, IEEE Transactions on*, 41(4):461–468, Nov. 1992. 26

[Hog07] Hogben L. *Handbook of linear algebra*. CRC Press, 2007. 38

[Jak74] Jakes W. C. *Microwave Mobile Communications*. New York: John Wiley & Sons, Ltd/Inc., 1974. 26

[Jal05] Jaldén J., and Ottersten B. On the complexity of sphere decoding in digital communications. *Signal Processing, IEEE Transactions on*, 53(4):1474–1484, Apr. 2005. 45

[Jal08] Jaldén J., Seethaler D., and Matz G. Worst - and average - case complexity of LLL lattice reduction in MIMO wireless systems. *Acoustics, Speech and Signal Processing, IEEE International Conference on*, pages 2685–2688, March 2008. 52, 53, 54, 55, 113

[Jal09] Jaldén J., and Elia P. LR-aided MMSE lattice decoding is DMT optimal for all approximately universal codes. *Information Theory, IEEE International Symposium on*, pages 1263–1267, June 2009. 58

[Jeo06] Jeon K., Kim H., and Park H. An efficient QRD-M algorithm using partial decision feedback detection. *Signal, Systems, and Computers, Asilomar Conference on*, pages 1658–1661, Oct. 2006. 46

[Kat70] Kato T. *Perturbation Theory for Linear Operators*. Springer-Verlag, 2^{nd} edition, 1970. 95

[Kaw04] Kawamoto J., Kawai H., Maeda N., Higuchi K., and Sawahashi M. Investigations on likelihood function for QRM-MLD combined with MMSE-based multipath interference canceller suitable to soft-decision turbo decoding in broadband CDMA MIMO multiplexing. *Spread Spectrum Techniques and Applications, IEEE International Symposium on*, pages 628–633, Aug. 2004. 79, 80

[Kaw06] Kawai H., Higuchi K., Maeda N., and Sawahashi M. Adaptive control of surviving symbol replica candidates in QRM-MLD for OFDM-MIMO multiplexing. *IEEE Journal of Selected Areas in Communications*, 24(6):1130–1140, June 2006. 46

[Kim05] Kim K.J., Yue J., Iltis R.A., and Gibson J.D. A QRD-M/Kalman filter-based detection and channel estimation algorithm for MIMO-OFDM systems. *Wireless Communications, IEEE Transactions on*, 4(2):710–721, March 2005. 45

[Kle00] Klein P. Finding the closest lattice vector when it's unusually close. *Discrete Algorithms, ACM-SIAM Symposium on*, pages 937–941, 2000. 84, 85, 86

[Lam91] Lamacchia B.A. Basis Reduction Algorithms and Subset Sum Problems. Technical report, MSc Thesis, Massachusetts Institute of Technology, May 1991. 49

[Lar09] Larsson E.G. MIMO Detection Methods: How They Work. volume 26, pages 91–95, May 2009. 28, 29

[Len82] Lenstra A.K., Lenstra H.W., and Lovász L. Factoring polynomials with rational coefficients. *Mathematische Annalen*, 261(4):515–534, Dec. 1982. 49, 50

[Li 98] Li K., Pan Y., and Zheng S.-Q. Fast and processor efficient parallel matrix multiplication algorithms on a linear array with a reconfigurable pipelined bus system. *Parallel and Distributed Systems, IEEE Transactions on*, 9(8):705–720, 1998. 32

[Li 99] Li K., Pan Y., and Zheng S.-Q. Parallel Matrix Computations Using a Reconfigurable Pipelined Optical Bus. *Journal of Parallel and Distributed Computing*, 59:13–30, June 1999. 31, 98

[Li 08] Li Q., and W. Zhongfeng. Reduced Complexity K-Best Sphere Decoder for MIMO systems. *Circuits, Systems and Signal Processing*, 27:491–505, 2008. 46

[Lin06] Ling C. Approximate lattice decoding: Primal versus dual lattice reduction. *Information Theory, International Symposium on*, July 2006. 49

[Liu10] Liu S., Ling C., and Stehlé D. Randomized Lattice Decoding. *Submitted*, Available:http://arxiv.org/abs/1003.0064, 2010. 84, 85, 86

[Lov86] Lovász L. An Algorithmic Theory of Numbers, Graphs and Convexity. *Society for Industrial and Applied Mathematics*, 1986. 28

[Lov05a] Love D.J., and Heath R.W. Limited feedback unitary precoding for orthogonal space-time block codes. *Signal Processing, IEEE Transactions on*, 53(8):64–73, Jan. 2005. 92

[Lov05b] Love D.J., and Heath R.W. Limited feedback unitary precoding for spatial multiplexing systems. *Information Theory, IEEE Transactions on*, 51(8):2967–2976, Aug. 2005. 92, 93

[Lue07] Luethi P.,Burg A., Haene S., Perels D., Felber N., and Fichtner W. VLSI Implementation of a High-Speed Iterative Sorted MMSE QR Decomposition. *Circuits and Systems, IEEE International Symposium on*, pages 1421–1424, May 2007. 38, 41

[M.197] ITU-R M.1225. Guidelines for evaluation of radio transmission technologies for imt-2000. Technical report, International Telecommunication Union, 1997. 26

[Ma 08] Ma X., and Zhang W. Fundamental Limits of Linear Equalizers: Diversity, Capacity, and Complexity. *Information Theory, IEEE Transactions on*, 54(8):3442–3456, Aug. 2008. 103

[Mic05] Michalke C., Venkataraman H., Sinha V., Rave W., and Fettweis G. Application of SQRD Algorithm for Efficient MIMO-OFDM Systems. *European Wireless Conference*, 1:8–12, Apr. 2005. 41

[Mil06] Milliner D.L., and Barry J.R. A Lattice-Reduction-Aided Soft Detector for Multiple-Input Multiple-Output Channels. *Global Telecommunications Conference, IEEE*, pages 1–5, Nov. 2006. 70, 71

[Mil08] Milliner D.L., Zimmermann E., Barry J.R. and Fettweis G. Channel State Information Based LLR Clipping in List MIMO Detection. *Personal, Indoor and Mobile Radio Communications International, IEEE International Symposium on*, pages 1–5, Sept. 2008. 74, 78, 79, 80, 81, 82, 83

[Moh09a] Mohaisen M., and Chang K.H. On improving the efficiency of the fixed-complexity sphere decoder. *Vehicular Technology Conference, IEEE*, pages 1–5, Sept. 2009. 41, 47

[Moh09b] Mohaisen M., and Chang K.H. On the achievable improvement by the linear minimum mean square error detector. *Communication and Information Technology, International Symposium on*, pages 770–774, Sept. 2009. 30

[Moh09c] Mohaisen M., Chang K.H., and Koo B.T. Adaptive parallel and iterative QRDM algorithms for spatial multiplexing MIMO systems. *Vehicular Technology Conference, IEEE*, pages 1–5, Sept. 2009. 46

[Moh10] Mohaisen M., and Chang K.H. Upper-lower bounded-complexity QRD-M for spatial multiplexing MIMO-OFDM systems. *Wireless Personal Communications*, 2010. 46

[Mur08] Murray A.T., and Weller S.R. Enhanced lattice-reduction aided detection for MIMO systems. *Technical Report SPM386*, Available:http://sigpromu.org/publications.html, Mar. 2008. 100

[Mur09] Murray A.T., and Weller S.R. Performance and Complexity of Adaptive Lattice Reduction in Fading Channels. *Communications Theory Workshop, IEEE*, pages 17–22, 2009. 100

[Myl07] Myllyla M., Antikainen J., Juntti M., and Cavallaro J.R. The effect of LLR clipping to the complexity of list sphere detector algorithms. *Signals, Systems and Computers, Asilomar, Conference on*, pages 1559–1563, Nov. 2007. 77, 78

[Naj11] Najafi H., Jafari M.E.D., and Damen M.O. On Adaptive Lattice Reduction over Correlated Fading Channels. *Communications, IEEE Transactions on*, 59(5):1224–1227, 2011. 100

[Pak10] Paker O., Eckert S., and Bury A. A Low Cost Multi-standard Near-Optimal Soft-Output Sphere Decoder: Algorithm and Architecture. *Design, Automation and Test in Europe, Conference on*, pages 1402–1407, March 2010. 75

[Pau03] Paulraj A., Nabar R., and Gore D. Introduction to Space-Time Wireless Communications. *UK, Cambridge: Cambridge University Press*, 2003. 29

[Pon07] Ponnampalam V., McNamara D., Lillie A., and Sandell M. On Generating Soft Outputs for Lattice-Reduction-Aided MIMO Detection. *Communications, IEEE International Conference on*, pages 1–7, June 2007. 70, 71, 77

[Pro95] Proakis J.G. *Digital Communications, Third Edition.* McGraw-Hill, New York, 1995. 13, 14, 15, 16, 23, 26

[Qi 07] Qi X.-F., and Holt K. A Lattice-Reduction-Aided Soft Demapper for High-Rate Coded MIMO-OFDM Systems. *Signal Processing Letters, IEEE*, 14(5):305–308, May 2007. 56, 58, 77, 78

[Rag87] Raghavan P., and Tompson C.D. Randomized rounding: A technique for provably good algorithms and algorithmic proofs. *Combinatorica*, 7(4):365–374, Dec. 1987. 84

[Ral98] Raleigh G.G., and Cioffi J.M. Spatio-temporal coding for wireless communication. *Communications, IEEE Transactions on*, 46(3):357–366, March 1998. 22

[Ravil] Rave W. Quantization of Log-Likelihood Ratios to Maximize Mutual Information. *Signal Processing Letters, IEEE*, 16(4):283–286, 2009 April. 77

[Ray97] Rayleigh fading channels in mobile digital communication systems .I. Characterization. Sklar, B. *Communications Magazine, IEEE*, 35(7):90–100, 1997. 26, 27

[Rei05] Reid A.B., Grant A.J., and Alexander P.D. List detection for the K-symmetric multiple-access channel. *Information Theory, IEEE Transactions on*, 51(8):2930–2936, Aug. 2005. 71

[Ric01] Richardson T.J., and Urbanke, R.L. The capacity of low-density parity-check codes under message-passing decoding. *Information Theory, IEEE Transactions on*, 47(2):599–618, Feb. 2001. 17

[Rob95] Robertson P., Villebrun E., and Hoeher P. A comparison of optimal and sub-optimal MAP decoding algorithms operating in the log domain. *Communications, IEEE International Conference on*, 2:1009–1013, June 1995. 65

[Rog08] Roger S., Gonzalez A, Almenar V., and Vidal A. Combined K-Best sphere decoder based on the channel matrix condition number. *Communications, Control and Signal Processing, International Symposium on*, pages 1058–1061, Mar. 2008. 58

[Rog09] Roger S., Gonzalez A., Almenar V., and Vidal A.M. On Decreasing the Complexity of Lattice-Reduction-Aided K-Best MIMO Detectors. *European Signal Processing Conference*, pages 2411–2415, Aug. 2009. 46, 56, 57, 58

[Rog10] Roger S., Gonzalez A., Almenar V., and Vidal A.M. Extended LLL algorithm for efficient signal precoding in multiuser communication systems. *Communications Letters, IEEE*, 14(3):220–222, March 2010. 73

[Sal67] Saltzberg B. R. Performance of an Efficient Parallel Data Transmission System. *Communication Technology, IEEE Transactions on*, 15(6):805–811, Dec. 1967. 19

[Sch94] Schnorr C., and Euchner M. Lattice basis reduction: improved practical algorithms and solving subset sum problems. *Mathematical Programming*, 66:181–199, Sept. 1994. 43

[Sch06] Schubert B. Analysis of sphere decoding in linear cooperative wireless relay networks. *Master Thesis, Berlin University of Technology*, 2006. 29

[See04] Seethaler D., Matz G., and Hlawatsch F. An efficient MMSE-based demodulator for MIMO bit-interleaved coded modulation. *Global Telecommunications Conference, IEEE*, 4:2455–2459, Dec. 2004. 66

[See07] Seethaler D., Matz G., and Hlawatsch F. Low-complexity MIMO data detection using Seysen's lattice reduction algorithm. *Acoustics, Speech, and Signal Processing, IEEE International Conference on*, 3:53–56, Apr. 2007. 51

[Ses09] Sesia S., Toufik, I., and Baker M. *LTE, The UMTS Long Term Evolution: From Theory to Practice*. Wiley, Feb. 2009. 15, 19, 20, 21, 22, 23, 88, 89, 90, 106

[Sey93] Seysen M. Simultaneous reduction of a lattice basis and its reciprocal basis. *Combinatorica*, 13(3):363–376, Sept 1993. 49, 51

[Sha48] Shannon C.E. A Mathematical Theory of Communication. *Bell System Technical Journal*, 27:379–423 and 623–656, July/Oct. 1948. 16, 17

[Sha08] Shabany M., and Gulak P.G. The Application of Lattice-Reduction to the K-Best Algorithm for Near-Optimal MIMO Detection. *Circuits and Systems, IEEE International Symposium on*, pages 316–319, May 2008. 57, 58

[Shi99] Shiu D., and Kahn J. Layered space-time codes for wireless communications using multiple transmit antennas. *Communications, IEEE International Conference on*, pages 436–440, June 1999. 41

[Shi06] Shin M., Kwon D. S., and Lee C. Performance Analysis of Maximum Likelihood Detection for MIMO Systems. *Vehicular Technology Conference, IEEE*, pages 2154–2158, May. 2006. 15

[Ste92] Stewart G.W. *On the perturbation of LU, Cholesky and QR factorizations*. Preprint Series 949, 1992. 95, 97

[Tah05] Taherzadeh M., Mobasher A., and Khandani A.K. LLL lattice-basis reduction achieves the maximum diversity in MIMO systems. *Information Theory, International Symposium on*, Sept. 2005. 49, 54

[Tar98] Tarokh V., Seshadri N., and Calderbank A.R. Space-time codes for high data rate wireless communication: performance criterion and code construction. *Information Theory, IEEE Transactions on*, 44(2):744–765, March 1998. 23

[Tar03] Tarokh B., and Sadjadpour H.R. Construction of OFDM M-QAM sequences with low peak-to-average power ratio. volume 51, pages 25–28, Jan 2003. 16

[Tel99] Telatar E. Capacity of Multi-antenna Gaussian Channels. *Telecommunications, European Transactions on*, 10(6):585–595, Nov. 1999. 24

[Tep04] Tepedelenlioğlu C. Maximum multipath diversity with linear equalization in precoded OFDM systems. *Information Theory, IEEE Transactions on*, 50(1):232–235, Jan. 2004. 94

[Tse05] Tse D., and Viswanath P. *Fundamentals of wireless communicatione*. Cambridge University Press, 2005. 24

[Van76] Van Etten W. Maximum likelihood receiver for multiple channel transmission systems. *Communications, IEEE Transactions on*, pages 276–283, Feb. 1976. 28

[van05] van Berkel K., Heinle F., Meuwissen P.P.E., Moerman K., and Weiss M. Vector processing as an enabler for software-defined radio in handheld devices. *Applied Signal Processing, EURASIP Journal on*, pages 2613–2625, Jan. 2005. 32

[Vik04] Vikalo H., Hassibi B., and Kailath T. Iterative decoding for MIMO channels via modified sphere decoder. *Wireless Communications, IEEE Transactions on*, 3(6):2299–2311, Nov. 2004. 43

[Vit67] Viterbi A.J. Error Bounds for Convolutional Codes and an Asymptotically Optimum Decoding Algorithm. *Information Theory, IEEE Transactions on*, IT-13:260–269, April 1967. 17

[Vit99] Viterbo E., and Boutros J. A universal lattice code decoder for fading channels. *Information Theory, IEEE Transactions on*, 45(5):1639–1642, 1999. 43, 57

[Wan00] Wang Z., G.B. and Giannakis. Wireless multicarrier communications. *Signal Processing Magazine, IEEE*, 17(3):29–48, May 2000. 19, 22

[Wan02] Wang C.C. A bandwidth-efficient binary turbo coded waveform using QAM signaling. *Communications, Circuits and Systems and West Sino Expositions, IEEE International Conference on*, 1:37–41, June 2002. 83

[Wan04] Wang R., and G.B. Giannakis. Approaching MIMO channel capacity with reduced-complexity soft sphere decoding. *Wireless Communications and Networking, IEEE Conference on*, 3:1620–1625, March 2004. 74, 75

[Wan05] Wang J., and Daneshrad B. A comparative study of MIMO detection algorithms for wideband spatial multiplexing systems. *Wireless Communications and Networking, IEEE Conference on*, 1:408–413, March 2005. 33

[Wan06] Wang R., and G.B. Giannakis. Approaching MIMO channel capacity with soft detection based on hard sphere decoding. *Communications, IEEE Transactions on*, 54(4):587–590, April 2006. 75

[Wan08] Wang L., Xu L., Chen S., and Hanzo L. MMSE Soft-Interference-Cancellation Aided Iterative Center-Shifting K-Best Sphere Detection for MIMO Channels. *Communications, IEEE International Conference on*, pages 3819–3823, May 2008. 48

[Wat04] Waters D.W., and Barry J.R. The Chase family of detection algorithms for multiple-input multiple-output channels. *Global Telecommunications Conference, IEEE*, 4:2635–2639, Dec. 2004. 75

[Wei71] Weinstein S., and Ebert P. Data Transmission by Frequency-Division Multiplexing Using the Discrete Fourier Transform. *Communication Technology, IEEE Transactions on*, 19(5):628–634, Oct. 1971. 19, 21

[Wid04] Widdup B., Woodward G., and Knagge G. A Highly-Parallel VLSI Architecture for a List Sphere Detector. *Communications, IEEE International Conference on*, 5:2720–2725, June 2004. 79

[Win03a] Windpassinger C., and Fischer R.F.H. Low-complexity near-maximum-likelihood detection and precoding for MIMO systems using lattice reduction. *Information Theory Workshop, IEEE*, pages 345–348, 2003. 49, 51, 52

[Win03b] Windpassinger C., Lampe L.H.-J., and Fischer R.F.H. From lattice-reduction-aided detection towards maximum-likelihood detection in MIMO systems. *Wireless and Optical Communications, International Conference on*, pages 144–148, July 2003. 56

[Win04] Windpassinger C. Detection and precoding for multiple input multiple output channels. *PhD Dissertation, Erlangen-Nurnberg University*, 2004. 29

[Wol98] Wolniansky P., Foschini G., Golden G., and Valenzuela R. V-BLAST: an architecture for realizing very high data rates over the rich-scattering wireless channel. *Signals, Systems, and Electronics, URSI International Symposium on*, pages 295–300, Oct. 1998. 36

[Won02] Wong K.-W., Tsui C.-Y., Cheng S.-K., and Mow W.-H. A VLSI Architecture of a K-Best Lattice Decoding Algorithm For MIMO Channels. 3:272–276, 2002. 45, 48

[Won05] Wong K.K.Y., and McLane P.J. A Low-Complexity Iterative MIMO Detection Scheme Using the Soft-Output M-Algorithm. *IST Mobile & Wireless Communications Summit*, June 2005. 76

[Wue01] Wuebben D., Böhnke R., Rinas J., Kühn V., and Kammeyer K.-D. Efficient algorithm for decoding layered space-time codes. *Electronics Letters, IEEE*, 37(22):1348–1350, Oct. 2001. 39, 41

[Wue03] Wuebben D., Böhnke R., Kühn V., and Kammeyer K.-D. MMSE extension of V-BLAST based on sorted QR decomposition. *Vehicular Technology Conference, IEEE*, pages 508–512, Oct. 2003. 39, 40, 41

[Wue04] Wuebben D., Boehnke R., Kuehn V., and Kammeyer K.-D. MMSE-based lattice-reduction for near-ML detection of MIMO systems. *Smart Antennas, ITG Workshop on*, pages 106–113, 2004. 49, 50, 54

[Wue06] Wuebben D.,and Kammeyer K.-D. Interpolation-Based Successive Interference Cancellation for Per-Antenna-Coded MIMO-OFDM Systems using P-SQRD. *Smart Antennas, International ITG Workshop on*, March 2006. 95

[Wue07] Wuebben D., and Seethaler D. On the Performance of Lattice Reduction Schemes for MIMO Data Detection. *Signals, Systems and Computers, Asilomar Conference on*, pages 1534–1538, Nov. 2007. 50, 51

[Yao02] Yao H., and Wornell G.W. Lattice-reduction-aided detectors for MIMO communication systems. *Global Telecommunications Conference, IEEE*, 1:424–428, Nov. 2002. 49

[Yee93] Yee N., Linnartz J.-P., and Fettweis G. Multi-Carrier-CDMA in indoor wireless networks. *Personal, Indoor and Mobile Radio Communications, IEEE International Conference on*, pages 109–113, Sept. 1993. 26

[Zha06] Zhao W., and Giannakis G.B. Reduced Complexity Closest Point Decoding Algorithms for Random Lattices. *Wireless Communications, IEEE Transactions on*, 5(1):101–111, Jan. 2006. 56, 57, 58

[Zha07a] Zhang W., and Ma X. Approaching Optimal Performance By Lattice-Reduction Aided Soft Detectors. *Information Sciences and Systems, Conference on*, pages 818–822, May 2007. 72, 73

[Zha07b] Zhang W., and Ma X. What determines the diversity order of linear equalizers? *Acoustics, Speech and Signal Processing, IEEE International Conference on*, 3:57–60, Apr. 2007. 27, 93

[Zhu04] Zhu H., Lei Z., and Chin F. An improved square-root algorithm for BLAST. *Signal Processing Letters, IEEE*, 11(9):772–775, Sept. 2004. 36

[Zim06] Zimmermann E., and Fettweis, G. Adaptive vs. Hybrid Iterative MIMO Receivers Based on MMSE Linear and Soft-SIC Detection. *Personal, Indoor and Mobile Radio Communications, IEEE International Symposium on*, pages 1–5, Sept. 2006. 69

[Zim07] Zimmermann E. *Complexity Aspects in Near-Capacity MIMO Detection-Decoding*. PhD thesis, Technische Universität Dresden, 2007. 60, 65, 68, 69, 74, 75, 76

[Zim08] Zimmermann E., Milliner D.L., Barry J.R., and Fettweis G. Optimal LLR Clipping Levels for Mixed Hard/Soft Output Detection. *Global Telecommunications Conference, IEEE*, pages 1–5, Nov. 2008. 81

Résumé

Cette thèse traite des systèmes MIMO à multiplexage spatial, associés à la modulation OFDM. L'étude s'attarde particulièrement sur les systèmes 4x4, inclus ou à l'étude dans les normes 3GPP LTE et 3GPP LTE-A. Ces dimensions particulières nécessitent une étude de conception poussée du récepteur. Il s'agit notamment de proposer des détecteurs qui affichent à la fois de bonnes performances, une faible latence et une complexité de calcul réalisable dans un système embarqué.

Le défi consiste plus particulièrement à proposer un détecteur offrant des performances quasi-optimales, tout en ne nécessitant qu'une complexité de calcul polynomiale. Une attention particulière est prêtée aux problèmes d'implantation. Ainsi, avantage est donné aux algorithmes à complexité fixe et permettant la réalisation d'opérations en parallèle. En réponse aux problématiques rencontrées, l'architecture du détecteur requiert une attention particulière. Le choix stratégique adopté est de chercher à transférer au prétraitement - qui ne dépend pas des données - le plus possible de complexité de calcul.

Au cours de ce travail et suite à l'introduction du contexte général et des principaux pré-requis, l'inventaire des grandes tendances dans la littérature en ce qui concerne les détecteurs à décision dure est fait. Ils constituent le cœur du sujet et un détecteur original est proposé, incluant notamment les aspects de réduction de réseau et de décodage sphérique. Son avantage par rapport aux techniques existantes est ainsi démontré, et les résultats prometteurs sont maintenus lors de son extension à la décision souple. Comme attendu, le choix de transférer au prétraitement la complexité de calcul s'avère gagnant. Notamment, la réduction de complexité de calcul qu'il permet est présentée dans cette thèse.

Parmi les principaux résultats, ce travail a débouché sur la proposition d'un détecteur original, qui a démontré un compromis entre performance et complexité de calcul efficace. Notamment, il requiert une complexité de calcul presque constante - selon les tailles de constellation -, tout en offrant des performances proches du maximum de vraisemblance. Par conséquent, le détecteur à décision souple proposé se positionne par rapport à l'état de l'art comme une solution d'une grande efficacité dans les systèmes 4x4.

Abstract

In this thesis, spatial multiplexing-MIMO communication schemes with OFDM modulation are considered with a focus on 4x4 systems. In order to achieve the 3GPP LTE and 3GPP LTE-A requirements, the design of detector's architecture with high performance, low latency and applicable computational complexity is a challenging research topic at the receiver due to the power and latency limitations of mobile communication systems.

The challenge consists in providing a detector that achieves near-optimum performance, while offering polynomial computational complexity. Simultaneously, implementation aspects are carefully considered, thus parallel and fixed computational complexity algorithms are strongly favoured.
As an answer to the encountered issues, particular attention is paid to the detector's architecture. In particular, the adopted strategy lies in shifting as much as possible of the computational complexity to the preprocessing step that is data-independent.

Throughout the present work and in addition to the background and preliminaries introduction, an inventory of the main existing hard-decision solutions is introduced. It presents the heart of the subject and an original detector is subsequently proposed. It includes - among others - both lattice reduction and sphere decoding aspects. Its advantage over the existing techniques is presented and is shown to be preserved through its soft-decision extension. As expected, the strategic choice of shifting the computational complexity to the preprocessing step is shown to be winning. It is due to significant decrease in the computational complexity, which is addressed in this thesis.

As a result, the present work has led to the proposal of an original detector that is promising from both the computational complexity and the performance points of view. Namely, it leads to an almost constant - in the constellation size - computational complexity, while offering near-maximum likelihood performance. Consequently, the proposed soft-decision detector compares to existing 4x4 detectors as a very efficient solution.

N° d'ordre : D11-17

Institut National des Sciences Appliquées de Rennes
20, Avenue des Buttes de Coësmes . CS 14315 . F-35043 Rennes Cedex
Tel : 02 23 23 82 00 – Fax : 02 23 23 83 96